

Comparison of Microwave Vs. Conventional Heating Polymerizations and Possible MW Applications in Polymers.

Bertha Teresa Pérez Martínez

March 2021

(c) 2021 Bertha Teresa Pérez Martínez

eman ta zabal zazu



**Universidad Euskal Herriko
del País Vasco Unibersitatea**



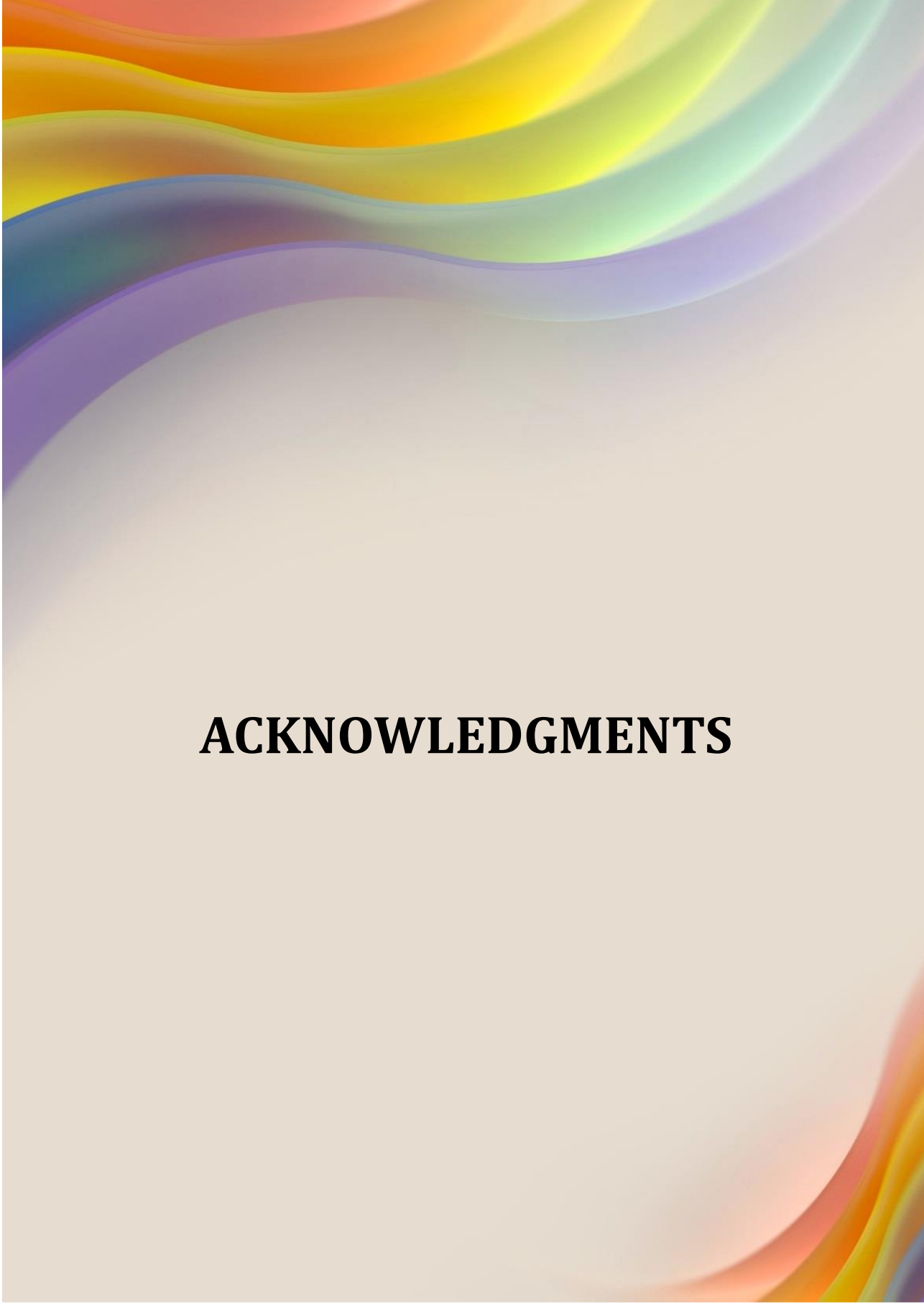
To

Mi abuela, Lydia Valdez
&
Dr. Juan Genaro Osuna Alarcón

“We come here to be philosophers; and I hope you will always remember that whenever a result happens, especially if it be new, you should say, “What is the cause? Why does it occur?” and you will, in the course of time, find out the reason.”

Michael Faraday





ACKNOWLEDGMENTS

ACKNOWLEDGMENTS

Quiero agradecer a todas las personas que van a leer este trabajo, y las personas que estuvieron involucradas en el proceso.

Al Consejo de Ciencia y Tecnología de México **CONACYT** por la beca **No. 410922**.

A mi asesora **Profra. Radmila Tomovska** por todo su apoyo, su tiempo y su dedicación en mi trabajo y por confiar en mí para poder realizar este proyecto. Виe најдобро знаете дека без вашата помош не би ја постигнала оваа цел, благодарам што верувавте во мене и бевте повеќе од мој советник, ми бевте пријател; знаевте како да ме охрабрите за да не се откажам, иако во почетокот имав погрешна насока и никој не ме сфаќаше сериозно, Виe секогаш верувавте во мојот потенцијал. Секогаш ќе имате многу важно место во мојот живот и моето срце. Неизмерно Ви благодарам.

Gracias a todos los profesores que hacen POLYMAT, por todos sus consejos y rigor académico, porque gracias a ello me han dado la oportunidad de crecer profesionalmente, muchas gracias **Prof. José M. Asua, Prof. Jose Ramón Leiza, Profra. Maria Paulis, Dr. Nicollas Ballard, Dr. David Mecerreyes, Dr. Alejandro Müller** y aunque ya se jubilaron también gracias a **Profra. Maria de Jesús Barandiaran** y sobre todo a **Prof. José Carlos de la Cal** por toda su paciencia y apoyo que me brindó.

A una gran persona y administrativa, **Inés Plaza**, gracias por tu gran amabilidad, trabajo y amistad. Eres la mejor, y una columna muy grande para POLYMAT.

A todos los que hacen los servicios de la Universidad SGIker por su ayuda en las diferentes técnicas de caracterización, **Dr. José Ignacio Miranda, Dra. Loli Martin y Dra. Ana Martínz**, así como a la **Dra. Itxaso Calafel, Dra. Mercedes Fernández y Dra. Patrica Leal**.

ACKNOWLEDGMENTS

A mis estudiantes de fin de grado **Niky Alexander** y **Oier Azkue**, por su ayuda en algunas partes experimentales.

A mi gran amigo y colega **Alfonso Arevalillo**, por todo su apoyo, su paciencia para explicarme cromatografía de gases, y todos los consejos que me dió como amigo, profesional y científico.

A mi gran familia adoptiva, por acojerme y hacer me sentir en casa a pesar de la distancia, **Patricia Leal**, **Stefano Paganini** y **Alessandra Paganini**.

A mi primo **Jorge Olmedo**, por todo su apoyo, discusiones científicas, por su infinita amistad y apoyo cuando más lo necesité.

A mis amigas del alma **Ana Belén López**, **Samane Mehravar**, **Gordana Siljanovska**, **Sevilay Bilgin**, **Aurélie Destephen**, **Samantha Molina**, **Claudia de León**, **Elodie Limousin**, **Alicia Simons**, **Nagore Redondo** y **Naroa Pérez**.

Gracias a todos los que me apoyaron para realizar cosas varias de última hora en el laboratorio: **Ana Trajcheva**, **Aurélie Destephen** y **Aitor Barquero**.

Y a **todos** mis **compañeros de laboratorio**, por su ayuda, consejos varios, risas y momentos vividos a lo largo de estos cuatro años.

Quiero agradecer a mi amada familia, porque sin su apoyo, no hubiera tenido la fuerza para poder llegar hasta aquí. Mis padres **María T. Martínez Valdez** y **Juan A. Pérez Blackaller**; mis queridos hermanos **Jesús** y **Araceli**, los amo muchísimo.

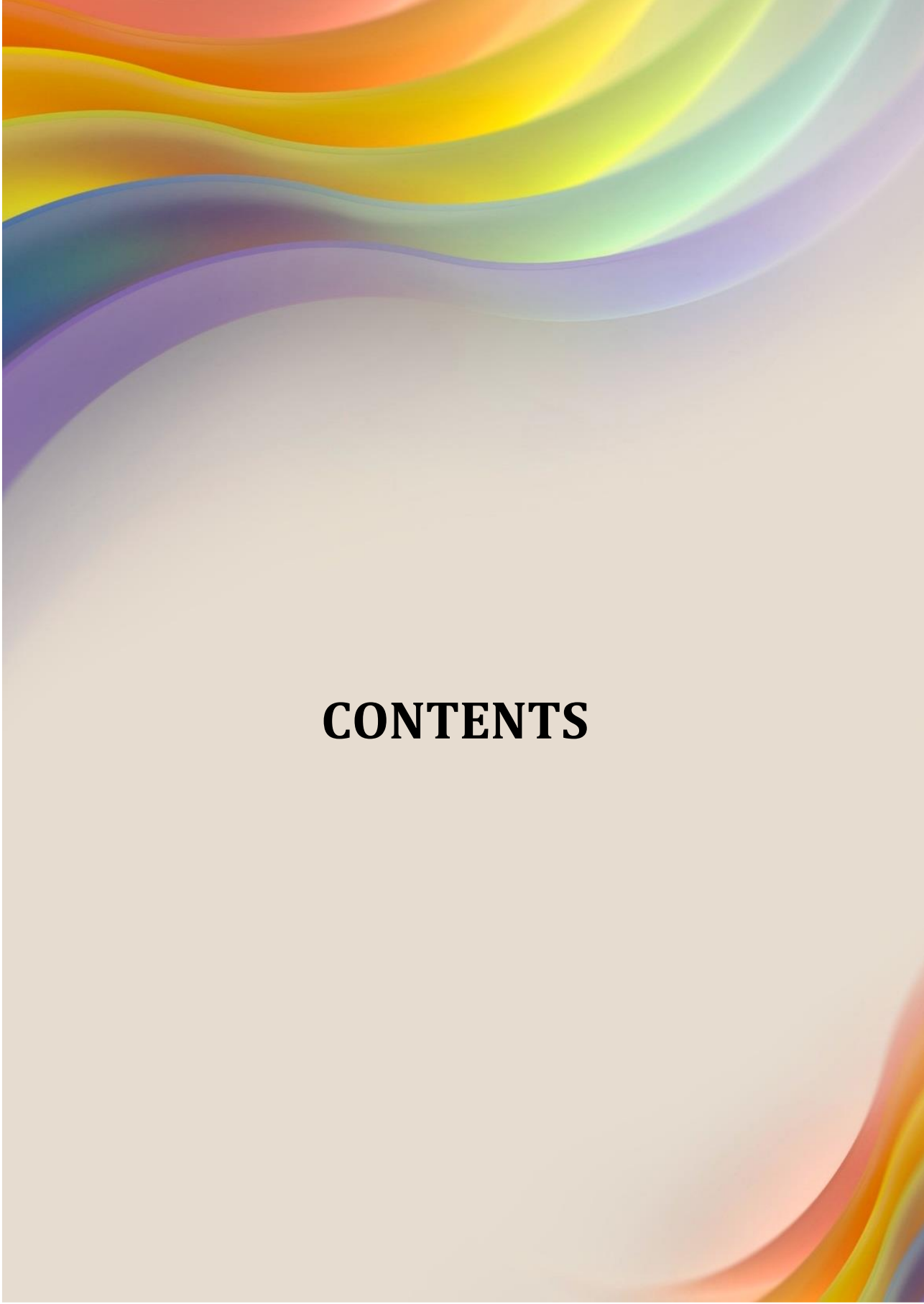
Y por último pero no menos importante quiero darle las gracias a mi compañero de vida **Álvaro Martín**, por si infinito amor, comprensión y todo el apoyo que me brinda todos los días.

ACKNOWLEDGMENTS

Este trabajo considero que no es sólo mío, hubo muchísimas personas a mí alrededor durante todo el camino, que me dieron su mano, una sonrisa, un abrazo (**Nerea Jiménez**), una llamada, mensajes de texto (**Maialen Arg aiz**) y cualquier otro afecto y consejo, tanto personal como en el área profesional. No puedo mencionar con detalle a todos ustedes pero, **GRACIAS** por haber sido parte de este logro.

Muchas gracias ;)





CONTENTS

TABLE OF CONTENT

CHAPTER 1: INTRODUCTION, STATE OF THE ART AND OBJETIVE

1.1 INTRODUCTION	1
1.1.1 DIFFERENCE BETWEEN MW AND CH HEATINGS.....	4
1.1.2 MICROWAVE PHENOMENA.....	7
1.2 POWER AND ENERGY	10
1.3 STATE OF THE ART	12
1.3.1 FREE-RADICAL POLYMERIZATION	13
1.3.2 SOLUTION POLYMERIZATION.....	15
1.3.3 EMULSION POLYMERIZATION	21
1.3.4 MINIEMULSION POLYMERIZATION.....	31
1.4 PhD MOTIVATION	34
1.5 OBJECTIVE OF THE THESIS	39
1.6 ORGANIZATION OF THE THESIS	39
1.7 REFERENCES	42

CHAPTER 2: SOLUTION POLYMERIZATION

2.1 INTRODUCTION	51
2.2 EXPERIMENTAL	53
2.2.1 MATERIALS	53
2.2.2 POLYMERIZATIONS.....	53
2.2.3 CHARACTERIZATIONS.....	54
2.3 RESULTS AND DISCUSSIONS	56
2.3.1 EFFECT OF INITIATOR TYPE.....	60

CONTENT

2.3.2	EFFECT OF SOLVENT AND MONOMER SYSTEM MMA/BA.....	65
2.3.3	EFFECT OF SOLVENT AND MONOMER SYSTEM MMA/St.....	68
2.3.4	EFFECT OF SOLVENT AND MONOMER SYSTEM MMA/VFc.....	71
2.4	CONCLUSIONS.....	80
2.5	REFERENCES.....	82

CHAPTER 3: EMULSION POLYMERIZATION

3.1	INTRODUCTION.....	87
3.2	EXPERIMENTAL.....	89
3.2.1	MATERIALS.....	89
3.2.2	POLYMERIZATIONS.....	89
3.2.3	CHARACTERIZATIONS.....	91
3.3	RESULTS AND DISCUSSIONS.....	91
3.3.1	TEMPERATURE PROFILES.....	91
3.3.2	POLYMERIZATION KINETICS AND POLYMER MICROSTRUCTURE.....	95
3.3.3	POLYMER FILM PROPERTIES.....	103
3.3.4	MICROWAVE ENERGY CONSUMPTION.....	110
3.4	CONCLUSIONS.....	111
3.5	REFERENCES.....	113

CONTENTS

CHAPTER 4: MINIEMULSION POLYMERIZATION IN THE PRECENCE OF MWCNTs

4.1 INTRODUCTION	117
4.2 EXPERIMENTAL	118
4.2.1 MATERIALS	118
4.2.2 POLYMERIZATIONS	118
4.2.2.1 MWCNTs PRE-TREATMENT AND, WATER DISPERSIONS.....	118
4.2.2.2 MINIEMULSIONPOLYMERIZATIONS.....	119
4.2.3 CHARACTERIZATIONS.....	120
4.3 RESULTS AND DISCUSSIONS	121
4.3.1 TEMPERATURE PROFILES.....	121
4.3.2 POLYMERATION KINETICS AND POLYMER MICROSTRUCTURE...	123
4.3.3 PROPERTIES OF POLYMER AND COMPOSITE FILMS.....	131
4.3.4 LATEX STABILITY AFTER TWO YEARS.....	137
4.3.5 MICROWAVE ENERGY CONSUMTION	141
4.4 CONCLUSIONS	142
4.5 REFERENCES	143

CHAPTER 5: GRAPHENE SURFACE MODIFICATION UNDER MWH AND THEIR POLYMER COMPOSITES

5.1 INTRODUCTION	145
5.2 EXPERIMENTAL	146
5.2.1 MATERIALS	146
5.2.2 GRAPHENE SURFACE MODIFICATION UNDER MWH.....	146
5.2.3 POLYMERIZATIONS	147

CONTENT

5.2.4	CHARACTERIZATIONS.....	148
5.3	RESULTS AND DISCUSSIONS.....	149
5.3.1	GRAPHENE SURFACE MODIFICATION.....	149
5.3.2	POLYMERIZATION KINETICS & POLYMER MICROSTRUCTURE	153
5.3.3	POLYMER MECHANICAL PROPERTIES.....	156
5.4	CONCLUSIONS.....	161
5.5	REFERENCES.....	162

CHAPTER 6: EMULSION POLYMERIZATION TOWARDS WATERBORNE HYDROPHOBIC DISPERSIONS

6.1	INTRODUCTION.....	165
6.2	EXPERIMENTAL.....	168
6.2.1	MATERIALS.....	168
6.2.2	POLYMERIZATIONS.....	168
6.2.3	CHARACTERIZATIONS.....	170
6.3	RESULTS AND DISCUSSIONS.....	170
6.3.1	HYBRID LATEX CHARACTERISTICS.....	170
6.3.2	INCORPORATION OF EPOXY INTO THE CO-POLYMER.....	177
6.4	CONCLUSIONS.....	184
6.5	REFERENCES.....	184

CONTENTS

CHAPTER 7: CONCLUSIONS

7.1	GENERAL CONCLUSIONS.....	187
7.2	FUTURE PERSPECTIVES.....	192
7.3	PUBLICATIONS AND CONFERENCES PRESENTATIONS	193

RESUMEN Y CONCLUSIONES

8.1	RESUMEN Y CONCLUSIONES.....	195
-----	-----------------------------	-----

APPENDIX I: MATERIALS AND CHARACTERIZATION METHODS

I.1	MATERIALS.....	203
I.2	CONVENTIONAL HEATING SET-UP.....	207
I.3	MICROWAVE HEATING SET-UP.....	208
I.4	CHARACTERIZATION METHODS OF DISPERSED POLYMERS.....	209
I.5	CHARACTERIZATION METHODS OF POLYMER FILMS.....	217
I.6	CALCULATION OF MW-ENERGY CONSUMPTION.....	219

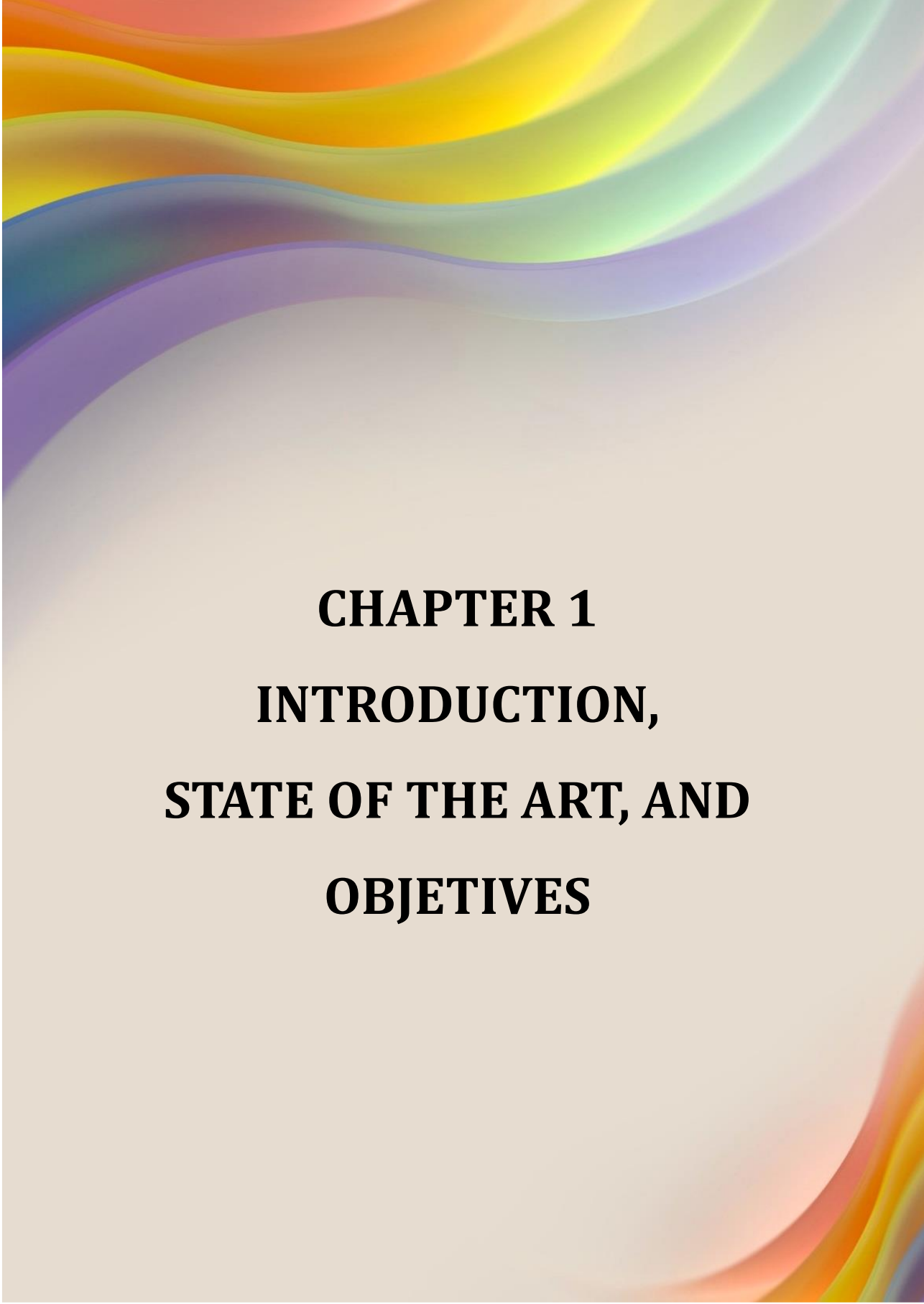
APPENDIX II: SUPPORTING INFORMATION

II.1	SUPPORTING INFORMATION FOR CHAPTER 1.....	221
II.2	SUPPORTING INFORMATION FOR CHAPTER 2.....	227
II.3	SUPPORTING INFORMATION FOR CHAPTER 3.....	229
II.4	SUPPORTING INFORMATION FOR CHAPTER 4.....	233

CONTENT

APPENDIX III: DISENTANGLEMENT OF LARGE MWCNTs BY SONICATION

III.1	INTRODUCTION	235
III.2	EXPERIMENTAL	237
III.2.1	MATERIALS.....	237
III.2.2	METHODS.....	237
III.2.3	CHARACTERIZATIONS.....	239
III.3	RESULTS AND DISCUSSIONS	239
III.3.1	MWCNTs SONICATION TREATMENT IN AIR AND WATER	239
III.3.2	PERFORMANCE OF THE TREATED MWCNTs IN POLYMERS	247
III.4	CONCLUSIONS	251
III.5	REFERENCES	253



CHAPTER 1
INTRODUCTION,
STATE OF THE ART, AND
OBJETIVES

1.1 INTRODUCTION

When the Second World War came to its end, so did the market of the magnetron tubes that generate short-range microwaves, developed initially for military radars. Therefore, the companies (as Raytheon, for example) searched for new applications of this technology. However, it was not until **1946** when the engineer **Percy LeBaron Spencer** discovered by accident that a peanut bar began to melt into his pocket when he was near the radar tubes. The idea of using microwaves for cooking was patented in the same year [1,2]. From that moment, the challenge was to develop equipment that, not just could be able to heat food faster, but will also be a safe and affordable device. The first commercialized models were expensive and large (1947). However, it was not until Japanese technology (Sharp Corporation) reached the global transfer to the market, where the majority of the people could get microwave ovens, which happened in the period between the 1970s-1980s [3,4].

Nowadays, 90% of the EU and the USA population use a microwave oven as a heating alternative for food preparation [5]. However, it is not the only application of this technology since its inception. In 1970 [6], microwave (MW) irradiation began to be used within laboratories as an alternative way to initiate chemical reactions because it promotes so-called internal, non-contact, or gradient-free heating, which is faster and less energy-consuming [7]. However, it was not essential until Nature journal published an article entitled “Microwave chemistry: out of the kitchen” written by David Adam in 2003 [8]. In this article, the advantage of MW organic synthesis reactions was highlighted by optimizing the process in terms of time and energy.

Application of the microwave irradiation in the fields of chemistry is broad; however, it may be divided into two main areas, the first and the largest one, Microwave-Assisted-Organic Synthesis (MAOS) [9], and the second one, which is our interest in

this work, **Microwave-Assisted Polymer Synthesis**, in other words, Microwave Polymerization [10].

At the same time that households purchased microwave ovens for food preparation, laboratories began to acquire them, as well. The first scientific publication about microwave application in polymerization reaction was in 1971, where the spontaneous MW polymerization of 1,5-dicarbopentaborane was studied using a kitchen microwave oven [11]. Thirty years later, there are more than **234** published works, as shown in Figure 1.1, whereas since 2000 to the 2019, this number increased to **2,074** publications, which partially was due to the development of specialized microwave equipment for scientific use. However, this number is significantly lower than **47,526** works published in the field of organic synthesis. The probable reason for such a lower interest may be that in the MW polymerization, no clear advantages over CH were observed, as it is the case for MW organic synthesis, where it was proven that the reactions are fast, less energy-consuming, and more selective [12–14].

The progress in the field of MW assisted polymerization is well documented in the few relatively recent reviews [15–17], where the increased interest in the topic is reported. However, most of the investigations are limited to the comparison of **microwave heating (MWH)** and **conventional heating (CH)** polymerization reactions and products. Besides, the comparison in most of the cases was made under not-comparable conditions and, the results are quite scattered and contradictory, as it will be shown later.

INTRODUCTION, STATE OF THE ART, AND OBJETIVES

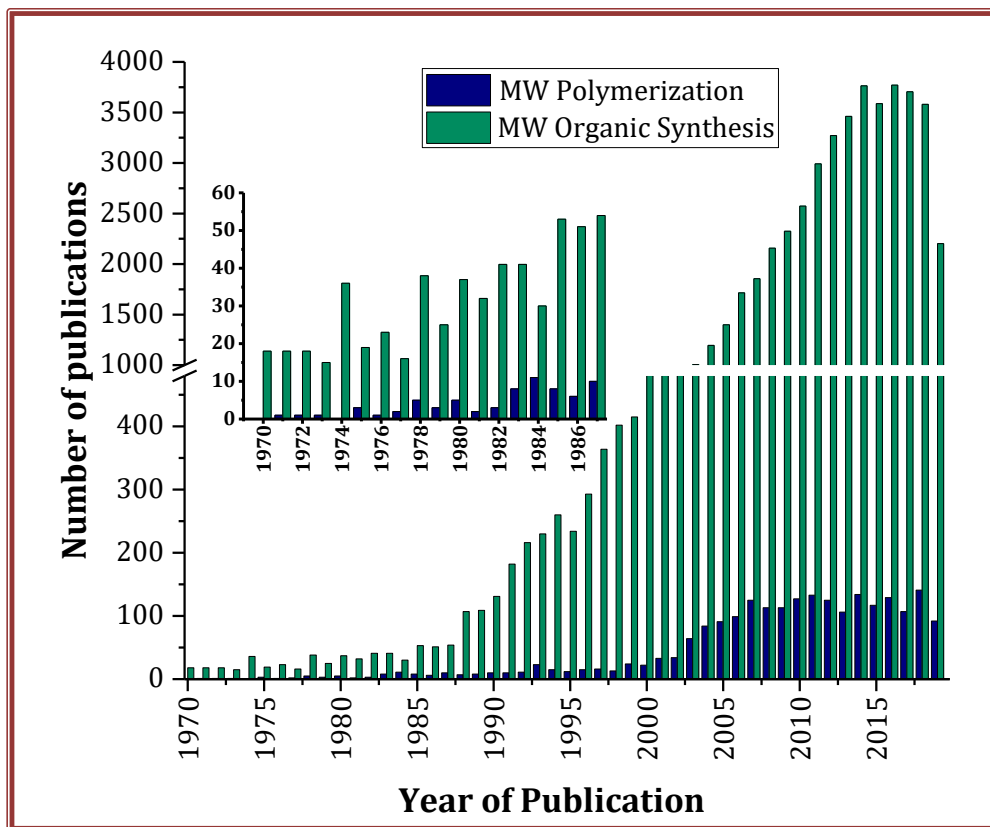


Figure 1.1. Numbers of publications on microwave-assisted polymerization and microwave-assisted organic synthesis per year, obtained from the SciFinder database on the 11th of July 2019 using the key “microwave polymerization” and “microwave organic synthesis.” (including books, journals, patents, preprints, and reviews), as well as the different and most used microwave ovens.

1.1.1 DIFFERENCE BETWEEN MWH AND CH

Conventional polymerization reactions can be initiated using different heat sources, for example, oil baths, heating plates, reactors with jackets, among others and, all of them can be classified as conventional heating, based on heat transfer by convection. **Convection** is the mode of energy transfer between a solid surface and the adjacent liquid that is moving, and it has to do with the combined effects of conduction and Brownian movement; the faster it is, the higher is the heat transfer by convection [18]. Therefore, the heat is introduced from the heating fluid into the reactor through the walls of the vessel, which is a slow and inefficient method for transferring energy into the reacting system that additionally creates a temperature gradient in the reactor.

On the contrary, MW heating starts from the inside of the molecules after the adsorption of MW irradiation. Within the Electromagnetic spectrum (Figure 1.2), MW electromagnetic waves are placed within the wavelength range of 1 cm and 1 m, due to this frequency range, this type of radiation is considered as non-ionized radiation [19]. Household microwave ovens and specialized MW equipment for laboratories work under **2.45 GHz** of frequency that means a wavelength of **12.23 cm** [20,21].

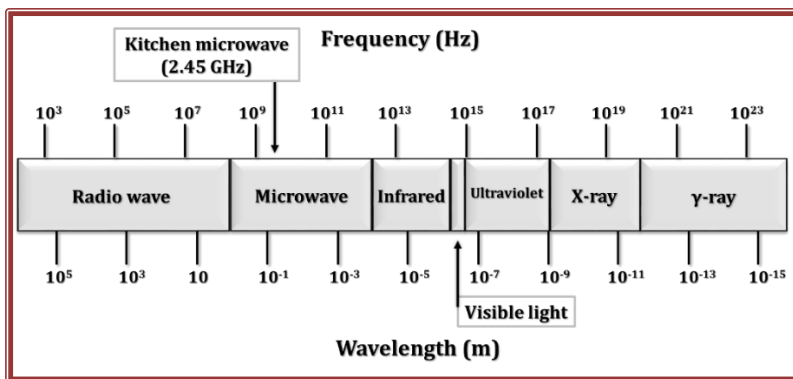


Figure 1.2. The electromagnetic spectrum.

INTRODUCTION, STATE OF THE ART, AND OBJETIVES

Microwave irradiation interacts in different ways with the matter, depending on the nature of the exposed materials. The radiation can be reflected from the surface (e.g., metals, Figure 1.3-a), transmitted through the material without any interaction (insulating materials, Figure 1.3-b), or absorbed by materials with dielectric loss (Figure 1.3-c). The materials containing dipole moment capable of undergoing dielectric losses (Figure 1.3-c) can interact with MW irradiation. MW is high wavelength irradiation that does not wear sufficient energy to break bonds within the substance; thus, when matter interacts with MW, it results in molecular rotation [22–24] and transforms absorbed MW energy into heat, thorough dielectric loss [25].

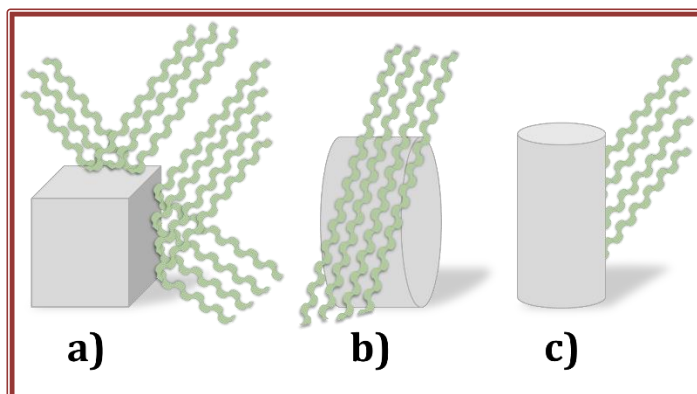


Figure 1.3. Interaction of microwaves with different materials: (a) electrical conductor, (b) insulating, (c) with dielectric loss.

The polarization of dielectric loss materials arises from the rotation of dipoles when a sinusoidal electric field as electromagnetic waves (microwaves) is applied. This should not be confused with electrical conduction, which results from the translational motion of the charges when the electric field is applied [26,27]. This rotation of dipole molecules in the condensed phase induces a lot of friction that hinders the alignment of the movement with the frequency of the applied electric field,

giving rise instead to relaxation processes and dissipation of the absorbed radiation as heat than to resonant processes[25].

Dipolar polarization, occurring through the torque on the permanent dipole moment exerted by the oscillating electric field, will tend to orient the molecule in the direction of the applied field. The energy loss and concomitant heating are caused by frictional losses during the reorientation or rotational diffusion of the dipoles. In short, **it is the dipolar relaxation process that converts the work done by the electric field to heat**. These polarization processes can be expressed in terms of their real and imaginary components corresponding to the in-phase (storage) and out-of-phase (loss) processes, respectively. Energy dissipation in a dielectric medium is often quantified by the loss tangent ($\tan \delta$), which can be obtained from permittivity via the ratio of loss over storage component, according to Equation 1 [28,29].

$$\tan \delta = \frac{\epsilon''}{\epsilon'} \quad (\text{eq. 1})$$

In other words, **$\tan \delta$ is the ability** of a specific material or solvent **to convert microwave energy into heat** at a given frequency and temperature. Dielectric loss (ϵ'') is indicative of the efficiency with which the electromagnetic radiation is converted to heat and dielectric constant (ϵ') described the polarizability of molecules in the electric field and determined the absorptivity of the MW irradiation of the molecule. This means that when a material or solvent has a high dielectric constant, it will absorb a significant amount of MW irradiation. In contrast, if the $\tan \delta$ value is high, the transformation of MW irradiation into heat will be important [30].

In contrast to CH polymerization, where the heat transfer relies on convection, MWH can be considered that produces efficient internal heating of the whole liquid volume simultaneously by direct coupling of MW energy with the molecules that are present in the reaction mixture, **where different MW phenomena can be produced**.

1.1.2 MICROWAVE PHENOMENA

The phenomena observed in MWH reactions have been divided into two categories: (i) **thermal microwave effects** based on the faster heating in the MW reactors than in CH reactors; and (ii) **non-thermal or specific microwave effects** refer to differences between the MW and CH assisted reactions under identical temperature and heating rate [31]. The last one has been the most controversial and most questioned effect.

Thermal microwave effects usually result in different macroscopic heating processes comparing with CH, such as:

- 1) **Volumetric heating:** as explained, certain molecules exposed to MW irradiation create the heat from the molecules and all at once, **creating non-contact heating**, as shown in Figure 1.4 [32].
- 2) **Different heating rates:** The interaction of the substance with the microwave irradiation depends on the polarity of the molecules and their dielectric properties. For example, if it is applied MW irradiation with the same power during the same time to the same volume of two different substances, the first one, water with a polarity of $\mu=1.8$ and dielectric constant of $\epsilon'=80$ and, the second one, toluene with $\mu=0.35$ and $\epsilon'=2.38$, their heating rate will be different, and of course, higher for water [33].
- 3) **Selective heating:** As the interactions of the substances with MW irradiation are determined by the nature and properties of the substance, this means that they will affect not only the heating rates but as well the heating extent, which leads to the significantly different behavior of chemically distinct phases of a heterogeneous system. Heterogeneity itself can lead to changes in effective temperatures at the phase. This phenomenon allows carrying out polymerization reactions using non-polar solvents, such as toluene, for

example. In such a case, the monomers are directly heated by absorption of MW irradiation and transfer the heat by conduction to the toluene. Each monomer will be heated differently, which results in selective heating.

Apart from selective heating, the presence of components within the reaction mixture that interact with MW irradiation and transform the energy into significant heat amount (such as magnetic or metallic particles) will induce an effect known as “hot-spots” or local overheating. These components provide a convenient way of assessing rate accelerations in MW reactions. Since the local overheating cannot be studied directly, their properties can only be investigated indirectly by measuring their effects on the reaction rates [31,34].

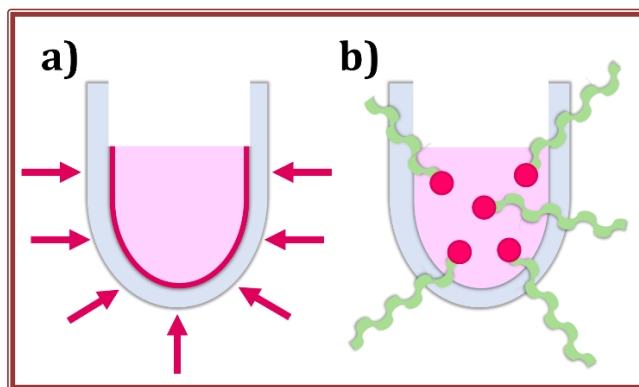


Figure 1.4. Scheme of sample heating: a) by heating conduction and b) by microwave heating.

INTRODUCTION, STATE OF THE ART, AND OBJETIVES

The non-thermal or specific microwave effect occurs when the system absorbs microwave irradiation, which is not immediately converted into heat, but instead, it induces changes within a chemical reactivity, resulting in acceleration rates and different characteristics of the products [28]. In an attempt to understand this non-thermal effect, reactions performed under MWH are usually done under CH, too.

According to published results by many researchers, the non-thermal MW effect is claimed when the experimental evidence cannot be explained due to temperature differences. Therefore, the results should be explained similarly to the effect that provokes UV irradiation, where the absorption of a UV photon is a way of radicals generation [35].

However, one should take into account that MW irradiation photon wears significantly lower energy (**0.00096 kJ/mol at MW= 2.45 GHz**) in comparison to the energy required for exciting electronic or vibration transitions (for carbon-carbon double bond, it is 613 kJ/mol). For that reason, MW irradiation is considered as non-ionizing energy because there is no mechanism in which microwave radiation can provoke the activation of a chemical bond [28,36]. Hence, this is the reason why the non-thermal MW effects are still controversial and unlike. According to the fundamental physics of **MW interaction with molecules in the solution, MW irradiation can generate heat by relaxation processes; this is not a quantum mechanical resonant phenomenon**. Transitions between quantized rotational bands are not involved, and the energy transfer is not a property of a specific molecule but the result of a collective phenomenon involved in the bulk. Hence, "heat is heat," regardless of how it is generated [28]. If non-thermal microwave effects exist, to demonstrate them experimentally, more specialized methods and experimental design are necessary to detect and separate them from the temperature effects, which is not easy.

1.2 POWER AND ENERGY

Microwave (MW) radiation is created by an oscillating electric or magnetic field produced by a magnetron. Indeed, a high voltage is applied between the positive (cathode) and negative (anode) electrodes of the magnetron, which induces oscillations of the electric field through cavities present on the anode. A magnetic field is then created perpendicular to the electric field thanks to two permanent magnets situated at the extremities of the magnetron. The frequency determines the velocity of these oscillations. For standard MW reactors, the frequency is 2.45 GHz, which represents about 4.5 billion oscillations per second. Microwaves are a combination of electric and magnetic fields in oscillation, and one field does not exist without the other (Figure 1.5).

The **MW-power** is supplied by the electrical energy (measured in watts) used to operate the magnetron. This power is reflected in the amplitude of the wave (Figure 1.5); at higher power applied, the amplitude and the strength of the MW increase; however, the frequency of the MW does not change.

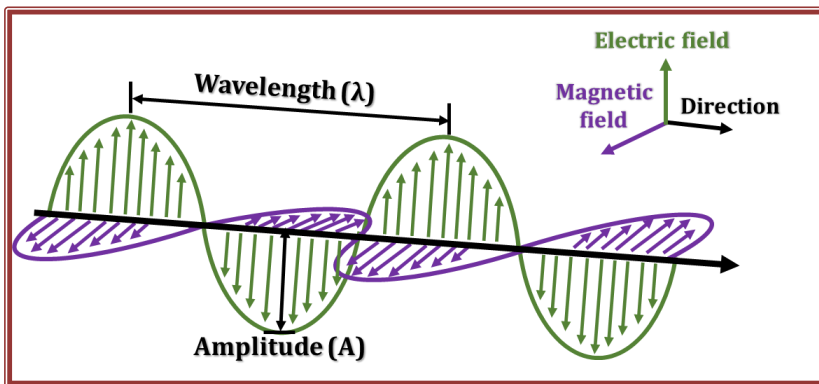


Figure 1.5. Scheme of a microwave, combination of electric (green), and magnetic (purple) fields.

INTRODUCTION, STATE OF THE ART, AND OBJETIVES

The **MW-energy** depends on the period of the time that microwaves are applied at a certain power, thanks to the magnetron. This energy is just for the magnetron work and not for the whole electric circuit of the MW-device. The MW-energy can be calculated with the following equation:

$$E = P \times t \quad \text{with E: Energy (J)} \quad (\text{eq. 2})$$

P: Power (W)
t: time (s)

However, the MW-energy should not confuse with the energy of the **MW-photons** defined by the Planck equation, as followed:

$$E = h \times \nu \quad \text{with E: Energy (J)} \quad (\text{eq. 3})$$

h: Planck's constant
($h = 6.63 \times 10^{-34}$ J.s)
 ν : Frequency (Hz)

A photon is a particle of light, which essentially is a packet of electromagnetic radiation. The energy of the photon depends on its frequency (how fast the electric field and magnetic field wiggle). The higher the frequency, the more energy the photon has. Following the Planck equation, the energy which wears a single microwave at 2.45 GHz of frequency has resulted in **1.623x10⁻²⁴J**. It is pointing out that this energy of the photons will not be changed along the exposure time or the power input because this energy is given by the frequency. Furthermore, the greater the increase in power, the greater the number of photons emitted (in the same period); however, each photon's energy is always the same.

1.3 MW ASSISTED POLYMERIZATION: STATE OF THE ART

Since 1971, when the first publication of microwave-assisted polymerization appears, to nowadays, many investigation topics in polymers have been studied. Richard Hoogenboom *et al.* [37] classified the most important works in different polymerization areas. In Figure 1.6, the different areas in microwave-assisted polymerization can be seen.

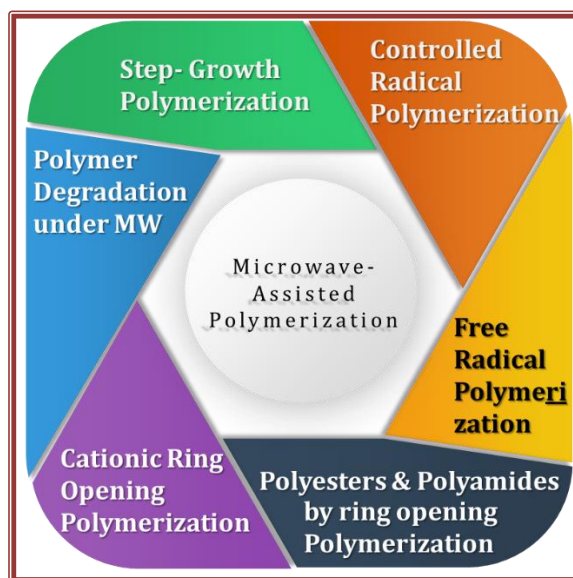


Figure 1.6. Scheme of the classification of microwave-assisted polymerization.

The present investigation work is focused on the MW induced **free-radical polymerization**.

1.3.1 FREE-RADICAL POLYMERIZATION

Free-radical polymerization is a method of formation of polymer that consists of at least three steps, the first one called **initiation**, when the radicals are formed, the second one called **propagation**, when the products are developed, and finally, the **termination** when the free-radicals reaction chains end. Figure 1.7 illustrates the steps in this process. The initiation process creates free radicals from free-radical initiators that start the polymerization reaction by addition to monomer units. For that aim, the initiators must be activated.

There are three different processes to activate the initiator and to generate radicals: heating, ultraviolet (UV) radiation and, electron transfer (redox) processes [38]. In the polymerizations, the propagations are usually chain reactions; a series of very rapid repetitive steps follow every single act of initiation, leading to the addition of thousands of monomer units. In a propagation reaction, a radical reacts with monomer unit to form a covalent bond and to generate a new radical.

In a termination reaction, two radicals interact in a mutually destructive reaction in which both radicals form covalent bonds, and the reaction ceases. Termination can occur by combination or disproportion. Termination by combination is when two reactive centers meet and react with each other, while termination by disproportionation is when hydrogen atom from a donor polymeric radical is transferred to acceptor polymer radical, and this results in the formation of two polymer molecules, one saturated and one unsaturated.

Chain reactions, in addition to the three stages indicated, usually comprise an additional stage that is called transfer reaction and consists of a transfer of active center from a growing chain to another molecule present in the reaction medium, which it may, in turn, initiate the formation of a new polymer molecule. The effect of

this type of reaction is to terminate the growth of one polymer chain and initiate the growth of another [39,40].

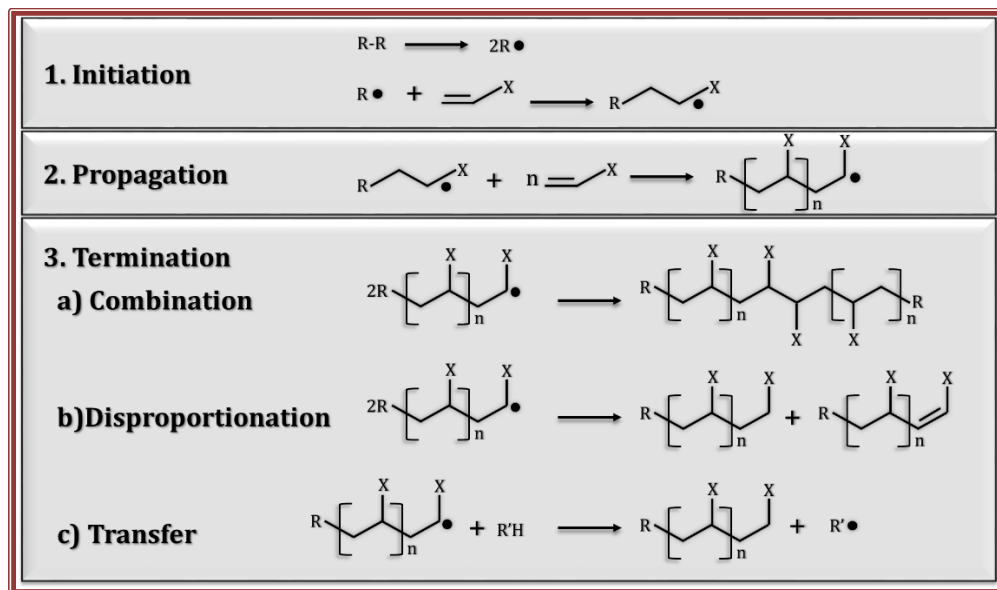


Figure 1.7. Scheme of free-radical polymerization mechanism.

As mentioned, the interest of this work is microwave-assisted free-radical polymerization in general; therefore, it was attempted to prepare exhaustive state-of-the-art in relation to it. According to the **SciFinder database**, there are; **1,956 publications** founded (11th of July 2019) into the field of **microwave-assisted polymerization**, from which only 138 corresponds to free radical polymerization that involved bulk, solution, dispersion, emulsion, and miniemulsion polymerizations. All those works are reviewed in the next section.

1.3.2 MW-ASSISTED SOLUTION POLYMERIZATION

Solution polymerization refers to a polymerization process in which the monomer, or mixture of monomers, and the initiators are dissolved in a non-monomeric solvent at the beginning of the polymerization reaction. The polymerization media, in this case, is usually also a solvent for the resulting polymer or co-polymer [41]. Figure 1.8 represented all processes involved in solution polymerization by a free-radical mechanism.

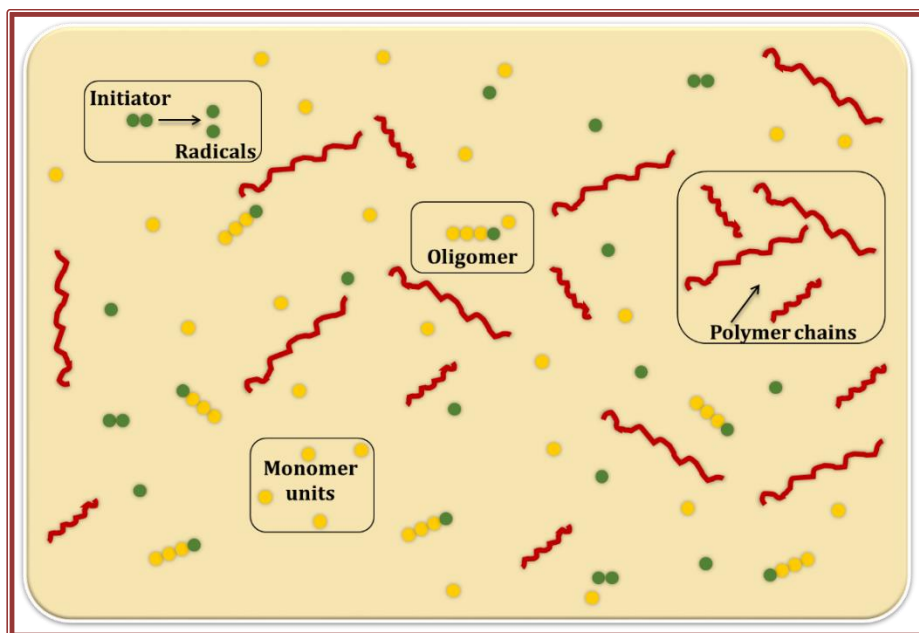


Figure 1.8. Solution polymerization method. Light orange color represents the organic solvent, yellow spheres the monomer units, green spheres represent the initiator and their radicals, and oligomers and polymer chains are as well represented.

Dikusar *et al.* [42] investigated the polymerization of 4-nitrophenyl acrylate (NPA) in dimethyl sulfoxide (DMSO) solvent, changing the temperature, monomer concentration, and initiator concentration. They compared both MWH and CH assisted polymerizations. It was found that CH had achieved full monomer conversion, in 24 hours, whereas it was in 10-20 min for MWH. Moreover, the average molecular weight (M_n) was higher, and molecular weight distribution (MWD) was narrower for MWH polymers. Among MW advantages, the authors claim good reproducibility and that the procedure can be scalable from 5 to 10 times using 300 μl as a base volume. Nevertheless, they added the initiator (AIBN) before starting the heating, which likely contributed to the observed differences. Namely, MW irradiation provides much faster heating than CH, leading towards sooner initiator decomposition and the creation of many more radicals. The temperature profiles were not reported for any of the reactions.

Madras and Karmore [43] studied the kinetics of polymerization of methyl methacrylate (MMA) and the simultaneous depolymerization of poly-MMA, using chlorobenzene solvent and varying the initiator concentration under MW irradiation. Their experimental results were confirmed using a mathematical model. Their data indicate that polymerization under the conditions studied occurred in 40 sec. However, in this work, they used a domestic oven using a beaker without any condenser, without details on how the MW experiment was carried out (agitation, control of temperature, and the most important possible monomer evaporation).

Buruiana *et al.* [44] synthesized co-polymers of n-acryloyl-(S)-phenylalanine benzyl ester (AcPheBz) and n,n-dimethyl aminoethyl acrylate (DMA) in dioxane under MW and compare it with CH reaction. The polymer obtained was quaternized with 4-chloromethylphenylcarbamoyloxy-methylstilbene, leading to a co-polymer with fluorescence response, able to detect various amine or ferrocene compounds into polymeric solutions.

INTRODUCTION, STATE OF THE ART, AND OBJETIVES

The synthesis of a co-polymer with high hydrophobicity and high glass transition temperatures was reported by **Agarwal *et al.*** [45], where polymerization reaction was induced by both MWH and CH. 2,3,4,5,3-pentafluorostyrene (PFS) and N-phenylmaleimide (NPMI) were co-polymerized in anisole. Under MWH, an enhanced reaction rate was observed; thus, at the beginning of the reaction in 5 min, the conversion was 40%, after which the conversion was changed slightly, achieving a final conversion of 58% in 270 min. CH polymerization rate was about 14 times slower than MWH, but after 300 min, the final conversion reached 83%. The molecular weight of the MW polymers was lower than these of CH polymers, which according to the authors, was due to the increase of the initiator efficiency, in this case, 2,2'-azobisisobutyronitrile (AIBN). However, in MW experiments, the initiator was added to the reaction mixture from the beginning, and before the reaction temperature was achieved. Such a reaction mixture was exposed to fast MW heating; therefore, the radicals were created into the MW system much before these in the CH system, in which initiator was added after the reaction temperature was achieved. We hypothesize that the observed differences reported in this work probably were due to these differences. The faster reaction was likely due to faster heating of the initiator until reaching the reaction temperature (before 0 time), whereas the difference in final conversion was probably due to faster exhausting of the initiator under MW. Apart from this, it was clearly demonstrated that the way of heating of the AIBN initiator (either MWH or CH) did not influence the efficiency and rate of decomposition [46,47].

Singh *et al.* [48] investigated the homopolymerization of acrylamide (AM) in an aqueous solution, using potassium persulfate (KPS) as initiator under MWH and CH. The authors claimed that MWH polymerization was performed with very low KPS concentration ($2 \times 10^{-3} \text{M}$), for which CH polymerization did not proceed. Furthermore, under MW irradiation, an inert atmosphere was not necessary. According to the

authors, by increasing the power of MW (up to 80% of the maximum), higher molar mass polymer chains were obtained. For further increase of MW power, depolymerization was reported. Nevertheless, it is necessary to point out that, in this work, a domestic MW oven was used without any type of temperature control and a condenser on the reaction flask.

The super absorbent polymer was synthesized by **Ren *et al.*** [49], co-polymerizing acrylic acid (AA), AM and, soluble starch, using water as a solvent and KPS as initiator, under both MWH and CH varying the reaction temperature from 30°C to 50°C and reaction times of 1 to 3 hours. The water absorption of the polymers was studied. In all cases, the polymers made by MW presented superior properties than polymers obtained under CH. The authors concluded that under MWH, the reaction times were significantly reduced in comparison with CH, and the whole process did not require nitrogen gas purging. The authors reported that the kinetics was changed due to changes in activation energies. However, no data on the kinetics of both polymerization methods (MWH and CH) were presented in this study.

Another approach in solution polymerization is to use ionic-liquids as a solvent. Due to the presence of ions in the solvent, it led towards the ionic conduction heating mechanism under MW irradiation. Therefore, the heating is faster and occurred without any significant pressure build-up, minimizing safety issues coming from over pressurization.

Guerrero-Sanchez *et al.* [50] investigated the MW-assisted polymerization of MMA in bulk and in a solution using two types of ionic-liquids named 1-butyl-3-methylimidazolium trifluoromethane sulfonate (IL-1) or 1-butyl-3-methylimidazolium tetrafluoroborate (IL-2). AIBN was used as an initiator. In this work, the reaction temperature profiles were presented, demonstrating that bulk polymerization proceeded slower than solution polymerization because the heating

INTRODUCTION, STATE OF THE ART, AND OBJETIVES

of the ionic liquids under MWH is faster than the heating of the monomers. Additionally, the authors claimed that the ionic-liquids could be recovered and reused, approaching the principles of green chemistry.

Two years later, **Glück *et al.*** [51] studied the homo and co-polymerization of MMA, styrene (St), acrylonitrile (AN), and n-phenylmaleimide (NPMI) using two kinds of solvents: conventional solvents, such as N,N'-dimethyl formamide (DMF) or methanol; and, ionic-liquids 1-ethyl-3-methylimidazolium ethylsulfate (IL-3) or 1-butyl-3-methylimidazolium tetrafluoroborate (IL-4), under MWH and CH methods. There was no difference observed between MWH and CH polymerization rates when DMF or methanol was used as solvents. However, higher polymerization rates under MW were noticed in the case of ionic-liquids solvent. Taking into consideration that the initiator was added from the beginning of the reaction before the reaction temperature was achieved, the comparison is not convincing. The authors presented the temperature profile for both methods (MWH and CH), showing that the reaction temperature in MW was achieved in two minutes and in 10 minutes under CH. Likely this fact contributed to the observed differences between MWH and CH experiments.

Slightly more than a decade ago, **H. Stange *et al.*** [52,53] performed a comprehensive study of MW-assisted free-radical homopolymerization of styrene (St) and its co-polymerization with methyl methacrylate (MMA). The effect of different peroxide initiators, different solvents (toluene, cyclohexane, and N,N-dimethylformamide, DMF), and different MW powers was studied, and MW and CH reactions were compared. Using both heating type methods, relatively similar homo and co-polymerization rates were obtained in toluene, whereas, remarkable acceleration of polymerization rate was observed in DMF under MW irradiation when tert-butylperbenzoate (tBPB) was used as the initiator, leading to monomer conversion of 92% (the corresponding conversion under CH was 37%). The authors related this higher rate of polymerization obtained in DMF to the much stronger microwave

absorbing ability of the polar DMF than non-polar toluene and cyclohexane, and to the increased decomposition rate of the initiator in DMF, which resulted in more radicals formed during an early stage of the co-polymerization. Nevertheless, the molar masses were not as different as might be expected in such conditions. Co-polymer composition of MMA/St was studied too, as the authors expected that the difference in polarity between these two monomers could affect the heating rates of both, and in toluene it may result in a difference in reactivity ratios of the two monomers. However, no differences in co-polymer composition were observed between MW and CH polymer. It is worth mentioning that, as in previous studies, the initiator was added before the reaction temperature was achieved for both MW and CH reactions, which obviously affected the results, and the conclusions should be taken with precaution.

Moreover, comparing these two studies [46,47], certain irreproducibility was noticed as different conversions, and molar masses for the same co-polymer obtained under the same reaction conditions were reported in both studies. All these differences in the final results leave uncertainty in the final discussions.

It is clear that the experimental conditions are key factors to create comparable conditions between MWH and CH, but none of the presented works has achieved it. Therefore, the true advantage of MW heating in comparison to CH for performing free-radical polymerization in solution remains uncertain.

In Table II.1.1 in Appendix II, the summary of the different published works reviewed previously about solution polymerization by free-radical polymerization under MWH is presented.

1.3.3 EMULSION POLYMERIZATION

INTRODUCTION, STATE OF THE ART, AND OBJETIVES

Emulsion polymerization is a method that involves the polymerization of hydrophobic monomer(s) dispersed in a continuous aqueous phase in the presence of an emulsifier. The concentration of the emulsifier needs to be above critical micellar concentration (CMC) in order to ensure the presence of micelles. The final product, called latex, consists of suspended polymer particles in water stabilized by the emulsifier.

The mechanism of the emulsion polymerization process is shown in Figure 1.9. When water-soluble initiators are used, the radicals are generated in the aqueous phase, and they are too hydrophilic to enter into the micelles swelled with monomers or in polymer particles if they are present in the system. Therefore, the initiator radicals start the polymerization reaction in the aqueous phase forming oligo-radicals, which may:

- Enter into the polymer particles
- Enter into micelles forming new particles (heterogeneous nucleation)
- Propagate in the aqueous phase until they become insoluble and precipitate, forming new polymer particles (homogenous nucleation)
- Terminate with other radicals in the aqueous phase.

The probability of each of these events depends not only on the formulation (the type and concentration of the monomers, initiator, and emulsifier) but as well on the process variables like agitation rate, temperature, type of reactor, etc.

Within the polymer particles, the number of radicals per particle depends on three competitive reactions that take place simultaneously: radical entry from the aqueous phase, radical exit from the polymer particle, and bimolecular termination in the polymer particle [54–56].

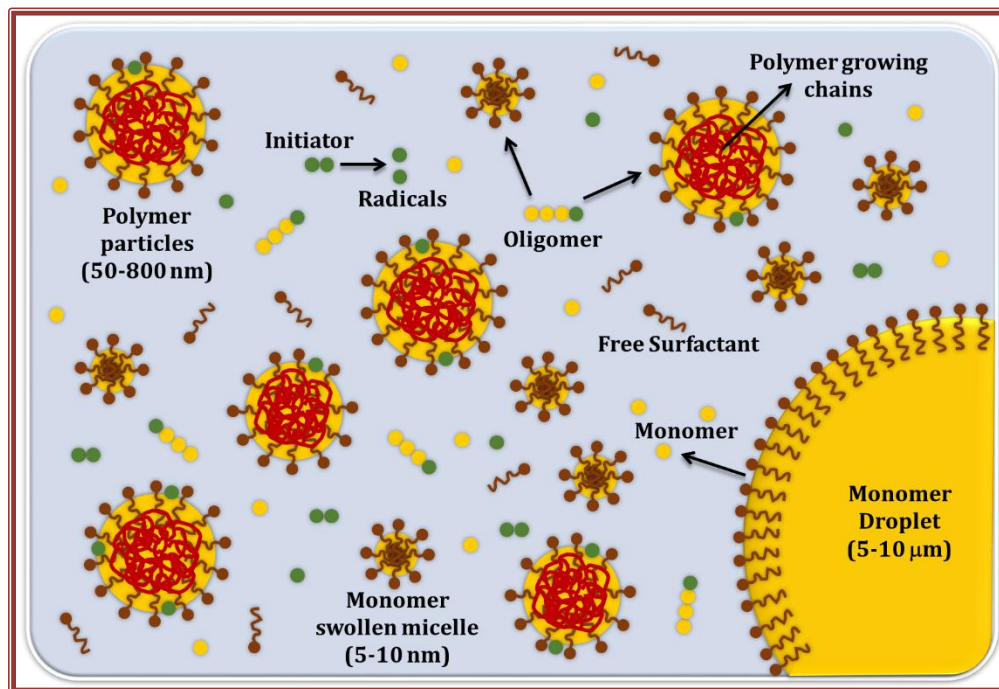


Figure 1.9. Mechanism of emulsion polymerization. The blue background refers to water as a continuous phase, in which there are monomer droplets, swollen monomer micelles, polymer particles, polymer growing chains as well the initiator; their radicals and oligomers are presented simultaneously.

Various (meth)acrylic and styrene monomers were homo and co-polymerized in the emulsion, performed in CH or MW reactors (in batch). In the following, MW-assisted polymerization performed in an oil-in-water emulsion, with and without surfactant, is presented.

Correa *et al.* [57] synthesized polystyrene by emulsion polymerization using sodium dodecyl sulfate (SDS) as surfactant and potassium persulfate (KPS) as an initiator in self-designed MW equipment. To prevent pressure increase in the reactor, they applied MW irradiation in cycles (for 800 W power the pulses were of 20 s “on” and

INTRODUCTION, STATE OF THE ART, AND OBJETIVES

600 s “off”; for the power of 175 W the “on” cycle was 60 s and the “off” was 300 s). They investigated two different programs (800 W and 175 W) and found that the reactions performed at 175 W presented a lower polymerization rate than the reactions performed at 800 W. The authors compared MWH and CH assisted polymerization, finding that the CH reaction was slower than the MW reaction under the same conditions. However, there was no proper temperature control (the temperature was followed by an external thermocouple); therefore, the temperature in both reactors and the heating rates likely were importantly different. The important conclusion of this work was that energy and time saving may be achieved by MWH polymerization of styrene in an emulsion because of the polarity of water solvent that heats faster and more efficient under MW, and the energy consumption can be controlled by irradiation in pulses.

Emulsion polymerization of PMMA [58] or PS [59] under MWH was done by **Zhu et al.** using SDS as a surfactant and KPS as initiator. The MW device was self-designed apparatus. In this case, an MW frequency of 1.25 GHz was used, a half less than conventional MW devices used in chemistry (2.45 GHz). Compared with the same reaction performed under CH, higher conversions were achieved under MWH due to faster polymerization. The PMMA or PSt polymers obtained under MWH presented higher molar masses than CH polymers. According to the ^{13}C -NMR results, both polymers from MW and CH assisted reactions were with very similar microstructure and presented very similar glass transition temperature (T_g) $\sim 127^\circ\text{C}$ of PMMA and $\sim 109^\circ\text{C}$ of PSt. Nevertheless, the authors remarked that the accelerated polymerization rate under MW “should be an instantaneous action of high electric field by MW irradiation instead of the thermal effect by MW energy”. Furthermore, they claim that the higher molar masses of MW-polymers were consequence of the rotation and oscillation of molecules of initiator and monomer at high speed, which polarized and even deformed them. This could promote the initiator decomposition

itself, resulting in a strong “gel-effect”, however, this did not explained the higher molar masses of MW polymer. They followed the decomposition rate of KPS under MW irradiation. It was found that at 68.5°C, the decomposition constant (K_d) of KPS was $8.05 \times 10^{-5} \text{ s}^{-1}$, whereas, for CH, they reported a theoretical value of K_d of $3.35 \times 10^{-5} \text{ s}^{-1}$ at 70°C. This enhancement of KPS decomposition under MWH was the main explanation for the higher polymerization rates observed under MWH. For PSt, average particle size (D_p) of $\sim 70.2 \text{ nm}$ (at 86.5% conversion) for MWH and $\sim 86.9 \text{ nm}$ (for 33.48% conversion) for CH were reported, whereas, for PMMA, D_p was not reported.

Hyun *et al.*[60] polymerized St and butyl acrylate (BA) as homopolymers and copolymers under MWH and CH, using KPS as initiator and SDS as a surfactant, at 70°C, using a cooling fan to control the temperature. For BA homopolymer, the polymerization rate was faster under MWH than CH. The addition of St in the formulation resulted in a decrease of the polymerization rate under MWH, and for the homopolymerization of St, there were no differences between both methods. The authors explained these results on the basis of the different susceptibilities of each monomer on MW irradiation. To demonstrate it, they exposed the monomers to continuous MW irradiation at 500 W. It was observed that the temperature elevation rates were mainly dependent upon the dipole moments of the monomers.

Sierra *et al.* [62] synthesized nanoparticles of PMMA, under both MWH and CH, using SDS as a surfactant, and KPS as initiator, obtaining an enhancement of polymerization rate and higher molar mass in comparison to CH. First, they performed the polymerization under MWH using different amounts of KPS, and they found that at higher concentrations of KPS, the number average molar mass (M_n) slowly decreases, while the weighted average (M_w) remains constant. However, PDI increases accordingly at higher KPS concentration. The author claimed that these results are characteristic of “living” systems and might be explained by the fast initiation rate,

INTRODUCTION, STATE OF THE ART, AND OBJETIVES

promoted by MW irradiation, where it could be possible that the propagation rate is favored over the bimolecular termination rate, thus making the system more “living”-like. On the other hand, when they compare the kinetics of the MW and CH assisted polymerization using 1.125g/L of initiator, they found that under MWH, they achieved 100% conversion just in 12 minutes. In contrast, in CH, they just achieved 73.7% in 90 min. The molar mass, 987×10^3 Da, and 588×10^3 Da were found, respectively, and all experiments were carried out at 50°C.

Cosa et al. studied emulsion polymerization of methyl methacrylate (MMA) or BA using different initiator types, as cationic azo-initiator or KPS under MW irradiation [63,64]. In these works, a specialized MW device (Synthos 3000 Anton Paar) was used. First [63], MMA, or BA as the monomer, a combination of surfactants (Disponil FES32 and Disponil A3065), KPS as initiators were used in the formulation. Emulsion polymerization under MWH and CH were compared. When MWH and CH MMA polymerization were compared, initially polymerization rate is faster for MWH than for CH, but after 12 minutes, polymer conversions are the same. However, the final average particle size is smaller for MWH (~60 nm) than for CH (~90 nm). This was ascribed to an increased thermal decomposition rate of KPS under MWH. For BA polymerizations, the differences between MWH and CH are negligible. For these results, the authors concluded that the differences between both monomers were attributed to the different aqueous phase solubility and dielectric parameters of the monomers. As a consequence, specific microwave effects on each monomer system was claimed to occur. However, the methodology was not the same for both heating methods. For MWH, the initiator was added before the reaction temperature was reached, and in the CH, the initiator was added after the reaction temperature was reached. Taking into account the fast heating in MW, the flux of radicals was probably already very high in MW, before the reaction was even started in CH, making this conclusion doubtful. These differences are even more important during emulsion

polymerization because they may affect the nucleation process, which has influence on the reaction rates and polymer molar mass.

The same authors [64] performed emulsion polymerization of MMA but in this case, using a water-soluble cationic azo-initiator, 2-2'-azo(2-methylpropionamidine) dihydrochloride (V-50) at two different concentration (0.013 wt% and 0.005 wt%), and dodecyltrimethylammonium bromide (DTAB) as a surfactant. The reaction temperature was 80°C. For both initiator concentrations, the initial polymerization rate was faster under MWH than CH, but at a certain time, they achieved the same conversion, and the final average particle sizes were very similar, ~85 nm for higher surfactant concentration and ~100 nm for lower surfactant concentration. The conclusion of the authors was that the improvement of polymerization rate for MWH using V-50 as initiator was ascribed to the presence of ions that provides specific heating by ionic conduction mechanism under MW irradiation. Indeed, in the same work, they present experimental results that confirm the differences in the decomposition rate of different initiators under MWH and CH.

Ergan *et al.*[65] has used a specialized multi-mode microwave oven from Milestone-Start-S-model. In this case, they studied the polymerization of St in the emulsion, varying some parameters such as the relation of water/monomer, surfactant/monomer, initiator/monomer, as well as temperature, reaction time, and MW power input. Polymerization reactions performed under CH were done to compare with the MWH method. They found that the polymerization rate was higher under MWH than CH method, but the final conversion, as well as the thermal and structural polymer characteristics, were very similar. However, the initiator was added before the reaction temperature was reached in both MW and CH. The heating profiles were very similar in both heating methods. Additionally, the vessel reactor was not sealed hermetically; hence the pressure factor is not playing a role in these comparisons. Beside all of these, the authors reported a difference between these

INTRODUCTION, STATE OF THE ART, AND OBJETIVES

polymerizations. Namely, the time necessary to achieve the conversion of about 95% on MWH experiments was 40 min, whereas for CH was 90 min for the same conversion. The higher polymerization rate under MWH was attributed to the fast decomposition of KPS as initiator, and they support this with an own study reported previously [66]. However, the presented kinetic curves were very similar (less than 5% difference in conversion may be observed at 40 min). **An et al.** [67] presented a novel one-step strategy to prepare PMMA nanoparticles with sizes ~20 to 50 nm and solid content up to 10% using microwave irradiation and surfactant-free emulsion polymerization. Polymer particles were crosslinked with hydroxyl functional groups using different corss-linkers like ethylene glycol dimethacrylate (EGDM) or N,N'-methylenebisacrylamide (MBA) and, the average particle size could be readily adjusted by simply varying the polarity of the solvent; in this case, the ratio of acetone to water and, increasing the temperature. This method was published in a short communication and more described in a Patent No. US2008/0009558 A1. [68]. Eight (Biotage) single-mode microwave reactor was used.

The research group of Professor To Ngai and Chi Wu of the Chinese University of Hong Kong published several works of emulsion polymerization of St or MMA under MW irradiation, with and without surfactant. In all these experiments, they used the same MW-oven Whirlpool-VIP20. In one of these works, **Gao et al.** [69] reported the control of the particle size but also to predict the monomer concentration dependence of the number of the resultant latex particles. They performed polymerization of St at 70°C, using SDS as surfactant and KPS as initiator. They claimed that the polymerization under MWH is ~10 times faster than the polymerization under CH. In other study, **Wu et al.** [70] performed MW polymerization of St or MMA, with and without surfactant. For the PSt reaction, they claimed 98% of polymer conversion reached approx. in ~40 minutes under MWH, and narrower hydrodynamic radius distribution than the polymer particles obtained by CH. **Zhang et al.** [71] presented the

preparation of narrowly distributed surfactant-free stable PSt nanospheres. The authors claimed that for MWH, 98% of monomer conversion was achieved in 40 min, whereas for CH, it was achieved in more than 10 hours. Nevertheless, for the MWH reaction, the initiator concentration was 1.13×10^{-2} g/mL, whereas for CH was 3.02×10^{-4} g/mL. This can be the reason for the observed differences in their results.

He et al. [72] used a self-design MW device to produce polymer nanoparticles of butyl methacrylate (BMA) by emulsion polymerization without any surfactant and KPS as initiator; varying the amount of monomer, initiator and, by adding into the reaction mixture a small amount of ethanol. Additionally, they determined the KPS decomposition rate (k_d) under MWH and CH methods, finding that under CH conditions, k_d was $2.33 \times 10^{-5} \text{ s}^{-1}$ whereas under MWH was $3.10 \times 10^{-4} \text{ s}^{-1}$; thus, it was expected to observe a polymerization rate enhancement under MWH vs. CH. Larger particle size with narrower distributions and higher conversion was observed for MWH experiments in comparison to CH.

Free-emulsifier emulsion co-polymerization of styrene with different acrylic monomers like methyl methacrylate (MMA), butyl methacrylate (BMA), ethyl acrylate (EA), and maleic anhydride (BDA) in water/acetone continuous phase, under the microwave, has been investigated by **Li-Sha et al.**[73], **with an aim of control of particle size and distribution, as well as the latex colloidal stability.** KPS as initiator was used. The effect from the content of each monomer and its hydrophilicity on the hydrodynamic radius (R_h) were discussed. They concluded that at a higher concentration of hydrophilic co-monomer, the R_h decreased remarkably. The authors have added a remark that when performed under CH, the reactions were slower, giving rise to a broader particle distribution and poor reproducibility.

Another attempt to improve the particle size distribution control of nanoparticles free of emulsifier was made by **Hu et al.**[74], where submicron-size particles of PMMA

INTRODUCTION, STATE OF THE ART, AND OBJETIVES

were prepared in the presence of europion octanate (EOA) in surfactant-free emulsion polymerization under MWH or CH. Additionally, they performed surfactant-free emulsion polymerization to prepare nanoparticles of neat PMMA, varying the monomer content, under both heating ways. In conclusion, the final R_h for neat PMMA particles did not present significant differences between MWH or CH, but polymerization rate was faster (5 hours) than conventional heating (6 hours). It was found that EOA molecules were distributed on the surface of PMMA particles forming a layer 5 nm thick, therefore the applied MW-assisted emulsion polymerization has shown to be a good choice for production of MMA submicron polymer particles doped with EOA.

Bao and Zhang [75] studied the polymerization of MMA by MWH and CH. Both polymerizations present an induction period for MWH was 2 min and for CH was 15 min. After 20 min of reaction, the conversion for MWH experiment was 60%, whereas for CH it was only 5%. In both cases, similar final conversions were obtained at the end of the polymerization (after 2 h), and the difference of the final conversion were not more than 10% between each other. The faster MW polymerization rate was explained on the base of their results about the faster KPS decomposition rate under MW irradiation. They found a faster decomposition rate under MWH than CH at 60°C and 70°C, but at 80°C and 90°C, there was almost no difference. The authors claimed that KPS's activation energy was 128 kJ/mol for CH and 97.1 kJ/mol for MWH. Moreover, they supported this finding with literature results reported by Lewis *et al.* (1992) [76], in which the solution imidization reaction's activation energy dropped from 105 to 55 kJ/mol when MW irradiation instead of CH was used.

Yi. et al. [77] and **Deng et al.** [78] have studied the same co-polymer system (poly(St-co-NIPAAm)), obtained under different agitation rates: 550 rpm, and 350 rpm. Monodisperse emulsifier-free nanoparticles were obtained by co-polymerization of styrene (St) and N-isopropylacrylamide (NIPAAm), using KPS as initiator and water

as a solvent. As a result, nanoparticles with a size of fewer than 150 nm were obtained. At a higher amount of NIPAAm monomer, the particle size decreased to 109 nm. In CH method, nanoparticle with average size of 493 nm were obtained. Additionally, the time of polymerization was extremely different; for MWH, it took 1 hour, whereas, for CH, 24 hours, at the same temperature, even though, they did not report the final conversion or the kinetics for the reactions. The enhancement of the MWH polymerization rate was assigned to the faster MW decomposition of KPS, quoting at **Zhu et al.** [59] but not considering that Zhu et al measured the K_d of KPS under different MW frequency (1.25 GHz) than the used in references 77 and 78 (2.45 GHz).

Yan et al.[79] presented preparation of monodisperse polymeric microspheres by emulsifier-free emulsion co-polymerization of MMA, St, and N-hydroxymethyl acrylamide (NMA), using KPS as initiator, and water as a continuous phase. They compared the same polymerization reaction under MWH and CH, finding that the polymerization rate under MWH was faster than CH. They calculated the apparent activation energy of polymerization (MMA/St/NMA) under both heating methods, having 61.04 kJ/mol for MWH, and 83.75 kJ/mol for CH, calculated using the Arrhenius equation. The final conversion for MWH was ~90% after 1 hour and for CH ~80% after 2 hours. Particle size and distribution were measured by an electronic transmission microscope (TEM), showing that the particles obtained under MWH were in the range of 115 nm to 187 nm, whereas under CH, they were in a range of 199 nm to 238 nm. Additionally, they examined the effects of variations in NMA, KPS, and microwave power. Those results indicate that the polymerization rate under MWH is proportional to the initiator concentration on the power of $\frac{1}{2}$, the NMA monomer concentration to the power of $\frac{2}{3}$, and MW power to 0.78 ($R_p \propto [I]^{0.52} [NMA]^{0.66} P^{0.78}$).

In Table II.1.2 in Appendix II, the summary of the different published works reviewed previously about emulsion polymerization by free-radical polymerization under MWH is presented.

1.3.4 MINIEMULSION POLYMERIZATION

When highly hydrophobic monomers have to be polymerized in aqueous dispersed media, or the polymer particles should be combined with some inorganic nanomaterial, in such case, a method of choice is a miniemulsion polymerization. For that aim, miniemulsion is prepared by dispersing the monomer (or monomer mixture with polymer or with inorganic nanomaterial) in an aqueous surfactant solution. By applying a high energy homogenizing device in the pre-formed emulsion, the large monomer droplets are broken and form small droplets (50-300 nm).

The small droplets are protected from diffusional degradation (Ostwald ripening) by addition of a low molar mass hydrophobic costabilizer. On the other hand, the small droplets are protected against coagulation by the presence of the surfactant. In such conditions, the large surface area formed by the formation of small droplets consumes the surfactant, and hence, no micelles are formed. The miniemulsion is a kinetically stable colloid system; thus, it is stable for a period ranging from hours to months. The main distinctive feature of miniemulsion polymerization is the droplet nucleation that ensures that no mass transfer through the aqueous phase is needed during the polymerization.

Droplet nucleation occurs when the initiator radicals enter into the monomer droplets and turn them into polymer particles. Ideally, one to one copy is achieved, which means each droplet is turned into polymer particle

Figure 1.10 is represented as the miniemulsion polymerization process.

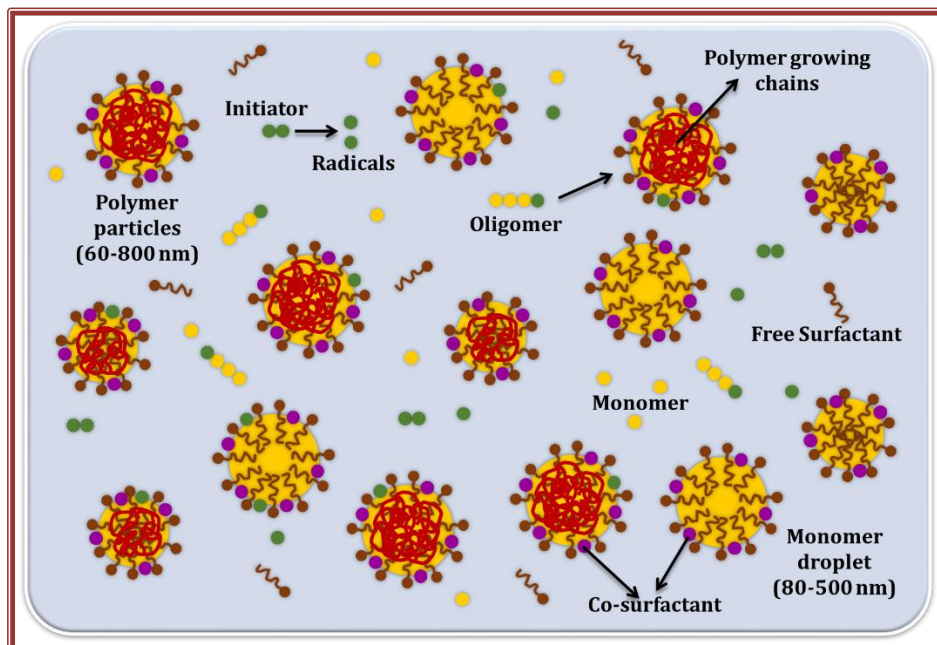


Figure 1.10. Mechanism of miniemulsion polymerization. The blue background refers to water as a continuous phase. Other components in the system are: monomer droplet stabilized by surfactant and co-stabilizer, polymer particles, polymer growing chains as well the initiator, their radicals and oligomers are represented at once.

Holtze and Tauer [80,81] reported two works, where St was homopolymerized in miniemulsion under MWH and CH, reporting a carefully temperature control into the reaction in the two heating methods.

For MWH two strategies were done, the first one using pulsed microwave irradiation by cycles of heating. At the beginning, MW-irradiation was applied at maximum power (100W) for few seconds until the reaction temperature was achieved. after which the MW-irradiation was turned off by few seconds. The second MWH strategy was the usual one, where the equipment applied the necessary MW power to achieve the reaction temperature and then it was kept during the whole reaction. Important

INTRODUCTION, STATE OF THE ART, AND OBJETIVES

results were obtained under pulsed MW-irradiation, as very higher molar mass polymers, up to 10^7 g/mol were achieved. Additionally, the molar masses were independent on the initiator concentration. In the other MW-strategy used and in the CH reactions, the molar masses were dependant on the initiator concentration and lower molar masses were obtained ($\approx 10^5$ – 10^6 g/mol) in comparison with pulsed MW-irradiation. According to the authors, this occurred because during pulsed MW-irradiation, the radicals produced react or recombine until only one radical is left in each droplet, then the radical could be able to grow efficiently during the cooling period, when no other radical can be produced provoking higher molecular weight. Polymerization rate was faster in MWH than CH, for MWH 100 s (pulsed MW-irradiation) and 24 min (MWH), whereas for CH 55 min were taken to obtain a polymer of styrene with final conversion of 80 to 93%.

Xiong *et al.* [82] synthesized fluoroacrylate co-polymer using MMA, BA and dodecafluoroheptyl methacrylate (DFHMA) in miniemulsion polymerization under MWH and CH with AIBN as initiator and SDS and hexadecane as surfactant and co-stabilizer, respectively. The reaction temperature was 80°C. The characterization of these polymer materials indicates that DFHMA takes part in copolymerization by both methods. However, polymerization rate was faster under MWH (90% in 2 h) than CH (85% in 7.5 h). Final particle size were measured by TEM imaging, finding smaller particle size and narrow distribution under MWH (56.7 nm) than CH (75.5 nm).

Hayden *et al.* [83] focused their work to elucidate the existence of special microwave effects in heterogeneous polymerization of styrene or methyl methacrylate using two different initiators (KPS or AIBN). SDS and HD were used as surfactant and co-stabilizer, respectively. For MWH experiments dual temperature-sensors were used, infrared sensor (external) and fibre optical probe (internal), thus obtaining a temperature measurement more accurate. Besides, the decomposition rate under MWH of the water soluble radical initiators was studied (V-50 or KPS). Additionally

homopolymerization of St under pulsed MW-irradiation was performed as well as some experiments under CH to compare the results.

For decomposition rate of initiators V-50 or KPS under MWH or CH, they did not find any significant difference between the two heating methods, arguing that the possible high differences founded by other authors were possibly due to the unfair temperature measurement into MW-reactor. For homopolymerization of St or MMA using KPS or AIBN, no significant effect on the polymerization rate was found in any of the polymer system studied. In the case for polymerization of St under pulsed MW-irradiation, they tried to mimic the same temperature ramp performed previously by C. Holtze [ref], in which higher molar masses were found. However, no significant differences were found between MWH and CH in terms of polymerization rate nor the molar masses. According to the authors, it was due to the better temperature control during the reaction, . The authors concluded that after replicate all previous experiments through careful and accurate internal temperature control, the observed effects by other authors when non-thermal MW-effects are claimed, could be due to classical bulk temperature effects.

In Table II.1.3 in Appendix II, the summary of the different published works reviewed previously about miniemulsion polymerization by free-radical polymerization under MWH is presented.

1.4 Ph.D. THESIS MOTIVATION

Based on the presented state of the art and analysis of the available information on how the matter interacts with microwave, their subsequent effects on polymerization reactions are still a bit cloudy due to all the parameters involved in the MWH process and the design of the MW experiments, as well as, the unfair comparison between MWH and CH methods done until now, due to either difference in experimental methodology or due to unprecise temperature measurements.

INTRODUCTION, STATE OF THE ART, AND OBJETIVES

In most of the work presented in the previous section an infrared detector placed externally have been used for measurements and control of temperature. Kappe [30] has shown experimentally that this way of temperature measurments brings numerous errors. In Figure 1.11, it is represented the difference of the measured temperature between an **external** (infrared, IR) versus an **internal** (fiber optic, FO) **sensor** of 3mL 1-butyl-3-methylimidazolium bromide (bmimBr) into a vial of 10 ml with magnetic stirring. The set temperature was 100°C, and the maximum power program was 65 watts.

From Figure 1.11 it can be observed that the external IR sensor measured 100°C (blue line) and it was kept constant during the applied MW power (the profile of which is presented with green line in Fig. 1.11). However, the FO sensor measured much higher temperature within the vial, as it is shown with the red line. Thus, at 60 s, while the IR sensor marked 100°C, the temperature in the reactor was 220°C. Later on, the difference in the reaction temperatures, the measured and the actual was stabilized to about 50°C and was kept so.

This fact opens uncertainty and doubts with respect to the all the published literature regarding MW assisted polymerization reaction and the results and conclusions reported so far.

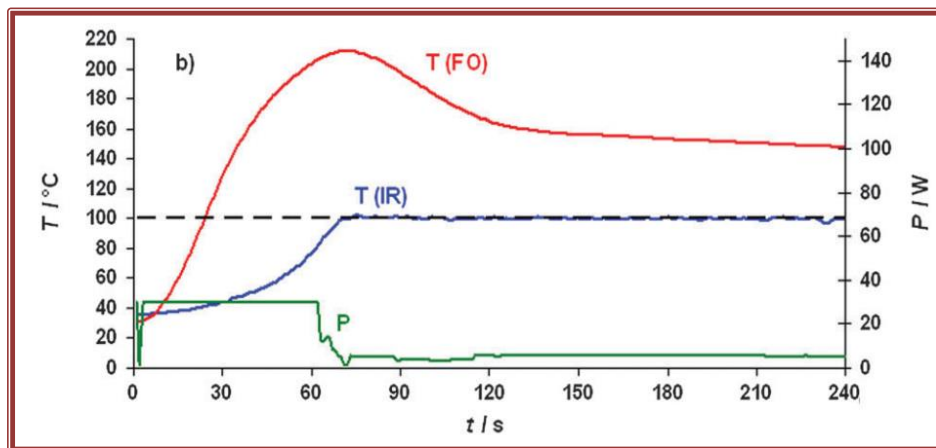


Figure 1.11. Temperature profiles using internal, fiber optic (red curve) and external, infrared (blue line) temperature sensors, and MW power profile using in a CEM Discover LabMate device[30].

In free-radical polymerization using thermal initiators, temperature control is crucial, because, when the temperature increases, the initiator decomposition rate increased as well [38]. Thus, the moment of the initiator addition in the reactor is important, too. Usually, the heating program consists of two stages, the first one in which the heating up to reaction temperature is controlled (we called it **heating rate**), and the second one, when the reaction temperature is hold (we call it reaction temperature), as it is shown in Figure 1.12. When the initiator is added before the start of the heating or during the heating, the initiator decomposition can be started before the reaction temperature was achieved, which could create important differences in the polymerization rate. It would be better to add the initiator in the reaction mixture when the reaction temperature was reached in both cases (CH and MWH), as shown in Figure 1.12. However, all of the reported works, the initiator was added before the heating was started, because a “**sealed vessel**” was used in **the reported works**. Speaking about the “sealed vessels”, it can be additional source of errors and misleading information, because most of the CH reactors are not sealed,

thus, in the MWH reactors the pressure increase created additional effects on the reaction rates and products.

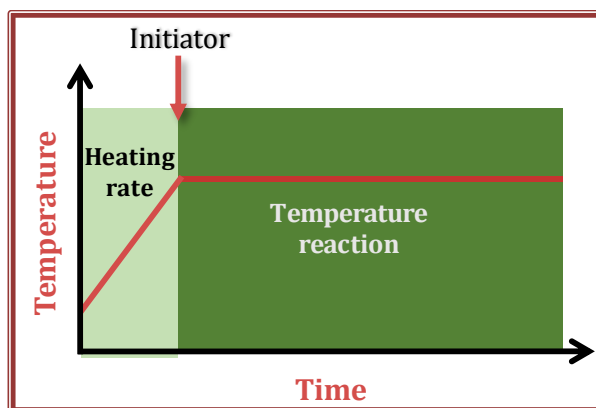


Figure 1.12. The advisable addition of an initiator during the polymerization process.

Therefore, in the majority of the published works in which CH and MWH assisted polymerizations were compared, likely fair comparison conditions were not ensured, even in the case when more specialized equipment was used and the temperature control was adequate.

Therefore, in order to be able to compare the polymerization reactions assisted by MWH and CH, it was necessary to design new experiments under MW irradiation by improving all the parameters described previously.

In this work, the advantage was taken of technically advanced MW equipment (Synthwave from Milestone)(Figure 1.13) that offers **higher reaction volume** (from 150 mL to 500 mL), **mechanical stirrer, inlets** in the reactor that enable the introduction of the initiator after reaching the reaction temperature, double monitoring and control of the reaction temperature: **external IR sensor** to measure the walls of the vessel and **internal sensors** (shielded thermocouple max. 200°C), **cooling jacket** for better temperature control, and spatially homogeneous heating.

Hence **similar reaction temperature profiles can be created in both CH and MWH** reactors. Under such conditions, it can be expected to compare the MWH and CH assisted polymerization reliably.

Additionally, this work **will contribute to the scale-up of the polymerization reactions under MWH**. So far, up to our best knowledge, the MW assisted polymerization reactions were performed at few mL scale (2-10 mL). Here the reactions were performed in 250 mL, the highest scale, so far. This will place a base for future works on a larger scale.



Figure 1.13. Microwave device, SynthWave from Milestone.

1.5 OBJECTIVE OF THE THESIS

The objective of this thesis is to compare the polymerization processes assisted by two different methods: microwave heating (MWH) and conventional heating (CH), using identical: heating rates, stable temperature profiles, stirring rates and, initiator addition at the same time and temperature at atmospheric pressure. Three different polymerization techniques, solution, emulsion, and miniemulsion, are investigated to analyse if there are differences in polymerization rate, co-polymer composition, polymer microstructure, and mechanical properties between MWH and CH processes and products. For that aim, co-polymerization of various monomer types, including functional monomers, and even some hybrid acrylic-epoxy systems were studied, as well as in situ polymerization in composite systems with graphene and carbon nanotubes.

1.6 ORGANIZATION OF THE THESIS

Chapter 1: Introduction, state of the art, and objectives.

This chapter described the leading theory behind the heat transfer mechanisms of microwave heating and their possible effects, as well all the state of the art of different polymerization methods in solution, emulsion, and miniemulsion performed under microwave heating. The aim and the organization of this thesis is presented, too in this chapter.

Chapter 2: Solution polymerization.

In this chapter, solution free-radical copolymerization was performed in order to study if the way of heating (either MWH or CH) affects the copolymerization kinetics and product characteristics (the microstructure and copolymer composition). For that aim, different monomer systems (different in polarity and dielectric properties, as well as use of organometallic monomer), different initiators were used, and the reaction was performed in either a highly MW absorbing solvent such as dimethylformamide (DMF) or MW transparent solvent as toluene.

Chapter 3: Emulsion Polymerization.

In this chapter, the comparison of the CH and MWH assisted emulsion polymerization processes was performed. Methyl methacrylate and butyl acrylate (MMA/BA) was the main copolymers using 1% of three different functional monomers (2-hydroxyethyl methacrylate (HEMA), sodium styrene sulfonate (NaSS), and acrylamide (AM)); potassium persulfate (KPS) was used as initiator and the effect of its content was studied. The main aim was to evaluate if, by changing the functional monomer type or initiator amount, we can induce selective heating and, thus, affect the polymerization rate, particle size distribution, polymer microstructure, mechanical properties, and water uptake.

Chapter 4: Miniemulsion Polymerization in the presence of MWCNTs.

In this chapter, monomers are combined with inorganic nanoparticles (multi-wall carbon nanotubes, MWCNTs) and polymerized in miniemulsion to synthesize polymer nanocomposites. The copolymer was composed of MMA/BA/HEMA, in which different amounts of MWCNTs were added (0.25%, 0.5%, 0.75%, and 1%). A comparison of the reaction kinetics, hybrid latexes, and composite films' properties for the nanocomposites obtained under MWH or CH was performed.

Chapter 5: Graphene modification under microwave irradiation and their polymer composites.

In this chapter, the graphene surface modification was performed under microwave heating using different monomers as acrylic acid (AA) and acrylamide (AM) to induce "grafting from" in order to improve the compatibility between graphene and polymer. After graphene modification, polymerization of MMA/BA/HEMA in presence of 0.5% of graphene by miniemulsion polymerization was performed using MWH method. The kinetics, polymer microstructure, and mechanical properties of the polymer films were studied.

Chapter 6: Emulsion polymerization towards waterborne hydrophobic dispersions.

Hybrid systems, in which acrylic monomers are copolymerized in presence of highly hydrophobic resins, such as polyurethane, epoxy or alkyds, are usually polymerized in miniemulsion, because the resins have limited diffusion throughout aqueous phase. However, miniemulsion polymerization is not of practical importance for large scale production, due to the additional step of high energy homogenizing to produce small monomer or hybrid droplets. In this chapter, the idea was to use the advantage of the MWH reactor to achieve fast very high temperature, and instead of miniemulsion, to perform emulsion polymerization of MMA/BA/AA with a highly hydrophobic epoxy resin. At high temperature, the diffusion of the hydrophobic components may be promoted. Therefore, the reactions were performed in the following temperature range: 80°C to 150°C, using different initiators (VA-086 or KPS)

Chapter 7: Conclusions.

In this chapter the most relevant conclusions are summarized.

Appendix I: Materials and Characterization methods.

In this appendix, all materials and characterization techniques are well described, as well as the schemes of the set-ups that were used in this work.

Appendix II: Supporting information.

For each chapter, some supporting information was added in this section.

Appendix III: Disentanglement of large MWCNTs by sonication.

In this appendix, a reliable method for disentanglement of multi-wall carbon nanotubes using ultrasound is well described. This method can be used for subsequent polymerizations.

1.7 REFERENCES

- [1] E. Ackerman, A Brief History of the Microwave Oven, 2016. <https://spectrum.ieee.org/tech-history/space-age/a-brief-history-of-the-microwave-oven>.
- [2] A. Davis, A History of the Microwave Oven The popular appliance resulted from a chance discovery in the 1940s, (2016). <https://spectrum.ieee.org/the-institute/ieee-history/a-history-of-the-microwave-oven>.
- [3] E. Bálint, G. Keglevich, The Spread of the Application of the Microwave Technique in Organic Synthesis, in: G. Keglevich (Ed.), Milestones Microw. Chem., Springer International Publishing, Cham, 2016: pp. 1–10. doi:10.1007/978-3-319-30632-2_1.
- [4] D.K. Pradhan, T.S. Dharamrajan, M.R. Mishra, A. Mishra, G. College, AN OVERVIEW OF MICROWAVE OVEN IN THE FIELD OF SYNTHETIC CHEMISTRY, Int. J. Res. Dev. Pharm. L. Sci. 1 (2012) 44–50.
- [5] M. Jordan, Las 12 mentiras y verdades sobre el microondas que debes conocer, (2019). <https://www.lavanguardia.com/comer/tendencias/20190311/4696509400/microondas-mitos-verdades-cocina.html>.
- [6] G. Cristy, S.S.; Mamantov, Cryogenic mass spectrometry of reactive fluorine-containing species:II. Applications to synthesis via pyrolysis, photolysis and microwave discharge, Int. J. Mass Spectrom. Ion Phys. 5 (1970) 319–328.
- [7] F. Wiesbrock, U.S. Schubert, Microwaves in chemistry: The success story goes on, Chim. Oggi. (2006). doi:10.1002/chin.200710273.
- [8] D. Adam, Out of the kitchen, Nature. 421 (2003) 571–572.
- [9] N. Horikoshi, S.; Schiffmann, R.F.; Fukushima, J.; Serpone, Chapter 9. Microwave-Assisted Chemistry, in: Microwave-Assisted Chem. Microw. Chem. Mater. Process., Singapore, 2018: pp. 243–320.
- [10] K. Hirao, H. Ohara, Microwave-Assisted Polymerizations, in: S. Kobayashi, K. Müllen (Eds.), Encycl. Polym. Nanomater., Springer Berlin Heidelberg, Berlin, Heidelberg, 2015: pp. 1261–1267. doi:10.1007/978-3-642-29648-2_417.
- [11] A. B. Burg, T. J. Reilly, Chemical studies of closo-1,5-dicarbapentaborane(5), Inorg. Chem. - INORG CHEM. 11 (1972) 1962–1964.

INTRODUCTION, STATE OF THE ART, AND OBJETIVES

doi:10.1021/ic50114a052.

- [12] C. Oliver Kappe, Microwave dielectric heating in synthetic organic chemistry, *Chem. Soc. Rev.* (2008). doi:10.1039/b803001b.
- [13] A. de la Hoz, A. Diaz-Ortiz, A. Moreno, Activation of Organic Reactions by Microwaves, in: *Adv. Org. Synth.* (Volume 1), 2012. doi:10.2174/978160805197710501010119.
- [14] S. Horikoshi, J. Tsuzuki, M. Kajitani, M. Abe, N. Serpone, Microwave-enhanced radical reactions at ambient temperature Part 3: Highly selective radical synthesis of 3-cyclohexyl-1-phenyl-1-butanone in a microwave double cylindrical cooled reactor, *New J. Chem.* (2008). doi:10.1039/b810142f.
- [15] C. Ebner, T. Bodner, F. Stelzer, F. Wiesbrock, One Decade of Microwave-Assisted Polymerizations: Quo vadis?, *Macromol. Rapid Commun.* 32 (2011) 254–288. doi:10.1002/marc.201000539.
- [16] K. Kempe, C.R. Becer, U.S. Schubert, Microwave-Assisted Polymerizations: Recent Status and Future Perspectives, *Macromolecules.* 44 (2011) 5825–5842. doi:10.1021/ma2004794.
- [17] R. Hoogenboom, U.S. Schubert, Microwave-Assisted Polymer Synthesis: Recent Developments in a Rapidly Expanding Field of Research, *Macromol. Rapid Commun.* 28 (2007) 368–386. doi:10.1002/marc.200600749.
- [18] C.Y.A. B. M.A., *Termodinámica*, Séptima ed, Mc Graw Hill, México D.F., 2012.
- [19] M.H. Weik, microwave, in: *Comput. Sci. Commun. Dict.*, Springer US, Boston, MA, 2001: p. 1017. doi:10.1007/1-4020-0613-6_11518.
- [20] H.P. Groll, Industrial Applications of Microwaves, in: H. Groll, W. Waidelich (Eds.), *Microw. Appl.*, Springer Berlin Heidelberg, Berlin, Heidelberg, 1987: pp. 12–27.
- [21] J. Lucas, What are Microwaves, (2018). <https://www.livescience.com/50259-microwaves.html>.
- [22] J.W. Gooch, Electromagnetic Spectrum, in: J.W. Gooch (Ed.), *Encycl. Dict. Polym.*, Springer New York, New York, NY, 2011: p. 260. doi:10.1007/978-1-4419-6247-8_4292.
- [23] S.Z. Li, A. Jain, eds., Electromagnetic Spectrum, in: *Encycl. Biometrics*, Springer US, Boston, MA, 2009: p. 254. doi:10.1007/978-0-387-73003-5_504.

- [24] D. Rouan, Electromagnetic Spectrum, in: M. Gargaud, R. Amils, J.C. Quintanilla, H.J. (Jim) Cleaves, W.M. Irvine, D.L. Pinti, M. Viso (Eds.), *Encycl. Astrobiol.*, Springer Berlin Heidelberg, Berlin, Heidelberg, 2011: p. 482. doi:10.1007/978-3-642-11274-4_493.
- [25] K.R. Surati, M.A.; Jauhari, S.; Desai, A brief review: Microwave assisted organic reaction, *Arch. Appl. Sci. Res.* 4 (2012) 645–661.
- [26] C. Gabriel, S. Gabriel, E. H. Grant, E. H. Grant, B. S. J. Halstead, D. Michael P. Mingos, Dielectric parameters relevant to microwave dielectric heating, *Chem. Soc. Rev.* 27 (1998) 213–224. doi:10.1039/A827213Z.
- [27] N. Hammack, B.; Ryan, P.; Ziech, *Eight Amazing Engineering Stories*, first, Articulate Noise Books, 2012.
- [28] G.B. Dudley, R. Richert, A.E. Stiegman, On the existence of and mechanism for microwave-specific reaction rate enhancement, *Chem. Sci.* 6 (2015) 2144–2152. doi:10.1039/C4SC03372H.
- [29] D.M.P. Mingos, D.R. Baghurst, Tilden Lecture. Applications of microwave dielectric heating effects to synthetic problems in chemistry, *Chem. Soc. Rev.* 20 (1991) 1–47. doi:10.1039/CS9912000001.
- [30] C.O. Kappe, How to measure reaction temperature in microwave-heated transformations, *Chem. Soc. Rev.* 42 (2013) 4977–4990. doi:10.1039/C3CS00010A.
- [31] P. Bana, I. Greiner, Interpretation of the Effects of Microwaves, in: G. Keglevich (Ed.), *Milestones Microw. Chem.*, Springer International Publishing, Cham, 2016: pp. 77–110. doi:10.1007/978-3-319-30632-2_4.
- [32] M.J. Collins, Chapter 1: Introduction to Microwave Chemistry, in: *Microw. Synth. Chem. Speed Light*, CEM Publishing, U.S.A., 2002: pp. 11–25.
- [33] J.H. Mishra, A.; Vats, T.; Clark, Chapter 1 Microwave Radiations: Theory and Instrumentation, in: *Microwave-Assisted Polym.*, The Royal Society of Chemistry, 2016: pp. 1–18. doi:10.1039/9781782623182-00001.
- [34] C.O. Kappe, B. Pieber, D. Dallinger, Microwave Effects in Organic Synthesis: Myth or Reality?, *Angew. Chemie Int. Ed.* 52 (2013) 1088–1094. doi:10.1002/anie.201204103.
- [35] A. Albini, *The Framework of Photochemistry: The Laws*, in: *Photochem. Past*,

INTRODUCTION, STATE OF THE ART, AND OBJETIVES

- Present Futur., Springer Berlin Heidelberg, Berlin, Heidelberg, 2016: pp. 9–40. doi:10.1007/978-3-662-47977-3_2.
- [36] M. Nüchter, B. Ondruschka, W. Bonrath, A. Gum, Microwave assisted synthesis – a critical technology overview, *Green Chem.* 6 (2004) 128–141. doi:10.1039/B310502D.
- [37] F. Hoogenboom, Richard; Schubert, Ulrich S; Wiesbrock, Microwave-assisted Polymer Synthesis, Springer International Publishing, Switzerland, 2016.
- [38] T.N. Myers, Initiators, Free-Radical, in: *Encycl. Polym. Sci. Technol.*, American Cancer Society, 2002. doi:10.1002/0471440264.pst425.
- [39] G. Odian, *Principles of Polymerization*, 2004. doi:10.1002/047147875x.
- [40] A. Ravve, *Principles of polymer chemistry*, third edition, 2012. doi:10.1007/978-1-4614-2212-9.
- [41] J.W. Gooch, ed., *Solution polymerization*, in: *Encycl. Dict. Polym.*, Springer New York, New York, NY, 2007: p. 902. doi:10.1007/978-0-387-30160-0_10684.
- [42] M.A. Dikusar, I. V Kubrakova, A.A. Chinarev, N. V Bovin, Polymerization of 4-Nitrophenyl Acrylate under Microwave Heating Conditions, *Russ. J. Bioorganic Chem.* 27 (2001) 408–412. doi:10.1023/A:1012949005183.
- [43] G. Madras, V. Karmore, Evolution to similarity solutions for polymerization and depolymerization with microwave radiation, *Polym. Int.* 50 (2001) 1324–1330. doi:10.1002/pi.779.
- [44] E.C. Buruiana, M. Zamfir, V. Melinte, T. Buruiana, Photo-polymers Containing (S)-Phenylalanine and Stilbene Pendants: Synthesis and Properties of Ionic Polyacrylates, *Des. Monomers Polym.* 13 (2010) 21–32. doi:10.1163/138577209X12591392377694.
- [45] S. Agarwal, M. Becker, F. Tewes, Synthesis, characterization and properties evaluation of copolymers of 2,3,4,5,6-pentafluorostyrene and N-phenylmaleimide, *Polym. Int.* 54 (2005) 1620–1625. doi:10.1002/pi.1890.
- [46] B.T. Ergan, M. Bayramoğlu, The effects of microwave power and dielectric properties on the microwave-assisted decomposition kinetics of AIBN in n-butanol, *J. Ind. Eng. Chem.* (2013). doi:10.1016/j.jiec.2012.08.015.
- [47] A.D. Smith, E.H. Lester, K.J. Thurecht, S.W. Kingman, J. El Harfi, G. Dimitrakis, J.P. Robinson, D.J. Irvine, Temperature dependence of the dielectric properties

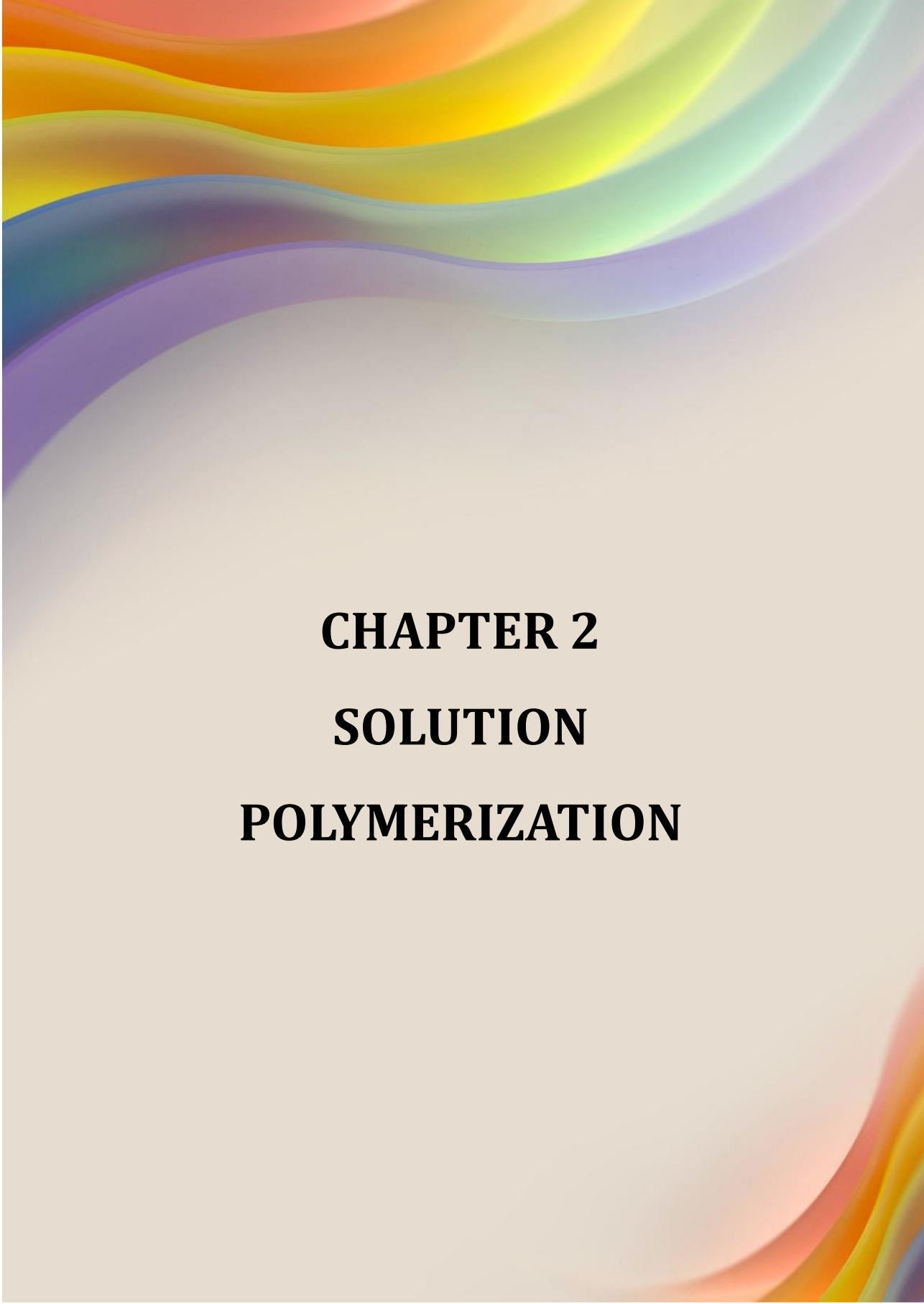
- of 2,2'-azobis(2- methyl-butyronitrile) (AMBN), *Ind. Eng. Chem. Res.* (2010). doi:10.1021/ie901389a.
- [48] V. Singh, A. Tiwari, P. Kumari, A.K. Sharma, Microwave accelerated synthesis and characterization of poly(acrylamide), *J. Appl. Polym. Sci.* 104 (2007) 3702–3707. doi:10.1002/app.25682.
- [49] H. Ren, Y.F. Zhang, T.Z. Huang, J. Wang, Study on Synthesis of Superabsorbent Using Microwave Heating and Water Absorbency, in: *Adv. Mater. CEAM 2011*, Trans Tech Publications Ltd, 2011: pp. 1854–1857. doi:10.4028/www.scientific.net/AMR.239-242.1854.
- [50] C. Guerrero-Sanchez, M. Lobert, R. Hoogenboom, U.S. Schubert, Microwave-Assisted Homogeneous Polymerizations in Water-Soluble Ionic Liquids: An Alternative and Green Approach for Polymer Synthesis, *Macromol. Rapid Commun.* 28 (2007) 456–464. doi:10.1002/marc.200600728.
- [51] T. Glück, I. Woecht, A. Schmalfuß, G. Schmidt-Naake, Modification of the Solvent Influence on the Free Radical Polymerization in Ionic Liquids by Microwave Irradiation, *Macromol. Symp.* 275–276 (2009) 230–241. doi:10.1002/masy.200950125.
- [52] H. Stange, M. Ishaque, N. Niessner, M. Pepers, A. Greiner, Microwave-Assisted Free Radical Polymerizations and Copolymerizations of Styrene and Methyl Methacrylate, *Macromol. Rapid Commun.* 27 (2006) 156–161. doi:10.1002/marc.200500640.
- [53] H. Stange, A. Greiner, Microwave-Assisted Free Radical Copolymerizations of Styrene and Methyl Methacrylate, *Macromol. Rapid Commun.* 28 (2007) 504–508. doi:10.1002/marc.200600841.
- [54] R. Tomovska, J.C. de la Cal, J.M. Asua, Reactions in Heterogeneous Media: Emulsion, Miniemulsion, Microemulsion, Suspension, and Dispersion Polymerization, in: *Monit. Polym. React. From Fundam. to Appl.*, 2014. doi:10.1002/9781118733813.ch4.
- [55] P.A. Lovell, M.S. El-Aasser, Features of Emulsion Polymerization, in: *Emuls. Polym. Emuls. Polym.*, 1997. doi:10.1016/S1381-5148(97)84204-6.
- [56] J.M. Asua, Emulsion polymerization: From fundamental mechanisms to process developments, *J. Polym. Sci. Part A Polym. Chem.* (2004).
- [57] R. Correa, G. Gonzalez, V. Dougar, Emulsion polymerization in a microwave

- reactor, *Polymer (Guildf)*. (1998). doi:10.1016/S0032-3861(97)00413-8.
- [58] X. Zhu, J. Chen, N. Zhou, Z. Cheng, J. Lu, Emulsion polymerization of methyl methacrylate under pulsed microwave irradiation, *Eur. Polym. J.* (2003). doi:10.1016/S0014-3057(02)00363-4.
- [59] X. Zhu, J. Chen, Z. Cheng, J. Lu, J. Zhu, Emulsion polymerization of styrene under pulsed microwave irradiation, *J. Appl. Polym. Sci.* (2003). doi:10.1002/app.12089.
- [60] M.J. Hyun, Y. Youngjae, S.K. Yong, H.L. Jae, Microwave-irradiated copolymerization of styrene and butyl acrylate, in: *Macromol. Symp.*, 2007. doi:10.1002/masy.200750430.
- [61] E. Ginsburger, F. Pla, C. Fonteix, S. Hoppe, S. Masseur, P. Hobbes, P. Swaels, Modelling and simulation of batch and semi-batch emulsion copolymerization of styrene and butyl acrylate, *Chem. Eng. Sci.* (2003). doi:10.1016/S0009-2509(03)00320-8.
- [62] J. Sierra, J. Palacios, E. Vivaldo-Lima, Effect of microwave activation on polymerization rate and molecular weight development in emulsion polymerization of methyl methacrylate, *J. Macromol. Sci. - Pure Appl. Chem.* (2006). doi:10.1080/10601320600575223.
- [63] C. Costa, A.F. Santos, M. Fortuny, P.H.H. Araújo, C. Sayer, Kinetic advantages of using microwaves in the emulsion polymerization of MMA, *Mater. Sci. Eng. C.* (2009). doi:10.1016/j.msec.2008.08.013.
- [64] C. Costa, V.H.S. Santos, P.H.H. Araujo, C. Sayer, A.F. Santos, C. Dariva, M. Fortuny, Rapid decomposition of a cationic azo-initiator under microwave irradiation, *J. Appl. Polym. Sci.* (2010). doi:10.1002/app.32409.
- [65] B.T. Ergan, M. Bayramoğlu, S. Özcan, Emulsion polymerization of styrene under continuous microwave irradiation, *Eur. Polym. J.* (2015). doi:10.1016/j.eurpolymj.2015.06.021.
- [66] B.T. Ergan, M. Bayramoğlu, S. Özcan, Experimental data in support of continuous microwave effect on emulsion polymerization of styrene, *Data Br.* (2015). doi:10.1016/j.dib.2015.07.009.
- [67] Z. An, W. Tang, C.J. Hawker, G.D. Stucky, One-step microwave preparation of well-defined and functionalized polymeric nanoparticles, *J. Am. Chem. Soc.* (2006). doi:10.1021/ja065250f.

- [68] G.A. Hawker, Craig; Stucky, ONE-STEP MICROWAVE PREPARATION OF WELL-DEFINED AND FUNCTIONALIZED POLYMERIC NANOPARTICLES, US 2008/0009558 A1, 2008.
- [69] J. Gao, C. Wu, Modified structural model for predicting particle size in the microemulsion and emulsion polymerization of styrene under microwave irradiation, *Langmuir*. (2005). doi:10.1021/la048972y.
- [70] C. Wu, J. Gao, M. Li, W. Zhang, M. Jiang, Formation, stabilization and application of polymeric nanoparticles, in: *Macromol. Symp.*, 2000. doi:10.1002/1521-3900(200002)150:1<219::AID-MASY219>3.0.CO;2-1.
- [71] W. Zhang, J. Gao, C. Wu, Microwave preparation of narrowly distributed surfactant-free stable polystyrene nanospheres, *Macromolecules*. (1997). doi:10.1021/ma970208d.
- [72] H.Q. Xie, J.S. Guo, G.Q. Yu, J. Zu, Soapless emulsion polymerization of butyl methacrylate through microwave heating, *J. Appl. Polym. Sci.* (2001). doi:10.1002/app.1352.
- [73] U.-S. You, H.-Q. Wu, W.-M. Zhang, Z. Fu, L.-J. Shen, Preparation and Stabilization of Emulsifier-free Macromolecule Nanoparticle Latex Particles, *Chinese J. Chem.* (2010). doi:10.1002/cjoc.20010190819.
- [74] J. Hu, H. Zhao, Q. Zhang, W. He, Synthesis and characterization of submicron PMMA particles containing rare earth ions on the surface, *J. Appl. Polym. Sci.* (2003). doi:10.1002/app.12298.
- [75] J. Bao, A. Zhang, Poly(methyl methacrylate) nanoparticles prepared through microwave emulsion polymerization, *J. Appl. Polym. Sci.* (2004). doi:10.1002/app.20758.
- [76] D.A. Lewis, J.D. Summers, T.C. Ward, J.E. McGrath, Accelerated imidization reactions using microwave radiation, *J. Polym. Sci. Part A Polym. Chem.* (1992). doi:10.1002/pola.1992.080300817.
- [77] C. Yi, Z. Deng, Z. Xu, Monodisperse thermosensitive particles prepared by emulsifier-free emulsion polymerization with microwave irradiation, *Colloid Polym. Sci.* (2005). doi:10.1007/s00396-005-1318-1.
- [78] Z.W. Deng, X.X. Hu, L. Li, Z.S. Xu, C.F. Yi, Self-assembled poly(styrene-co-N-isopropylacrylamide) film induced by capillary force, *J. Appl. Polym. Sci.* (2006). doi:10.1002/app.22977.

INTRODUCTION, STATE OF THE ART, AND OBJETIVES

- [79] W. Yan, X. Hu, G. Zhang, M. Deng, C. Yi, Z. Xu, Microwave assisted preparation of monodisperse polymeric microspheres and its morphologies and kinetics, *J. Wuhan Univ. Technol. Mater. Sci. Ed.* (2012). doi:10.1007/s11595-012-0609-x.
- [80] C. Holtze, M. Antonietti, K. Tauer, Ultrafast conversion and molecular weight control through temperature programming in microwave-induced miniemulsion polymerization, *Macromolecules.* (2006). doi:10.1021/ma060608d.
- [81] C. Holtze, K. Tauer, Surviving radicals: Promises of a microwave effect on miniemulsion polymerization for technical processes, *Macromol. Rapid Commun.* (2007). doi:10.1002/marc.200600714.
- [82] S. Xiong, X. Guo, L. Li, S. Wu, P.K. Chu, Z. Xu, Preparation and characterization of fluorinated acrylate copolymer latexes by miniemulsion polymerization under microwave irradiation, *J. Fluor. Chem.* (2010). doi:10.1016/j.jfluchem.2009.12.015.
- [83] S. Hayden, A.F.H. Studentschnig, S. Schober, C.O. Kappe, A critical investigation on the occurrence of microwave effects in emulsion polymerizations, *Macromol. Chem. Phys.* (2014). doi:10.1002/macp.201400279.
- [84] A. Valério, M. Fortuny, A.F. Santos, P.H.H. Araújo, C. Sayer, Poly(urea-urethane) synthesis by miniemulsion polymerization using microwaves and conventional polymerization, *Macromol. React. Eng.* (2015). doi:10.1002/mren.201400029.



CHAPTER 2
SOLUTION
POLYMERIZATION

2.1 INTRODUCTION

Free-radical solution polymerizations under microwave heating have been investigated so far, as it was presented in Chapter 1 [1–10], wherein some publications reported using different organic solvents [1–6,11,12], water [7–9], or ionic liquids [3,4,10]. In some of these works, non-specialized MW-devices (domestic MW-oven) were used [2,4,7], which are characterized by non-homogeneous heating and poor temperature control in the reactor. Probably due to such conditions, depolymerization was reported to occur after achieved certain monomer conversion [2,7]. In most of the reports, MWH and CH assisted polymerizations were compared, reporting on increased polymerization rate and lower average molar masses of the polymers obtained in the MW reactions [1,5,6,8,9], even though in some of the reports, no differences were claimed between both methods [3].

However, in all the presented studies, the reactions were performed in batch mode, which means all the reactants, including the initiator, were charged in a closed system and subjected to MW irradiation or CH, under the same conditions. In other words, the temperature profiles during these reactions were distinct. In such conditions, as MWH is much faster than CH and provides volumetric heating, the initiator is decomposed sooner and to a higher extent under MWH than in CH reaction (often before the target reaction temperature was achieved in CH). Likely this is the reason behind frequently observed irreproducibility [3] and faster reaction under MWH compared to CH [1,5,6,8,9]. Usually, the increased reaction rates were observed in polar solvents, such as DMF [11,12], whereas in toluene, no difference in reaction rates was noticed [11,12], which confirms that all observed differences were results of the different heating rates and initiator decompositions in early reaction stages.

Furthermore, in some of the specialized MW reactors (CEM discover) [1,5,6,8,10–12], an external (infrared) sensor was exclusively used for the temperature monitoring,

which often does not represent the real reaction temperature, as recently demonstrated by Oliver Kappe [13]. This study confirms that even if specialized MW devices are used for the experiments, the reaction temperature is not controlled if there is no double monitoring of the temperature by IR external and fiber optic internal sensors. This fact may open a new uncertainty into the assertiveness of the previously published works, in which, even specific MW effects were claimed [1,5,7,11,12] they can be attributed exclusively to thermal effects. To the best knowledge of the authors, no comparable MWH and CH assisted polymerization were reported so far.

In this chapter and in complementation of previous pioneering works (presented previously in chapter 1), we analyzed the effect of the different experimental variables (initiator, solvent, and monomer mixture type) on the polymerization behavior and the macromolecular characteristic of the obtained polymers. First, we have thoroughly examined and compared the microwave-assisted copolymerization of methyl methacrylate (MMA) with butyl acrylate (BA) in toluene as a solvent and using either 2,2-azobisisobutyronitrile (AIBN), benzoyl peroxide (BPO), or Lauroyl peroxide (LPO) as an initiator with the polymerizations performed under CH or MWH. After choosing the most appropriate initiator, in order to study the effect of solvent on both heating types, the rest of the experiments have been done in DMF as well as in toluene. Furthermore, with the aim of investigating the effect of co-monomer type, respectively, the copolymerization of MMA with styrene (St) or vinyl ferrocene (VFc) was investigated in both solvents using either microwave or conventional heating.

The objective of this work is to update the overall understanding of free-radical copolymerization in solution under MW heating that has to be optimized well in future research works. Besides, the novelty of this study from previous studies includes addressing the best solvent and monomer mixture to demonstrate the economic issues and energy-efficiency of the reaction.

SOLUTION POLYMERIZATION

Additionally, the demonstration of how **increasing the temperature control** in the experiments under MW irradiation **results in a more precise and reliable** comparison between both MWH and CH methods are obtained.

2.2 EXPERIMENTAL

2.2.1 MATERIALS

The materials are given in Appendix I.

2.2.2 POLYMERIZATIONS

Solution polymerization was carried out at 15% of solid content, considering 200 mL as a total volume. A monomer mixture of MMA/BA, MMA/St and, MMA/VFc in a molar ratio of 1:1 was dissolved in solvents (Toluene or DMF) for 15 min under magnetic stirring and nitrogen purging at 200 rpm; then the mixture was placed in their respective vessel for CH or MW reactor. Afterward, it was heated over 15 min from room temperature to 80°C (VFc at 70°C), then the first addition of initiator (3.8 wt% referred to the amount of monomer) was done. The addition of the initiator was slowly approx in 60 seconds due to moderate solubility of the initiator in both solvents toluene and DMF. If the initiator was added rapidly, the temperature into reaction would go down considerably, even so in CH experiments was observed a decreasing of temperature in the first minutes. After passing 3 hours, the reaction temperature increased to 90°C (Vfc at 70°C by 5 hours) following by the second addition of initiator (1.1 wt% referred to the amount of monomer), and it kept at this temperature for another 2 hours, thereafter the reaction was quenched. All experiments were carried out under a nitrogen atmosphere and stirred at 250 rpm. The total reaction time for

all experiments was 5 hours, except for experiments where VFc is used. In this case, the full reaction time was 8 hours.

Characteristics of conventional heating and microwave setups are described in detail in Appendix I. The reaction conditions for the different polymerizations performed in this study are summarized in Table 2.1.

Apart from 1:1 mol ratio, MMA/VFc monomer couple was polymerized in 3:7 molar ratio (DMF solvent, AIBN initiator). The reaction was carried out at 70°C for 1 hour, under both MWH and CH (Table 2.1).

To follow the kinetics, several samples were taken during the reaction, directly from the reaction mixture, at different interval times, quenched the samples first using an ice-bath at ~ -5 to -7°C (because some salt (NaCl) was added into ice) to stop the reaction and after that, a few drops of hydroquinone solution (1%) was added.

It is worth mentioning that **all experiments were carried out by duplicate** to ensure the reproducibility of results.

2.2.3 CHARACTERIZATIONS

The overall conversion of the copolymerization and the co-monomer conversion was measured via two methods. First, by gas chromatography with a Head-Space HP6890, in which Helium gas as the carrier and internal standard were used. Second, by gravimetry to have a confirmation from the first method. For systems, MMA/VFc were used ^1H NMR on a Bruker 500 NEO spectrometer at room temperature by dissolving small amounts of the reaction mixtures after the polymerizations in a proper deuterated solvent.

SOLUTION POLYMERIZATION

The molar mass distribution (MMD) of the soluble fraction was determined by gel permeation chromatography (GPC) at 35°C. To measure the MMD of the samples, the sol part obtained after Soxhlet extraction was concentrated and then directly analyzed by GPC. The gel fraction was measured by Soxhlet extraction, using THF as the solvent.

More details about the methodology and characteristics of all equipment used are described in Appendix I.

Table 2.1. Reaction formulations for different copolymerizations performed under conventional and microwave heating with various solvents and initiators.

Exp.	Heating method	Monomer mixture	Solvent	Initiator	Reaction temperature and time
1	CH	MMA/BA	Toluene	LPO	80°C/3h then 90°C/2h
3			Toluene	BPO	
5			Toluene	AIBN	
7		DMF			
9		Toluene			
11		MMA/ST	DMF		
2	MWH	MMA/BA	Toluene	LPO	
4			Toluene	BPO	
6			Toluene	AIBN	
8		DMF			
10		Toluene			
12		MMA/ST	DMF		
13	CH	MMA/VFc (50/50)	Toluene	AIBN	70°C/8h
14	MWH		DMF		
15			Toluene		
16			DMF		
17	CH	MMA/VFc (30/70)	DMF	AIBN	70°C/1h
18	MW				

2.3 RESULTS AND DISCUSSIONS

In order to assure continuous irradiation of the reaction mixture, which increases the probability to observe any MW effect, the heating conditions in MW reactor were selected in a way to assure that the reaction mixture is under continuous MW irradiation, as is shown in Figure 2.1.

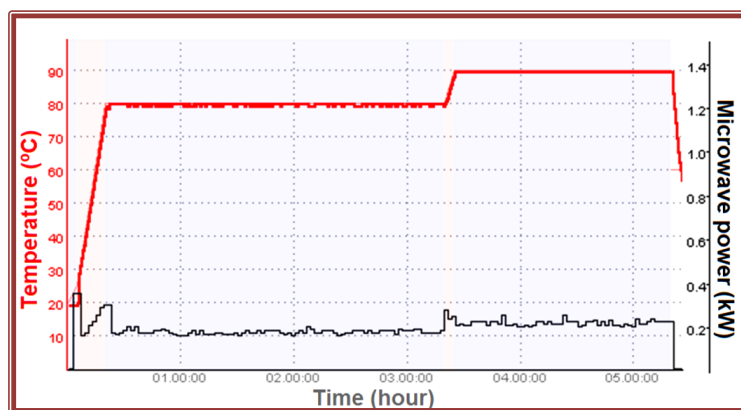


Figure 2.1. Temperature profile (red line) and microwave power (black line) for polymerization reaction of MMA/BA in toluene using AIBN initiator.

As was mentioned above, in this work, we were able to create very similar temperature profiles for CH and MWH induced polymerization reactions by charging the initiator into the reactor after the reaction temperature was achieved in both reactors and a better temperature control system in both reactors. The temperature profiles for all reactions are presented in the next figures (Figures 2.2-2.5).

SOLUTION POLYMERIZATION

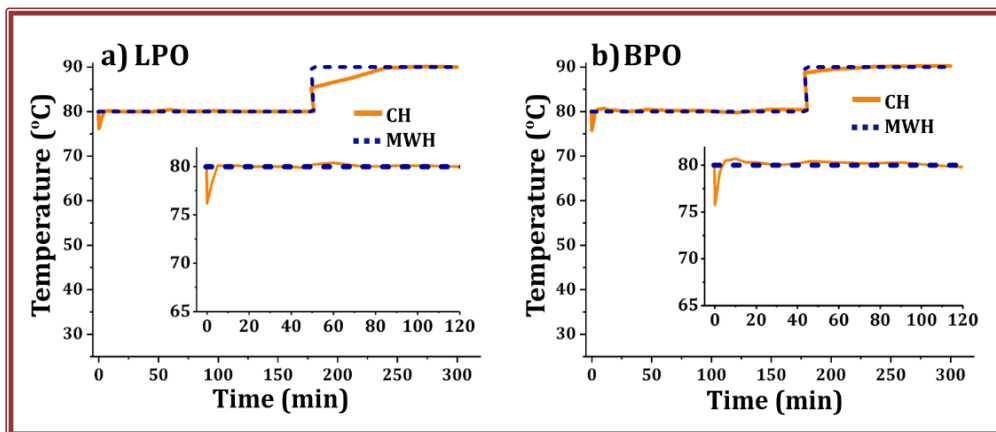


Figure 2.2. Comparison of the temperature profiles of CH and MWH assisted polymerization reaction of **MMA/BA** monomer couple in **Toluene** using different initiators: **a) lauroyl peroxide** and **b) benzoyl peroxide**. Insets: enlarged initial reaction region.

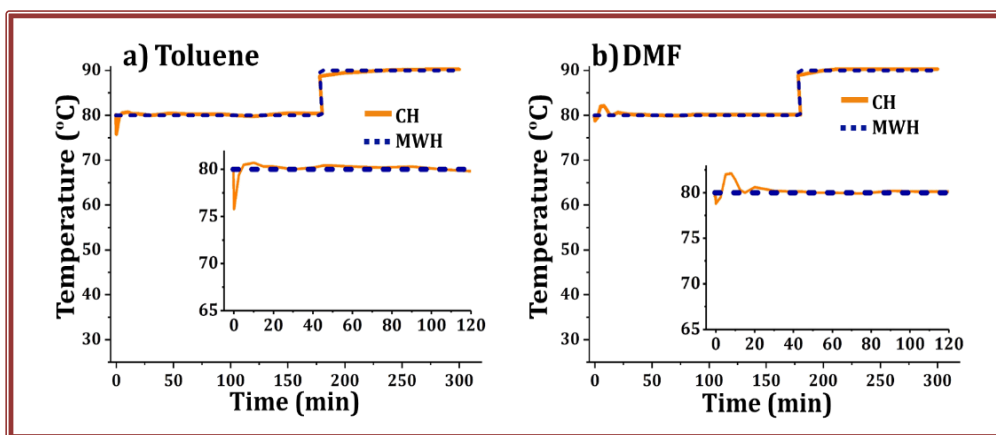


Figure 2.3. Comparison of the temperature profiles of CH and MWH assisted polymerization reaction of **MMA/BA** monomer couple and **AIBN** as initiator, using different solvents: **a) Toluene** and **b) DMF**. Insets: enlarged initial reaction region.

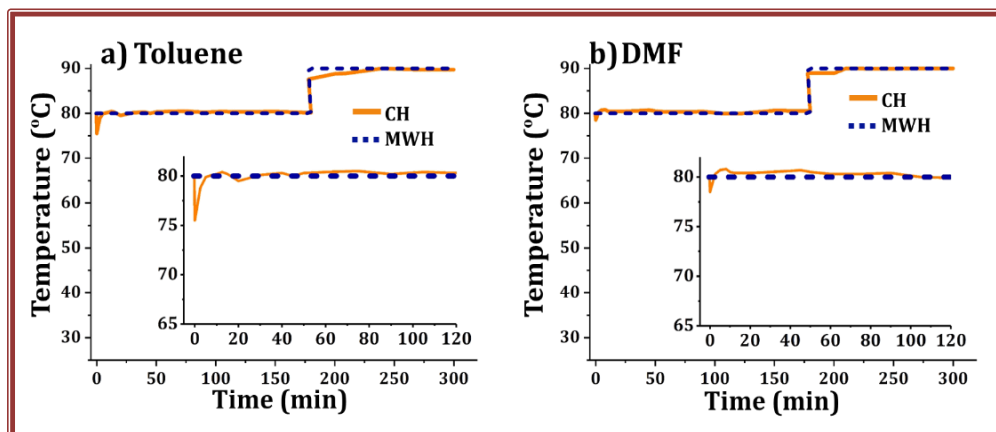


Figure 2.4. Comparison of the temperature profiles of CH and MWH assisted polymerization reaction of **MMA/St** monomer couple and **AIBN** as initiator, using different solvents: **a) Toluene** and **b) DMF**. Insets: enlarged initial reaction region.

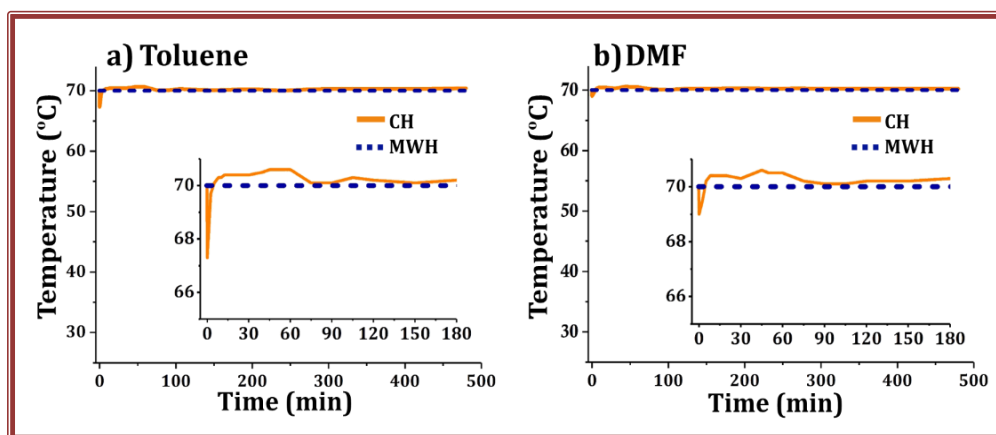


Figure 2.5. Comparison of the temperature profiles of CH and MWH assisted polymerization reaction of **MMA/VFc** monomer couple and **AIBN** as initiator, using different solvents: **a) Toluene** and **b) DMF**. Insets: enlarged initial reaction region.

SOLUTION POLYMERIZATION

With an aim to induce observable changes in the reaction rate or copolymer composition and microstructure (molar mass and distribution and gel fraction), we selected different initiators (AIBN that creates carbon-centered radical, LPO aliphatic oxygen centered radicals, and BPO aromatic oxygen centered radicals), different couples of monomers (MMA/BA, MMA/St and MMA/VFc), and different solvents (toluene and DMF). The monomer couple either with a difference in polarity as MMA/St or in dielectric properties as MMA/BA were selected (Table 2.2). The organometallic monomer VFc was selected to co-polymerize with MMA, as it was already reported that selective heating of organometallic compounds directly contributed to the changes in reaction conditions in ring-opening polymerization [14]. The polymerization reactions were performed in two solvent types, toluene, and DMF; the former a non-polar solvent known by low absorption of MW irradiation and poor transfer of the irradiation into heat (dielectric constant of toluene is 2.29 [15], and its loss tangent is 0.04 [13]) and the latter prone to fast heating under MW irradiation and to high MW irradiation absorption and efficient transfer to heat (dielectric constant of DMF is 35.23 [15], and its loss tangent is 0.16 [13]). The dielectric constant of the solvent determines its ability to absorb MW irradiation, whereas the loss tangent value indicates the ability to transform the absorbed irradiation into heat. The effect of the solvent on the polymerization kinetics and polymer properties was studied, too, with the aim to elucidate if the solvent selection may influence the energy demand of the process. Furthermore, the reactions performed within solvent transparent to MW irradiation (toluene) are expected to be more conclusive about the effect of different monomers and possible microwave effects.

Table 2.2. Polarity and dielectric constant (at 45°C) values of different monomers and solvents used.[15,16].

Reactive	Polarity (μ)	Dielectric constant (ϵ')
MMA	1.60	6.44
BA	1.79	2.49
St	0.13	2.4
Toluene	0.31-0.38	2.29
DMF	3.85	35.23

2.3.1 EFFECT OF INITIATOR TYPE

The effect of LPO as an initiator on the overall conversion and cumulative copolymer composition and molar mass distribution for MMA/BA polymerization (1:1 molar ratio) in toluene for CH and MWH reactions is presented in Figures 2.6, 2.7, and Table 2.3.

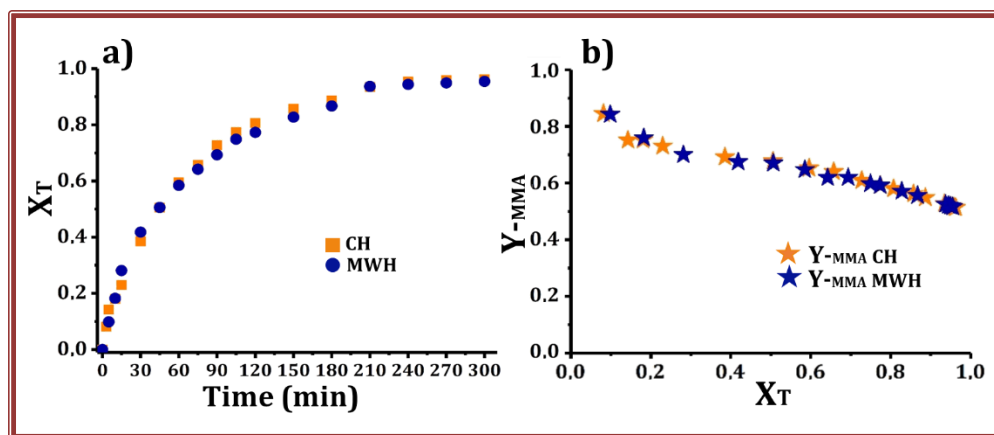


Figure 2.6. (a) Time evolution of conversion of **MMA/BA** copolymerization under CH and MWH using **LPO** initiator in **Toluene**; (b) Cumulative copolymer compositions for both reactions, presented as MMA fraction within the copolymer.

SOLUTION POLYMERIZATION

In the case of the LPO initiator, the time evolution of conversion profiles and MMA/BA copolymer compositions obtained in CH and MWH reactors are identical (Figure 2.6a). According to the reactivity ratios of MMA and BA ($r_{MMA}=2.15$ and $r_{BA}=0.26$ [17,18]), at low total conversion, the polymer is mostly composed of MMA units ($\sim 80\%$ at $X_T=0.2$). By increasing X_T , MMA fraction in the polymer chains decreased due to the faster disappearance of this monomer, whereas at high X_T the fraction of BA in copolymer chains increased. The MMA/BA copolymerization was not affected by way of heating, which means that under-investigated conditions, the MWH, which provides direct volumetric heating of the reaction mixture, did not influence the reactivity ratios of the individual monomers and the molar masses and distributions (Figure 2.7, Table 2.3). Both polymers did not present any gel content, which means that in both cases, linear polymer chains soluble in THF were synthesized.

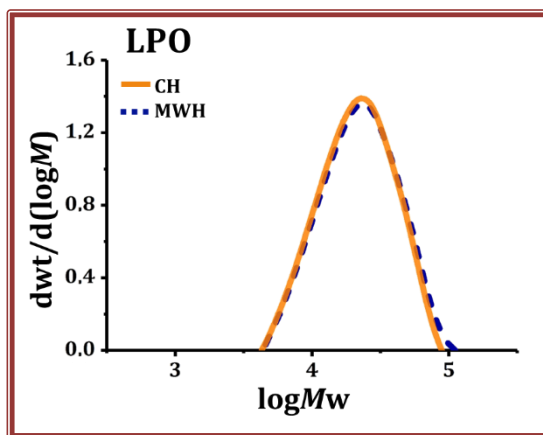


Figure 2.7. Final molar mass distribution of **MMA/BA** copolymerization under CH and MWH using **LPO** initiator in **Toluene**.

Figure 2.8 shows the result of the same copolymerization using an aromatic BPO initiator. Similarly, there were few differences observed for the kinetic curves (Figure 2.8a), the cumulative copolymer compositions (Figure 2.8b), and the molar masses and distributions (Figure 2.9, Table 2.3).

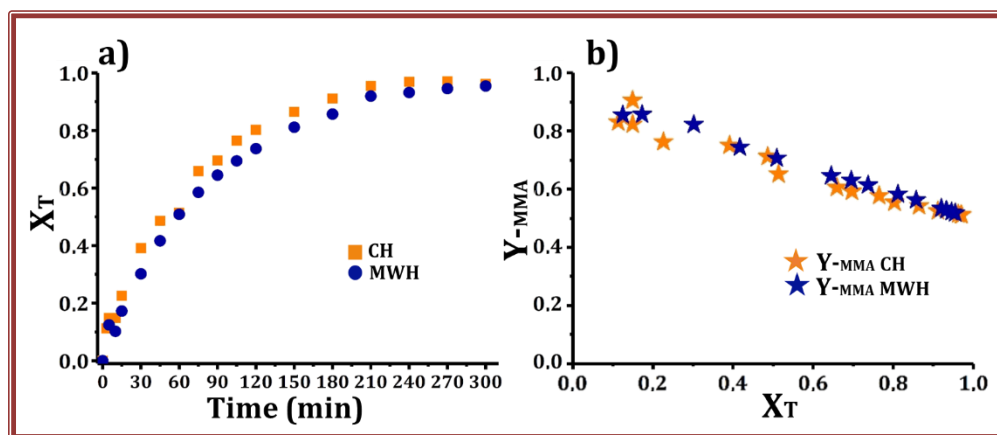


Figure 2.8. (a) Time evolution of conversion of MMA/BA copolymerization under CH and MWH using BPO initiator in Toluene; (b) Cumulative copolymer compositions for both reactions, presented as MMA fraction within the copolymer.

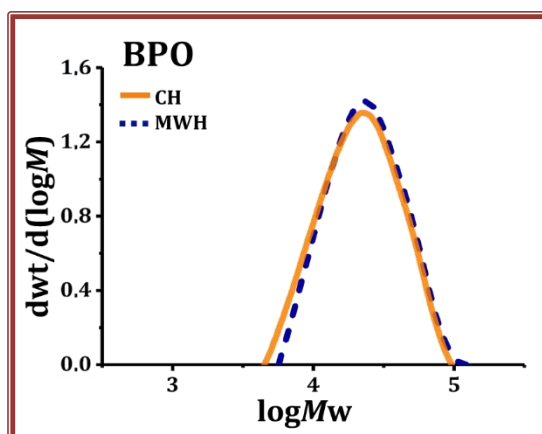


Figure 2.9. Final molar mass distribution of MMA/BA copolymerization under CH and MWH using BPO initiator in Toluene.

SOLUTION POLYMERIZATION

Figure 2.10 compares conversions, copolymer composition, and Figure 2.11 molar mass distributions for the MMA/BA copolymerization carried out with AIBN with CH and MWH. Insignificant differences were noticed in the molar mass distributions and in the average molar mass (Table 2.3).

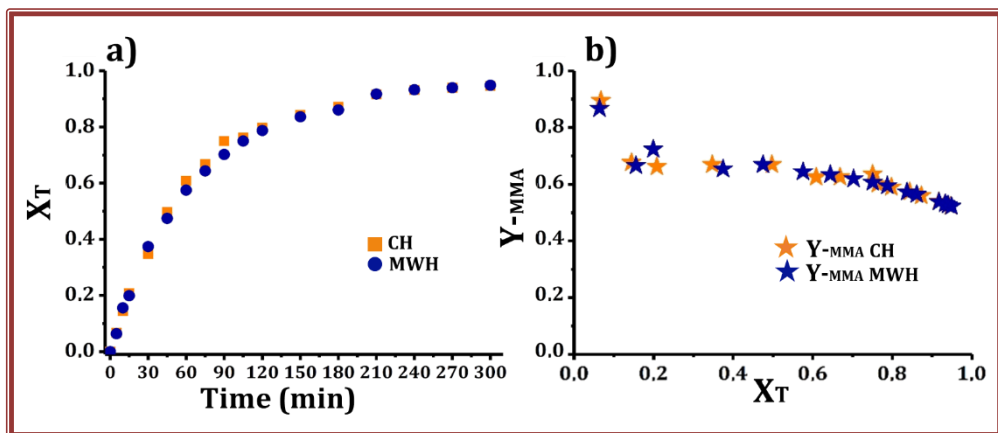


Figure 2.10. (a) Time evolution of conversion of **MMA/BA** copolymerization under CH and MWH using **AIBN** initiator in **Toluene**; (b) Cumulative copolymer compositions for both reactions, presented as MMA fraction within the copolymer.

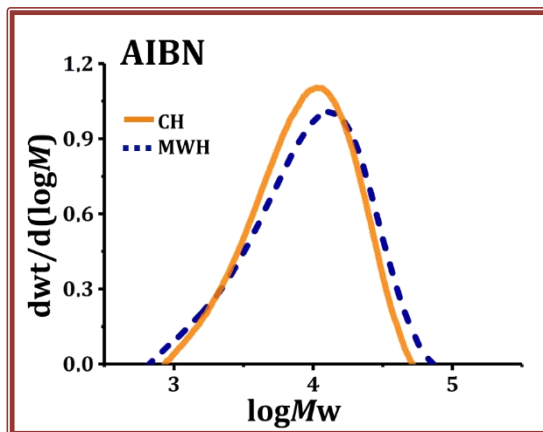


Figure 2.11. Final molar mass distribution of **MMA/BA** copolymerization under CH and MWH using **AIBN** initiator in **Toluene**.

Table 2.3. Overall conversions and molecular weight distributions of **MMA/BA** polymerization in **Toluene**, using different initiators under CH and MWH.

Initiator	Overall conversion (%)		Molecular weight distribution (g/mol)			
			MWH		CH	
	MWH	CH	\overline{M}_w	PDI	\overline{M}_w	PDI
LP	95.4	96.2	25731	1.45	25205	1.43
BPO	95.4	97.0	27568	1.40	26666	1.46
AIBN	94.5	94.6	13233	2.19	11388	1.84

These results demonstrate two findings. On the one hand, under similar temperature profiles with both heating approaches, the difference in the heating did not influence the decomposition rate of selected initiators, in agreement with already reported observation for AIBN [19] and BPO [20]. On the other hand, if selective heating of the two monomers happened due to different polarities in the MW-assisted polymerization, it was not enough to induce any increase of the reaction rate or changes in reactivity ratios of the monomers in relation to the same reaction assisted by CH.

Benefits accomplished with the usage of peroxide initiators for copolymerization of MMA/BA have not been observed, and almost the same polymerization rates and final conversions were achieved in all cases; this can be shown in Figure 2.12 where all conversion of the polymerization are compared separately for each heating method.

SOLUTION POLYMERIZATION

Moreover, molecular weight distribution was measured during the reaction time, and no differences were found in any experiment (Appendix II, Figure II.2.1).

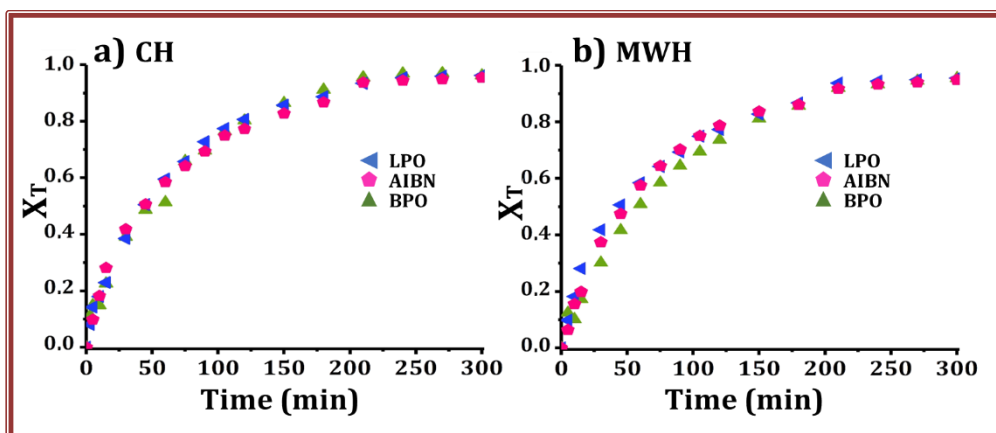


Figure 2.12. Comparison of time evolution of conversion of MMA/BA copolymerization, using different initiators under (a) CH and (b) MWH.

Therefore **for the rest of the study, AIBN was chosen as initiator**, as AIBN and some of its derivatives are usually safer to use than peroxides because the explosion risk is much lower. However, these compounds are still considered explosives [21].

2.3.2 EFFECT OF SOLVENT AND MONOMER SYSTEM MMA/BA

Using AIBN initiator, copolymerization of different monomer pairs under CH and MWH in the two solvents was studied. With both heating approaches, similar temperature profiles were ensured (Figure 2.3). Figure 2.13 presents the time evolution of conversion for MMA/BA copolymerization (mol ratio of 1) in both solvents, wherein the insets, the copolymer compositions of both CH and MWH reactions are compared.

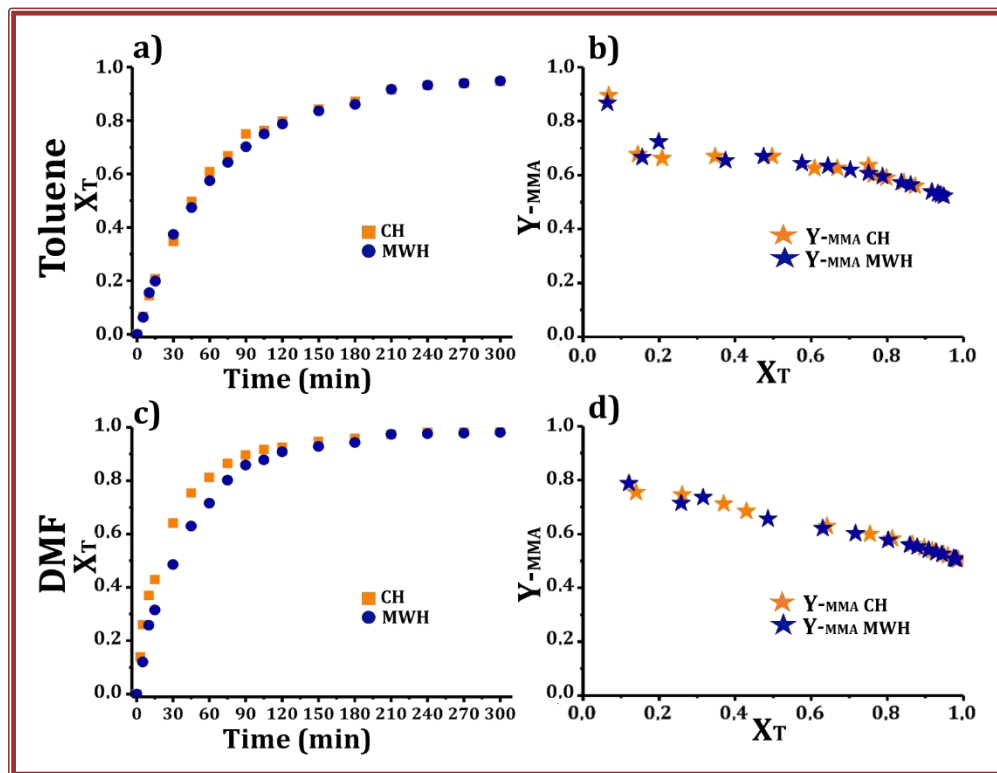


Figure 2.13. (a) Time evolution of conversion of **MMA/BA** copolymerization under CH and MWH using **AIBN** initiator in **Toluene**; (b) Cumulative copolymer compositions for both reactions, presented as MMA fraction within the copolymer. (c) Time evolution of conversion of **MMA/BA** copolymerization under CH and MWH using **AIBN** initiator in **DMF**; (d) Cumulative copolymer compositions for both reactions, presented as MMA fraction within the copolymer.

According to the time evolution of conversion curves of MMA/BA copolymerization presented in Figure 2.13, except for the slightly faster CH reaction rate in DMF solvent, the heating approach did not have any noticeable effect neither in the reaction rates and the cumulative copolymer composition (Figure 2.13b) and d)) nor in the molar mass distributions (Figure 2.14, Table 2.4).

SOLUTION POLYMERIZATION

The small difference observed was attributed to the overshoot of temperature in the CH reactor after the addition of initiator, as shown in the temperature profiles of this reaction (Figure 2.3), due to the poorer temperature control in this reactor.

Copolymer compositions demonstrate that the monomers co-polymerized similarly under CH and MWH in both solvents producing linear polymer chains. The molar mass distributions presented in Figure 2.14 indicate the unimodal distribution of molar masses that were not significantly affected by way of heating. In toluene, CH polymer has a slightly lower average molar mass than MWH polymer (Table 2.4) which likely is due to the slightly faster CH reaction due to temperature overshoot in the initial reaction stage that resulted in faster initiator decomposition, a higher number of radicals created simultaneously and increased termination.

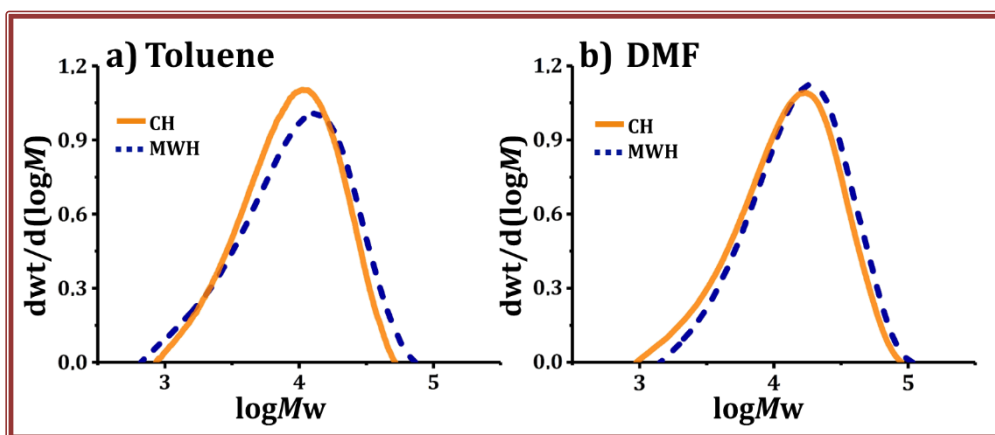


Figure 2.9. Final molar mass distribution of **MMA/BA** copolymerization under CH and MWH using **AIBN** initiator in (a) **Toluene** and (b) **DMF**.

2.3.3 EFFECT OF SOLVENT AND MONOMER SYSTEM MMA/St

The time evolution of conversion curves of the MMA/St copolymerization (1:1 mol ratio) is presented in Figure 2.15. Similarly, as in previous cases, the reaction rates were not influenced by way of heating in either of the two solvents. The reaction rates and the final conversions in St/MMA system are much lower than in MMA/BA due to the lower propagation rate constant of St [22,23].

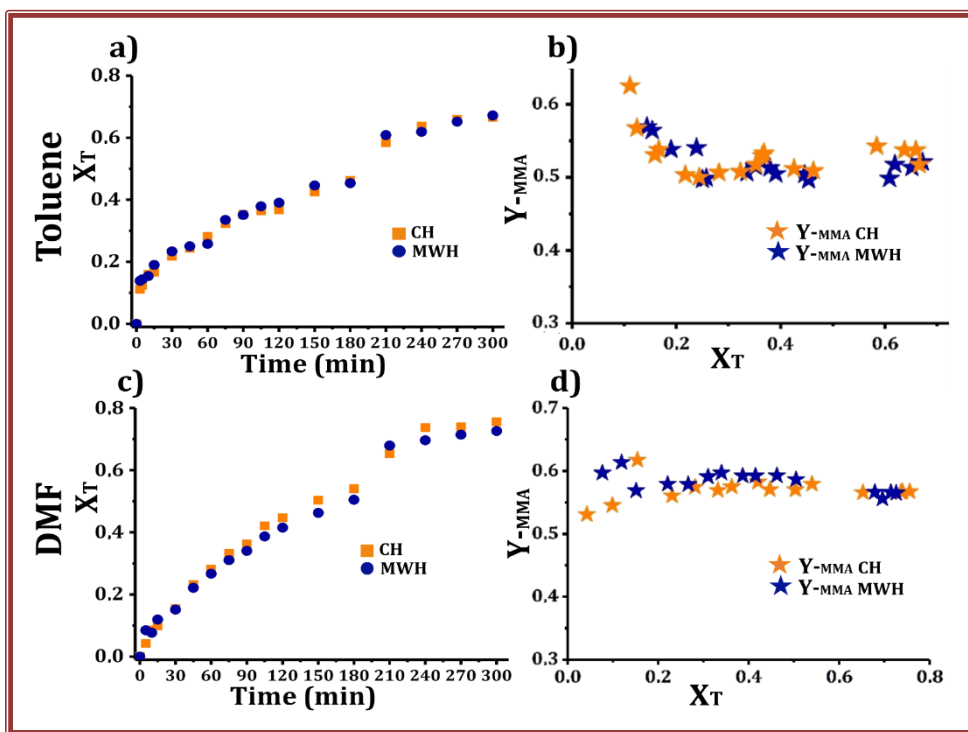


Figure 2.15. (a) Time evolution of conversion of MMA/St copolymerization under CH and MWH using AIBN initiator in **Toluene**; (b) Cumulative copolymer compositions for both reactions, presented as MMA fraction within the copolymer. (c) Time evolution of conversion of MMA/St copolymerization under CH and MWH using AIBN initiator in **DMF**; (d) Cumulative copolymer compositions for both reactions, presented as MMA fraction within the copolymer.

SOLUTION POLYMERIZATION

A similar effect of a slightly higher rate of polymerization was noticed under CH in DMF, assigned to the temperature overshoot in CH reactor, for which the cooling system was not fast enough to prevent it (see Figure 2.4). The copolymer composition corresponds to the reactivity ratios of MMA and St copolymerization in a batch reactor ($r_{MMA} = 0.46$ and $r_{St} = 0.52$ [24]) and, it was not influenced by way of heating nor by the solvent type (in both solvents, the cumulative copolymer compositions in CH and MWH were very similar). MMA and St have different polarities (1.60 of MMA and 0.13 of St), and dielectric constants, 6.44 of MMA versus 2.4 of St. Nevertheless, no sufficient difference was created in the energy absorbed and converted into heat to permit observable differences in the reactions and products. The comparison of molar mass distribution, presented in Figure 2.16, demonstrates that the MMA/St copolymers synthesized under CH and MWH have almost identical molar mass distribution and no difference in average molar mass (Table 2.4).

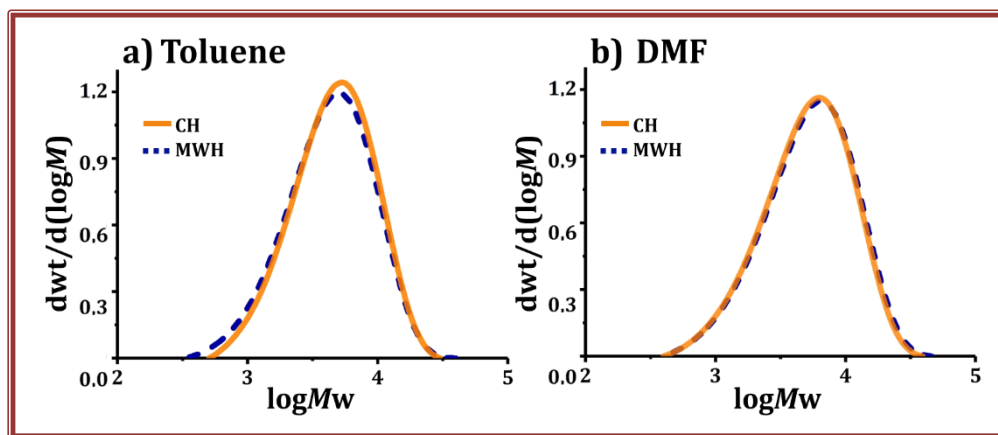


Figure 2.11. Final molar mass distribution of **MMA/St** copolymerization under CH and MWH using AIBN initiator in (a) **Toluene** and (b) **DMF**.

Even though out of the scope of this work, it is worth mentioning that an important difference between the reaction and product composition in both solvents was observed. In the DMF solvent, the reaction rate at low conversion and the incorporation of MMA within the copolymer is lower than in toluene. DMF as a polar solvent likely creates hydrogen bonds with polar monomers, such as MMA, decreasing its reactivity towards styrene, an effect that was demonstrated in solution copolymerization of various monomers theoretically[25] and experimentally [26].

Table 2.4. Overall conversions and molecular weight distributions of **MMA/BA**, **MMA/St**, or **MMA/VFc** polymerization in **Toluene or DMF**, using **AIBN** as initiators under CH and MWH.

Monomer system	Solvent	Overall conversion (%)		Average molar mass (g/mol)			
				MWH		CH	
		MWH	CH	\overline{M}_w	PDI	\overline{M}_w	PDI
MMA/BA	Toluene	94.5	94.6	13233	2.19	11388	1.84
	DMF	97.6	98.6	20106	1.85	17305	2.0
MMA/St	Toluene	67.2	66.5	5528	1.76	5759	1.64
	DMF	72.6	75.6	6919	1.85	6641	1.81
MMA/VFc	Toluene	44.2	54.5	1562	2.33	1827	1.9
	DMF	45.2	52.8	2420	2.04	2428	2.06

2.3.4 EFFECT OF SOLVENT AND MONOMER SYSTEM MMA/VFc

Figure 2.17 presents the time evolution of conversion curves and the cumulative copolymer compositions of the MMA/VFc (1:1 mol ratio) copolymerization performed with AIBN under CH and MWH in toluene and DMF solvents. The reaction rate is much lower than in other copolymer systems, probably due to the slow polymerization rate of VFc (similar to that of St [27] (reactivity ratios $r_{MMA}=1.22$ and $r_{VFc}=0.52$ [24])), thus much lower conversions were achieved. Additionally, the reaction was performed at a lower temperature than the previous one. Even though the CH and MWH polymerizations were intended to be performed under similar temperature profiles, due to poorer temperature control in CH reactor, a slight increase of reaction temperature was noticed after initiator addition to the system (Figure 2.5). In MW reactor, perfect temperature control was kept during the reaction. In spite of that, the MMA/VFc copolymerization reaction was faster under MWH in toluene in the initial stage, as shown in Figure 2.17a. For example, in 5 min the overall conversion of MMA/VFc is less than 5% under CH and about 8% under MWH, whereas in 30 min the conversion is less than 10% under CH and more than 30% under MWH.

In Figure 2.17b the cumulative copolymer compositions are shown. Due to the faster reaction in MW reactor, the compositions of the copolymer extracted at 5 min reaction from both CH and MW reactor have significantly different overall conversions and copolymer compositions. In CH reaction, the incorporation of both monomers follows the reactivity ratios (reactivity ratios $r_{MMA}=1.22$ and $r_{VFc}=0.52$ [27]); therefore, in the initial reaction stages, the copolymer is richer in MMA. With the decrease of MMA concentration, the incorporation of VFc increased. Under MWH, the first data available for copolymer composition corresponds to an overall conversion of around 10%, and the MMA fraction in the copolymer is already closed to 0.5, which did not change during the reaction. As it was determined that AIBN decomposition was not influenced by way of heating, the enhanced reaction rate in MW reactor may be

related to the overheating effect of VFc monomer molecules within the reaction mixture, which in bulk has the same temperature as in CH reactor.

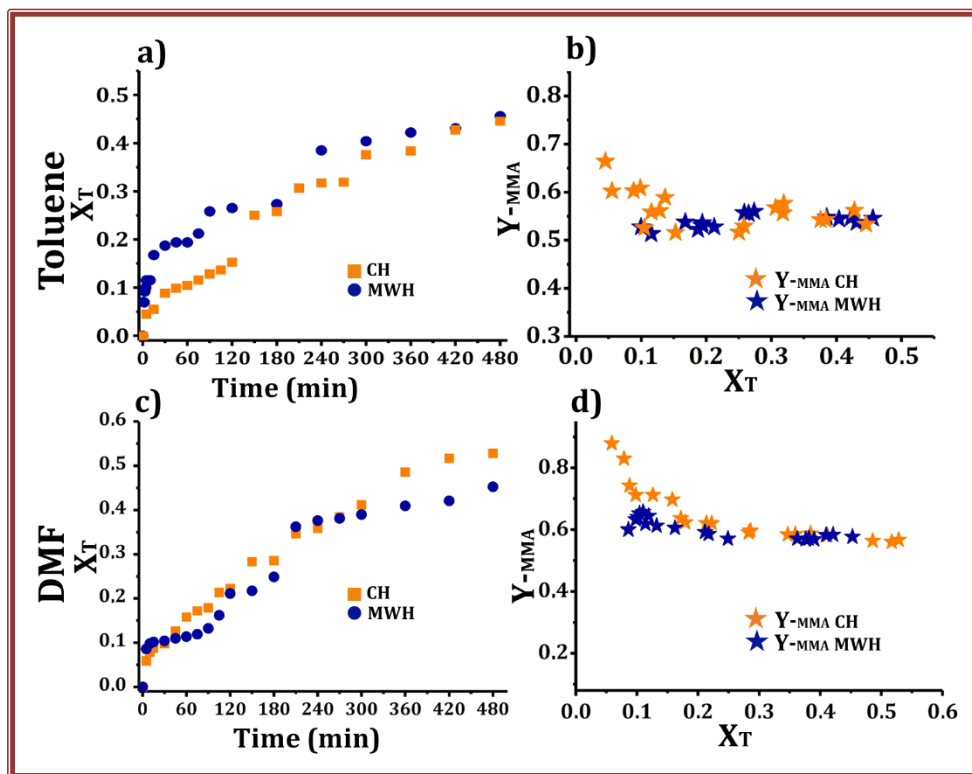


Figure 2.17. (a) Time evolution of conversion of **MMA/VFc** copolymerization under CH and MWH using **AIBN** initiator in **Toluene**; (b) Cumulative copolymer compositions for both reactions, presented as MMA fraction within the copolymer. (c) Time evolution of conversion of **MMA/VFc** copolymerization under CH and MWH using **AIBN** initiator in **DMF**; (d) Cumulative copolymer compositions for both reactions, presented as MMA fraction within the copolymer.

SOLUTION POLYMERIZATION

On the other hand, when the MMA/VFc copolymerization was performed in DMF (Figure 2.17b), the evolution of overall conversion is similar in both CH and MWH. However, under MWH, it presents peculiar behavior, oscillating around the evolution of overall conversion achieved during CH, which presents typical behavior. This difference is likely due to the high absorbing MW nature of DMF; therefore, the effect of VFc overheating was not so strong. However, the inset of Figure 2.17d, where cumulative copolymer compositions are compared, presents a discrepancy in the copolymer compositions at low total conversion between CH and MWH polymers. At 5% total conversion, the CH copolymer is made mostly of MMA (90%), whereas the MWH copolymer contains 60% MMA and 40% VFc. The MMA/VFc copolymers obtained have linear chains with molar mass distributions presented in Figure 2.18 (the average values of molar mass are presented in Table 2.4). According to Figure 2.18, short molar mass oligomers were obtained, probably on the one hand due to low reaction rate and, on the other, due to the fact that VFc acts as an electron transfer agent that intramolecularly terminate the growing chains [28].

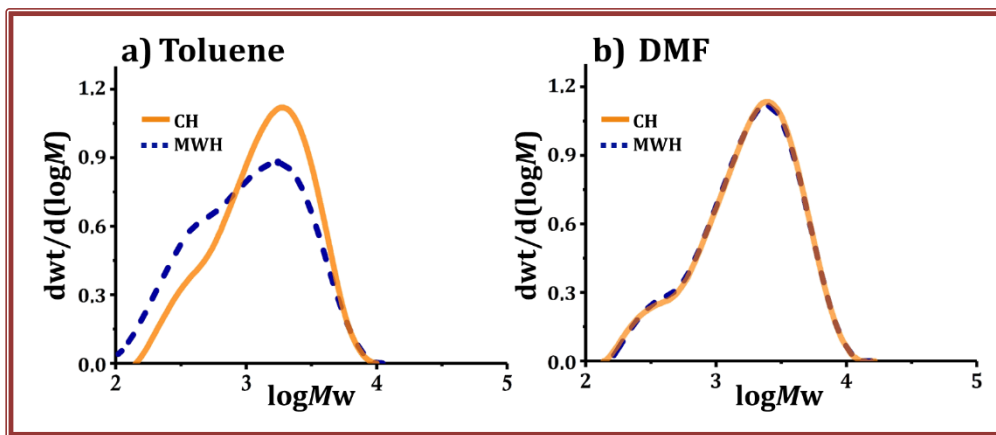


Figure 2.13. Final molar mass distribution of **MMA/VFc** copolymerization under CH and MWH using **AIBN** initiator in (a) **Toluene** and (b) **DMF**.

CHAPTER 2

The molar masses are lower, and the fraction of oligomers is higher for MWH copolymer obtained in toluene, as shown in Figure 2.18a, which may result in an increasing rate of intramolecular termination of superheated VFc molecules. The lack of this effect was observed in DMF (Figure 2.18b), probably because VFc was exposed to much lower MW power in DMF than in toluene; thus, no sufficient energy was accumulated within the domains to affect the molar mass distribution of MMA/VFc copolymer.

The magnitude of the observed effect in the two solvents is different and probably takes place due to the distinct dielectric properties of each of them. The reaction rate enhancement effect is clearly stronger in toluene, which was expected due to its MW transparent nature. Namely, to heat the same monomer mixture (and amount) up to the same temperature in toluene would likely require much more MW energy than in DMF. This is clearly shown in Figure 2.19, where the time evolution of the main reaction parameters (reaction temperature, the external temperature on the reaction wall, and MW power) are compared for both solvents in MW reactor. In toluene, the MW power applied is almost 300 W, whereas, in DMF, it is around 100 W. Therefore, in toluene VFc was exposed to importantly more intensive MW irradiation, and likely due to it, the observed effects were more significant.

SOLUTION POLYMERIZATION

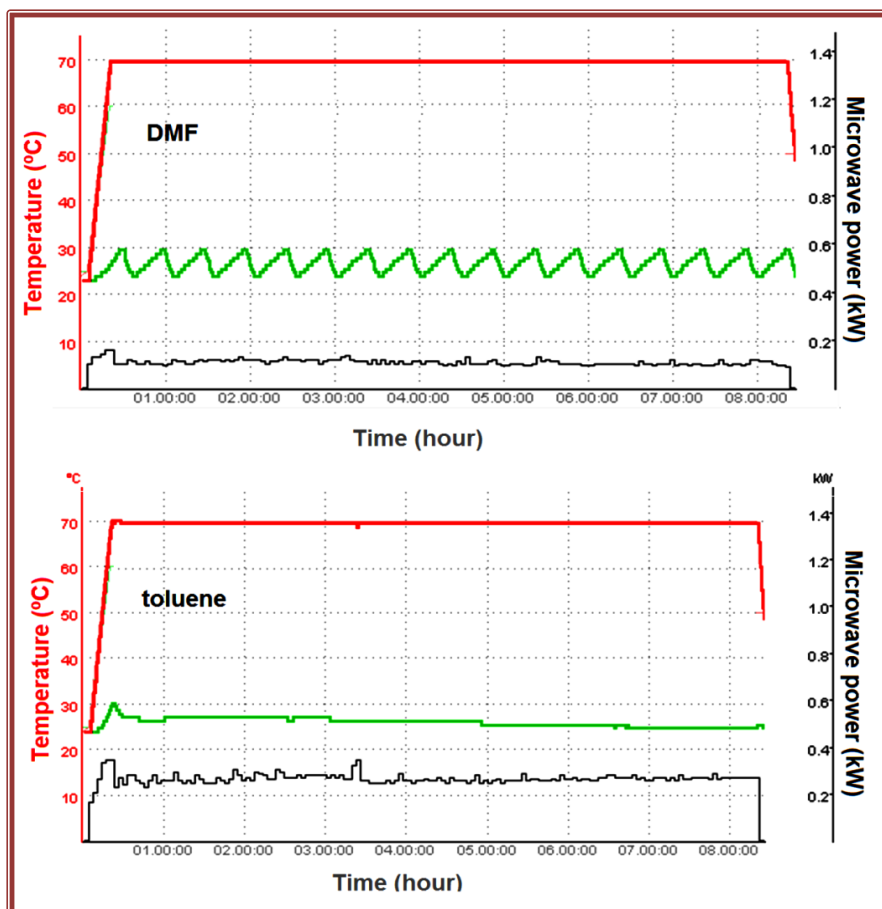


Figure 2.19. Reaction temperature profile (red lines), **MW power** (black lines), and external temperature on the reaction wall profile (green line) during **MMA/VFc** copolymerization under MWH in **DMF** (above) and **toluene** (bellow) and with **AIBN** initiator.

The differences observed in DMF solvent for the reaction rate of MMA/VFc monomer couple and the cumulative copolymer compositions are rather tiny. If the observed changes resulted from the presence of the VFc in the monomer mixture, by increasing its content in the monomer mixture, one would expect a stronger effect. Therefore, MMA/VFc copolymerization was performed in both CH and MWH reactors at an increased molar fraction of VFc (30 mol% MMA and 70 mol% VFc) in DMF with AIBN initiator. The reaction was selected to be performed in DMF solvent because of the alteration of copolymer compositions observed (Figure 2.17d). **The results of 3:7 mole ratios MMA/VFc** are shown in Figure 2.20.

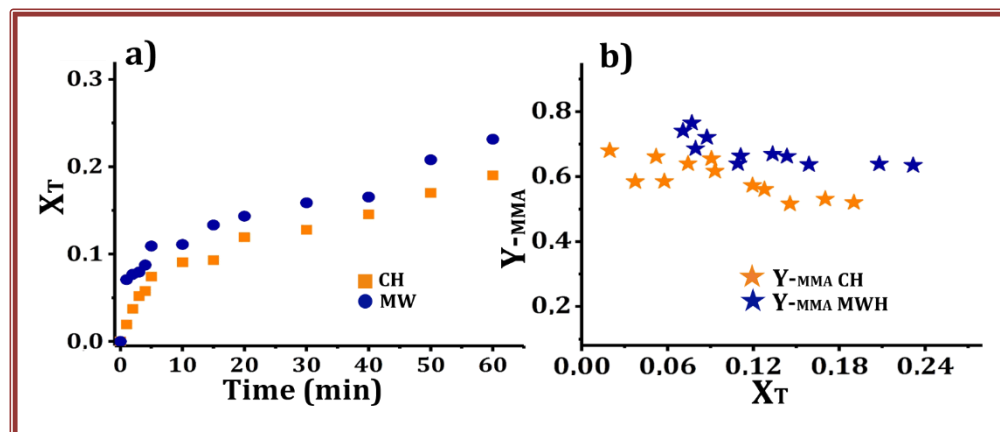


Figure 2.20. (a) Time evolution of conversion of **MMA/VFc (3:7)** copolymerization under CH and MWH using **AIBN** initiator in **DMF**; (b) Cumulative copolymer compositions for both reactions, presented as MMA fraction within the copolymer.

Apparently, the effects observed in Figure 2.17c,b are enhanced in Figure 2.20. According to the time evolution of conversion curves presented in Figure 2.15a, initially, the MW reaction is importantly faster than CH reaction and presents continuously higher conversion in the whole investigated period. MWH polymer has altered copolymer composition in comparison to the CH polymer, as displayed in

SOLUTION POLYMERIZATION

Figure 2.20b. In CH reaction, the higher VFc concentration in the initial mixture resulted in increased VFc fraction in the copolymer. Thus, at 6% overall conversion, the MMA fraction in the copolymer is about 60%, compared to 90% in the case of 1:1 mixture of MMA/VFc (Figure 17c). Oppositely, in MWH copolymer, the fraction of MMA increased to almost 80%, indicating affected reactivity ratios r_{MMA} and r_{VFc} under MWH. The higher incorporation of MMA under MWH may be achieved only if the $(r_{MMA}/r_{VFc})_{MWH} > (r_{MMA}/r_{VFc})_{CH}$, where r_{MMA} is the ratio of the propagation constants of the addition of MMA to growing chains ended with MMA to that ended with VFc unit ($r_{MMA} = k_{pMMA\ MMA}/k_{pMMA\ VFc}$), whereas r_{VFc} is the ratio of propagation constants of the addition of VFc to a growing copolymer chain ended with VFc to that ended with MMA unit ($r_{VFc} = k_{pVFc\ VFc}/k_{pVFc\ MMA}$). As it is expected that MWH affects the VFc reactivity ratio, this means that in order to increase $(r_{MMA}/r_{VFc})_{MWH}$ the propagation constant of VFc addition to MMA ending growing copolymer chain ($k_{pMMA\ VFc}$) must be higher under MWH, which will lead to increased incorporation of MMA in the copolymer mixture as it was noticed in Figure 2.20b.

The clear differences between the CH and MWH polymerization in MMA/VFc comonomer system, observed in Figures 2.17 and 2.20, indicate reaction rate enhancement and alteration of the copolymer composition, which may be considered specific microwave effects. The magnitude of the observed effects, although noticeable, is substantially smaller than the claimed enhancement of polymerization rate reported in the literature [1,6,9]. However, having in mind the equal bulk temperature in both CH and MWH reactors; apparently, the observed results can not be rationalized by means of the measured bulk temperature and Arrhenius equation. The unique heat properties of the MW irradiation in solution, based on the dielectric relaxation processes, creates, in this case, deviations that can be explained by means of selective heating mechanisms in dynamically distinct domains in macroscopically homogenous multi-component solutions [29–31]. These authors reproduced MW

heating experiments by performing dielectric relaxation experiments in simple supercooled liquids. They found out that, after absorption of MW photon that excites the configuration mode of the absorbing molecules, they will either overtake the relaxation process and dissipate the absorbed energy into heat or will be exposed to excess configurational temperature and accumulate heat. In the last case, if the local temperature is higher than the bulk one, the absorbing molecules have increased molecular mobility over that at actual bulk temperature. However, what is crucial for the appearance of the microwave specific effect is the time scale of the relaxation process. For components with fast relaxation dynamics (the absorption of MW is a slower process than the energy transfer into heat), probably the specific MW effects remain absent. These components under MW behave similarly to CH. On the other hand, for components characterized by slow configurational relaxation time, the transfer of the absorbed energy into heat is intrinsically ineffective. Under these conditions, MW specific effects may be eventually observed.

In a solution of different components, MMA, VFc, AIBN, and DMF, each of them with different dielectric properties and polarity, dynamically distinct domains are formed, as it is shown in Figure 2.21a. Under MW irradiation, each domain absorbs a different amount of energy and converts it into heat at different rates, depending mostly on the configurational relaxation time of each of them, but as well on the thermal properties of the solvent. The relaxation time of different domains may differ in order of magnitude. DMF solvent is a highly absorbing species; however, the copolymerization of MMA/BA and MMA/St in this solvent demonstrated identical behavior under both CH and MWH. As the observed MW effects were clearly related to the presence of VFc molecules that absorb MW irradiation efficiently, we hypothesize that the dielectric relaxation in VFc is slow and inefficient in energy dissipation as heat in the reaction media. Thus, such components will accumulate heat within the domain leading to the prolonged time excess of configurational temperature, likely higher than the

SOLUTION POLYMERIZATION

measured bulk temperature (Figure 2.21b). This probably induces increased mobility of VFc domains over the domains at the actual temperature, affecting the reactivity of VFc, as it was observed experimentally.

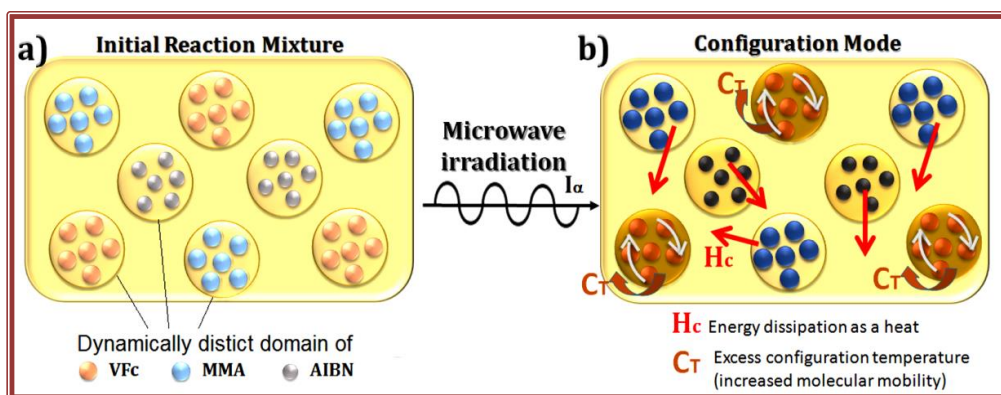


Figure 2.21. (a) Initial reaction mixture made of dynamically distinct domains of the reaction component in the solvent; (b) the reaction mixture during MW irradiation, the components are in the configuration excited mode.

Table 2.5. Total energy spent during the polymerization reaction **per mL** of the reaction mixture under conditions explained in the experimental section; In all cases, AIBN was used.

Co-monomers (solvent)	MMA/BA (Toluene)	MMA/BA (DMF)	MMA/St (Toluene)	MMA/St (DMF)	MMA/VFc (Toluene)	MMA/VFc (DMF)
E (kJ/mL)	14	7.7	18	8	33	11

The energy spent in the MWH reaction in this system, presented in Table 2.5, may provide additional evidence on the inefficiency of the VFc to convert the absorbed energy into heat.

According to the data in Table 2.5, due to the much higher dielectric constant and loss tangent of DMF, the MWH reactions in this solvent are much more cost-efficient. Apparently, in monomer mixture containing VFc monomer, the total energy spent is much higher than in the respective solvent system and other monomer mixture, which may be an indirect proof of the hypothesis that VFc, besides high MW absorption ability as an organometallic compound, is completely inefficient in the dissipation of the absorbed energy as heat.

The data presented in Table 2.5 additionally demonstrates that by the selection of appropriate solvent for the MW assisted polymerization, the required energy is importantly reduced, without significant change in the polymer properties, as shown by the similar microstructural characteristics measured (copolymer composition, MWD, and polymer architecture).

2.4 CONCLUSIONS

A reliable comparison of free radical CH and MWH assisted polymerization was reached by creating similar reaction temperature profiles, eliminating the possibility to attribute the observed effects to thermal differences. Under such conditions, the copolymerization of different monomer couples was studied. The most common monomers for free-radical polymerization, such as MMA, BA, and St, as well as organometallic monomer VFc, presenting different polarities and dielectric properties, were selected. Two types of organic solvents were studied.

SOLUTION POLYMERIZATION

On the one hand, toluene as MW transparent solvent (low dielectric constant and low loss tangent), and on the other, DMF characterized with high dielectric constant and loss tangent, fast absorption, efficient heating under MWH. Finally, three different initiators have studied: AIBN and two peroxides LPO and BPO.

It was found that under similar reaction temperature profiles in both CH and MWH reactors in the case of MMA/BA and MMA/St monomer couples, no changes were observed neither in polymerization rates nor in the polymer composition and molar masses. Nevertheless, in the case of MMA/VFc monomer couple in both investigated solvents, slightly enhanced polymerization rates were observed, especially in the early reaction stages. This effect was accompanied by a difference in copolymer composition, suggesting altered reactivity ratios of MMA and VFc during polymerization under MWH. The observed effects were more pronounced in toluene, considered as MW transparent solvent because the toluene system was exposed to more intense MW irradiation in order to keep the same temperature profile as the one of the DMF system. Increasing the concentration of VFc in the initial co-monomer mixture, the observed effects in DMF solvent increased, too. As a result, the copolymer obtain in MW irradiation in shorter reaction times was richer in VFc than the respective CH copolymer.

The observed effects were explained by the unique heat properties of the MW irradiation in a multi-component solution, which provided selective heating and creation of dynamically distinct domains. Depending on the interaction of the components with MW irradiation within each domain, they will either absorb the MW irradiation and efficiently transfer it to heat or will remain in the configurational mode and accumulate the heat, which likely increased the mobility of the molecules within such domain. The last case results in the creation of microwave specific effect, as the ones observed in the case of MMA/VFc mixture. The MW energy requirement of MMA/VFc monomer system, which was higher than for other systems besides the

high capability of VFc of MW absorption, demonstrates the inefficiency of VFc to convert the absorbed energy into heat.

Finally, the comparison of the energy consumption between the different polymerization systems in MW reactor leads to the conclusion that the selection of appropriate solvent may be an important tool to save energy without altering the product quality.

The presented study, up to the best knowledge of the authors, is the first presenting microwave effects in free-radical polymerization in solution as rate enhancement and copolymer composition alteration.

2.5 REFERENCES

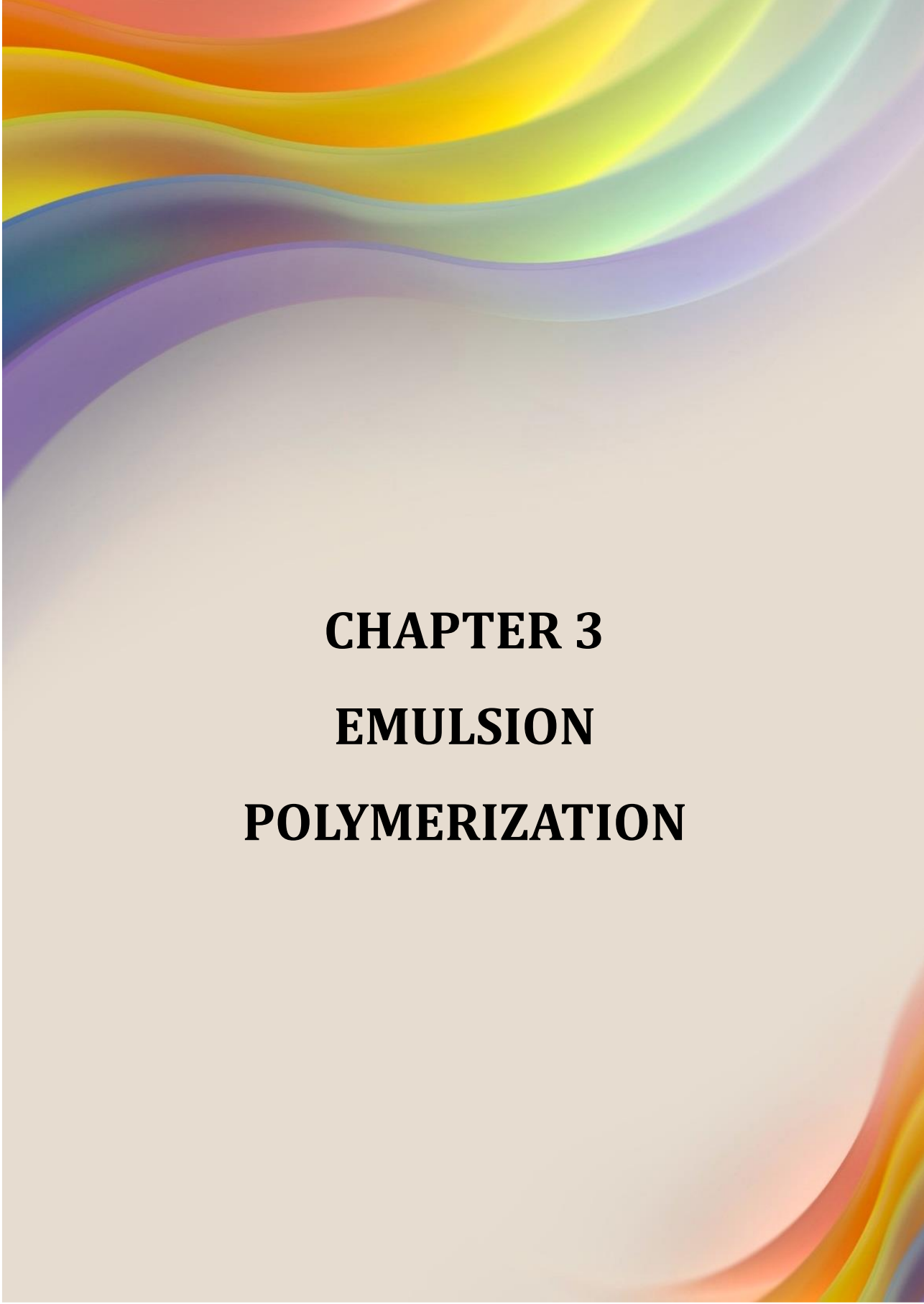
- [1] M.A. Dikumar, I. V Kubrakova, A.A. Chinarev, N. V Bovin, Polymerization of 4-Nitrophenyl Acrylate under Microwave Heating Conditions, *Russ. J. Bioorganic Chem.* 27 (2001) 408–412. doi:10.1023/A:1012949005183.
- [2] G. Madras, V. Karmore, Evolution to similarity solutions for polymerization and depolymerization with microwave radiation, *Polym. Int.* 50 (2001) 1324–1330. doi:10.1002/pi.779.
- [3] T. Glück, I. Woecht, A. Schmalfuß, G. Schmidt-Naake, Modification of the Solvent Influence on the Free Radical Polymerization in Ionic Liquids by Microwave Irradiation, *Macromol. Symp.* 275–276 (2009) 230–241. doi:10.1002/masy.200950125.
- [4] Y.-H. Shih, B. Singco, W.-L. Liu, C.-H. Hsu, H.-Y. Huang, A rapid synthetic method for organic polymer-based monoliths in a room temperature ionic liquid medium via microwave-assisted vinylization and polymerization, *Green Chem.* 13 (2011) 296–299. doi:10.1039/C0GC00803F.
- [5] E.C. Buruiana, M. Zamfir, V. Melinte, T. Buruiana, Photo-polymers Containing (S)-Phenylalanine and Stilbene Pendants: Synthesis and Properties of Ionic Polyacrylates, *Des. Monomers Polym.* 13 (2010) 21–32. doi:10.1163/138577209X12591392377694.

- [6] S. Agarwal, M. Becker, F. Tewes, Synthesis, characterization and properties evaluation of copolymers of 2,3,4,5,6-pentafluorostyrene and N-phenylmaleimide, *Polym. Int.* 54 (2005) 1620–1625. doi:10.1002/pi.1890.
- [7] V. Singh, A. Tiwari, P. Kumari, A.K. Sharma, Microwave accelerated synthesis and characterization of poly(acrylamide), *J. Appl. Polym. Sci.* 104 (2007) 3702–3707. doi:10.1002/app.25682.
- [8] M.M. Azad, M.G. Sandros, Microwave-assisted polymerization: Superabsorbent polymer with improved properties, *J. Appl. Polym. Sci.* 133 (2016). doi:10.1002/app.43325.
- [9] H. Ren, Y.F. Zhang, T.Z. Huang, J. Wang, Study on Synthesis of Superabsorbent Using Microwave Heating and Water Absorbency, in: *Adv. Mater. CEAM 2011*, Trans Tech Publications Ltd, 2011: pp. 1854–1857. doi:10.4028/www.scientific.net/AMR.239-242.1854.
- [10] C. Guerrero-Sanchez, M. Lobert, R. Hoogenboom, U.S. Schubert, Microwave-Assisted Homogeneous Polymerizations in Water-Soluble Ionic Liquids: An Alternative and Green Approach for Polymer Synthesis, *Macromol. Rapid Commun.* 28 (2007) 456–464. doi:10.1002/marc.200600728.
- [11] H. Stange, M. Ishaque, N. Niessner, M. Pepers, A. Greiner, Microwave-Assisted Free Radical Polymerizations and Copolymerizations of Styrene and Methyl Methacrylate, *Macromol. Rapid Commun.* 27 (2006) 156–161. doi:10.1002/marc.200500640.
- [12] H. Stange, A. Greiner, Microwave-Assisted Free Radical Copolymerizations of Styrene and Methyl Methacrylate, *Macromol. Rapid Commun.* 28 (2007) 504–508. doi:10.1002/marc.200600841.
- [13] C.O. Kappe, How to measure reaction temperature in microwave-heated transformations, *Chem. Soc. Rev.* 42 (2013) 4977–4990. doi:10.1039/C3CS00010A.
- [14] N.T. Nguyen, E. Greenhalgh, M.J. Kamaruddin, J. El harfi, K. Carmichael, G. Dimitrakakis, S.W. Kingman, J.P. Robinson, D.J. Irvine, Understanding the acceleration in the ring-opening of lactones delivered by microwave heating, *Tetrahedron.* 70 (2014) 996–1003. doi:https://doi.org/10.1016/j.tet.2013.11.031.
- [15] W. Liptay, *Tables of Experimental Dipole Moments*. Von A. L. McClellan. Verlag W. H. Freeman, *Angew. Chemie.* 77 (1965) 276.

doi:10.1002/ange.19650770627.

- [16] Landolt-Börnstein, Static Dielectric Constants of Pure Liquids and Binary Liquid Mixtures No Title, Springer Materials, 2008. doi:10.1007/978-3-540-75506-7.
- [17] S.G. Roos, A.H.E. Müller, K. Matyjaszewski, Copolymerization of n-Butyl Acrylate with Methyl Methacrylate and PMMA Macromonomers: Comparison of Reactivity Ratios in Conventional and Atom Transfer Radical Copolymerization, *Macromolecules*. 32 (1999) 8331–8335. doi:10.1021/ma9819337.
- [18] E.L. Madruga, M. Fernández-García, A kinetic study of free-radical copolymerization of butyl acrylate with methyl methacrylate in solution, *Macromol. Chem. Phys.* 197 (1996) 3743–3755. doi:10.1002/macp.1996.021971120.
- [19] B.T. Ergan, M. Bayramoğlu, The effects of microwave power and dielectric properties on the microwave-assisted decomposition kinetics of AIBN in n-butanol, *J. Ind. Eng. Chem.* (2013). doi:10.1016/j.jiec.2012.08.015.
- [20] O.A. Haidukevich, E.D. Skakovskii, L.Y. Tychinskaya, T.D. Zvereva, E.A. Dikumar, S.A. Lamotkin, S. V Rykov, NMR analysis of diacyl peroxide decomposition in methanol in response to temperature and microwave radiation, *J. Appl. Spectrosc.* 79 (2012) 302–306. doi:10.1007/s10812-012-9598-y.
- [21] T.N. Myers, Initiators, Free-Radical, in: *Encycl. Polym. Sci. Technol.*, American Cancer Society, 2002. doi:10.1002/0471440264.pst425.
- [22] M. Buback, R.G. Gilbert, R.A. Hutchinson, B. Klumperman, F. -D Kuchta, B.G. Manders, K.F. O'Driscoll, G.T. Russell, J. Schweer, Critically evaluated rate coefficients for free-radical polymerization, 1. Propagation rate coefficient for styrene, *Macromol. Chem. Phys.* (1995). doi:10.1002/macp.1995.021961016.
- [23] J.M. Asua, S. Beuermann, M. Buback, P. Castignolles, B. Charleux, R.G. Gilbert, R.A. Hutchinson, J.R. Leiza, A.N. Nikitin, J.P. Vairon, A.M. Van Herk, Critically evaluated rate coefficients for free-radical polymerization, 5: Propagation rate coefficient for butyl acrylate, *Macromol. Chem. Phys.* (2004). doi:10.1002/macp.200400355.
- [24] M.G. Baldwin, K.E. Johnson, Free-radical polymerization of vinyl ferrocene, *J. Polym. Sci. Part A-1 Polym. Chem.* (1967). doi:10.1002/pol.1967.150050825.

- [25] T. Furuncuoğlu Özaltın, B. Dereli, O. Karahan, S. Salman, V. Aviyente, Solvent effects on free-radical copolymerization of styrene and 2-hydroxyethyl methacrylate: A DFT study, *New J. Chem.* (2014). doi:10.1039/c3nj00820g.
- [26] L.A. Idowu, R.A. Hutchinson, Solvent effects on radical copolymerization kinetics of 2-Hydroxyethyl methacrylate and butyl methacrylate, *Polymers (Basel)*. (2019). doi:10.3390/polym11030487.
- [27] J.C. Lai, T. Rounsfell, C.U. Pittman, Free-radical homopolymerization and copolymerization of vinylferrocene, *J. Polym. Sci. Part A-1 Polym. Chem.* (1971). doi:10.1002/pol.1971.150090307.
- [28] M.H. George, G.F. Hayes, Free-radical polymerization of vinylferrocene. I. Kinetics, *J. Polym. Sci. Polym. Chem. Ed.* 13 (1975) 1049–1070. doi:10.1002/pol.1975.170130503.
- [29] G.B. Dudley, R. Richert, A.E. Stiegman, On the existence of and mechanism for microwave-specific reaction rate enhancement, *Chem. Sci.* 6 (2015) 2144–2152. doi:10.1039/C4SC03372H.
- [30] W. Huang, R. Richert, Dynamics of glass-forming liquids. XIII. Microwave heating in slow motion, *J. Chem. Phys.* (2009). doi:10.1063/1.3139519.
- [31] W. Huang, R. Richert, The Physics of Heating by Time-Dependent Fields: Microwaves and Water Revisited, *J. Phys. Chem. B.* 112 (2008) 9909–9913. doi:10.1021/jp8038187.



CHAPTER 3
EMULSION
POLYMERIZATION

3.1 INTRODUCTION

As shown in Chapter 2, the MW effect may be observed in a heterogeneous system, in which there is sufficient difference between the components to induce a different level of MW heating of the components. Consequently, the reaction rate and the polymer composition obtained in the MWH assisted polymerization to differ than these obtained in CH reactor. Therefore, the aim of the present work is to investigate the emulsion polymerization as a heterogeneous system that contains two phases (aqueous continuous and monomers dispersed phase) and numerous additional components (surfactant, initiator) to check if the way of heating would induce selective heating and as a consequence changes in the process and products.

For that aim, potassium persulfate (KPS) was selected as initiator, for which it is already demonstrated in the literature that it decomposed faster under MWH ($k_d=1.03 \times 10^{-4}$) than under CH ($k_d=2.87 \times 10^{-5}$) at 70°C [1,2]. Therefore, we expect to observe a difference because it will affect the nucleation process, the number of particles and their size and distribution, and subsequently, the polymer properties [3].

Free-radical emulsion polymerization under MW irradiation has been investigated so far, as shown in Chapter 1 [1,2,4–22]. However, all these studies present the same experimental method as the studies performed in solution. The reactions were performed in batch mode, with all the reactants, including the initiator, added to the reaction mixture from the beginning of the reaction. However, under MW the heating rate is faster, making differences in temperature profiles and having the temperature initially higher in the MW reactor. Under such conditions, the decomposition of the initiator is faster in MW than in CH, where the initiator was usually added when the temperature reaction was achieved. Consequently, the nucleation process is expected to be affected substantially, and this effect would result in the difference in the

methodology between both MW and CH processes and not in the difference in the heating. We believe that the difference in temperature profiles, especially in the initial reaction stages, is the reason behind the observed increased reaction rates [1,2 4-22]. However, we consider that so far, no fair comparison of MWH and CH assisted emulsion polymerization was reported.

In this chapter, a few reaction series of MMA/BA co-polymerization were performed. The effect of the concentration of KPS on the polymerization processes performed under MWH and CH was studied. In the second set of reactions, 1% of different functional monomers were added to the MMA/BA copolymer. We selected hydroxyethyl methacrylate (HEMA), which is more polar than the main monomers, and two ionic monomers (sodium styrene sulfonate, NaSS, and acrylamide, AM), which are expected to be heated by the ionic conduction mechanism of heating under MW. The main challenge of these systems is the incorporation of the functional monomers into the MMA/BA polymer particles [23,24]. The functional monomers are dissolved in the aqueous phase, whereas the main monomers are placed within the dispersed phase. As a result, the functional monomers polymerized mostly in the aqueous phase, giving rise to water-soluble oligomers, which negatively affect the colloidal stability of the dispersions and polymer properties [23,24]. Here, the main idea was to introduce selective heating into the system, as it was expected that these functional monomers would absorb and be heated importantly by MWH into the reaction mixture. In this way, between others, their partitioning between the two phases and the diffusion properties may be affected and, subsequently, their incorporation into the copolymer.

Despite the still controversial discussion on the specific non-thermal MW effect in the free-radical polymerization performed in dispersed media, it is worth investigating MW as an alternative heating method for chemical reactions because of the possible

EMULSION POLYMERIZATION

energy saving and the possibility of developing new waterborne products with improved properties.

3.2 EXPERIMENTAL

3.2.1 MATERIALS

The materials are given in Appendix I.

3.2.2 POLYMERIZATIONS

Emulsion polymerization was carried out at 30% of solid content in 200 mL of a total volume. The aqueous phase is composed of a water solution of 1 wt % of sodium dodecyl sulfate (SDS) surfactant. The organic phase is composed of a monomer mixture of MMA/BA in 50/50 wt ratio. Both phases were stirred separately for 5 minutes at 200 rpm, and then both phases were mixed and stirred for 15 minutes at 300 rpm. When functional monomers were used (1%wt), in the case of 2-hydroxyethyl methacrylate (HEMA), it was dissolved in the organic phase along with main monomers; on the other hand, the ionic monomers sodium styrene sulfonate (NaSS) or acrylamide (AM), were dissolved into the water phase.

The emulsion was placed into the respective setup (MWH or CH) and polymerized in batch at 70°C for two hours, under a nitrogen atmosphere using potassium persulfate (KPS) as initiator, which was added as a shot in both cases, after the reaction temperature was achieved. The temperature was monitored during all reactions under both methods (MWH and CH). For better temperature control in CH experiments, the addition of ice directly into the heating bath was necessary.

Before starting any polymerization, an oxygen degasification process was required; for CH experiments were done using constant nitrogen flux for 25 min, whereas for MWH experiments, 60 minutes of nitrogen flux was necessary due to the dimensions of the vessel.

Characteristics of conventional heating and microwave setups are described in detail in Appendix I. The formulations and the reaction conditions for the different polymerizations performed in this study are summarized in Table 3.1.

It is worth mentioning that **all experiments were duplicated** to check the reproducibility of the results.

Table 3.1. Reaction formulations for different co-polymerizations performed under CH and MWH with various functional monomers.

Exp.	Heating method	Monomer mixture	Functional monomer	Initiator KPS	Reaction temperature and time
1	CH	MMA/BA	---	0.5%	70°C/2h
2			---	1.5%	
3			---	1%	
4			HEMA		
5			NaSS		
6			AM		
7	MWH	MMA/BA	---	0.5%	
8			---	1.5%	
9			---	1%	
10			HEMA		
11			NaSS		
12			AM		

3.2.3 CHARACTERIZATION

The overall conversions of the main monomers were measured gravimetrically. Particle size distribution was determined by dynamic light scattering (DLS). The gel fraction (fraction of the polymer insoluble in THF) was measured by soxhlet extraction, using THF as a solvent. Molar mass distribution (MMD) of the soluble fraction in THF was determined by gel permeation chromatography (GPC) at 35°C. For MMD measurements, the sol part was analyzed by GPC. Visco-elastic properties of the polymers were determined by dynamic mechanical thermal analysis (DMTA) and differential scanning calorimetry (DSC).

More details about the methodology and characteristics of all equipment used are described in Appendix I.

3.3 RESULTS AND DISCUSSION

3.3.1 TEMPERATURE PROFILES

Temperature profiles for CH and MWH induced polymerization reactions since the moment of charging the initiator into the reactor at reaction temperature (70°C) developed in both reactors are presented in Figures 3.1 and 3.2.

At the beginning of all CH reactions, there is a pick of 2-3°C temperature decrease from 70°C. It lasted ~3 min (Figures 3.1-a and 3-1-b) and occurred due to the addition of the initiator aqueous solution as a shot in the reactor. Obviously, the system did not respond sufficiently fast to keep the temperature unchanged. The exception is the system with 1.5% of KPS (Figure 3.1-c), where the temperature drop was 10°C due to a higher amount of aqueous solution added. This effect is not present in MW reactor

due to the faster heating by MW irradiation; thus, when the initiator solution was incorporated into the system, the temperature was kept constant.

Around minute five of the reaction, the temperature starts increasing above 70°C due to the exothermic polymerization reaction. For the reaction with 1.5% of KPS (Figure 3.1-c), the temperature in both methods (MWH and CH) was difficult to control; thus, it was increased by approx. 5°C. As well, in the system where NaSS was used, a temperature rise of around 6 degrees was observed in both reactions (Figure 3.2-b). When HEMA was used, an increased temperature of more than 6 degrees was observed just for reaction with CH. In all cases, better temperature control was provided by the MW reactor system. Nevertheless, the temperature differences are rather small.

EMULSION POLYMERIZATION

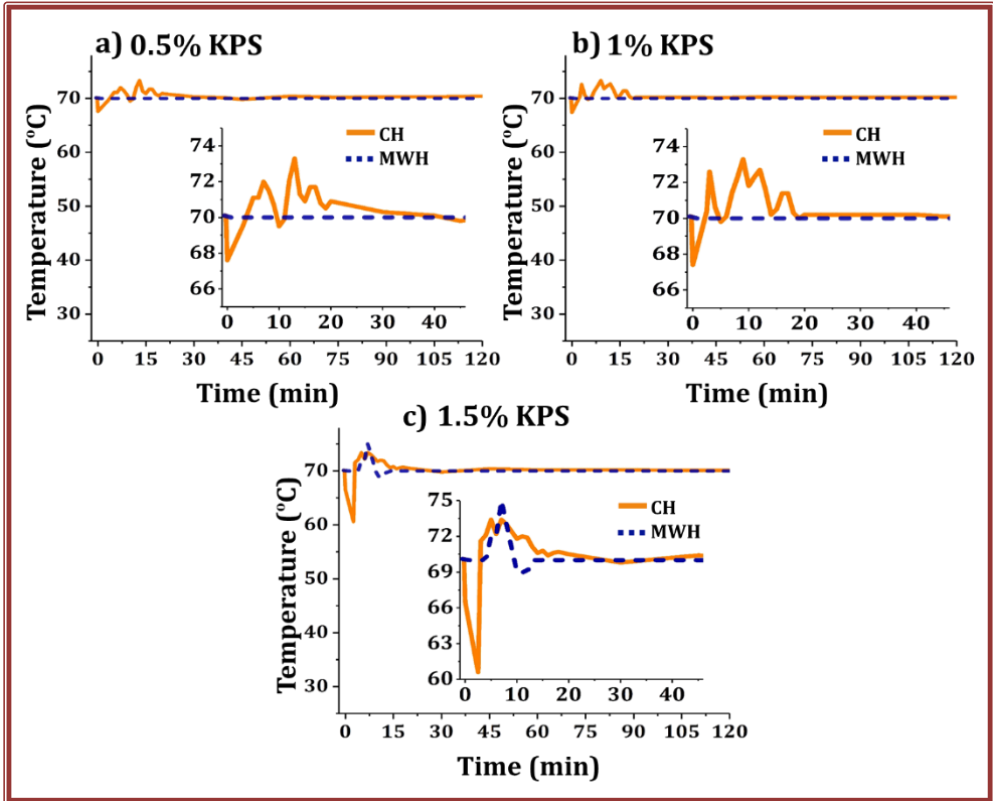


Figure 3.1. Comparing the temperature profiles of CH and MWH assisted polymerization reaction of MMA/BA monomer couple using different amounts of KPS initiator: a) **0.5% KPS**, b) **1% KPS**, and c) **1.5% KPS**. Insets: enlarged initial reaction region.

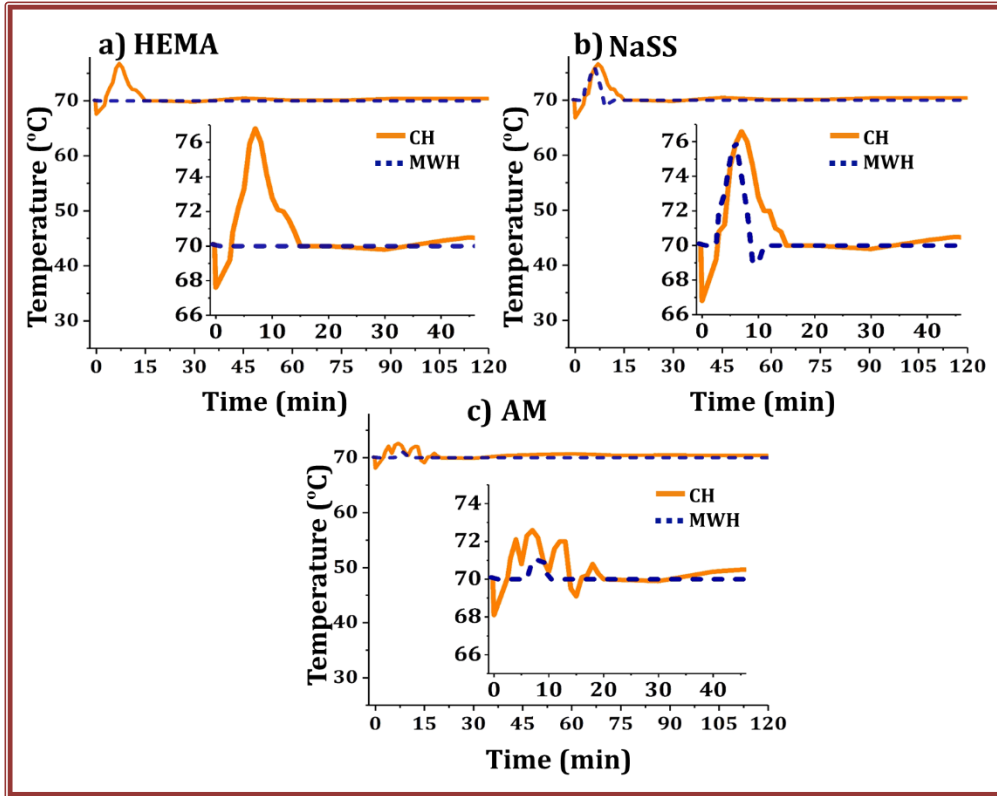


Figure 3.2. Comparison of the temperature profiles of CH and MWH assisted polymerization reaction of **MMA/BA** monomer couple using different functional monomers: a) **HEMA**, b) **NaSS**, and c) **AM**. Insets: enlarged initial reaction region.

It is worth mentioning that in the aqueous dispersion in **MMA/BA** monomer system, the temperature control under MWH was worst than in the solution system (see Chapter 2), which is likely due to the water used as a solvent. Water is a polar molecule with a high dielectric constant of 71.46 at 45°C [25], and its loss tangent is 0.123 [26].

Therefore, the aqueous dispersion reactions performed under MWH may be an important way of saving energy.

3.3.2 POLYMERIZATION KINETICS AND POLYMER MICROSTRUCTURE

Time evolution of conversion of MMA/BA using different amounts of KPS and different functional monomers, performed under MWH and CH, are presented in Figures 3.3 and 3.4, respectively. The area of the graphs presenting the first 20 min of the reactions, in which most of the changes have already occurred, is presented zoomed in at the intersection of each graph. Contrary to what was expected, **no significant differences in polymerization rate** were observed between CH and MWH methods for all reactions (experiments from 1 to 12 in Table 3.1). This finding is the opposite to almost all reported examples in literature [2,3,5-23], in most of which faster polymerization rate under MWH than under CH was claimed. We believe that it is so because of the similar temperature profiles ensured for both reactions.

Figure 3.3 presents the comparison of the evolution of monomer conversions in CH and MWH reactors, using the three different concentrations of KPS. The almost full conversion was achieved in all cases. As expected, the polymerization rate increased with the amount of initiator, no matter the heating method (CH or MWH). The difference between both heating methods is obvious just in the first 5 min., for which the conversion in MW reaction is higher. This effect increases with increasing KPS concentration. For the case of 1.5% of KPS (Figure 3.3-c), at 5 min, the conversion in MW reactor was 50%, whereas, in the CH reactor, it was 40%. This may be a result of the decreased temperature in the CH reactor when KPS aqueous solution was added (temperature drop of 10°C was observed, Figure 3.1-c). However, exactly at 5 min, the temperature in the CH reactor is already at the peak of higher temperature than in MW reactor. Even though the effect is small, being present in all reactions, it indicates that under MW the reaction is initially faster.

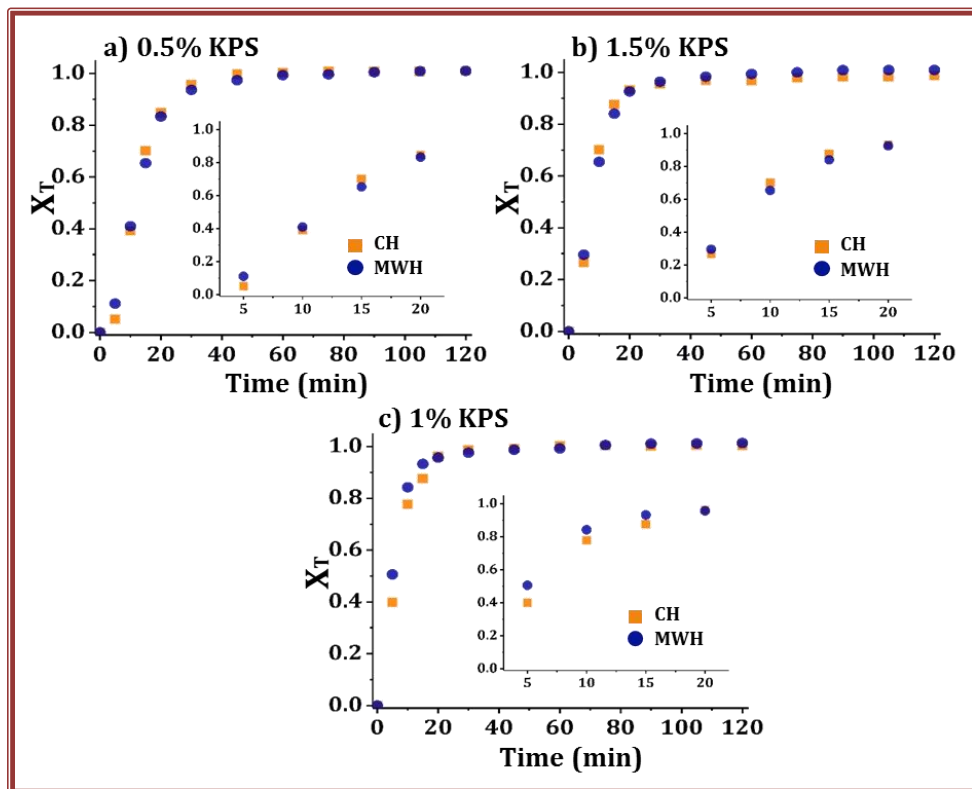


Figure 3.3. Time evolution of conversion of MMA/BA under CH and MWH using different amounts of KPS initiator: a) 0.5%, b) 1%, and c) 1.5%.

In Figure 3.4, the time evolution of the conversion of MMA/BA with functional monomers is shown for both MWH and CH reactions. No significant difference between MWH and CH reactions was noticed. In the case of HEMA and NaSS (Figures 3.4-a and 3.4-b, respectively), CH polymerization was slightly faster than the MWH reaction initially (at 5 min, polymer conversion difference of 10% for HEMA and 5% for NaSS were observed). This can be due to the higher temperature observed in CH reactor as shown in Figures 3.2-a and -b, where the peak of about 6°C higher temperature in CH lasts for about 0 min. However, in the case of AM, the reaction in

EMULSION POLYMERIZATION

MWH is faster than in CH reactor (at 5 min, the conversion difference of 10% is observed), even though the temperature is higher in CH reactor according to Figure 3.2-c. This indicates that a certain acceleration of the reaction occurred in this system due to the difference in the heating method. This difference decreased with time.

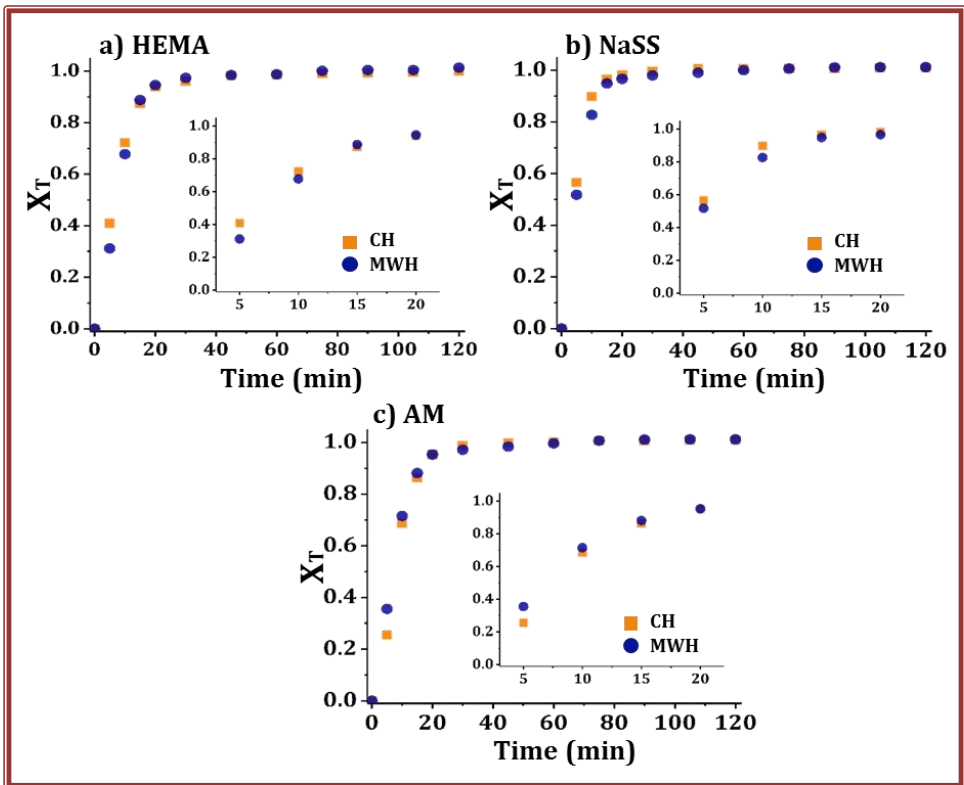


Figure 3.4. Time evolution of conversion of MMA/BA using different functional monomers under CH and MWH with 1% KPS.

The evolution of the number of particles along with the polymerization, calculated from the Z average size (more details are shown in Appendix I) for all experiments, is shown in Figure 3.5.

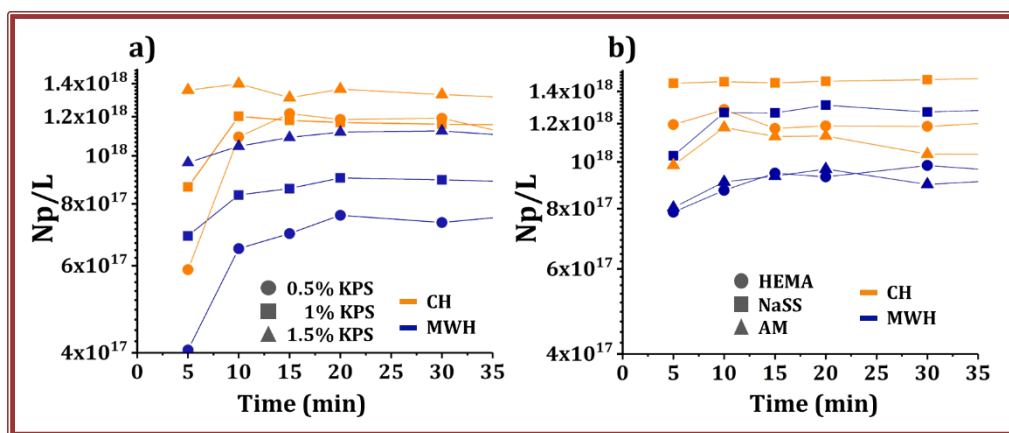


Figure 3.5. The number of particles for **MMA/BA** co-polymerization: a) using **different amounts of KPS** and b) using **different functional monomers** with 1% of KPS.

According to Figure 3.5-a, the effect of initiator amount on the number of particles is more pronounced for MW than for CH reactions. This indicates that the nucleation process is affected by way of heating. We may observe that in CH the nucleation finished until 10 min reaction (the period in which the temperature was unstable in the reactor), after which the number of particles slightly decreased, probably due to some coagulation. In MW reactor, new particles were formed until 20 min. All of this indicates that the nucleation is affected on the one hand by the temperature and on the other by way of heating, and it is extremely difficult to see each effect individually. For all initiator amounts, the number of particles in CH reaction is higher than in MWH reaction. The differences are not significant; however, the effect is again opposite than

EMULSION POLYMERIZATION

expected. We think that this is because in CH, up to 3 min reaction time, the temperature is lower than under MWH. This would induce decreased KPS decomposition rates under CH and a lower number of particles nucleated. This means that the radical creation process under MWH is affected on the one hand by the slightly higher temperature and, on the other hand, supposedly by the faster decomposition of KPS under MWH. Nevertheless, the data shown in Figure 3.5-a demonstrate that much fewer particles were nucleated in MW reactor. From the point of view of classical nucleation theory [27], the nucleation in MW reactor is postponed slightly because the higher temperature increases the free energy of nucleus formation with respect to the same reaction in CH reactor. On the other hand, from the point of view of Smith-Ewart theory [28], at a lower temperature in CH reaction, the volumetric grow rate of particles is lower than for MWH, which allows additional nucleation of new particles in CH reaction. The difference between MWH and CH for the lower KPS amounts (0.5% and 1%) is more important than for 1.5%. Probably, the higher number of radicals created in MW in the case of 1.5% KPS compensates the other effects.

The effect of different functional monomers on the particle number is shown in Figure 3.5-b. In all cases, the number of particles in CH reactor is higher than in MWH, being the difference largest for HEMA and NaSS. Additionally, the ionic monomers NaSS and AM, contribute to the colloidal stability, being the effect largest in the case of NaSS; thus, for this system, the number of particles is higher than for the other systems, independently on the way of heating and MWH.

The characteristics of the latexes and the polymers are summarized in Table 3.2. The average particle size (d_z) in the MWH reactions is slightly larger than in the CH, likely due to the reasons already discussed in relation to the number of particles.

Regarding the gel content, no gel was found for all polymers without ionic monomers. This is in agreement with what is known for the batch co-polymerization of MMA/BA, namely that no gel could be formed for MMA content higher than 25 wt% [29]. The lack of gel was attributed to the combined effect of the low reactivity of the MMA terminated active chains for hydrogen abstraction, the absence of abstractable hydrogens in MMA units, and the fact that MMA radicals terminate by disproportionation (whereas BA terminates by combination)[30], whereas no gel was formed in the same CH reaction.

For the experiments with ionic functional monomers, the gel content was found to be in a range of 30 to 60%. This could be due to the presence of the ionic groups coming from NaSS or AM in the polymer chains that make these chains insoluble in THF.

The difference between AM functional monomer in MWH and CH reaction in the gel content is not significant ($\sim 4\%$), whereas, for the NaSS functional monomer in MWH and CH reaction, the difference in gel content was $\sim 10\%$. This difference indicates that a slightly higher content of NaSS was incorporated into polymer particles under MWH than in CH method. This may be a result of the locally overheated NaSS molecules that may improve their mobility and their partition between the water and monomer phase. Namely, it was already observed a higher concentration of ionic compounds in the organic phase at an increased temperature [31]. By increasing their concentration in the organic phase, their incorporation would increase.

EMULSION POLYMERIZATION

Table 3.2. Characteristics of latexes and polymers produced by MMA/BA co-polymerization using different amounts of KPS and different functional monomers.

Exp.	Particle size (nm)		Gel (%)		Average molar mass (kDa)			
	MWH	CH	MWH	CH	MWH		CH	
					M_w	\bar{D}	M_w	\bar{D}
0.5%	85	78	0	0	2632	3.4	2364	3.6
1%	81	75	0	0	2597	4.2	2475	3.5
1.5%	76	76	0	0	2496	4.5	2260	4.2
HEMA	76	72	0	0	2576	5.0	2356	3.1
NaSS	71	68	60	50	698	2.9	364	2.1
AM	80	78	39	43	1967	3.7	1429	2.3

According to emulsion polymerization kinetics theory, lower molar masses (M_w) is observed when the amount of initiator is increased due to the higher number of radicals, promoting bimolecular termination of the chains. This trend is observed separately in both heating methods. When the amount of initiator was increased, the M_w decreased with higher polydispersity. However, at the same amount of initiator between both heating methods, higher M_w for MWH-polymers than CH is observed. The fact of having a higher number of particles at the same amount of initiator in CH than in MWH means that the average number of radicals per particle (\bar{n}) is lower in CH reaction, expecting to obtain larger M_w [32,33]. The observed effect here is the opposite; **the larger M_w polymers were obtained under MWH**, with increased polydispersity. Even though the difference is rather small, as it may be observed in Figure II.3.2 in Appendix II, the trend is obvious for all the reactions (Table 3.2). It is difficult to find the reason behind this behavior. In MWH, two effects are simultaneously present. On the one hand, and initially higher temperature than in CH and, on the other, a faster decomposition rate of KPS because of higher temperature and MW irradiation, both leading to higher \bar{n} and expectedly lower molar mass. However, the average molar mass is higher in this system. Even though these results

point towards the existence of an effect in MW assisted polymerization, the observed differences are rather small, and the clear conclusion of possible MW non-thermal effect cannot be taken, additionally supported by the small effects observed on the polymerization rates (Figure 3.3). The fact that the molar masses are higher at no important difference of conversion or particle size, at higher number of radicals per particle, indicates that probably the bimolecular termination was postponed under MW.

When different functional monomers were used, the difference in the molar masses of the polymer chains produced by MWH and CH is more important, especially for NaSS for which the molar masses were doubled under MWH (Table 3.2), Figure II.3.1e (Appendix II), despite the larger in average particles and higher \bar{n} . In the case of NaSS, 10% higher gel content was obtained under MWH; thus, the soluble molar mass should be lower than in CH, because the higher molar mass chains were supposed to be incorporated into the gel. However, again opposite trend was observed. If the gel fraction indeed is just the insoluble part of the polymer in THF due to the presence of ions in the polymer chains (not a real crosslinked structure), these results show that indeed higher amount of NaSS was incorporated into polymer particles due to the MW heating and that indeed the molar masses of MW polymers are importantly higher than these of CH polymers. The first effect was explained by increased solubility of NaSS into the organic phase due to the fact that NaSS molecules will be locally overheated with respect to MMA/BA molecules. It is well known that the ionic species overheat under MWH due to the ionic conduction mechanism of heating. According to this mechanism, the ions oscillate back and forth, influenced by the electric field created by the microwaves. Consequently, an internal electric current is formed, which faces internal resistance due to collisions of charged species with neighboring molecules or atoms, causing the heating up of the material. This is usually a stronger

effect in comparison to dipolar polarization for the capacity of heating materials [34,35].

On the other hand, the insoluble fraction in THF in the case of cationic functional monomer AM is rather similar in both reactions MW and CH assisted, indicating similar incorporation of AM into polymer particles. The molar masses are higher for MW polymer, similar to the other analysed systems and similar to the system with HEMA functional monomer. This occurrence demonstrates an effect occurring due to the difference in heating. Even though in this study, the differences are rather small, where higher molar masses were found in emulsion polymerization of acrylates under MWH [16,18,19].

3.3.3 POLYMER FILM PROPERTIES

The coating films, prepared by drying of the latex at 25°C and 55% relative humidity, were analyzed using DSC, DMTA, and water uptake, in order to understand if there are some differences in the polymer microstructure, thermal and mechanical properties, and the water sensitivity of the polymers produced by the CH and MWH.

Table 3.3 shows the glass transition temperature (T_g) of the prepared polymer films by both heating methods determined from DSC results. A broad peak from -30°C to 67°C in all experiments was found for all polymers, which is a result of the heterogeneous composition of the polymer chains formed in the batch polymerization of MMA/BA monomers, due to their different reactivity ratios ($r_{MMA} = 2.02 \pm 0.36$, $r_{BA} = 0.26 \pm 0.14$) [36]. This yield polymer chains rich in MMA-units (MMA with $T_g \sim 100.1^\circ\text{C}$) [37,38] at the beginning of the process, and chains rich in BA-units at the end (BA with $T_g \sim -52.1^\circ\text{C}$) [37,38]. As the MMA and BA are the main monomers in the composition, their heterogeneous composition is reflected in the T_g , showing

that the amount of the initiator or the addition of 1% of the functional monomer, nor the method of heating, did not modify the T_g of the final polymer significantly. We already demonstrated that the copolymer composition of MMA/BA was not affected by the heating method in Chapter 1 [39].

Table 3.3. Range of the glass transition temperature (T_g) measured by DSC of the prepared polymer films from both methodologies (MWH and CH).

Exp.	Glass transition temperature T_g (°C)	
	MWH	CH
0.5%	-30 to 67	-29 to 66
1%	-31 to 64	-30 to 60
1.5%	-31 to 64	-31 to 63
HEMA	-31.0 to 66.6	-31.5 to 63.7
NaSS	-30.6 to 63.7	-31.2 to 56.1
AM	-30.3 to 67.1	-31.2 to 63.8

The coating films presented wrinkles on the surface, especially for experiments with 1% KPS, 1.5% KPS, and HEMA, whereas for experiments with 0.5% KPS, NaSS, and AM, all films have a smooth surface. This could be due to a possible skin formation, a consequence of the inhomogeneous vertical drying process of a waterborne latex forming a solid layer of accumulated particles at the top of the film. A barrier to further evaporation forms and drying become extremely slow. In this case, all coating films were performed at 0.45-0.5mm of thickness.

The DMTA results of the formulated coating films are shown in Figures 3.6 and 3.7 and Table 3.4. For coating films with different amounts of KPS (Figure 3.6-a), the storage modules were slightly higher for MWH-films than CH-films for 0.5 and 1.5% of KPS in the whole temperature region. The reinforcing effect is the most obvious in

EMULSION POLYMERIZATION

the rubbery region, where the MWH films (0.5 and 1.5 % KPS) are stable at almost 20°C higher temperature than CH film (the MWH films still have the behaviour of solids, whereas the CH films already behave as a liquid). This is probably a result of the higher molar mass of the MWH-polymers. For the coating film with 1% of KPS, these differences were insignificant (as the M_w as well were very similar). Figure 3.6-b shows that $\text{Tan}\delta$ presents a single pick, which corresponds to a T_g of around 50°C, which is within the range determined from DSC measurements. The variation of the initiator or the heating method did not affect the T_g of the polymer films.

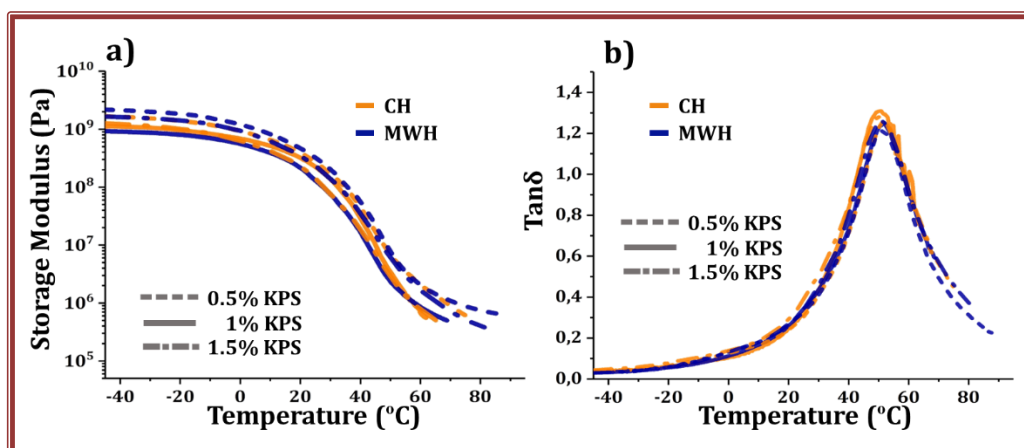


Figure 3.6. DMTA results of polymer films with **different amounts of KPS** a) Storage Modules, b) $\text{Tan}\delta$

In the case of coating films with different functional monomers (Figure 3.7), the MWH films present increased storage modulus. The effect is stronger in the rubbery region, indicating more thermally stable polymers were obtained in MWH than in CH reactor. For NaSS, this difference is the largest as MWH polymers behave as a solid until 90°C, presenting high storage modules. The CH polymer was stable until 72°C. There is no

effect on T_g , except in the case of NaSS, the T_g slightly shifts to 5 degrees higher temperature. The strongest effect in the case of NaSS is probably due to the higher molar mass of MWH polymer. The increased T_g under MWH over that obtained under CH is likely the result of the higher amount of incorporated NaSS. Namely, it was shown that the polymer chains reach in NaSS are placed on the surface of the particles, which after the formation of the film, create a reinforcing network [23].

The comparison of MWH and CH DMTA measurements separately is presented in Figure II.3.3 in Appendix II.

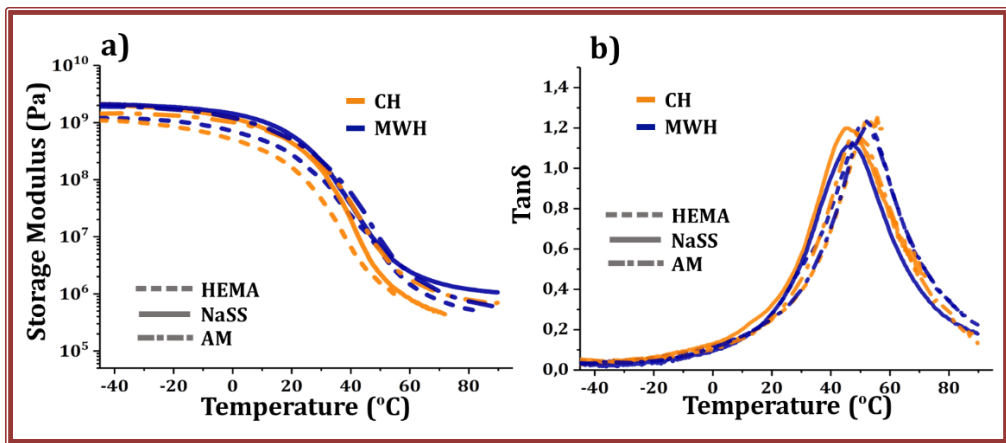


Figure 3.7. DMTA results of polymer films with **different functional monomers, and 1% KPS** dried at 25°C and 55% relative humidity. a) **Storage Modules**, b) **Tan δ**

EMULSION POLYMERIZATION

Table 3.4. Storage modulus at -40°C , glass transition temperature (T_g), and temperature at liquid like behaviour of the prepared **films at 25°C** with different amounts of KPS and different functional monomers.

Exp.	Storage (Pa) at -40°C		$T_g(^{\circ}\text{C})$		The temperature at liquid like behaviour ($^{\circ}\text{C}$)	
	MWH	CH	MWH	CH	MWH	CH
0.5%	2.12×10^9	1.65×10^9	51.2	51.4	89.4	74.9
1%	9.10×10^8	1.12×10^9	51.6	50.9	68.8	61.8
1.5%	1.62×10^9	1.23×10^9	52.4	50.2	81.3	67.9
HEMA	1.19×10^9	1.07×10^9	52.3	53.3	84.5	57.2
NaSS	2.07×10^9	2.05×10^9	46.2	45.6	89.7	71.8
AM	1.91×10^9	1.44×10^9	52.4	49.4	89.7	89.7

The water sensitivity was characterized by means of the water uptake by the films at 25°C , and the results are presented in Figure 3.8. In general, all CH films present a higher water uptake than MWH films. When different initiator amount was used (Figure 3.8-a), as it was expected, at a higher amount of KPS, the higher is the absorbed water because of a higher concentration of ionic species, which could increase the osmotic pressure as the major driving force for water uptake [40]. For 1% KPS, the difference in the water absorption is more than 30%, which indicates that the MWH films present decreased water sensibility, increasing the importance of these films for practical application. In the case of films with different functional monomers (Figure 3.8-b), the higher water uptake is observed for HEMA, followed by NaSS and finally AM, for both heating methods. It is well known that due to high water solubility and aqueous phase polymerization of the functional monomers, usually high amount of soluble oligomers were formed [23]. These oligomers are placed in the aqueous phase in the latex and are incorporated in the films, increasing their hydrophilicity, as observed in Figure 3.8b.

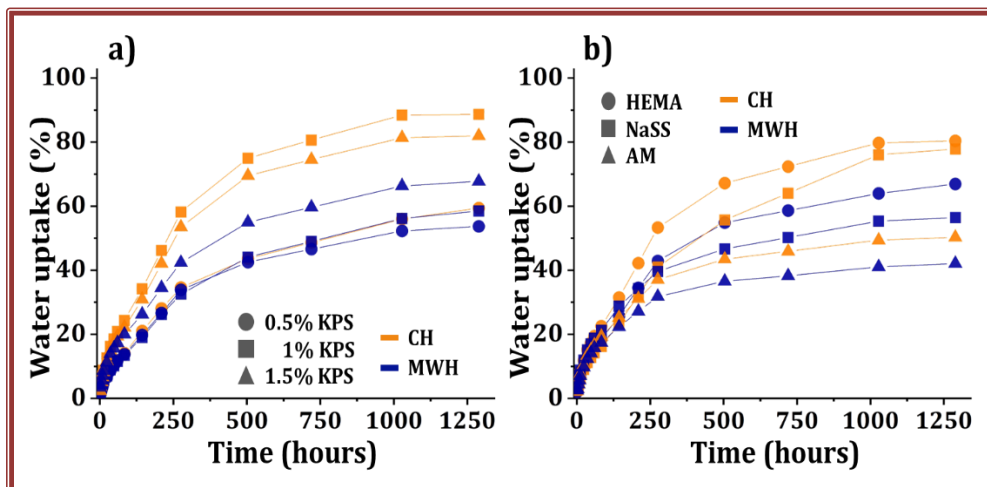


Figure 3.8. Water uptake of polymer films: a) using different amounts of KPS and b) using different functional monomers with 1% of KPS.

Table 3.5. Water uptake and the weight loss after water uptake test of polymer films and polymer films annealed. Reactions performed with functional monomers and different amounts of KPS.

Exp.	Water uptake of films (%)		Weight loss (%)	
	MWH	CH	MWH	CH
0.5%	53.7	59.4	1.36	1.26
1%	58.5	88.6	1.61	2.09
1.5%	67.7	81.9	2.31	2.56
HEMA	66.9	80.4	1.85	1.98
NaSS	56.4	77.8	1.73	1.88
AM	42.1	50.3	1.69	1.83

EMULSION POLYMERIZATION

To determine roughly the amount of these water-soluble species presented in the polymer films, the weight loss of the films after immersion in water for 52 days was calculated (Table 3.5). The weight loss corresponds to the number of water-soluble species presented within the film, such as a surfactant or ionic containing oligomers that diffuse from the film into the water during the water uptake measurements. Indeed, by increasing the amount of KPS, the higher is the quantity of the water-soluble oligomers. In the case of functional monomer, the presence of HEMA induced formation of the highest amount of these oligomers, followed by NaSS and AM. In both cases the observed results correspond perfectly to the water up-take. Finally, according to Table 3.5, the general trend is that the CH-films lost more mass than the MWH-films. It might be a result on the higher molar masses of MW polymers, but as well, on the improved incorporation of the functional monomers, demonstrated by this result. In Appendix II, Figure II.3.4; all polymer film pictures are presented after the immersion in water and after drying at 60°C.

The differences observed in the thermal properties and water absorption point out that there are differences in the properties of the polymers produced under MWH and CH that we did not observe so far. As the polymeric dispersions and the polymer microstructure were rather similar, we suppose that some change in the copolymer composition could be behind the distinct behaviour observed, which so far was not investigated. Even though in Chapter 2 we demonstrated that in MMA/BA system there was no effect of the heating method on copolymer composition, these reactions were performed in organic solvents. Here we had two phases and the small differences observed in temperature, and the possibility of the overheating of some of the components could produce alteration in the partitioning of the components between both phases and consequently in the composition of the polymer chains. Taking into account that the reactions were performed in batch, it is well known that the polymer chains under CH are heterogeneous, having some of the chains reach in

MMA, thus quite hard and the other reach in BA or soft. Consequently, the films are heterogeneous too. It is possible that by MWH, the chains are more homogeneous, producing more homogeneous films, thus improving slightly the mechanical, and more importantly, the thermal properties and water sensitivity. However, besides these improvements, we do not have a direct proof for this hypothesis.

3.3.4 MICROWAVE ENERGY CONSUMPTION

Table 3.6 shows the total energy consumption for all reactions performed under MWH. In the case of different amounts of initiator, The experiment with 1.5% of KPS spends less energy than the experiment with 0.5 or 1% of KPS. This is explained by, at the moment when the temperature reached higher temperature than required (70°C), the magnetron automatically turned off, and the remain heat still in there until the temperature down by itself, then the magnetron starts on again.

Regarding experiments with functional monomers, it was expected that the addition of these monomers could make the system more susceptible to MW irradiation, increasing the selectivity in heating in the system. Hence less MW-energy will be required to increase and keep the temperature. However, the differences in energy consumption are not reliable. Where NaSS was used, the less energy consumption is due to the same as it was explained before with the experiment of 1.5% of KPS.

In this case, where water is presented in the formulation, and its dielectric constant is higher than the other components, besides, it is in the majority of the system; hence, it is difficult to see a difference in energy consumption.

EMULSION POLYMERIZATION

Table 3.6. Microwave energy consumption (kJ) for all experiments performed by MWH in a volume of 200 mL for 2 hours of reaction.

Exp.	Total Energy (kJ)	Energy per mL (kJ/mL)
0.5%	733.9	3.66
1%	775.4	3.87
1.5%	713.2	3.56
HEMA	759.7	3.79
NaSS	717.5	3.58
AM	747.0	3.73

3.4 CONCLUSIONS

A comparison of free-radical CH and MWH assisted emulsion polymerization was performed under similar reaction temperature profiles, decreasing the possibility to attribute the observed effect to thermal differences. Under such conditions, the copolymerization of MMA/BA as the main monomers were studied, modifying the amount of initiator (KPS), or type of functional monomer (HEMA, NaSS, and AM) added in a small amount (1%) to the MMA/BA formulation.

Very small differences were observed between CH and MWH reactions in the initial reaction period, which were diminished during the reaction. The polymerization rate was slightly higher under MWH than CH, which was attributed to the initial drop of temperature in CH reactor when the initiator solution was introduced. Despite the higher temperature initially in the MWH reactor, under which it was expected to produce faster decomposition of KPS, fewer particles were nucleated. We think that the higher temperature-induced postponed nucleation process due to increased free energy of nucleus formation or because of the higher volumetric growth rate of the particles. The particle size was a little bit larger in the MWH reaction, signifying that

the average radical per particle is lower. Nevertheless, the molar masses of the polymer produced under MWH, in general, were larger than those obtained under CH. These effects were decreased when a higher amount of KPS initiator was used, and the effects were stronger when ionic functional monomers were, especially in the case of NaSS. These results even presented minor differences between both heating methods, a strong indication that there is an effect occurring under MW different from pure thermal effects.

In the case of functional monomers, the obtained results demonstrated that higher incorporation of the functional monomers was produced in the reaction under MWH, which was attributed to the improved partitioning of these highly hydrophilic monomers. DMTA results have shown that all polymers produced under MWH were slightly more mechanically stable; however, essential thermal stability was observed in MWH polymers. Namely, they kept the thermal stability at temperatures higher for about from 7°C to 27°C than that of CH polymers. Additionally, the MWH polymers absorbed up to from 5.7% to 30.1% less water absorption than their CH counter polymers.

Finally, this work demonstrated that the use of MWH to assist polymerization reaction in the emulsion is an important tool towards more sustainable polymer production, with eventually improved properties.

3.5 REFERENCES

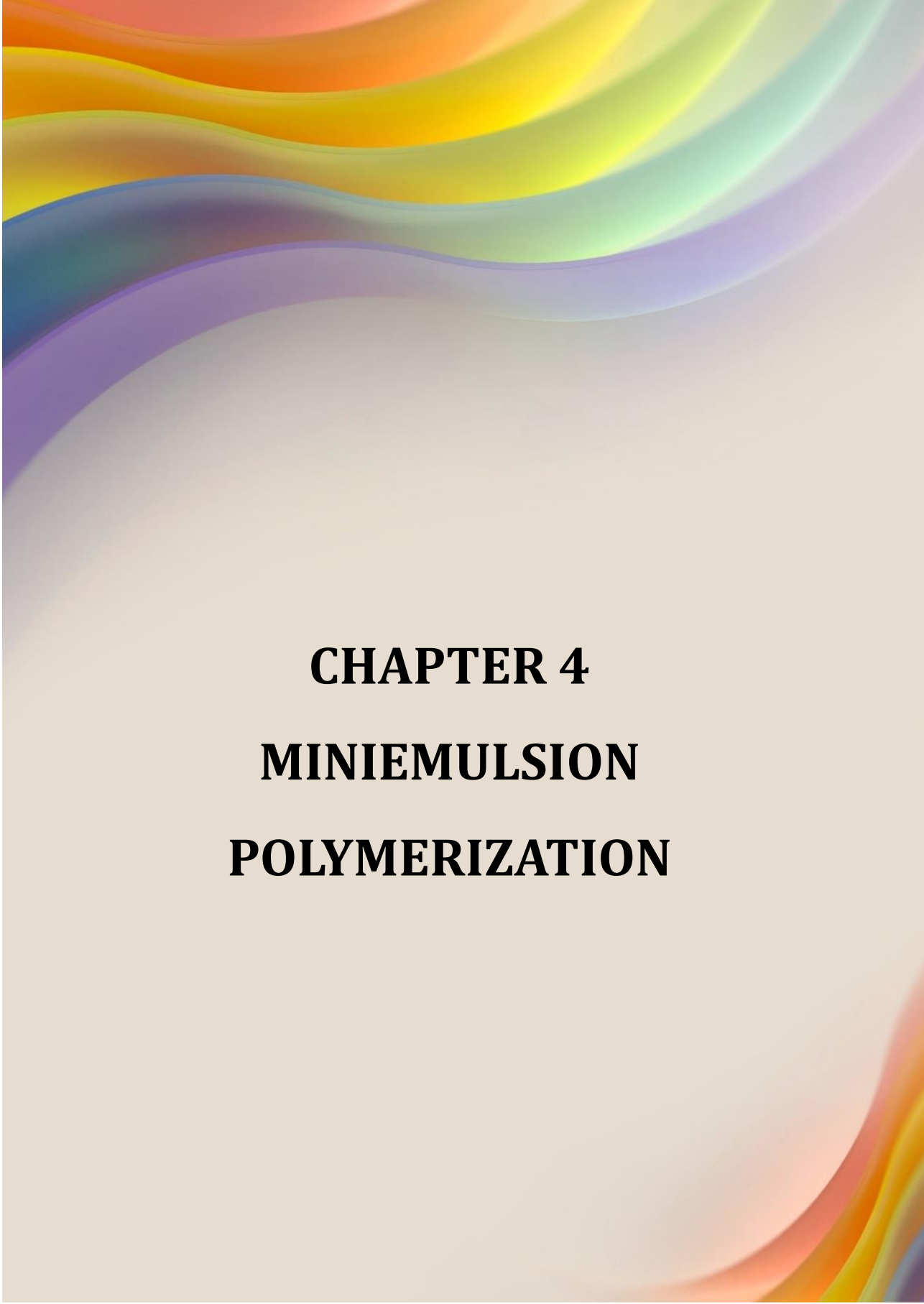
- [1] C. Costa, A.F. Santos, M. Fortuny, P.H.H. Araújo, C. Sayer, Kinetic advantages of using microwaves in the emulsion polymerization of MMA, *Mater. Sci. Eng. C.* (2009). <https://doi.org/10.1016/j.msec.2008.08.013>.
- [2] C. Costa, V.H.S. Santos, P.H.H. Araujo, C. Sayer, A.F. Santos, C. Dariva, M. Fortuny, Rapid decomposition of a cationic azo-initiator under microwave irradiation, *J. Appl. Polym. Sci.* (2010). <https://doi.org/10.1002/app.32409>.
- [3] R. Tomovska, J.C. de la Cal, J.M. Asua, Reactions in Heterogeneous Media: Emulsion, Miniemulsion, Microemulsion, Suspension, and Dispersion Polymerization, in: *Monit. Polym. React. From Fundam. to Appl.*, 2014. <https://doi.org/10.1002/9781118733813.ch4>.
- [4] C. Wu, J. Gao, M. Li, W. Zhang, M. Jiang, Formation, stabilization and application of polymeric nanoparticles, in: *Macromol. Symp.*, 2000. [https://doi.org/10.1002/1521-3900\(200002\)150:1<219::AID-MASY219>3.0.CO;2-1](https://doi.org/10.1002/1521-3900(200002)150:1<219::AID-MASY219>3.0.CO;2-1).
- [5] W. Zhang, J. Gao, C. Wu, Microwave preparation of narrowly distributed surfactant-free stable polystyrene nanospheres, *Macromolecules.* (1997). <https://doi.org/10.1021/ma970208d>.
- [6] T. Ngai, C. Wu, Double roles of stabilization and destabilization of initiator potassium persulfate in surfactant-free emulsion polymerization of styrene under microwave irradiation, *Langmuir.* (2005). <https://doi.org/10.1021/la0506630>.
- [7] H.Q. Xie, J.S. Guo, G.Q. Yu, J. Zu, Soapless emulsion polymerization of butyl methacrylate through microwave heating, *J. Appl. Polym. Sci.* (2001). <https://doi.org/10.1002/app.1352>.
- [8] U.-S. You, H.-Q. Wu, W.-M. Zhang, Z. Fu, L.-J. Shen, Preparation and Stabilization of Emulsifier-free Macromolecule Nanoparticle Latex Particles, *Chinese J. Chem.* (2010). <https://doi.org/10.1002/cjoc.20010190819>.
- [9] J. Hu, H. Zhao, Q. Zhang, W. He, Synthesis and characterization of submicron PMMA particles containing rare earth ions on the surface, *J. Appl. Polym. Sci.* (2003). <https://doi.org/10.1002/app.12298>.
- [10] J. Bao, A. Zhang, Poly(methyl methacrylate) nanoparticles prepared through microwave emulsion polymerization, *J. Appl. Polym. Sci.* (2004). <https://doi.org/10.1002/app.20758>.

- [11] C. Yi, Z. Deng, Z. Xu, Monodisperse thermosensitive particles prepared by emulsifier-free emulsion polymerization with microwave irradiation, *Colloid Polym. Sci.* (2005). <https://doi.org/10.1007/s00396-005-1318-1>.
- [12] Z.W. Deng, X.X. Hu, L. Li, Z.S. Xu, C.F. Yi, Self-assembled poly(styrene-co-N-isopropylacrylamide) film induced by capillary force, *J. Appl. Polym. Sci.* (2006). <https://doi.org/10.1002/app.22977>.
- [13] S.T. Camli, F. Buyukserin, M.S. Yavuz, G.G. Budak, Fine-tuning of functional poly(methylmethacrylate) nanoparticle size at the sub-100nm scale using surfactant-free emulsion polymerization, *Colloids Surfaces A Physicochem. Eng. Asp.* (2010). <https://doi.org/10.1016/j.colsurfa.2010.05.037>.
- [14] R. Correa, G. Gonzalez, V. Dougar, Emulsion polymerization in a microwave reactor, *Polymer (Guildf.)* (1998). [https://doi.org/10.1016/S0032-3861\(97\)00413-8](https://doi.org/10.1016/S0032-3861(97)00413-8).
- [15] W. Yan, X. Hu, G. Zhang, M. Deng, C. Yi, Z. Xu, Microwave assisted preparation of monodisperse polymeric microspheres and its morphologies and kinetics, *J. Wuhan Univ. Technol. Mater. Sci. Ed.* (2012). <https://doi.org/10.1007/s11595-012-0609-x>.
- [16] X. Zhu, J. Chen, Z. Cheng, J. Lu, J. Zhu, Emulsion polymerization of styrene under pulsed microwave irradiation, *J. Appl. Polym. Sci.* (2003). <https://doi.org/10.1002/app.12089>.
- [17] M.J. Hyun, Y. Youngjae, S.K. Yong, H.L. Jae, Microwave-irradiated copolymerization of styrene and butyl acrylate, in: *Macromol. Symp.*, 2007. <https://doi.org/10.1002/masy.200750430>.
- [18] X. Zhu, J. Chen, N. Zhou, Z. Cheng, J. Lu, Emulsion polymerization of methyl methacrylate under pulsed microwave irradiation, *Eur. Polym. J.* (2003). [https://doi.org/10.1016/S0014-3057\(02\)00363-4](https://doi.org/10.1016/S0014-3057(02)00363-4).
- [19] J. Sierra, J. Palacios, E. Vivaldo-Lima, Effect of microwave activation on polymerization rate and molecular weight development in emulsion polymerization of methyl methacrylate, *J. Macromol. Sci. - Pure Appl. Chem.* (2006). <https://doi.org/10.1080/10601320600575223>.
- [20] B.T. Ergan, M. Bayramoğlu, S. Özcan, Emulsion polymerization of styrene under continuous microwave irradiation, *Eur. Polym. J.* (2015). <https://doi.org/10.1016/j.eurpolymj.2015.06.021>.
- [21] Z. An, W. Tang, C.J. Hawker, G.D. Stucky, One-step microwave preparation of well-defined and functionalized polymeric nanoparticles, *J. Am. Chem. Soc.* (2006).

<https://doi.org/10.1021/ja065250f>.

- [22] J. Gao, C. Wu, Modified structural model for predicting particle size in the microemulsion and emulsion polymerization of styrene under microwave irradiation, *Langmuir*. (2005). <https://doi.org/10.1021/la048972y>.
- [23] S. Bilgin, R. Tomovska, J.M. Asua, Effect of ionic monomer concentration on latex and film properties for surfactant-free high solids content polymer dispersions, *Eur. Polym. J.* (2017). <https://doi.org/10.1016/j.eurpolymj.2017.06.029>.
- [24] S. Bilgin, R. Tomovska, J.M. Asua, Fundamentals of chemical incorporation of ionic monomers onto polymer colloids: Paving the way for surfactant-free waterborne dispersions, *RSC Adv.* (2016). <https://doi.org/10.1039/c6ra07486c>.
- [25] Landolt-Börnstein, Static Dielectric Constants of Pure Liquids and Binary Liquid Mixtures No Title, Springer Materials, 2008. <https://doi.org/10.1007/978-3-540-75506-7>.
- [26] C.O. Kappe, How to measure reaction temperature in microwave-heated transformations, *Chem. Soc. Rev.* 42 (2013) 4977–4990. <https://doi.org/10.1039/C3CS00010A>.
- [27] K. Tauer, I. Kühn, Particle Nucleation at the Beginning of Emulsion Polymerization, in: *Polym. Dispersions Princ. Appl.*, 1997. https://doi.org/10.1007/978-94-011-5512-0_4.
- [28] W. V Smith, R.H. Ewart, Kinetics of Emulsion Polymerization, *J. Chem. Phys.* 16 (1948) 592–599. <https://doi.org/10.1063/1.1746951>.
- [29] I. González, J.M. Asua, J.R. Leiza, The role of methyl methacrylate on branching and gel formation in the emulsion copolymerization of BA/MMA, *Polymer (Guildf)*. (2007). <https://doi.org/10.1016/j.polymer.2007.03.015>.
- [30] N. Ballard, S. Hamzehlou, F. Ruipérez, J.M. Asua, On the Termination Mechanism in the Radical Polymerization of Acrylates, *Macromol. Rapid Commun.* (2016). <https://doi.org/10.1002/marc.201600278>.
- [31] N.P. Bahadur, W.Y. Shiu, D.G.B. Boocock, D. Mackay, Temperature dependence of octanol-water partition coefficient for selected chlorobenzenes, *J. Chem. Eng. Data.* (1997). <https://doi.org/10.1021/je970020p>.
- [32] M.J. Barandiaran, J.C. de la Cal, J.M. Asua, Emulsion Polymerization, in: *Polym. React. Eng.*, John Wiley & Sons, Ltd, 2008: pp. 233–272. <https://doi.org/10.1002/9780470692134.ch6>.

- [33] J.M. Asua, Emulsion polymerization: From fundamental mechanisms to process developments, *J. Polym. Sci. Part A Polym. Chem.* (2004).
- [34] J. Anwar, U. Shafique, Waheed-uz-Zaman, R. Rehman, M. Salman, A. Dar, J.M. Anzano, U. Ashraf, S. Ashraf, Microwave chemistry: Effect of ions on dielectric heating in microwave ovens, *Arab. J. Chem.* (2015). <https://doi.org/10.1016/j.arabjc.2011.01.014>.
- [35] D.M.P. Mingos, D.R. Baghurst, Tilden Lecture. Applications of microwave dielectric heating effects to synthetic problems in chemistry, *Chem. Soc. Rev.* 20 (1991) 1–47. <https://doi.org/10.1039/CS9912000001>.
- [36] S.G. Roos, A.H.E. Müller, K. Matyjaszewski, Copolymerization of n-Butyl Acrylate with Methyl Methacrylate and PMMA Macromonomers: Comparison of Reactivity Ratios in Conventional and Atom Transfer Radical Copolymerization, *Macromolecules.* 32 (1999) 8331–8335. <https://doi.org/10.1021/ma9819337>.
- [37] M.N. Nguyen, Q.T. Pham, V.D. Le, T.B.V. Nguyen, C. Bressy, A. Margaille, Synthesis and characterization of random and block-random diblock silylated terpolymers via RAFT polymerization, *Asian J. Chem.* (2018). <https://doi.org/10.14233/ajchem.2018.21217>.
- [38] M. Fernández-García, R. Cuervo-Rodríguez, E.L. Madruga, Glass transition temperatures of butyl acrylate-methyl methacrylate copolymers, *J. Polym. Sci. Part B Polym. Phys.* (1999). [https://doi.org/10.1002/\(SICI\)1099-0488\(19990901\)37:17<2512::AID-POLB22>3.0.CO;2-2](https://doi.org/10.1002/(SICI)1099-0488(19990901)37:17<2512::AID-POLB22>3.0.CO;2-2).
- [39] B.T. Pérez-Martínez, M.A. Aboudzadeh, U.S. Schubert, J.R. Leiza, R. Tomovska, Microwave irradiation versus conventional heating assisted free-radical copolymerization in solution, *Chem. Eng. J.* (2020). <https://doi.org/10.1016/j.cej.2020.125761>.
- [40] A.F. Keddie, Joseph, Routh, Fundamentals of Latex Film Formation, in: *Fundam. Latex Film Form.*, 2010.



CHAPTER 4
MINIEMULSION
POLYMERIZATION

4.1 INTRODUCTION

As shown in previous chapters, some MW-effects were observed, especially in heterogeneous systems, in which, according to the nature of the components, microwaves can induce selective heating. The increase of heterogeneity in the investigated system likely increase the possibility to observe the MW-effect. Therefore, the aim of this chapter is to increase the number of the components into the polymerization system by adding a carbon nanomaterial conductive filler, such as multiwall carbon nanotubes (MWCNTs). The added conductive nanoparticles in the polymerization system under MWH will be heated by the mechanisms based on conduction heating (Joule heating), in which the motion of the electrons is induced by the electric field created under MW [1,2]. In this way, MW irradiation can generate localized superheating of the nanomaterials, acting as **hot-spots** during the polymerization. We expect that these hot-spots will change the interaction MWCNTs – polymer and will affect the structure and properties of the polymer composites. To check if it so, the MWCNTs-polymer composites were synthesized by in-situ polymerization assisted by both MWH and CH. For that aim, The aim is to synthesize water-borne nanocomposites by miniemulsion co-polymerization of MMA/BA/HEMA in the presence of MWCNTs in different concentrations. A minor amount of HEMA in the monomer mixture was added to further improve the interaction between the polymer and the MWCNTs.

Miniemulsion polymerization is a method suitable for synthesis of waterborne polymer composites, in which the polymerization is performed within the pre-formed nanosized monomer droplets dispersed in aqueous continuous phase. In miniemulsion, the monomer droplets are stabilized against coagulation using surfactant and against the diffusional degradation (Oswald ripening process) by co-surfactant.

The synthesis of polymer composites is still a challenging issue. The bottle-neck towards practical application of polymer composites is the difficulty to distribute the MWCNTs into the polymer matrix in a homogeneous manner without aggregation [3–5]. The interaction between the polymer and the MWCNTs is crucial to obtain a better distribution of MWCNTs within the polymer matrix and, therefore, the best performance of the nanocomposite [6]. For the improvement of the compatibility between MWCNTs and polymer matrix, in this work, a new dry strategy to disentangle the large MWCNTs bundles by air sonication was developed. This strategy is well described in Appendix III. After disentangling of the MWCNTs, polyvinylpyrrolidone (PVP) was used to obtain a stable aqueous dispersion of MWCNTs in water.

4.2 EXPERIMENTAL

4.2.1 MATERIALS

The materials used throughout this study are given in Appendix I.

4.2.2 POLYMERIZATIONS

4.2.2.1 MWCNTs PRE-TREATMENT AND WATER DISPERSIONS

MWCNTs were pre-treated by sonication in air. Ultrasound was applied for 1.5 h at 70% of power output and 50% duty cycle under magnetic stirring (200 rpm). More details about this procedure are well described in Appendix III.

The aqueous dispersions of MWCNTs used in composite preparation were prepared by dispersing the treated MWCNTs (max. 0.3 g) in water (50.5 g) in the presence of

MINIEMULSION POLYMERIZATION

polyvinyl pyrrolidone (PVP) (3g) and sonicated for 10 min (70% of power output and 50% duty cycle).

4.2.2.2 MINIEMULSION POLYMERIZATIONS

Miniemulsion polymerization was carried out at 20% of the solids content. The aqueous phase was composed of water and 2% wt of SDS surfactant. The organic phase was composed of a monomer mixture of MMA/BA/HEMA/SA with 47.6/47.6/0.96/3.84 wt%, in which MMA/BA/HEMA are the main monomers and, SA is a co-stabilizer to prevent the Oswald ripening process. Both phases were stirred separately for 15 minutes at 250 rpm, then mixed and stirred for 15 minutes at 300 rpm, and finally sonicated under magnetic stirring for 15 min at 80% power output and 50% duty cycle. Sonication was carried out in an ice bath to avoid overheating. After miniemulsion preparation, it was mixed under stirring (250 rpm, 15 min) with different amounts the aqueous dispersion of PVP stabilized MWCNTs (0.25, 0.5, 0.75, and 1.0 wt % with respect to monomers).

After that, the miniemulsion was placed into their respective setup (MWH or CH) and polymerized in batch at 70°C for 1.5 hours, under a nitrogen atmosphere using KPS as initiator, which was added as a shot.

Characteristics of conventional heating and microwave setups are described in detail in Appendix I. The reaction conditions for the different polymerizations performed in this study are summarized in Table 4.1.

It is worth mentioning that **all experiments were carried out by duplicate** to ensure the reproducibility of results.

Table 4.1. Reaction formulations for different copolymerizations performed under conventional and microwave heating with various MWCNTs amount.

Exp.	Heating method	Monomer mixture	MWCNTs (%)	Reaction temperature and time
1	CH	MMA/BA/HEMA	0	70°C/1.5 h
2			0.25	
3			0.5	
4			0.75	
5			1	
7	MWH	MMA/BA/HEMA	0	
8			0.25	
9			0.5	
10			0.75	
11			1	

4.2.3 CHARACTERIZATIONS

The monomer conversion was followed by gravimetry. Latex stability was studied by measuring light backscattered from the dispersions using a Turbiscan Lab expert apparatus. Particle size was measured by dynamic light scattering (DLS, Zetasizer Nano from Malvern Instruments). An insoluble fraction in tetrahydrofuran (THF) of the composite (gel content) was determined by the soxhlet extraction.

Films from the hybrid latexes were cast on Teflon molds and dried in a constant climate chamber (Espec Bench SH-641) at 25°C and 80% of relative humidity for five days. Fractured composite films were prepared under liquid nitrogen for SEM imaging, which was performed on Hitachi S-48000 and TEM on Jeol TM-1400. Differential scanning calorimetry (DSC, TA instrument Q1000), measurements, and the viscoelastic properties of the films were determined in a dynamic mechanical

MINIEMULSION POLYMERIZATION

thermal analyser (DMTA, Triton 2000 DMA) were done. The electrical conductivity of the films was measured using a four-point probe (Digital Lock-In, SR850), the absolute molar mass distribution was determined by size exclusion chromatography with a multi angle light scattering detector (SEC/MALS).

More details about the methodology and characteristics of all equipment used are described in Appendix I.

4.3 RESULTS AND DISCUSSIONS

4.3.1 TEMPERATURE PROFILES

The temperature profiles for all polymerization reactions are presented in Figures 4.1. The polymerization reactions was induced by charging the initiator into the reactor after the reaction temperature was reached in both reactors CH and MWH.

Due to the addition of the initiator solution as a shot at the beginning of the reaction, a pick of a decreasing temperature for 2-4 degrees appeared in the first ~3 minutes, observed only for CH reactions. Five minutes later, for CH reactions, the temperature increased above 70°C due to the exothermic polymerization reaction for 2 to 6 degrees, whereas, for MWH, this temperature increment was not higher than 2 degrees. Polymerization with 0.25% MWCNTs presents fewer differences in temperature between CH and MWH than all other reaction systems.

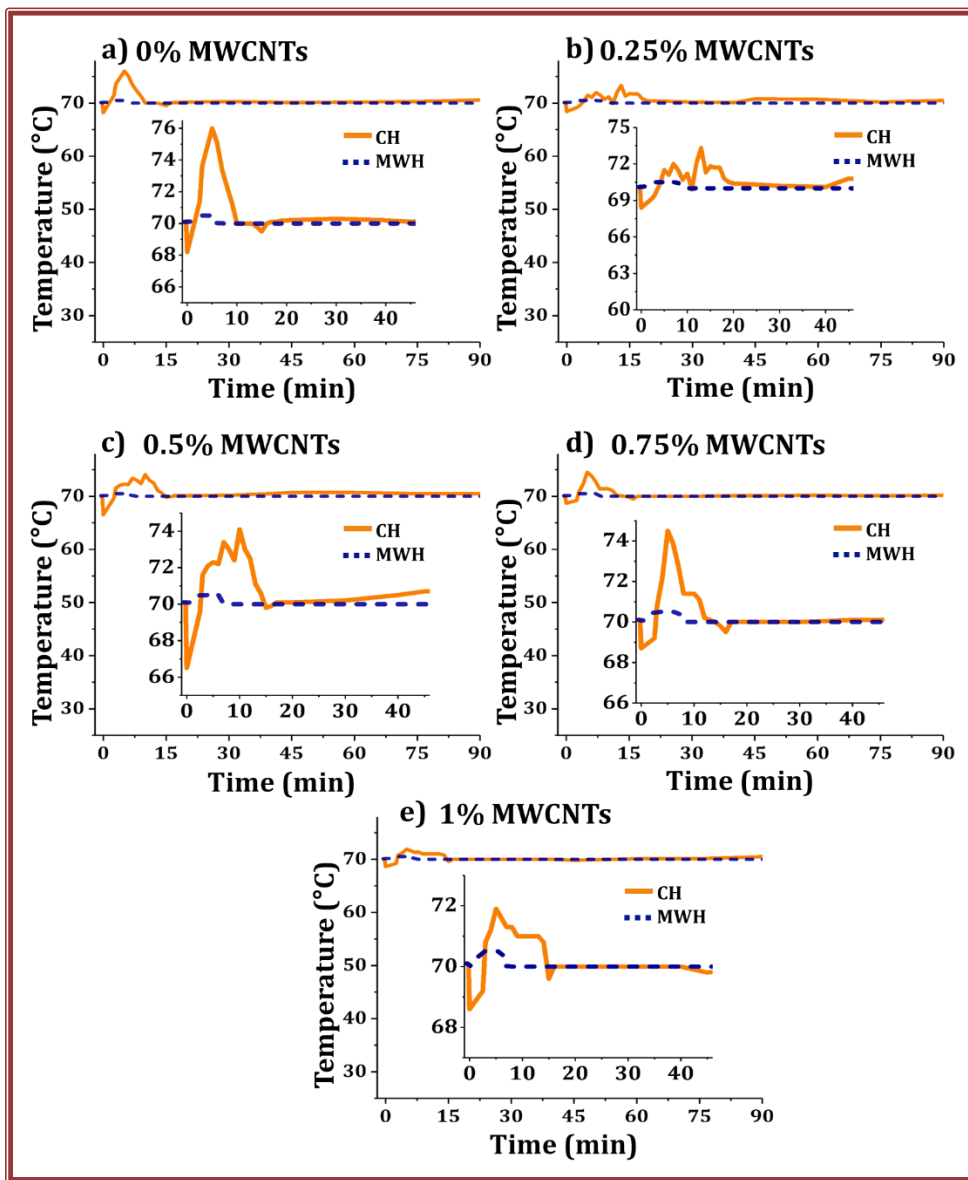


Figure 4.1. Comparison of the temperature profiles of CH and MWH assisted polymerization reaction of MMA/BA/HEMA using different amount of MWCNTs: **a) 0% MWCNTs, b) 0.25% MWCNTs, c) 0.5% MWCNTs, d) 0.75% MWCNTs, and e) 1% MWCNTs.** Insets: enlarged initial reaction region.

4.3.2 POLYMERIZATION KINETICS AND POLYMER MICROSTRUCTURE

The kinetics of the miniemulsion polymerizations carried out with the different amount of MWCNTs, performed under CH and MWH are shown in Figure 4.2. The characteristics of the produced latexes are presented in Table 4.2.

For all cases, final monomer conversion yields between 96 to 100%, achieved in 30 min for CH reactions and ~45 min for MWH reactions. The polymerization rate was slightly higher for CH than MWH in the initial reaction period, with the exception of the formulation of 0.25% MWCNTs for which MWH reaction was slightly faster than CH. This may be due to the very similar temperature profiles of the 0.25% MWCNT CH and MWH reactions (Figure 4.1-b). The observed faster CH reactions in all other investigated systems may be due to the important temperature increase observed in the CH reactor that likely induced faster initiator decomposition and radicals creation.

The most important difference in monomer conversion was noticed for the system without MWCNTs, for which the temperature difference in the first 15 min between CH and MWH reactor is the highest (6°C).

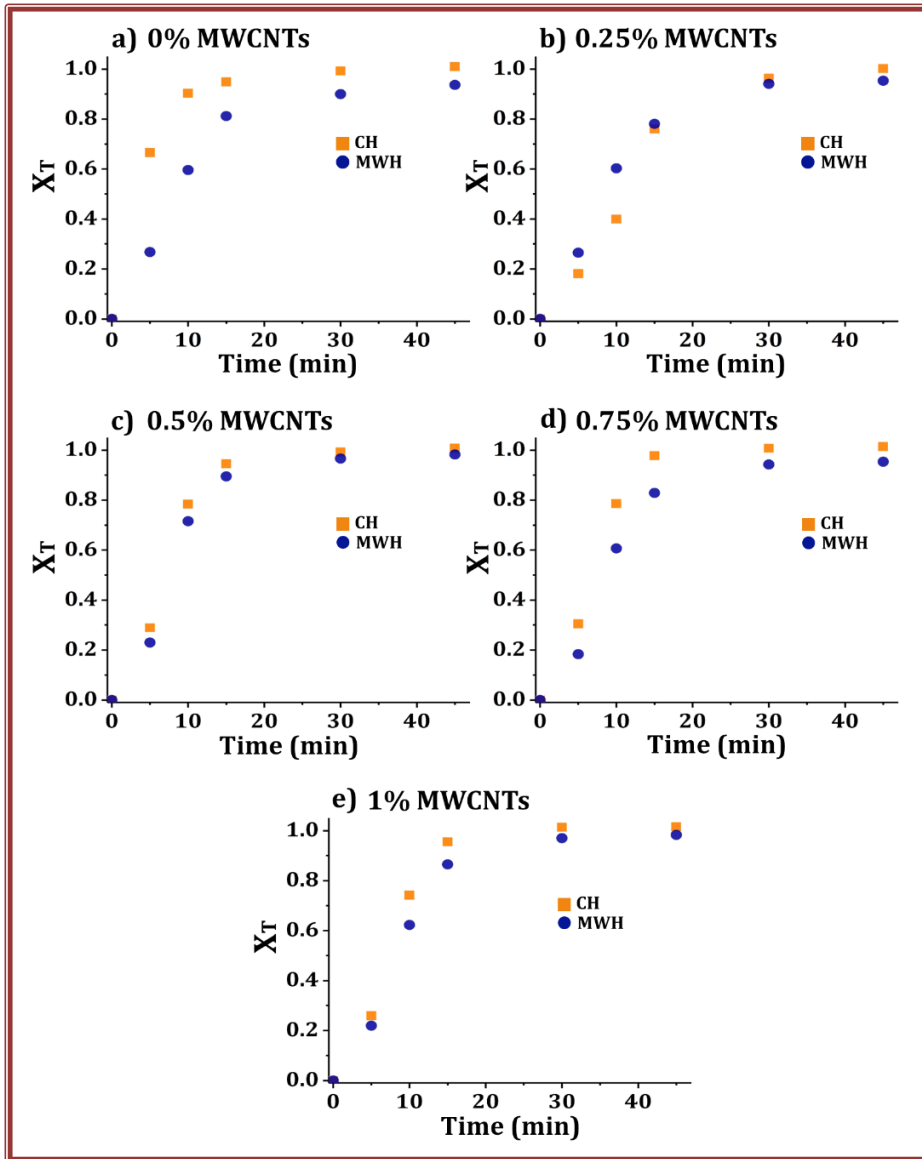


Figure 4.2. Comparison of the time evolution of conversion of MMA/BA/HEMA using different amount of MWCNTs: a) 0% MWCNTs, b) 0.25% MWCNTs, c) 0.5% MWCNTs, d) 0.75% MWCNTs, and e) 1% MWCNTs. Under CH and MWH.

MINIEMULSION POLYMERIZATION

In Appendix II, Figure 4.II.1a, the monomer conversion of all reactions performed in CH reactor, whereas in Figure 4.II.1b the same for MW reactor are shown. It may be observed that the addition of MWCNTs affected the reaction rate in CH heating reactor. The MWCNTs loading did not affect it, except for the lowest amount of 0.25% MWCNTs, for which the reaction is slowest. This effect is likely due to the lower temperature than for the other reactions, in which the important increase of temperature was noticed. In the case of MWH (Figure 4.II.-b, Appendix II), the addition of MWCNTs and their loading did not affect the polymerization rate.

Table 4.2 presents the characteristics of the miniemulsion and the corresponding in situ latexes prepared with MWCNTs.

Table 4.2. Characteristics of latexes produced by MMA/BA/HEMA copolymerization using different amounts of MWCNTs.

MWCNTs (wt%)	d_p (nm)		N_p (number/L)		*Gel (%)	
	CH	MWH	CH	MWH	CH	MWH
0	66	86	1.24×10^{18}	5.32×10^{17}	0	0
0.25	98	95	3.83×10^{17}	3.89×10^{17}	21	0
0.5	98	98	3.85×10^{17}	3.84×10^{17}	30	0
0.75	98	96	3.79×10^{17}	3.81×10^{17}	45	0
1	97	97	3.96×10^{17}	4.04×10^{17}	85	0

The final particle diameters (d_p) were not affected by the heating method nor by MWCNTs loading (Table 4.2). This suggests that the number of polymer particles was controlled by the available amount of surfactant, which was independent on the MWCNTs concentration for both heating methods. As well, the number of particles (Table 4.2) was not affected by the heating method and by the MWCNTs increased amount.

To add a bit of light to this issue, the number of particles was calculated in both systems and the results are presented in Figures 4.3 to 4.7, where the evolution of the particle size distribution of particles during the miniemulsion polymerization in the presence of different MWCNTs amounts is presented. It can be observed that most of the particles for CH experiments were formed by secondary nucleation. This effect is likely due to the combined effect of the presence of a highly water-soluble monomer (HEMA) that promoted the formation of oligomers in the aqueous phase and the large droplet size that reduced the total surface area of the droplets and consequently their ability to capture oligoradicals from the aqueous phase. For MWH reactions, the secondary nucleation is significantly lower, where the particle size distribution during the polymerization observed in the first 10 minutes of the reaction presents narrower particle distribution than observed in CH.

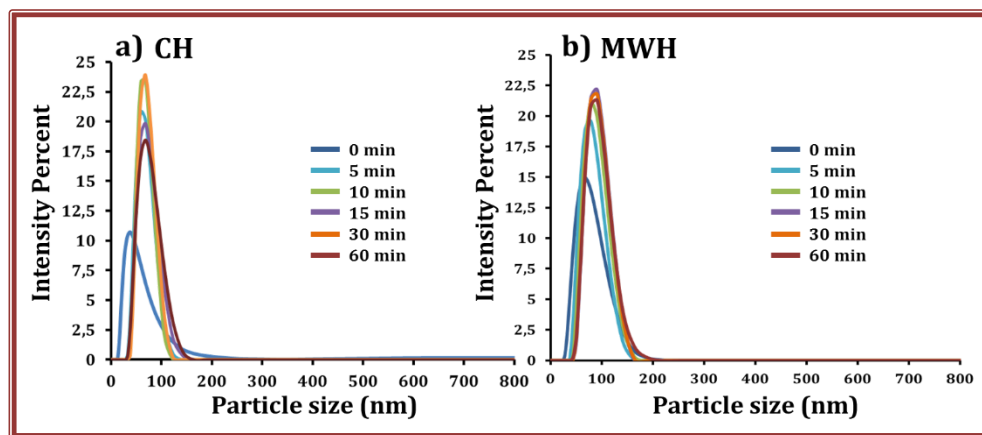


Figure 4.3. The **particle size distribution** for miniemulsion polymerization in the presence of **0% MWCNTs** at different reaction times by a) CH and, b) MWH.

MINIEMULSION POLYMERIZATION

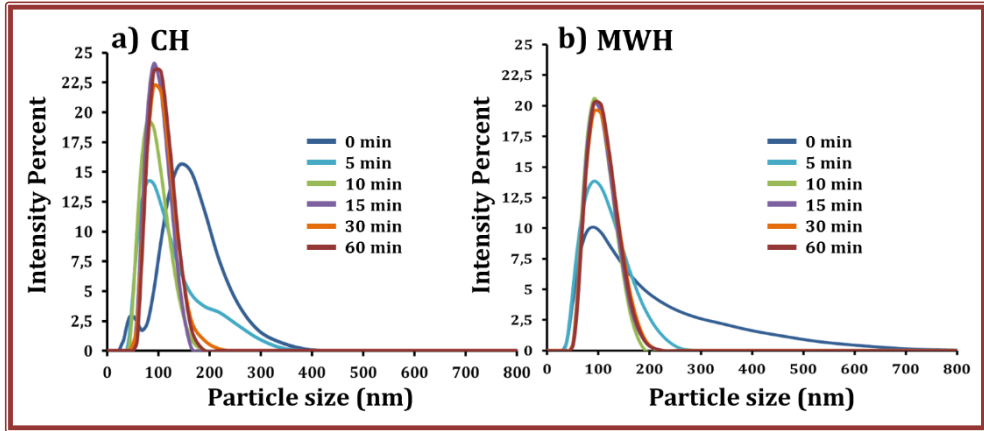


Figure 4.4. The **particle size distribution** for miniemulsion polymerization in the presence of **0.25% MWCNTs** at different reaction times by a) CH and, b) MWH.

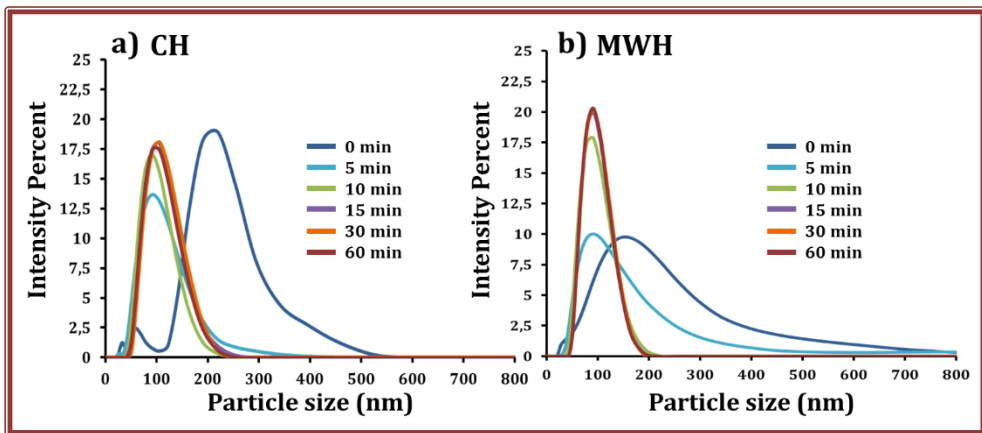


Figure 4.5. The **particle size distribution** for miniemulsion polymerization in the presence of **0.5% MWCNTs** at different reaction times by a) CH and, b) MWH.

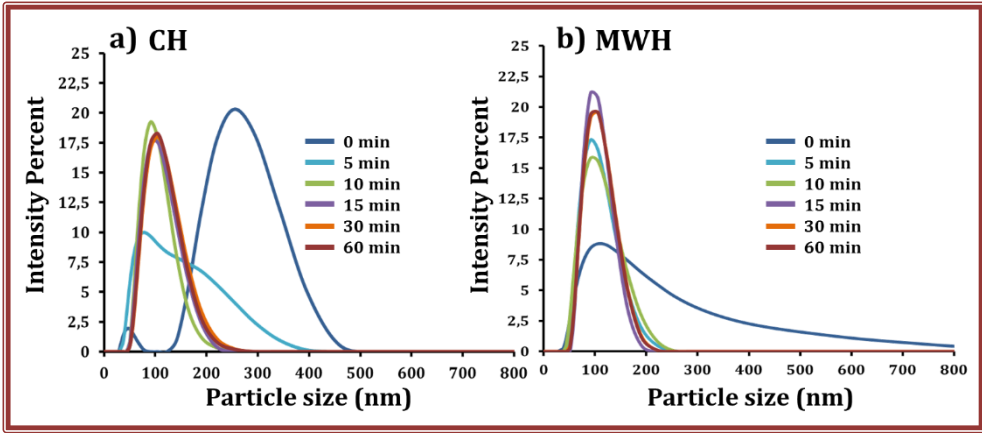


Figure 4.6. The **particle size distribution** for miniemulsion polymerization in the presence of **0.75% MWCNTs** at different reaction times by a) CH and, b) MWH.

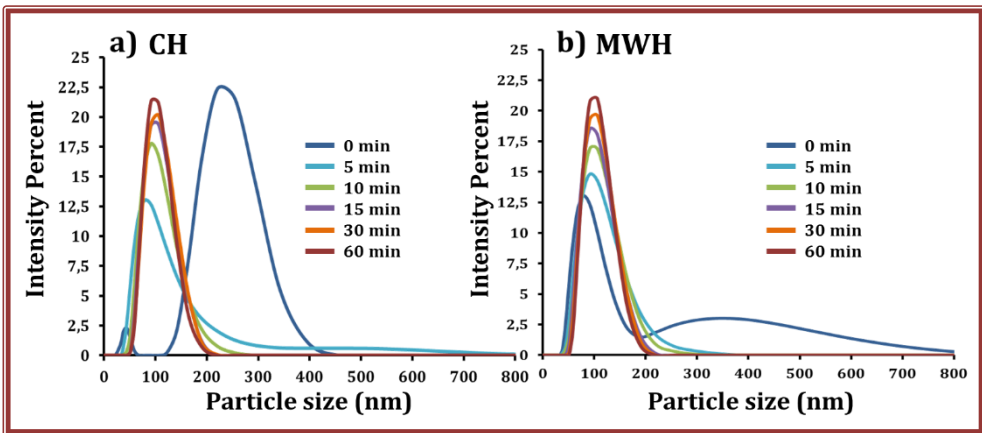


Figure 4.7. The **particle size distribution** for miniemulsion polymerization in the presence of **1% MWCNTs** at different reaction times by a) CH and, b) MWH.

MINIEMULSION POLYMERIZATION

The polymer and composite microstructures were determined by mean of gel content (the insoluble polymer fraction in THF) and molar mass of the soluble fraction. The gel fraction of all the materials is shown in Table 4.2. For the reactions with 0% MWCNTs, no gel was found for both CH and MWH, in agreement with previous results [7] for the monomer composition used. In the case of CH reactions, the gel increased with the concentration of MWCNTs, reaching values as high as 85% (1% MWCNTs). However, for MWH reactions, no gel was formed. In both cases (CH and MWH), it is worth pointing out that this fraction was measured in films, not in individual particles.

In the case of CH experiments, the increase in the gel fraction with addition and increase of MWCNTs load indicates highly cross-linked polymer-MWCNT composite film formation. The cross-linking might happen by grafting of the polymer chains onto the surface of MWCNTs, as already shown to happen in the case of emulsion polymerization of styrene initiated with KPS in the presence of MWCNTs [8]. According to this work, the initiator radicals created from KPS in the aqueous phase are able to break the C=C double bond in the graphic network of CNT, creating a radical that starts the polymerization with the monomer dissolved in water. Therefore a “grafting from” occurred resulting in highly crosslinked structures.

For MWH reactions, the cross-linking polymer-MWCNT did not occur, which means that the reaction proceeded differently. Probably, it may be related with the highly MW absorbing nature of MWCNT that results in their overheating and acting as hot-spots [1,2]. In such conditions, the fact that no cross-linked structure was created indicates that the initiator radicals did not create MWCNT C-centred radical. It has been demonstrated that in water under MW irradiation in presence of activated carbon creates abundant amount of OH radicals [9]. We think that in the aqueous phase of miniemulsion, where the MWCNT are placed, there are OH radicals created that induced MWCNT surface modification. The MWCNTs are highly MW adsorbing species [10], so in their presence the heating of the reaction system is through

convection from MWCNT towards the miniemulsion. In such conditions likely the OH modification of the MWCNT proceed preferentially over the C-centered radical creation.

The comparison of the molar mass distribution and molecular weight of the soluble part of the polymer in THF is presented in Figure 4.8 and Table 4.3. Where the molecular weight, and polydispersity is always higher for polymer performed under MWH than CH. The addition of MWCNTs reduced the molecular weight due to

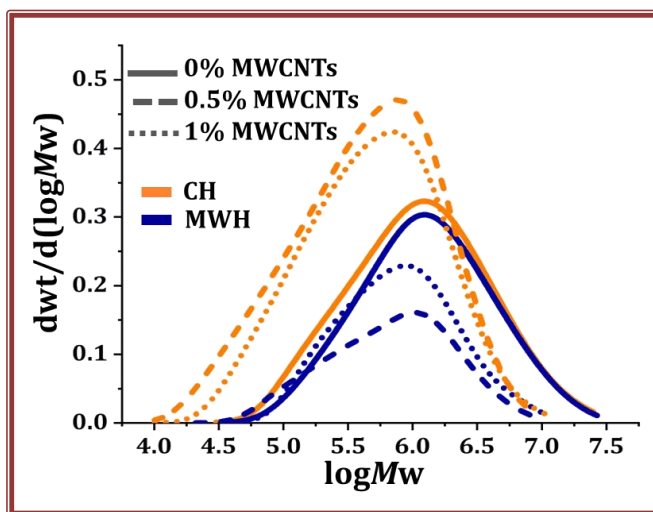


Figure 4.8. Molecular weight distribution between CH and MWH polymerization of 0% MWCNTs.

MINIEMULSION POLYMERIZATION

Table 4.3. Molar masses for the soluble polymer in THF for MMA/BA/HEMA copolymerization using different amounts of MWCNTs by both heating methods.

nanotubos	CH (peso molecular en kDa)		MWH peso molecular kDa	
	Mw	PDI	Mw	PDI
0%	2157	3.7	2333	3.4
0.25	---	---	1075	2.4
0.5	880.7	4.4	1115	2.9
0.75	---	---	1103	2.4
1	934.9	3.7	1215	2.4

4.3.3 PROPERTIES OF POLYMER AND COMPOSITE FILMS

Thermal and mechanical properties as well as the morphology were studied for the neat polymer and composites containing 0.5% and 1% MWCNTs. In Figure II.4.3 (Appendix II) the pictures of the studied films are shown.

The morphology of the composite films for the cross-section was studied by SEM, and the results are presented in Figure 4.9 for 0.5% and 1% MWCNT loadings by both heating methods. In the images, white/grey structures represent the MWCNTs distributed in the black polymer matrix. Comparing Figures 4.9 a and c, for 0.5% MWCNTs, a difference in the morphology may be observed. It seems that the MWCNTs in CH film are more rigid (Figure 4.9a) than in MWH film (Figure 4.9c), in which the nanotubes were more curved, encapsulating polymeric areas. It may be related to the type of interaction established between both phases, as likely the covalent bonding decreases the mobility of the MWCNTs.

1% MWCNT-discussion

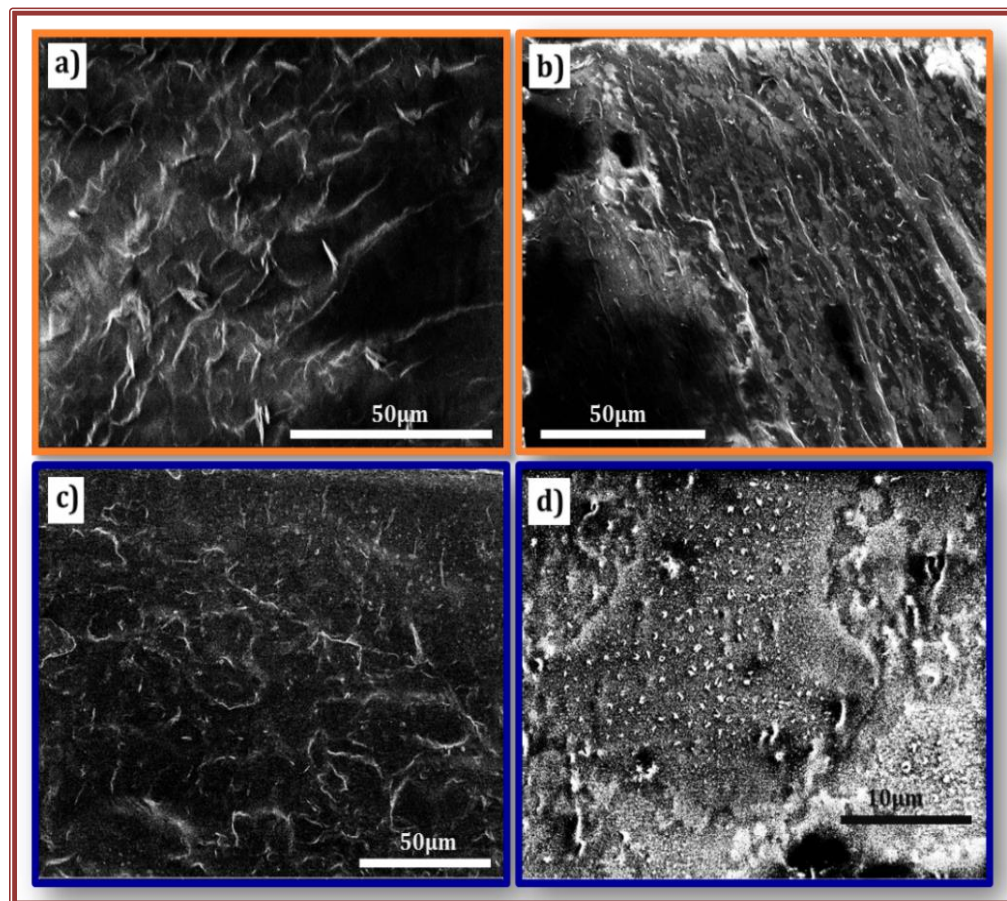


Figure 4.9. SEM images for polymer films fractured surface of MMA/BA/HEMA copolymer, using different amounts of MWCNTs; by CH: a) 0.5% MWCNTs; b) 1% MWCNTs and, by MWH: c) 0.5% MWCNTs; d) 1% MWCNTs.

MINIEMULSION POLYMERIZATION

Table 4.4 shows the glass transition temperature (T_g) of the prepared polymer films by both heating methods, measured by DSC and DMTA.

Table 4.4. The glass transition temperature (T_g) of the prepared coatings from MMA/BA/HEMA/SA and MWCNTs hybrids. Note: * is an additional T_g founded in the range of T_{g2} for polymer film performed by CH method.

MWCNTs (wt%)	Glass transition temperature T_g (°C) From DSC						T_g (°C) From DMTA	
	CH			MWH			CH	MWH
	T_{g1} region	T_{g2} region	T_{g3} region	T_{g1} region	T_{g2} region	T_{g3} region	T_g	T_g
0	-70	-40 to 57	93	-70	-40 to 50	93	38.5	41.5
0.5	-71	-45 to 75 ~50*	90	-69	-31 to 64	90	43.7	42.4
1	-70	-49 to 75 ~50*	90	-72	-49 to 54	90	41.2	44.6

The DSC results show the presence of few T_g regions. The first T_{g1} region was close to -70°C , indicating the formation of co-polymer of BA ($T_g=52.1^\circ\text{C}$) and SA ($T_g=-111^\circ\text{C}$) in the case of neat polymer and the composite films. In the T_{g2} region, a broad peak between -40°C and $50-75^\circ\text{C}$ appears in all polymer composites obtained by both heating methods. This region is narrower for the neat polymer, indicating the presence of composite phase in the films containing MWCNTs. This wide transition is a result of the heterogeneous composition of the polymer chains formed in the batch polymerization of monomers with different reactivity ratios ($r_{\text{MMA}} = 2.02 \pm 0.36$, $r_{\text{BA}} = 0.26 \pm 0.14$) [11]. This yield co-polymer chains reach in MMA-units (MMA- $T_g=100.1^\circ\text{C}$)[12,13] at the beginning of the process, and co-polymer chains reach in BA-units at the reaction end (BA- $T_g=-52.1^\circ\text{C}$)[12,13]. The T_{g3} region appeared at 90°C that corresponds to MMA-rich co-polymer chains. In the case of hybrids obtained under CH, an additional T_g was found at about 50°C . The lack of this transition within

the composite obtained under MWH indicates that it may be related to the grafted polymer onto MWCNT.

DMTA results for the CH and MWH polymer composites and the neat polymer are presented in Figure 4.10. Figure 4.10a shows comparison of the storage modulus, whereas $\text{Tan}\delta$ are compared in Figure 4.10b, from which the determined T_g 's are shown in Table 4.10. These T_g 's differ from the T_g 's determined by DSC, because of different principles of measurements of both techniques. The T_g increased when MWCNT were added to the polymers and when their content increased. This is due to the presence of MWCNTs in the polymer matrix, which acts as stiff cross-points and delays segmental oscillations of the polymer matrix, so more thermal energy is needed to excite the relaxational motions of the chains. This increase demonstrates excellent interactions between polymer and MWCNTs in both CH and MWH composites.

The storage modulus (Figure 4.10a) presents a clear trend that corresponds to the addition of MWCTs. The MWH films present a slightly higher storage modulus than CH films, which is especially obvious in the rubbery region, where the MW composite films have high storage modulus at temperatures higher than 80°C. This is rather strange if the gel fractions (crosslinking) is taken into account and indicates that there is something in the structures that we were not able to observe to now. Figure 4.10b shows that there are no significant differences between the MWH and CH films. The decrease in the height of the peak $\text{Tan}\delta$ with increasing MWCNTs amounts reveals that the amount of the mobile phase in the composites is fewer when the percentage of MWCNTs is higher. The comparison for MWH and CH DMTA measurements for each sample are presented sepately in Appendix II Figure II.4.4

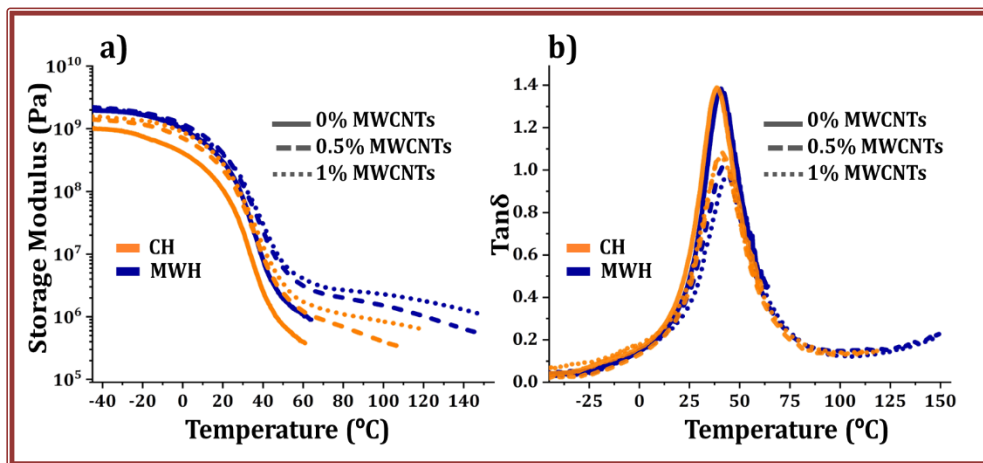


Figure 4.10. DMTA results of polymer and composite films containing different MWCNTs amounts: (a) Storage Modulus; (b) $\text{Tan}\delta$.

To get additional information on the structure of the composites, the solubility test of the polymer films in THF solvent was performed. The small pieces of the composite films obtained under CH and MWH with 1% MWCNT were placed in the solvent, and their behaviour in time was studied. The photos of this study are presented in Figure 4.11, in which, within an orange frames the photos of CH composite film, whereas in the blue frames the photos of MWH composite film are shown.

The behaviour of the MWH and CH films is completely different. As expected, CH film, due to very high gel content, presented behaviour of highly cross-linked film. Namely, when the cross-linked composite film is placed in solvent, it start swelling, and its volume increased substantially during the seven days. According to Figure 4.11, the volume of the films was increased at least 10 folds. This result demonstrates the cross-linked structure of CH composite film containing 1% MWCNT. The large volume increase indicates that there is a lot of space between the cross-linking points that is filled with solvent.

On the other hand, MWH composite film did not present swelling behaviour, but neither it was solubilized in THF. What happens is that a great part of the polymer was dissolved in the THF, whereas some composite hair-like interconnected structures were observed. Probably this interconnected structures are made of MWCNTs that were strongly interacting with some of the polymer chains. This interaction obviously is not covalent, as, during Soxhlet extraction, no insoluble fraction was determined, thus, they were solubilized in THF at 70°C. We believe that strong H-bonding occurs between the polymer chains containing OH (from HEMA monomer), with the oxygen functionalities presented on MWCNTs (OH or COOH). This is further supported by the possible functionalization of MWCNT under MWH by OH functionality.

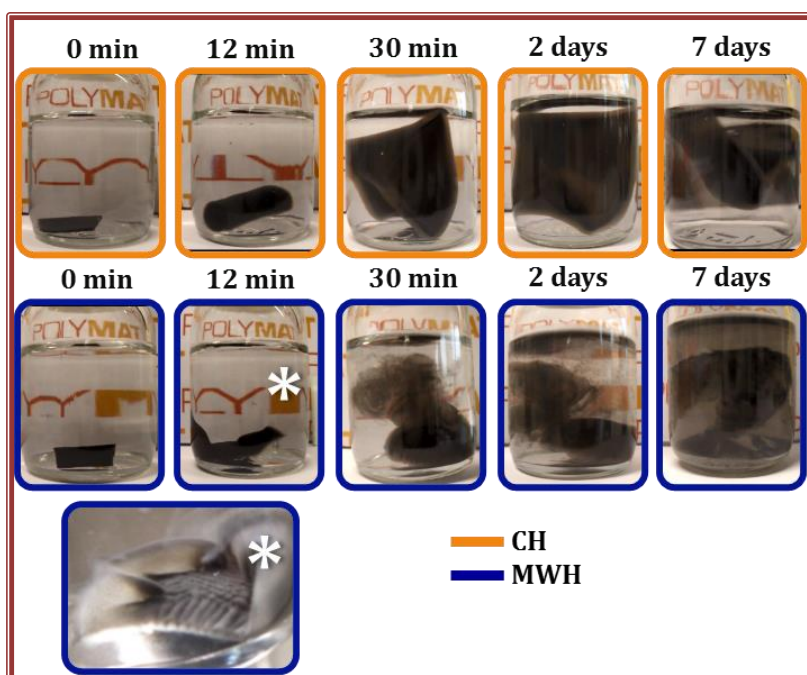


Figure 4.11. Images for **polymer films** of MMA/BA/HEMA co-polymer and **1% of MWCNTs**, into THF solvent during a week, Orange frame of the photos correspond to CH method and blue frame for MWH method.

4.3.4 LATEX STABILITY AFTER TWO YEARS

After two years of storage of the composite latexes, their shelf stability was checked. As it may be observed in Figure 4.12 for the composite latex containing 1% MWCNT, the CH latex was pretty much separated into two-phase: on the bottom, MWCNT rich phase, and on the surface neat polymer. This is probably related to the heterogeneity of the structures presented in CH composites: neat polymer, grafted polymer-MWCNTs and neat MWCNTs. However, MWH latex presented only one phase, showing incredible stability. Likely in the MWH composite the both phases polymer and MWCNTs are uniformly related by H-bonding forming colloiddally stable supramolecular structures.

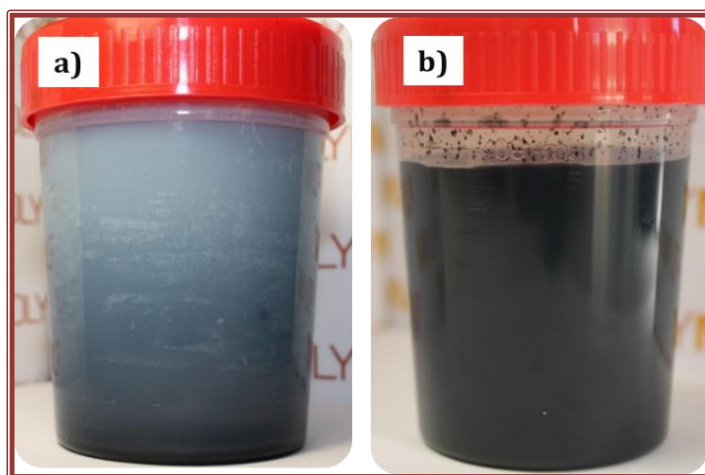


Figure 4.12. Images for **polymer latex's** with **1% of MWCNTs**, after two years of storage; **a) CH** synthesis and, **b) MWH** synthesis.

The distribution of different phases was checked by TEM imaging. In Figure 4.13 the CH latex is shown, presenting that in the top fraction (Figure 4.13 a) most of the particles are neat polymer, although some composite particles can be observed, too.

In Figure 4.13b and 4.13c, the fraction taken from the middle position of the vial shows that almost all particles are composite. Finally, the bottom fraction shown in Figure 4.13d presents a large aggregated structure, where the polymer particles tightly bonded by CNTs may be observed.

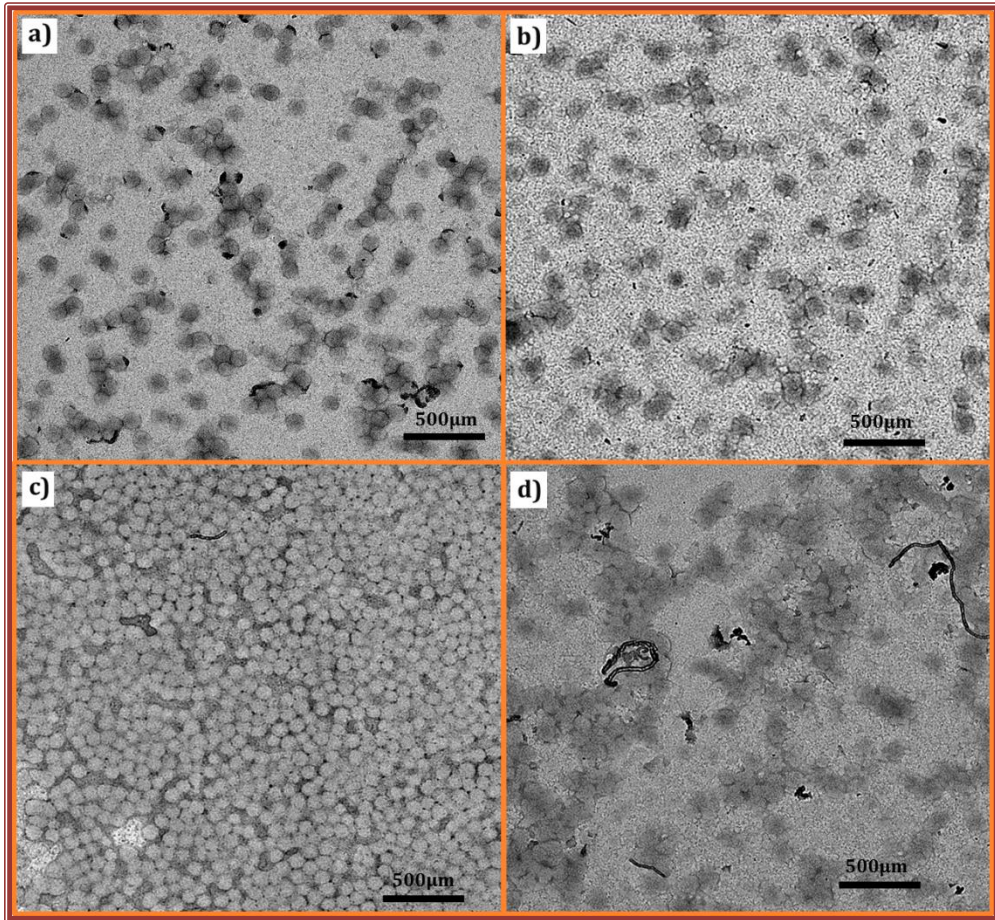


Figure 4.13. TEM images for polymer latex with 1% of MWCNTs synthesized by CH along the the bottle height (Figure 4.12) a) surface; b) middle diluted, c) middle concentrated; d) bottom.

MINIEMULSION POLYMERIZATION

Figure 4.14 reveals the distribution of different structures along the bottle (Figure 4.12b) of the MWH latex with 1% MWCNTs, determined by TEM imaging. A sample concentrated of the latex is presented in Figure 4.14a, where it is well noticed a homogeneous distribution of the polymer particle size, whereas Figures 4.14b, c, and d present the sample diluted at different locations through the sample. That almost all particles are composite, where the polymer particles are tightly bonded by MWCNTs may be observed.

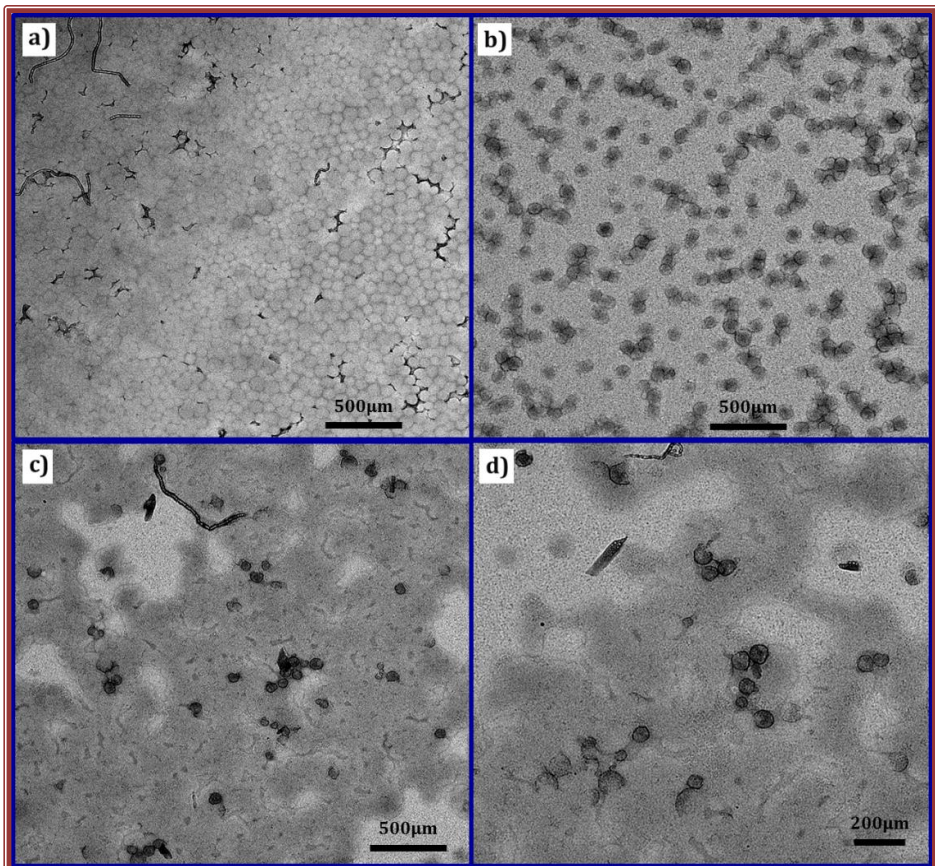


Figure 4.14. TEM images for polymer latex with 1% of MWCNTs synthesized by MWH from the middle of the bottle (Figure 4.12) **a) sample concentrated; b), c) and, d) sample diluted** at different locations through the sample.

4.3.5 MICROWAVE ENERGY CONSUMPTION

Table 4.5 shows the energy consumption for all reaction performed under MWH. It is clear that addition of MWCNTs in amount of 0.25% decreased the energy consumption, likely due to the high absorbance of the MWCNTs, their fast heating and transmitted heat to the reaction mixture. It has been already demonstrated that microwave absorbance of silicone oil was enhanced by 500 times with the addition of only 0.04 wt% CNT [10].

However, increasing the amount of MWCNT added in the reaction mixture, the energy consumption augmented, too. As the MWCNTs amount was increased, the differences in energy consumption between composites and the neat polymer are decreased. In the case of an experiment where 1% MWCNTs, the energy consumption was higher than the neat polymer.

If the MW-energy consumption is compared with the polymers performed in Chapter 3, when MMA/BA with 1% of KPS, the consumption was 3.9 kJ/mL in 200mL of the reaction mixture by 2 hours of reaction, thus if this value will divided by total time, it can say that 1.95 kJ/mL were consumed in one hour. Whereas for miniemulsion polymerization of MMA/BA with 0% and 1% of MWCNT the consumption per hour was 1.85 kJ/mL and 1.86 kJ/mL respectively. This means that at the same temperature reaction (70°C), miniemulsion polymerization technique could be save more MW-energy than emulsion, likely due to the more compartmentalization of the process.

MINIEMULSION POLYMERIZATION

Table 4.5. Microwave energy consumption (kJ) for all polymer composites using different amount of MWCNTs performed by MWH (200 mL reaction mixture, 1.5 h reaction).

MWCNTs (wt%)	MW-Energy (kJ)	MW-Energy (kJ/mL)
0	554.4	2.77
0.25	504.8	2.52
0.5	522.9	2.61
0.75	535.5	2.67
1	560.7	2.80

4.4 CONCLUSIONS

A reliable comparison of free-radical of CH and MWH assisted miniemulsion polymerization of MMA/BA/HEMA with the addition of the different amount of MWCNTs was reached by creating similar reaction temperature profiles.

It was found that, under similar reaction temperature profiles in both CH and MWH reactors, the polymerization rate was not significant, as well the number of particles and the final particle size, even with the addition of MWCNTs. In this polymer system, the use of KPS as initiator does not have any MW-effect in polymerization rate.

The molar mass between CH and MWH of the neat polymer was higher for MWH reaction than CH, due to...

The insoluble polymer fraction in THF was strongly increased with the addition of MWCNTs for CH reactions, attributed to the possible grafting between polymer chains onto MWCNTs, whereas polymers synthesized by MWH is likely that they do not present the insoluble polymer fraction. This was confirmed with polymer mechanical

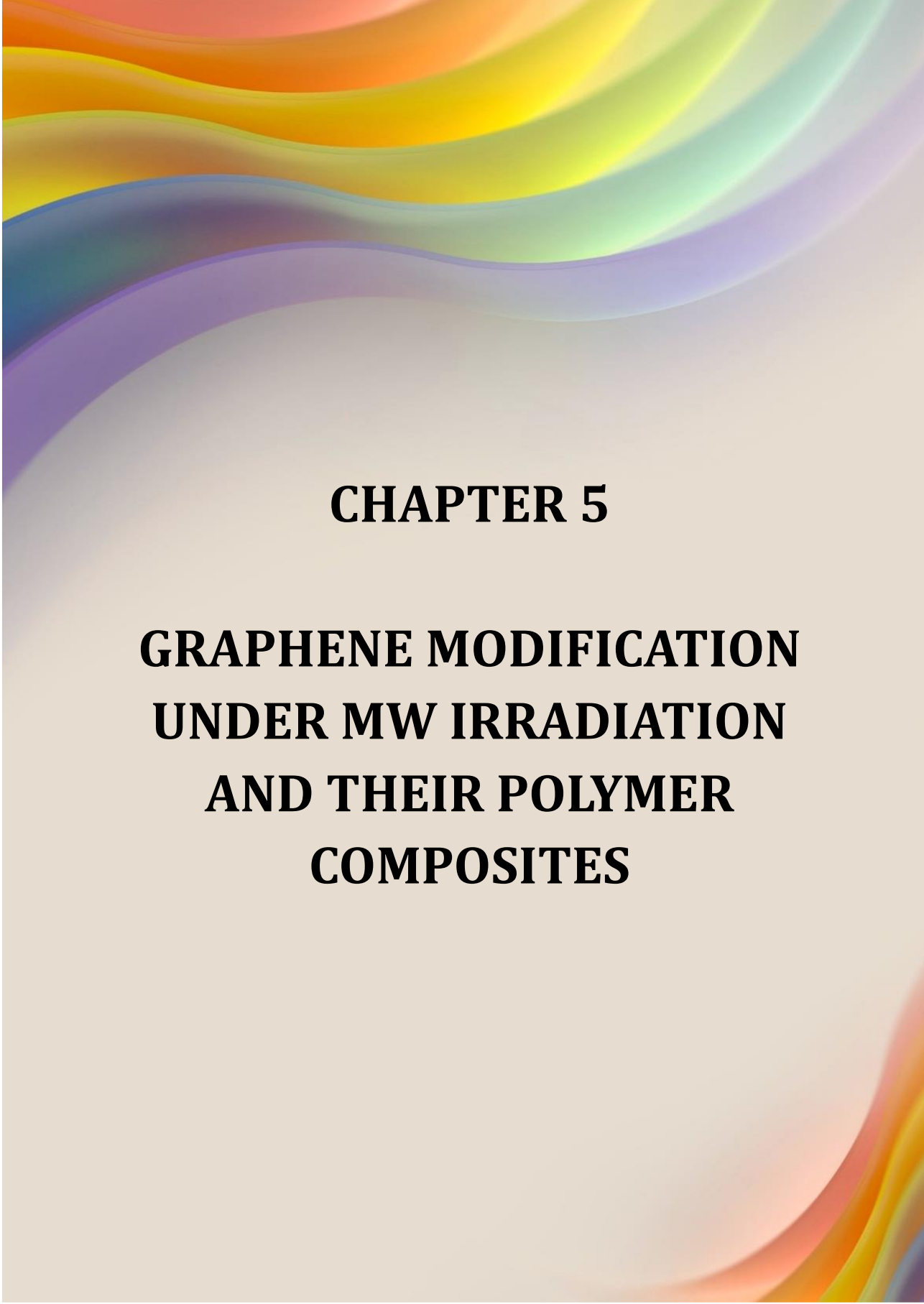
properties evaluated in DMTA where the reinforcement of the polymer was done with the addition of MWCNTs synthesized by both heating methods.

Additionally, the latex stability of the polymer composites after two years of storage was significantly different between both heating methods, probably due to the high cross-linked between the polymer and MWCNTs the latex synthesized under CH present less stability than the MWH-latex.

4.5 REFERENCES

- [1] E. Vázquez, M. Prato, Carbon nanotubes and microwaves: Interactions, responses, and applications, *ACS Nano*. (2009). doi:10.1021/nn901604j.
- [2] H.Y. Kim, J.W. Lee, H.M. Oh, K.J. Baeg, S. Jung, H.S. Yang, W. Lee, J.Y. Hwang, K.S. Kim, S.Y. Jeong, J.T. Han, M.S. Jeong, G.W. Lee, H.J. Jeong, Ultrafast Heating for Intrinsic Properties of Atomically Thin Two-Dimensional Materials on Plastic Substrates, *ACS Appl. Mater. Interfaces*. (2016). doi:10.1021/acsami.6b09677.
- [3] I.N. Seekkuarachchi, H. Kumazawa, Aggregation and disruption mechanisms of nanoparticulate aggregates. 2. Dispersion of aggregates using a motionless mixer, *Ind. Eng. Chem. Res.* (2008). doi:10.1021/ie0714955.
- [4] J.H. Bang, K.S. Suslick, Applications of ultrasound to the synthesis of nanostructured materials, *Adv. Mater.* (2010). doi:10.1002/adma.200904093.
- [5] J.S. Taurozzi, V.A. Hackley, M.R. Wiesner, Preparation of Nanoparticle Dispersions from Powdered Material Using Ultrasonic Disruption, *NIST Spec. Publ.* (2012).
- [6] M. Rahmat, P. Hubert, Carbon nanotube-polymer interactions in nanocomposites: A review, *Compos. Sci. Technol.* (2011). doi:10.1016/j.compscitech.2011.10.002.
- [7] I. González, J.M. Asua, J.R. Leiza, The role of methyl methacrylate on branching and gel formation in the emulsion copolymerization of BA/MMA, *Polymer*

- (Guildf). (2007). doi:10.1016/j.polymer.2007.03.015.
- [8] M.S.P. Shaffer, K. Koziol, Polystyrene grafted multi-walled carbon nanotubes, *Chem. Commun.* (2002). doi:10.1039/b205806p.
- [9] X. Quan, Y. Zhang, S. Chen, Y. Zhao, F. Yang, Generation of hydroxyl radical in aqueous solution by microwave energy using activated carbon as catalyst and its potential in removal of persistent organic substances, *J. Mol. Catal. A Chem.* (2007). doi:10.1016/j.molcata.2006.08.079.
- [10] K.R. Paton, A.H. Windle, Efficient microwave energy absorption by carbon nanotubes, *Carbon N. Y.* (2008). doi:10.1016/j.carbon.2008.08.001.
- [11] S.G. Roos, A.H.E. Müller, K. Matyjaszewski, Copolymerization of n-Butyl Acrylate with Methyl Methacrylate and PMMA Macromonomers: Comparison of Reactivity Ratios in Conventional and Atom Transfer Radical Copolymerization, *Macromolecules.* 32 (1999) 8331–8335. doi:10.1021/ma9819337.
- [12] M.N. Nguyen, Q.T. Pham, V.D. Le, T.B.V. Nguyen, C. Bressy, A. Margaillan, Synthesis and characterization of random and block-random diblock silylated terpolymers via RAFT polymerization, *Asian J. Chem.* (2018). doi:10.14233/ajchem.2018.21217.
- [13] M. Fernández-García, R. Cuervo-Rodriguez, E.L. Madruga, Glass transition temperatures of butyl acrylate-methyl methacrylate copolymers, *J. Polym. Sci. Part B Polym. Phys.* (1999). doi:10.1002/(SICI)1099-0488(19990901)37:17<2512::AID-POLB22>3.0.CO;2-2.



CHAPTER 5

GRAPHENE MODIFICATION UNDER MW IRRADIATION AND THEIR POLYMER COMPOSITES

5.1 INTRODUCTION

It is well known that carbon nanoparticles, such as graphene for example, could improve the mechanical and electrical properties when they are added into a polymer matrix [1–3]. The interaction between the polymer and graphene is crucial to obtain homogeneous distribution of the nanoparticles within the matrix and the best performance from nanocomposites. However, due to very high hydrophobicity of graphene, usually it is not compatible with the polymers, resulting in poor interactions and substantial aggregation of graphene. Surface functionalization of graphene is one of the ways to improve the interactions.

In Chapter 4, to obtain polymer nanocomposite with MWCNTs, colloidal water dispersion of the MWCNTs was a key point to obtain stable miniemulsion and subsequently a homogeneous distribution of MWCNTs within the polymer matrix. This process involved 3 steps, the first one was the air-sonication, then the physical functionalization using polyvinylpyrrolidone and finally the sonication process to ensure the water dispersion. As a result, the length of the MWCNTs was decreased within the nanocomposites.

In this chapter the main aim is to perform mild surface functionalization of graphene platelets under MWH taking the advantage of the mechanisms based on conduction heating (Joule heating), in which the motion of the electrons is induced by the electric field created under MW [4,5]. In this way localized superheating of the nanomaterials, acting as hot-spots could produce some MW-effects. When this process is performed in presence of some organic compound it is grafted onto the graphene surface. The surface modification of the CNT under MWH are well known [6–11], where different monomers like styrene [6,8], aniline [7,9,10], MMA [6,11], and PAN, GMA [9] were used. The authors claimed successful surface modification of the carbon nanomaterial by respective polymer chains that grown from the CNT surface. Up to our best knowledge, similar reactions with graphene have not been performed.

In this chapter, the surface modification of graphene under MWH was performed using acrylic acid (AA) and acrylamide (AM) in aqueous dispersion, in presence and absence of KPS initiator. During this procedure, the sonication step of graphene aqueous dispersion was eliminated, in order to avoid some graphene oxidation occurring due to ultrasound irradiation during sonication.

The surface modified graphene was dispersed in water and used during in-situ MWH initiated miniemulsion polymerization of MMA/BA/HEMA monomer mixture, using SDS and SA as surfactant and co-stabilizer, and KPS as initiator to prepare graphene/polymer waterborne composites.

5.2 EXPERIMENTAL

5.2.1 MATERIALS

The materials are given in Appendix I.

5.2.2 GRAPHENE MODIFICATION UNDER MWH

Graphene nano powder flakes were treated under MW irradiation in water and AA or AM, with and without initiator as potassium persulfate (KPS). First, graphene (0.4 g) was dispersed in water (196 g) or in aqueous solution of AA or AM (196 g water and 4 g monomer) under magnetic stirring (200 rpm) for 15 minutes. After that, the mixture was placed into MW reactor and heat-up at 70°C for 2 hours under a nitrogen atmosphere and stirring (250 rpm). The reactions were performed in presence and absence of KPS, added as a shot into the reactor, when 70°C was achieved. After this procedure, graphene was washed with double distilled water at least 7 times. It was characterized by Raman spectroscopy, transmission electron microscopy, and determination of water contact angle.

5.2.3 POLYMERIZATION

Miniemulsion polymerization was carried out at 20% of solid content in 200 mL total volume. The water phase was composed of water and 2%wt of SDS surfactant. The organic phase was composed of a monomer mixture of MMA/BA/HEMA/SA of 47.6/47.6/0.96/3.84 wt%; in which mixture SA was used as a co-stabilizer to prevent the Oswald ripening process. Both phases were stirred separately for 15 minutes at 250 rpm. Then, both phases were mixed and stirred for 15 minutes at 300 rpm. and this mixture was sonicated under magnetic stirring for 15 min at 80% power output and 50% duty cycle. Sonication was carried out in an ice bath to avoid overheating. After miniemulsion preparation, it was mixed under stirring (250 rpm, 30 min) with different surface-modified graphene water-dispersion (0.5 wt % with respect to monomers) using polyvinylpyrrolidone (PVP) to obtain a better water-dispersion.

After that, the complete mixture was placed into MW-reactor and polymerized in batch at 70°C for 2 hours, under a nitrogen atmosphere using KPS as an initiator (0.4 g) previously dissolved in water, which was added as a shot.

The reaction conditions for the different polymerizations performed in this study are summarized in Table 5.1. It is worth mentioning that **all experiments were carried out by duplicate** to ensure the reproducibility of the results.

Table 5.1. Reaction formulations for different copolymerizations performed under microwave heating with various modified graphene.

Exp.	Monomer mixture	Modified graphene (0.5 wt%)	Graphene acronym	Reaction temperature and time
1	MMA/BA/HEMA	Without graphene	B	70°C/2 h
2		Neat graphene	Gp	
3		MWH treated Graphene in water	GWt	
4		MWH treated Graphene by Acrylic Acid	GAc	
5		MWH treated Graphene by Acrylamide	GAm	
6		MWH treated Graphene by Acrylic Acid and KPS	GAc-KPS	
7		MWH treated Graphene MWH treated Acrylamide and KPS	GAm-KPS	

5.2.4 CHARACTERIZATIONS

Polymer conversions was followed gravimetrically. Particle size was measured by dynamic light scattering (DLS). An insoluble fraction in tetrahydrofuran (THF) of the composite (gel content) was determined by the Soxhlet extraction, molar masse of the soluble part in THF were measured in GPC. Films from the hybrid latexes were cast in Teflon molds and dried in a constant climate chamber (Espec Bench SH-641) at 25°C and 80% of relative humidity for five days. Differential scanning calorimetry (DSC) measurements and the viscoelastic properties of the films were determined in a dynamic mechanical thermal analyser (DMTA), and stress-strain by the tensile test

were done. More details about the methodology and characteristics of all equipment used are described in Appendix I.

5.3 RESULTS AND DISCUSSIONS

5.3.1 SURFACE GRAPHENE MODIFICATION

In order to check the nature of the changes induced by the MWH treatment of the graphene platelets, the dried samples were analysed by Raman spectroscopy. The Raman spectra of the neat graphene and the treated graphene under MWH are presented in Figure 5.1. Three peaks were observed in the spectra: G peak at about 1582 cm^{-1} assigned to sp^2 hybridized carbon atoms in the aromatic structure, D peak at about 1350 cm^{-1} assigned to the structural defects coming from the presence of sp^3 hybridized carbons within the graphene network, and 2D peak centred at 2700 cm^{-1} , which is the second overtone of the D peak [12]. Table 5.2 presents the ratios between peaks D/G and 2D/G, which should give an idea about the chemical change occurred during the graphene MW treatment. For all treated graphene, D/G ratio increased, which indicates creation of defects in the graphene structure during the treatment, probably due to introduction of functional groups. The effect is stronger in presence of monomers, and the highest modification obviously occurred in presence of monomers and initiator. On the other hand, the 2D/G ratio decreased slightly in the treated graphene, denoting enhanced exfoliation of the graphene platelets during the treatment. This effect is the highest during simple treatment of graphene in water, which show that using MWH treatment of graphene can modified it.

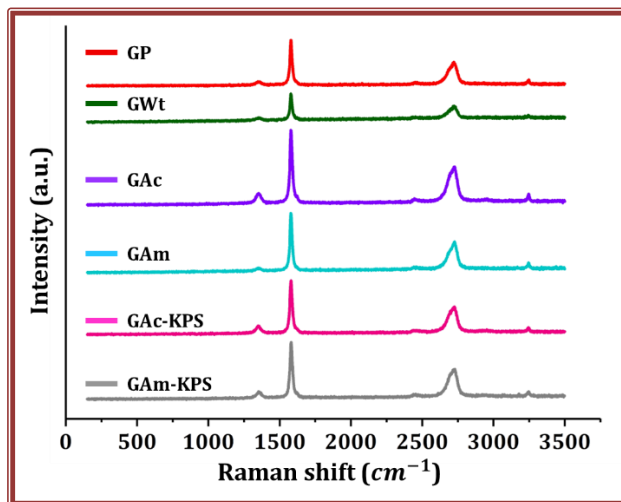


Figure 5.1. Raman spectra of neat and treated graphene under MWH.

Table 5.2. Intensity ratios of characteristic Raman peaks of the neat and treated graphene under MWH.

Experiment	D/G	2D/G
Gp	0.09	0.50
GWt	0.12	0.32
GAc	0.15	0.54
GAm	0.06	0.48
GAc-KPS	0.14	0.47
GAm-KPS	0.12	0.48

GRAPHENE MODIFICATION UNDER MW IRRADIATION AND THEIR POLYMER COMPOSITES

To confirm further the surface modification, the water contact angles of the dried samples were measured and shown in Figure 5.2. The neat graphene present the higher contact angle around 147° , which dropped to 134° when it was treated in water under MWH, which is accordance with the Raman results that the hydrophobicity of graphene was slightly reduced. The highest water contact angle between the treated graphene was observed for GAm 137° , again in accordance with Raman spectra results, where almost no changes were observed with respect to the neat graphene. The both graphene treated by AA present much lower contact angle, on one hand due to the hydrophilicity of AA and on the other hand due to the extent of modification, which likely was the highest in presence of KPS for both monomers. MWH.

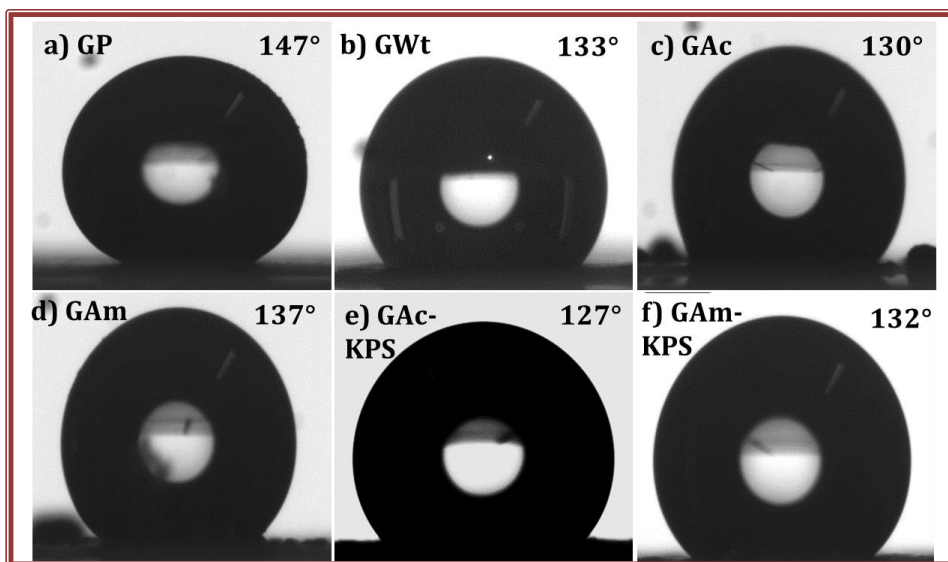


Figure 5.2. Contact angle of the neat and modified graphene samples under MWH.

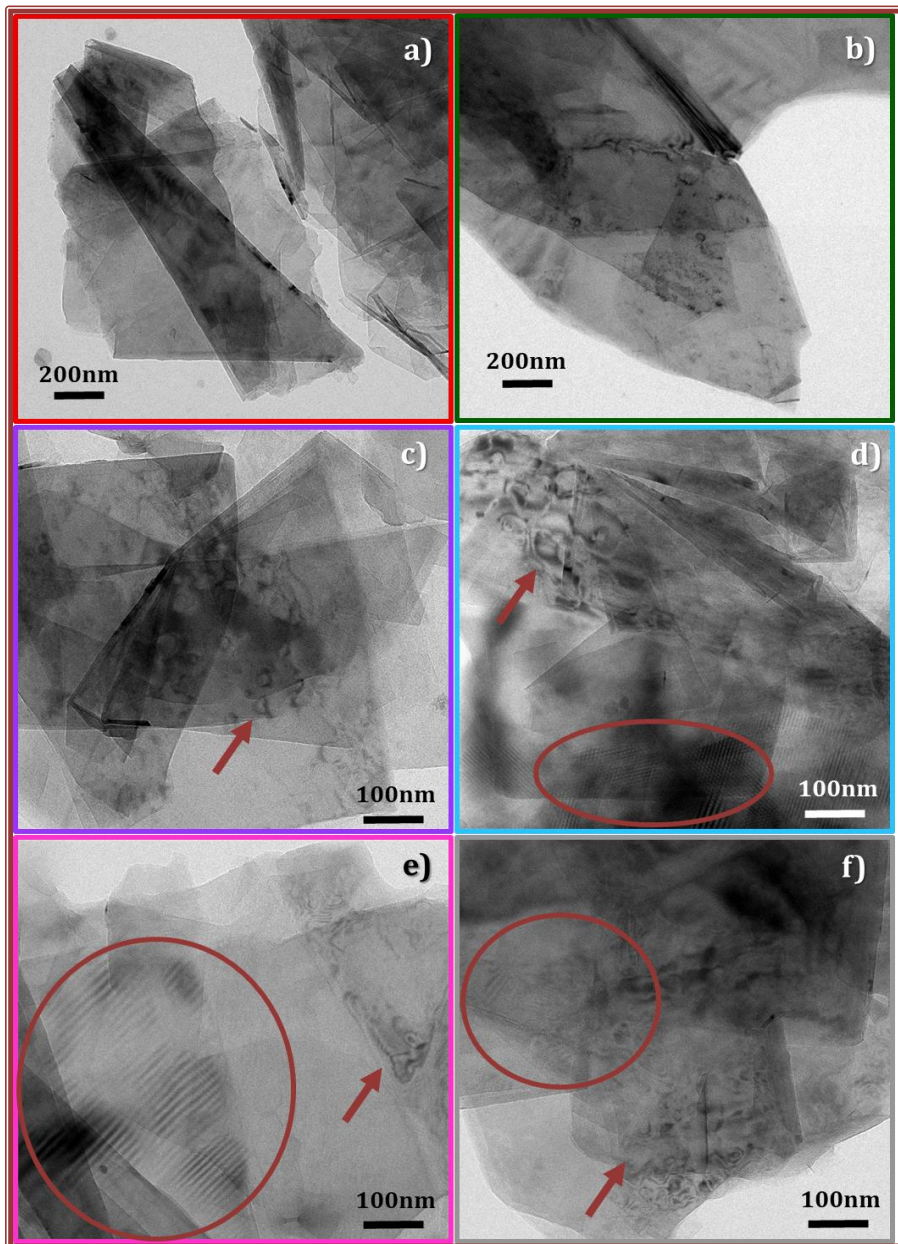


Figure 5.3. TEM images of the neat graphene and the treated graphene. a)GP, b)GWt, c)GAc, d)GAM, e)GAc-KPS, f)Gam-KPS

The structure of the treated graphene was determined by TEM imaging, shown in Figure 5.3.

Important difference cannot be observed between the neat and the treated graphenes. In the graphenes treated in presence of monomers presence of some amorphous material can be observed (shown with arrows). Additional distinction may be observed in Figures 5.3d, 5.3e, and 5.3f, where some ordered structures are visible (marked with red circles). The treatment affected the surface chemistry and morphology of the graphenes, but did not affect the size of the platelet.

5.3.2 POLYMERIZATION KINETICS AND POLYMER MICROSTRUCTURE

The modified graphenes were used to prepare polymer composites by MWH assisted miniemulsion polymerization of MMA/BA/HEMA. Neat monomers were polymerized under the same conditions for sake of comparison. Figure 5.4 presents the time evolution of conversion curves for all systems studied (Table 5.2).

According to the data presented in Figure 5.4, there is no substantial difference of the reaction rate and conversion between the neat polymer systems and the composite ones, as well as, there is no important variation between the unmodified graphene and modified ones.

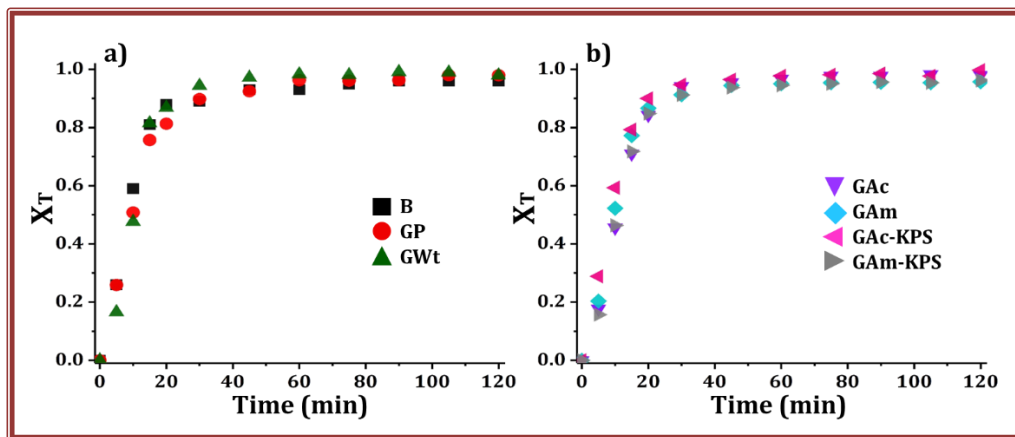


Figure 5.4. Time evolution conversion for different co-polymerizations performed under MWH with various modified graphene.

The characteristics of the miniemulsion and the final latexes are presented in Table 5.3. It may be seen that the droplet size of the neat polymer miniemulsion is lower than for the hybrids. The addition of graphene affected the miniemulsification process. It can be due to the methodology of the composite emulsion preparation, in which the graphene aqueous dispersion was added after miniemulsification process. Therefore the measured average droplet size already include larger particles. This increment is huge in case of the graphenes treated with both monomers AA and AM in presence of KPS, for which average droplet size was >300 nm.

GRAPHENE MODIFICATION UNDER MW IRRADIATION AND THEIR POLYMER COMPOSITES

Table 5.3. Characteristics of latex produced by MMA/BA/HEMA co-polymerizations performed under MWH with various modified graphene.

Experiment	d_d (nm)	d_p (nm)	N_p (number/L)	*Gel (%)	Average molar mass (kDa)	
					M_w	\bar{D}
B	63.4	86.1	5.3073×10^{17}	0	1952	3.6
Gp	83.3	97.3	3.7293×10^{17}	0	1194	3.0
GWt	87.4	100.1	3.4251×10^{17}	0	1196	2.9
GAc	98.6	103.5	3.4945×10^{17}	0	1213	2.6
GAm	97.7	99.6	3.3894×10^{17}	0	934	2.8
GAc-KPS	318.4	111.4	2.5355×10^{17}	0	1189	3.1
GAm-KPS	315.6	104.9	2.9261×10^{17}	0	1015	2.6

Beside these differences observed for the droplet sizes of different miniemulsions, the average particle size achieved after polymerization was rather similar and likely controlled by the available amount of surfactant. Comparing the droplet and particle size, one may conclude that there is negligible particle coalescence occurring during polymerization, except in the case of Am-KPS and Ac-KPS. For their case, the particle size was importantly decreased indicating important secondary nucleation occurring in these systems.

However, the small difference in particle size when translated to number of particles, the differences are more important: the neat polymer latex has almost doubled the number of particles in comparison to the composites. For the composite latexes, the ones prepared with Am-KPS and Ac-KPS the number of particles dropped further. This difference could be accounted for the variation of the average molar masses. The neat polymer presented the higher average molar mass probably due to higher number of particles in which the average number of radicals per particle dropped and as well the probability for bimolecular termination.

The polymer and composite microstructures were determined by gel content and molar mass of the soluble fraction. The gel fraction of all the materials is shown in Table 5.3. where, no gel was found for any sample, in agreement with previous results [13]. The absence of gel demonstrates that there is no cross-linking polymer-graphene, that has been observed previously (chapter 4). However it should be stated that in previous works, rGO was used and here it was graphene. The difference is not only in higher hydrophobicity to graphene but as well in the chemical composition, as rGO still contains high quantity of oxygen functional groups on the surface. Molar mass distributions were compared in Figure 5.5. It can be observed shifting from higher molar masses of neat polymer towards lower molar masses in the composites.

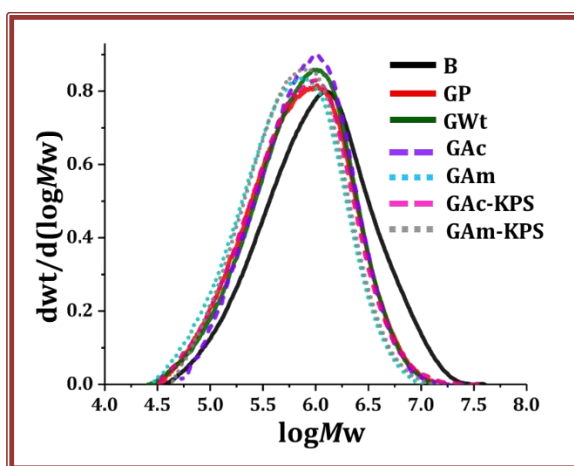


Figure 5.5. Molecular weight distributions of MMA/BA/HEMA copolymers with various modified graphene performed under MWH.

5.3.3 COMPOSITE PROPERTIES

Thermal and mechanical properties of the composite film were studied by means of DMTA and tensile test analyses.

In Figure 5.6 the photos of the neat polymer and composite films are presented. The insets in each photo is a zoomed area obtained with an optical microscope. It can be seen that all composites containing modified graphene present small graphene clusters. Untreated graphene seems to be dispersed much better than all treated ones, whereas the composite with GAm, present the larger clusters. This result is rather surprising and against the expectation that the treated graphene will enhance the compatibility with polymers, as it was experienced with reduced graphene oxide.

Nevertheless, except the GAm, which presented larger graphene aggregates than others, the other films presented homogenous dispersions of smaller aggregates. To check how this film morphology will affected the mechanical and thermal properties, they were further studied.

Table 5.4 shows the glass transition temperature (T_g) of the composite films, determined by DSC and DMTA methods.

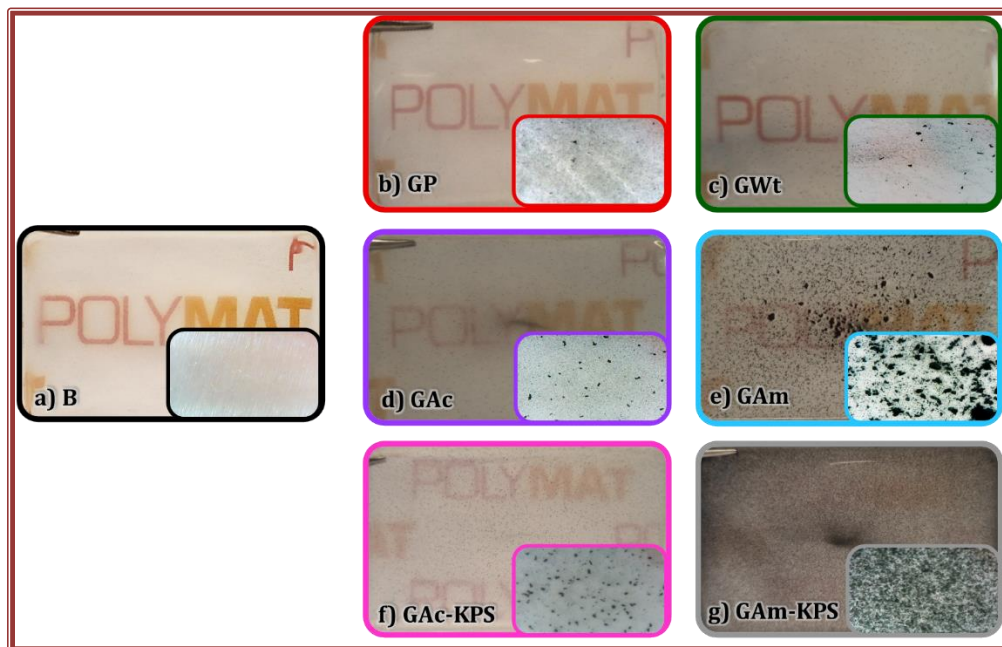


Figure 5.6. Polymer films of MMA/BA/HEMA copolymers with neat and various modified graphene, inserts images represent the zoom of the polymer film surface.

Table 5.4. The glass transition temperature (T_g) of the prepared coatings from MMA/BA/HEMA/SA and graphene hybrids.

MWCNTs (wt%)	Glass transition temperature T_g (°C) From DSC			T_g (°C) From DMTA
	T_{g1} region	T_{g2} region	T_{g3} region	T_g
B	-70	-40 to 50	93	41
Gp	-71	-30 to 56	90	43
GWt	-70	-31 to 65	89	43
GAc	-70	-31 to 64	90	43
GAm	-72	-36 to 61	87	43
GAc-KPS	-71	-32 to 56	90	43
GAm-KPS	-73	-48 to 66	87	43

GRAPHENE MODIFICATION UNDER MW IRRADIATION AND THEIR POLYMER COMPOSITES

The DSC results show the presence of few T_g regions. The first T_{g1} region was close to -70°C , indicating the formation of co-polymer of BA ($T_g=52.1^\circ\text{C}$) and SA ($T_g=-111^\circ\text{C}$). In the T_{g2} region, a broad peak between -30°C - -48°C to 50 - 66°C appears in all polymer composites obtained by MWH. It is a result of the heterogeneous composition of the polymer chains formed in the batch polymerization of monomers with different reactivity ratios ($r_{MMA} = 2.02 \pm 0.36$, $r_{BA} = 0.26 \pm 0.14$) [14]. This yield co-polymer chains reach in MMA-units (MMA- $T_g=100.1^\circ\text{C}$) [15,16] at the beginning of the process, and co-polymer chains reach in BA-units at the reaction end (BA- $T_g=-52.1^\circ\text{C}$)[15,16]. The T_{g3} region appeared at 90°C that corresponds to MMA-rich co-polymer chains. The broad T_{g2} region for the neat polymer could correspond to the change of the co-polymer composition during polymerization.

DMTA results for MWH polymer composites and the neat polymer are presented in Figure 5.7, where the storage modulus is compared in Figure 5.7a and the $\text{Tan}\delta$ in Figure 5.7b, from which the determined T_g 's are shown in Table 5.4. The T_g 's differ from the DSC determined ones because of different principles of measurements of both techniques. The T_g increased with respect to neat polymers when graphene was added. This is due to the presence of graphene in the polymer matrix, which acts as stiff cross-points and delays segmental oscillations of the polymer matrix, because higher amount of thermal energy is needed to excite the relaxational motions of the chains. The increase in T_g s of the composites demonstrates that there are stable interactions established between polymer and graphene. The storage modulus (Figure 5.7a) presents a clear trend that corresponds to the addition of graphene in comparison with the neat polymer. The worst behaviour was presented by composite film containing GAM, which could be due to the graphene clusters presented along the film, (Figure 5.6e) presented the less storage modulus than the other polymers. The composite with treated graphene with monomers and initiator (GAc-KPS and GAM-KPS) present improved storage modulus at high temperature (80°C) that the neat

polymer and other composites. Decreased area under the curve of $\text{Tan}\delta$ in Figure 5.7b denotes decreasing of the mobile phase in the composite films with respect to the neat polymer film.

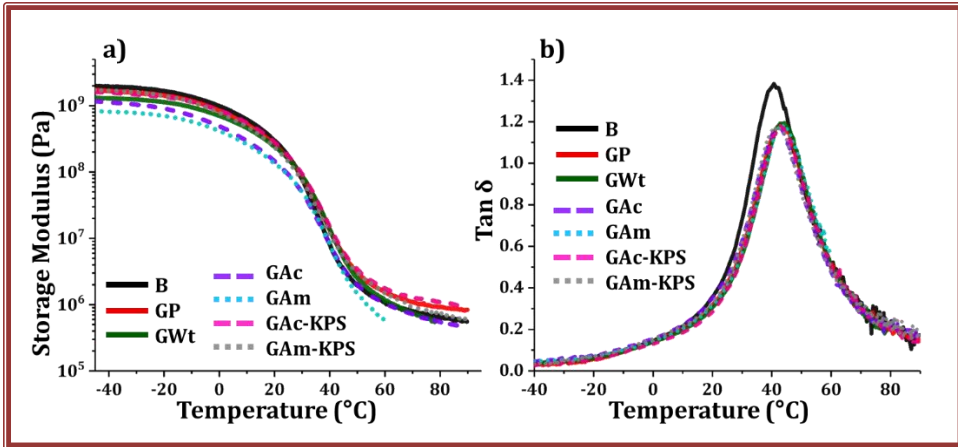


Figure 5.7. DMTA results of polymer and composite films containing different modified graphene under MWH. (a) Storage Modulus; (b) $\text{Tan}\delta$.

In Figure 5.8 and Table 5.5, the results of the stress-strain tests are presented for the neat polymer and the composite. It is clearly shown that the addition of graphene reinforced the neat polymer, as the Young modulus were higher in the composite sample than in the neat polymer film. However, the composite containing non-modified graphene presents the highest Young modulus than the other composites, which likely is due to the excellent graphene dispersion within the polymer matrix, as observed in the optical images in Figure 5.6. It is worth mentioning that the composites presented increased stiffness without significant drop of the elongation at break, which is unusual combination, as usually increasing the stiffness of nanocomposites decreases their flexibility.

GRAPHENE MODIFICATION UNDER MW IRRADIATION AND THEIR POLYMER COMPOSITES

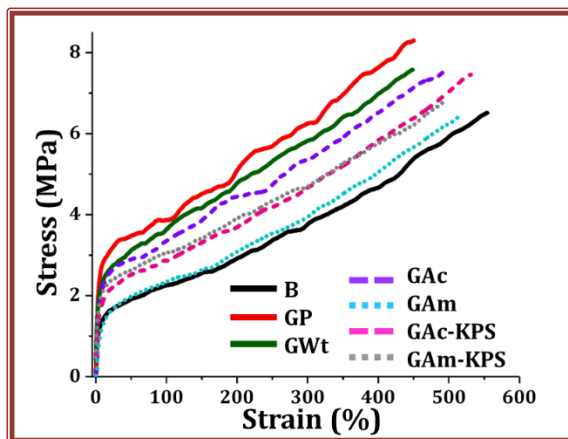


Figure 5.8. Stress-Strain measurements of polymer films of MMA/BA/HEMA copolymers with neat and various modified graphene.

Table 5.5. The glass transition temperature (T_g) of the prepared coatings from MMA/BA/HEMA/SA and graphene hybrids.

Experiment	Young's modulus (MPa)	Yield stress (MPa)	Ultimate tensile strength (MPa)	Elongation at break (%)
B	0.32	1.37	6.51	554.3
Gp	0.64	2.74	8.30	450.1
GWt	0.47	2.28	7.76	513.6
GAc	0.43	2.13	7.56	494.8
GAm	0.23	4.19	6.44	515.1
GAc-KPS	0.28	4.98	7.46	530.9
GAm-KPS	0.35	4.90	6.77	491.8

5.4 CONCLUSIONS

In this chapter it was demonstrated that MWH can provide facile way for surface modification of graphene, by simple irradiation in water either without any additives or in presence of water-soluble monomers and initiator. In all these strategies, mild graphene surface modification was induced, which was demonstrated by RAMAN spectroscopy in which it was observed that the defect sites in graphene structure were increased. The hydrophobicity of the treated graphene dropped with respect to the non-treated one, as it was shown by measurements of water contact angles.

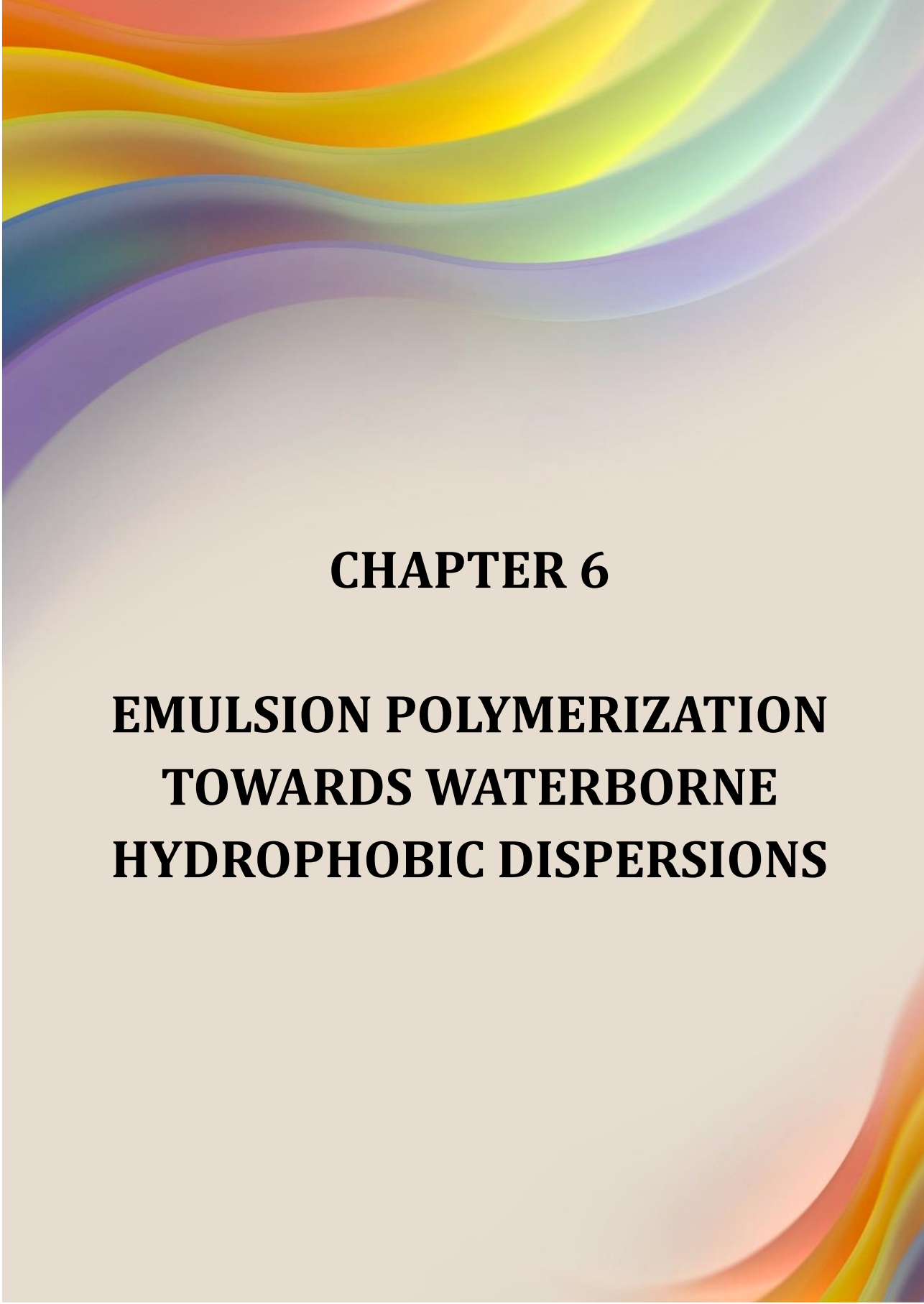
Such treated graphene were used to prepare miniemulsion using MMA/BA/HEMA monomer mixture and polymerized in MWH reactor. As a result nice composite films were obtained, in which the non-treated graphene was surprisingly dispersed better than the treated ones. This was the probable reason for the modest improvement of the mechanical and thermal properties.

5.5 REFERENCES

- [1] K. Balasubramanian, M. Burghard, Chemically functionalized carbon nanotubes, *Small*. (2005). <https://doi.org/10.1002/smll.200400118>.
- [2] S. Park, M. Vosguerichian, Z. Bao, A review of fabrication and applications of carbon nanotube film-based flexible electronics, *Nanoscale*. (2013). <https://doi.org/10.1039/c3nr33560g>.
- [3] X.J. Wang, Z. Liu, Carbon nanotubes in biology and medicine: An overview, *Chinese Sci. Bull.* (2012). <https://doi.org/10.1007/s11434-011-4845-9>.
- [4] E. Vázquez, M. Prato, Carbon nanotubes and microwaves: Interactions, responses, and applications, *ACS Nano*. (2009). <https://doi.org/10.1021/nn901604j>.
- [5] H.Y. Kim, J.W. Lee, H.M. Oh, K.J. Baeg, S. Jung, H.S. Yang, W. Lee, J.Y. Hwang, K.S. Kim, S.Y. Jeong, J.T. Han, M.S. Jeong, G.W. Lee, H.J. Jeong, Ultrafast Heating for Intrinsic Properties of Atomically Thin Two-Dimensional Materials on Plastic

- Substrates, ACS Appl. Mater. Interfaces. (2016). <https://doi.org/10.1021/acsami.6b09677>.
- [6] H.X. Wu, X.Q. Qiu, W.M. Cao, Y.H. Lin, R.F. Cai, S.X. Qian, Polymer-wrapped multiwalled carbon nanotubes synthesized via microwave-assisted in situ emulsion polymerization and their optical limiting properties, Carbon N. Y. (2007). <https://doi.org/10.1016/j.carbon.2007.10.009>.
- [7] H. Mi, X. Zhang, S. An, X. Ye, S. Yang, Microwave-assisted synthesis and electrochemical capacitance of polyaniline/multi-wall carbon nanotubes composite, Electrochem. Commun. (2007). <https://doi.org/10.1016/j.elecom.2007.10.013>.
- [8] J.M. Yuan, Z.F. Fan, X.H. Chen, X.H. Chen, Z.J. Wu, L.P. He, Preparation of polystyrene-multiwalled carbon nanotube composites with individual-dispersed nanotubes and strong interfacial adhesion, Polymer (Guildf). (2009). <https://doi.org/10.1016/j.polymer.2009.04.065>.
- [9] S. Pramanik, R. Konwarh, R.C. Deka, L. Aidew, N. Barua, A.K. Buragohain, D. Mohanta, N. Karak, Microwave-assisted poly(glycidyl methacrylate)-functionalized multiwall carbon nanotubes with a “tendrillar” nanofibrous polyaniline wrapping and their interaction at bio-interface, Carbon N. Y. (2013). <https://doi.org/10.1016/j.carbon.2012.11.062>.
- [10] J. Ding, X. Li, X. Wang, J. Zhang, D. Yu, B. Qiu, Fabrication of Vertical Array CNTs/Polyaniline Composite Membranes by Microwave-Assisted In Situ Polymerization, Nanoscale Res. Lett. (2015). <https://doi.org/10.1186/s11671-015-1201-z>.
- [11] S.R. Chowdhury, Y. Chen, Y. Wang, S. Mitra, Microwave-induced rapid nanocomposite synthesis using dispersed single-wall carbon nanotubes as the nuclei, J. Mater. Sci. (2009). <https://doi.org/10.1007/s10853-009-3259-4>.
- [12] L.M. Malard, M.A. Pimenta, G. Dresselhaus, M.S. Dresselhaus, Raman spectroscopy in graphene, Phys. Rep. (2009). <https://doi.org/10.1016/j.physrep.2009.02.003>.
- [13] I. González, J.M. Asua, J.R. Leiza, The role of methyl methacrylate on branching and gel formation in the emulsion copolymerization of BA/MMA, Polymer (Guildf). (2007). <https://doi.org/10.1016/j.polymer.2007.03.015>.
- [14] S.G. Roos, A.H.E. Müller, K. Matyjaszewski, Copolymerization of n-Butyl Acrylate with Methyl Methacrylate and PMMA Macromonomers: Comparison of Reactivity Ratios in Conventional and Atom Transfer Radical

- Copolymerization, *Macromolecules*. 32 (1999) 8331–8335. <https://doi.org/10.1021/ma9819337>.
- [15] M.N. Nguyen, Q.T. Pham, V.D. Le, T.B.V. Nguyen, C. Bressy, A. Margaillan, Synthesis and characterization of random and block-random diblock silylated terpolymers via RAFT polymerization, *Asian J. Chem.* (2018). <https://doi.org/10.14233/ajchem.2018.21217>.
- [16] M. Fernández-García, R. Cuervo-Rodríguez, E.L. Madruga, Glass transition temperatures of butyl acrylate-methyl methacrylate copolymers, *J. Polym. Sci. Part B Polym. Phys.* (1999). [https://doi.org/10.1002/\(SICI\)1099-0488\(19990901\)37:17<2512::AID-POLB22>3.0.CO;2-2](https://doi.org/10.1002/(SICI)1099-0488(19990901)37:17<2512::AID-POLB22>3.0.CO;2-2).



CHAPTER 6

EMULSION POLYMERIZATION TOWARDS WATERBORNE HYDROPHOBIC DISPERSIONS

6.1 INTRODUCTION

Since the high demand for synthetic alternatives to natural rubber latexes boosted the research in this field during World War II, the emulsion polymerization technique is nowadays considered as the basis of a massive global industry that continues to expand, mainly due to the versatility of the reaction and the ability to control the properties of the polymer latexes produced [1]. With a yearly production of synthetic polymer dispersions of more than 25% of the overall polymer production, emulsion polymerization is important industrial process with divers applications in the main markets of polymer dispersions, like paints and coatings, paper coatings, adhesives, carpet backings and even in biomedical applications as drug delivery system [1,2].

Hybrid coatings based on combination of acrylics with another functional polymer, as for example, epoxies, alkyds, urethanes, or silicones are common class of polymer species known as high performance due to advantageous combination of the main properties of both polymer species. [3,4]. Incorporating of the hydrophobic components within acrylic systems results in producing, for example, protective coatings, which have not only a decorative purpose and excellent mechanical and thermal properties, but are also able to confer anti-fouling and water resistance properties to painted substrates.

The main problem in these systems is that physical blends of the two different polymer dispersions or emulsion polymerisation reaction of two different polymer systems can produce an incompatible mixture that exhibits the worst properties of each polymer. Therefore, the great challenge in this kind of material is to compatibilize the both phases. Previous studies show that the copolymerization of, for example, acrylic/alkyd and acrylic/epoxy resins have been performed by both emulsion and miniemulsion polymerization [5,6]. Although emulsion polymerization has several advantages over miniemulsion polymerization in terms of less complexity,

lower costs, easier scale-up, and better reproducibility, it is stated in both studies that miniemulsion polymerization proved to be the most effective in incorporating the hydrophobic resins into the acrylic coating copolymers. **The hydrophobic nature of the resin caused diffusion limitations**, which made it impossible for emulsion polymerization to succeed since, in this technique, diffusion of the hydrophobic component through the water phase into the polymer particles is needed. Miniemulsion overcomes this limitation, as the locus of polymerization are the small monomer droplets prepared from monomer and resins mixed previously. Therefore, no transport across the aqueous phase is necessary. The colloidal stability of miniemulsion is improved by use of a small amount of costabilizer, which is low molecular weight and highly water-insoluble component, which prevent Ostwald ripening process, by which small monomer droplets disappear by monomer diffusion to the large droplets. [2,7].

Even though miniemulsion polymerization enables the production of good quality hybrid latexes on a lab-scale, the implementation in the industry is still challenging, due to the requirement of additional energy to pre-form the small monomer droplets, which increases the irreproducibility and scale-up possibilities [2].

Alternatively, emulsion polymerization at increase temperature may be used, (≥ 100 °C) **aimed to increase the diffusion of the more hydrophobic component through the aqueous phase** and may be the clear road of scaling up the emulsion copolymerization in acrylic hybrid systems. This idea has been developed in a published patent was found, which stated that: "Although water solubility is not always a linear function of temperature, high temperature can increase diffusivity for low polar and non-polar monomers. By elevating the temperature, it is possible to increase the saturation concentration of hydrophobic monomers in water, which makes it possible for emulsion polymerizing hydrophobic monomers"[8]. Although some possible monomers to perform this kind of reaction are proposed, there are no

EMULSION POLYMERIZATION TOWARDS WATERBORNE HYDROPHOBIC DISPERSIONS

details about methods, results, or specifications, and the increase of the diffusivity of hydrophobic monomers at elevated temperatures was not proved.

Conventional heating reactors, however, are not convenient to perform the reactions in aqueous dispersed media at higher temperatures due to the use of water as a continuous phase. Therefore, in this work, it is intended to use a microwave (MW) reactor, which allows precise control of the temperature and pressure in the reaction system.

The main goal of this work will, therefore, be to develop a method of high-temperature emulsion polymerization assisted by microwave heating, which will allow copolymerization of the acrylics/hydrophobic resin hybrid systems. It is expected to obtain similar products as usually obtained by conventional miniemulsion polymerization at lower temperatures. Therefore, the main challenge lies in eliminating the distribution in chemical composition within the different particles by controlling the temperature and, subsequently, the diffusion of hydrophobic compounds throughout the water phase.

In this chapter, we explore this possibility taking advantage of the MW reactor with excellent control of temperature and pressure. The acrylic monomers (MMA/BA/AA) were copolymerized in emulsion polymerization either with epoxy or alkyd resin.

6.2 EXPERIMENTAL

6.2.4 MATERIALS

The materials are given in Appendix I.

6.2.2 POLYMERIZATIONS

Emulsion polymerization was carried out at 20% solids content (S.C.) of acrylic monomers and 10% of S.C. of resin, in 400 mL total volume emulsion. The water phase was prepared by mixing water and of sodium dodecyl sulfate (SDS, 1 wt%) surfactant and 1.5wt % based to acrylic monomers amount of the initiator 2,2'azobis[2-methyl-N-(2-hydroxyethyl)propionamide](VA-086) or potassium persulfate (KPS). The organic phase was by mixing MMA/BA/AA of 49.5/49.5/1 wt% ratio as the main monomers and 10% of epoxy resin D.E.R. 732.

Miniemulsion polymerization was performed for comparison under CH (ME 11^{CH}). Miniemulsion was prepared similarly as explained, with addition of 7% of stearyl acrylate (SA) polymerizable co-stabilizer to the oil phase. Both phases were stirring separately for 5 minutes at 200 rpm, mixed together, and stirred for 15 minutes at 300 rpm. For miniemulsion preparation, the emulsion containing SA was subjected to sonication by 10 minutes at 80% power output and 50% duty cycle under magnetic stirred at 250 rpm, sonication was carried out in an ice bath to avoid overheating.

When azo-initiator type was used, it was dissolved into the organic phase along with the monomers. On the other hand, the water-soluble initiator KPS was dissolved into the water phase. After that, the complete mixture was placed into MW reactor and polymerized in batch, several variables were changed along with the chapter, so the

EMULSION POLYMERIZATION TOWARDS WATERBORNE HYDROPHOBIC DISPERSIONS

different experiments are described in Table 6.1, where temperature, heating time, and reaction time was changed.

The initiator was added in the reaction mixture since the beginning, before the reaction starts it was subjected to just five minutes degasification. After that time, the nitrogen inlet was closed. The reactions were performed in hermetically closed MW reactor, so during the reaction the pressure increased.

Table 6.1. Reaction formulations for different co-polymerizations performed under microwave heating with different reaction parameters. (Exp^{CH}: Performed by conventional heating).

Exp.	Temperature (°C)	Initiator type	Heating program (min)	Reaction Time (min)
E1 ^{CH}	80	VA-086	10	120
2	80	VA-086	10	120
3	100	VA-086	10	120
4	120	VA-086	10	120
5	150	VA-086	10	60
6	100	VA-086	3	15
7	100	VA-086	3	30
8	60	KPS	3	120
9	80	KPS	3	120
10	100	KPS	3	120
ME11 ^{CH}	60	KPS	10	120

6.2.3 CHARACTERIZATIONS

The final acrylic conversions were measured gravimetrically. Particle size distribution of the latexes were determined by dynamic light scattering (DLS). The molar mass distribution (MMD) of the soluble fraction in THF was determined by gel permeation chromatography (GPC) at 35°C. To measure the MMD of samples, the sol part obtained after soxhlet extraction was concentrated and then directly analysed by GPC. The gel fraction was measured by soxhlet extraction, using THF as the solvent. In order to identify if the epoxy resin was present in the copolymer, the final latex was centrifuged at 10000 rpm of 4°C by 1 h, and after that their fractions were analysed by DLS and FT-IR.

More details about the methodology and characteristics of all equipment used are described in Appendix I.

6.3 RESULTS AND DISCUSSIONS

6.3.1 HYBRID LATEX CHARACTERISTICS

Hybrid polymer system made of MMA/BA/AA and bi-functional epoxy resin pre-polymer were copolymerized in situ, expecting to obtain crosslinking between the copolymer acrylic chains and the epoxy resin throughout COOH-epoxy reaction at increased temperature. The reactions were performed in emulsion system, and we increased slowly the reaction temperature, expecting to improve the epoxy resin diffusion and subsequently its incorporation in the hybrid polymer (Figure 6.1). The effect of the following parameters, the reaction time, the heating program in MW reactor, and the initiator type on the emulsion polymerization reaction, stability of the latex and incorporation of the epoxy in the hybrid polymer were studied.

EMULSION POLYMERIZATION TOWARDS WATERBORNE HYDROPHOBIC DISPERSIONS

The reactions were performed at four different temperatures for 10 min. The reaction performed at the lowest temperature (80°C) was performed under CH for comparison. In Table 6.2 the final conversion achieved and the latexes characteristics are shown. It may be observed that in CH reaction at 80°C in 120 min 44% acrylic monomer conversion was achieved, whereas, when performed under MWH, the conversion was as high as 96%. This difference in conversion is likely a result of the fact that the initiator was added to the reaction mixture in MWH reactor before heating was started, whereas in CH it was added after achieving the reaction temperature. Furthermore, the heating profiles were not equalized as in previous chapters and the heating program to achieve the reaction temperature in MW reactor was 10 min, which is rather long. These results clearly demonstrate our points of view, that most of the differences between CH and MWH polymerizations in published literature were result of the poor comparison conditions established between CH and MWH.

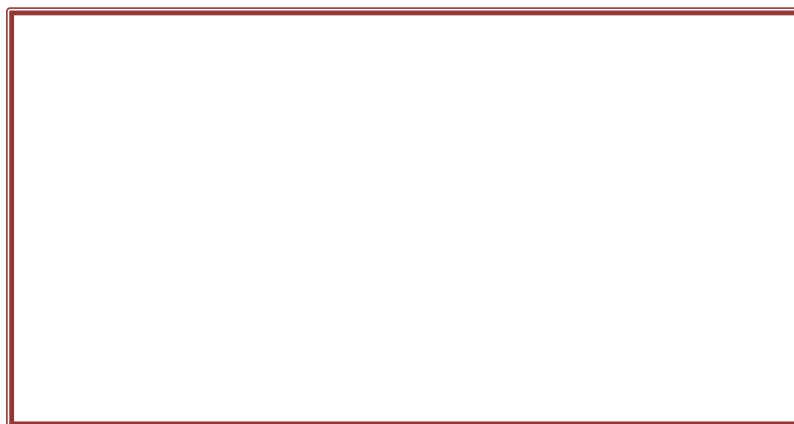


Figure 6.1. Scheme of the possible reaction of MMA/BA/AA/Epoxy resin.

CHAPTER 6

Table 6.2. Characteristics of **MMA/BA/AA/Epoxy resin** latexes produced at different reaction temperatures, using **V-086** as initiator. Reaction time is 10 min. (Exp^{CH}: Performed by conventional heating).

Exp.	Temperature reaction (°C)	Overall Conversion (%)	Dp (nm)	Coagulum (%)	% Gel	Mw (kDa)	Đ
1 ^{CH}	80	44	92	0	6	---	---
2	80	96	114	0	49	1066	2.79
3	100	95	116	2	0	644	2.30
4	120	87	126	11	0	197	2.21
5	150	66	378	19	0	184	2.37

Table 6.2 demonstrates that by increasing of the temperature in the MWH reactor, the conversion decreased. However, simultaneously, coagulation appeared in the system and its amount increased with the temperature, which explained the lower conversions observed as part of the polymer was incorporated in the coagulum. The amount of coagulum obtained may be observed in Figure 6.2, where the photos of the reactor and the coagulum obtained at the end of each reactions are shown.

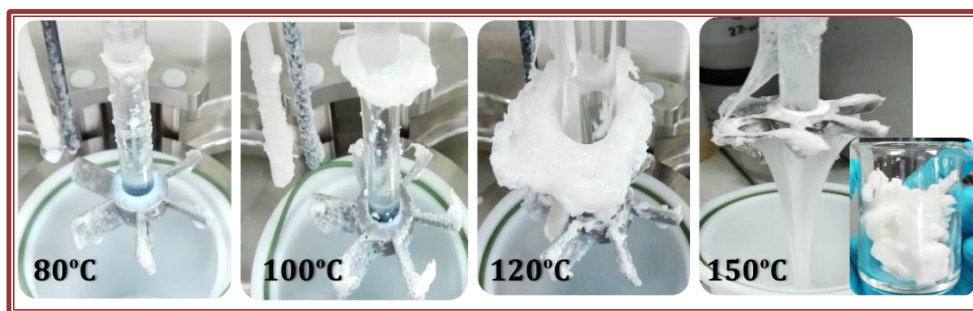


Figure 6.2. Coagulation of each reaction at different temperatures.

EMULSION POLYMERIZATION TOWARDS WATERBORNE HYDROPHOBIC DISPERSIONS

Table 6.2 shows that the average particle size of the latexes increased with temperature, probably due to the lower stability of the latexes at higher temperature. However, the increase coagulum production could be promoted as well due to the intensive mechanical stirring of the latex after achieving of full acrylic monomer conversion.

It is worth mentioning that the pressure was slightly increased during the higher temperature reaction. For reaction performed at 80°C, the pressure increased up to ~1.5 bar; for 100°C and 120°C the pressure was ~2 bar and, for 150°C the pressure increase up to ~3 bar..

According to Table 6.2, the insoluble polymer fraction in THF (% gel) of the latex produced at 80°C is 50%. This indicates that there is high incorporation of the epoxy resin within the acrylic polymer. In the same reaction done under CH, there was no insoluble polymer produced. As it was mentioned, this difference was likely due to the difference in temperature in the initial reaction period. Even though at higher temperature due to faster initiator decomposition, it is expected to obtain lower molar masses, the higher temperature may promote the chain transfer to polymer process which leads toward increased branching and gel formation within the acrylic polymer [??]. Additionally the epoxy group reactions are as well promoted by increasing the temperature [9,10]. However, surprisingly the polymers produced at higher temperatures in MWG reactor did not contain any gel fraction and the produced molar masses were low, decreasing further with the temperature. The low molar mass is likely the reason for the lack of gel, and were obtained because of the promoted bimolecular terminations at high temperature. On the other hand, the gel obtained within these reactions was probably incorporate within the coagulum.

In the next attempts in order to decrease the coagulum formation, it was decided to shorten the heating program (to achieve the reaction temperature) in MW reactor

from 10 min to 3 min and to decrease the reaction time from 120 min to 30 min, and to 15 min. The reactions were performed at 100°C and the results are presented in Table 6.3. As it may be observed in Figure 6.3, except the small amount of polymer adhered on the mechanical agitator, no coagulum was observed in the system. In the same reaction performed for 120 min (and with larger heating program of 10 min), apart of the polymer adhered on the agitator, there was 2% of the polymer present as solid coagulum.

Table 6.3. Characteristics of latexes produced by **MMA/BA/AA** copolymerization with **Epoxy resin**, using **V-086** as initiator at two different reaction times and, **100°C** reaction temperature.

Exp.	Reaction time (min)	Overall Conversion (%)	Dp (nm)	Coagulum (%)	% Gel	Mw (kDa)	Đ
6	15	84	121	0	17	609	2.1
7	30	85	115	0	10	611	2.2

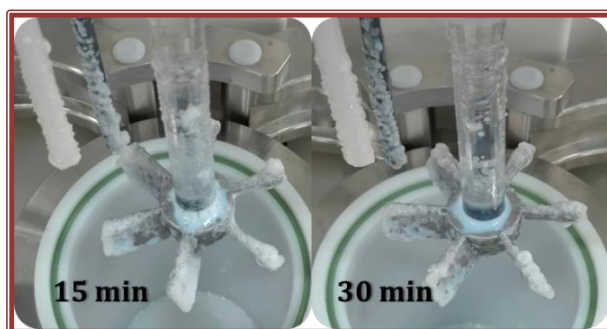


Figure 6.3. Photos of the coagulum of the reaction No.6 and No.7 at different reaction times.

EMULSION POLYMERIZATION TOWARDS WATERBORNE HYDROPHOBIC DISPERSIONS

Table 6.3 shows that very high acrylic monomer conversion was achieved, in both cases higher than 80%. The pressure into the reactor increased to ~2bar for both experiments, and the final particle size was similar between them (~118 nm). Under these conditions the incorporation of epoxy resin in the acrylic polymers, giving rise to formation of gel fraction was increased to about 17 % and 10 %, for both reactions, respectively. The sol molar masses were very similar of about 6000 kDa. These results indicate that the reaction was probably almost finished even in 15 min, and that the prolonged agitation was likely the reason of the creation of large coagulum. The lack of full conversion can be a result on fast consumption of initiator due to very high decomposition rate at such high temperature, and possible solution could be addition of second shot of initiator to achieve full conversion.

The second advantage of shortening the reaction time is the decrease in the energy consumption. For example, for experiment No.3, the total MW-energy consumption was 1606.0 kJ and, for Exp. 6 and 7, the MW-energy consumed were for 252.2 kJ and 414.5 kJ, for a volume of 400 mL, at same temperature and pressure. However, the conditions should be found at which 100% conversion of acrylic monomers would be achieved.

In the so far presented results, VA-086 water-soluble azo initiator was used. It is known that azo-initiator decomposition rate is not affected by MW heating [11]. In the next attempts, KPS initiator was used, to check if the MW can affected the polymerization reaction not only through different way of heating, but as well through initiation step, as it was demonstrated that it decomposed faster under MW [11,12].

The heating time was kept at 3 minutes and reaction time was 120 min. The reactions were performed at three different temperatures, 60°C, 80°C and 100°C. For comparison, conventional heating miniemulsion polymerization was performed at 60°C.

Table 6.4 shown the characteristics of final latexes. High monomer conversions >95% were obtained by MWH method, whereas, for miniemulsion polymerization under CH 87% of conversion was achieved. No significant differences were observed in the final particle size, for all cases D_p of ~90 nm was obtained and no coagulum in neither case was observed (Figure 6.4). The similar particle size in the MW emulsion polymerization with that of CH miniemulsion and the lack of coagulum indicate that the reactions were successful and probably beside the diffusion limitation of epoxy resin it was probably incorporated into the polymer particles homogeneously.

Table 6.4. Characteristics of latexes produced by **MMA/BA/AA** copolymerization with **Epoxy resin** at different reaction temperatures and, **KPS** as initiator.

Exp.	Temperature reaction (°C)	Overall Conversion (%)	D_p (nm)	Coagulum (%)	% Gel	M_w (kDa)	\bar{D}
8	60	96	87	1	48	2015	2.02
9	80	99	76	1	13	822	1.96
10	100	96	87	2	11	761	2.25
11 ^{CH}	60	87	91	0	7	---	---

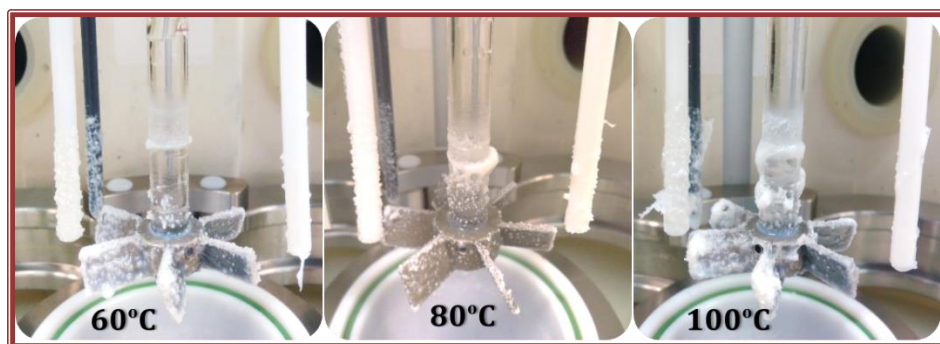


Figure 6.4. Coagulation of reaction No.6 and No.7 at different reaction times.

The gel content for MWH at 60°C was found to be almost 50%, which amount dropped at higher temperature to 13% and 11%. Surprisingly, the molar mass of the THF soluble fraction for 60°C reaction was very high (>2.000 kDa) and decreased at increased temperature in MW reactor. For CH miniemulsion polymerization just 7% gel was found, this could be due to a less epoxy resin incorporation into de polymer system, because of less COOH – epoxy reaction at lower temperature (60°C).

6.3.2 INCORPORATION OF EPOXY INTO THE CO-POLYMER

In order to identify if the composition of all polymer particles is similar and contain both components, the acrylics and the epoxy, the final latex was centrifuged at 10000 rpm of 4°C for 1 h, Different fractions along the length of the centrifugation tube were extracted the fractions and were analysed by DLS and FT-IR. FTIR spectra were used to distinguish the composition within each fraction, for which the ratio of the following bands were used as indicator for the composition: for acrylics C=O at 1721 cm^{-1} and for the epoxy resin C-O of oxirane group at 842 cm^{-1} . Representative FT-IR spectra of the neat epoxy, neat acrylics and their combination are shown in Figure 6.5, showing the characteristic peaks of both components used to calculate relative composition of the each fraction. The obtained results are shown in Table 6.5.

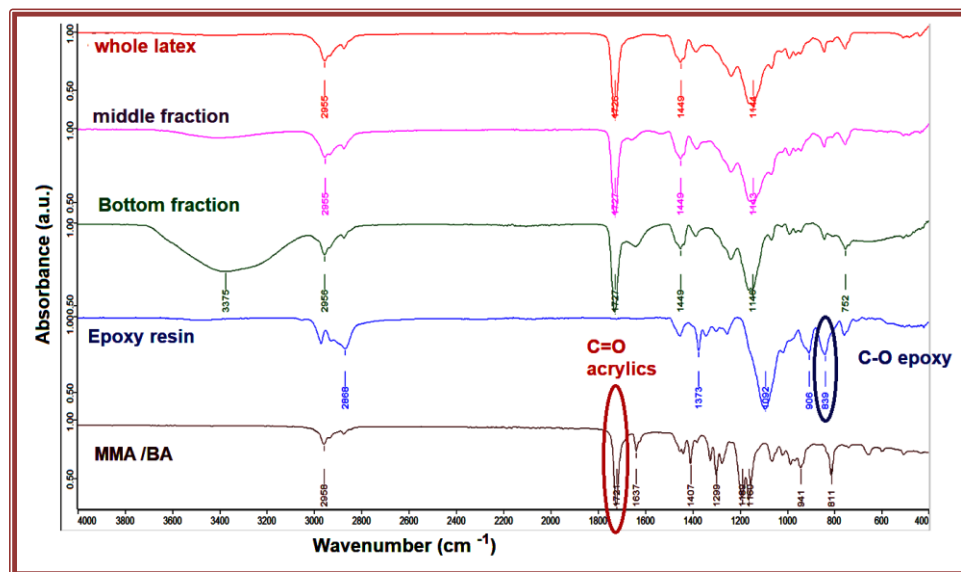


Figure 6.5. Representative FTIR spectra (reaction MW at 80°C with VA-086 initiator) and characteristic peaks used for evaluation of chemical composition of the polymer fraction after centrifugation.

In Figure 6.6 the particle size distribution from DLS (PSD) of the hybrid latex obtained at 80°C with VA-086 azo initiator. In the figure the PSD fraction after centrifugation of this latex are presented, too. By centrifugation of the latexes, 3 phases are obtained: a top fraction consisting mostly of water, a middle fraction containing the less dense particles and a bottom fraction consisting of more dense particles. The bottom fraction is not included in the Figure 6.6, because it was completely solid after centrifugation and could not be analyzed with DLS. Figure 6.6 presents that the whole latex and the middle fraction has completely same PSD, which indicates that the separation occurred during centrifugation is not due to the size of the particles but due to their composition.

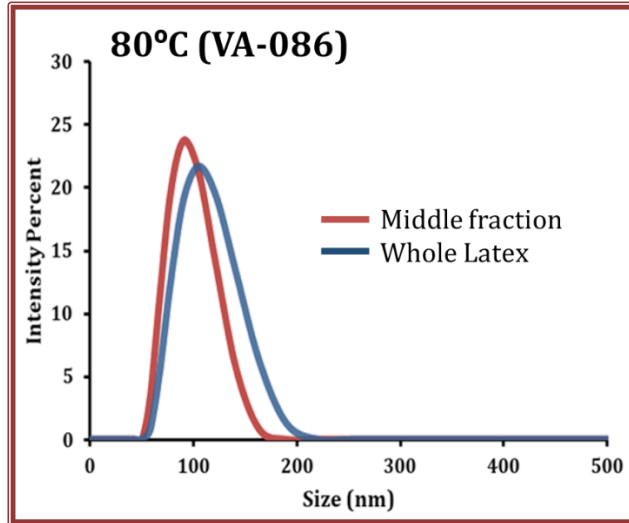


Figure 6.6. PSD of the latex obtained at 80°C with VA-086 and the middle fraction after its centrifugation.

Similar findings were obtained for all other latexes produced with VA-086 at different temperature, except the latex obtained at 150°C. As shown in Figure 6.7, there is an important difference in PSD between the middle fraction and the whole latex. The PSD of the middle fraction is shift towards the lower particle sizes with respect to the whole latex, indicating that the particles were separated in fractions with different sizes.

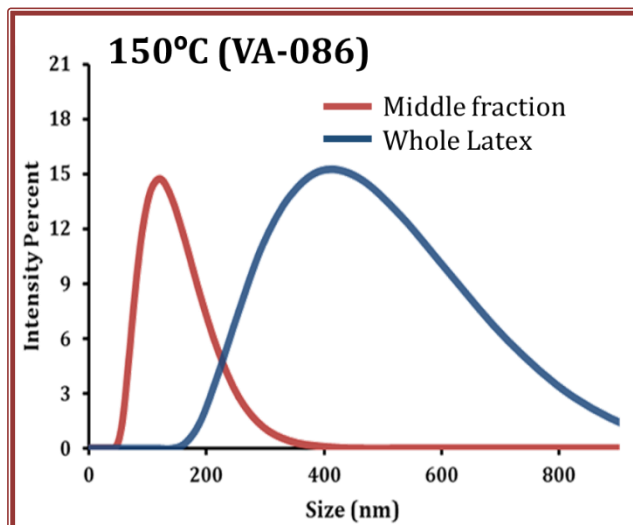


Figure 6.7. PSD of hybrid latex obtained at 150°C with VA-086 initiator and the middle fraction after its centrifugation.

The composition of the each of these fractions (including the bottom fraction that were not analyzed with DLS, was determined by FT-IR analysis and the intensity ratio of C=O representing acrylics and C-O representing epoxy resin. Table 6.5 shows the ratio of some of the representative materials obtained.

Table 6.5. Ratio of the FT-IR bands of acrylics and epoxy, of each latexes produced by MMA/BA/AA copolymerization with **Epoxy resin** at different reaction temperatures and, different **initiators** .

Exp.	Temperature (°C)	sample	Dp (nm)	Ratio between Acrylics/epoxy
1 ^{CH}	80	Final latex	92	7.35

EMULSION POLYMERIZATION TOWARDS WATERBORNE HYDROPHOBIC DISPERSIONS

2	80	Final latex	114	8.68
		Middle fracrtion	112	8.46
3	100	Final latex	116	7.59
		Middle fracrtion	109	7.47
		Coagulum	--	6.75
4	120	Final latex	126	8.045
		Middle fracrtion	120	8.249
		Coagulum	--	8.448
5	150	Final latex	378	5.54
		Middle fracrtion	119	2.32
		Coagulum	--	11.17
6	100	Final latex	121	6.493
		Middle fracrtion	112	6.085
7	100	Final latex	115	5.89
		Middle fracrtion	110	5.462
8	60	Final latex	87	6.528
		Middle fracrtion	81	6.886
9	80	Final latex	76	7.00
		Middle fracrtion	78	6.23
10	100	Final latex	87	7.953
		Middle fracrtion	77	6.24
11 ^{CH}	60	Final latex	91	9.12
		Middle fracrtion	67	5.63

In order to determine and visualize the distribution of compounds in the latexes by MALDI-IMS measurements, first the utilized latex is chosen from the GPC results. In this work the latex with epoxy resin and Azobis initiator performed at 150°C is chosen

for all upcoming MALDI-IMS results, which has a bimodal distribution of molar masses of which the low molecular weights can be detected by MALDI-IMS. After preparing films of this latex on ITO glass slides by using a film applicator and a 2-MBT matrix deposited on it by sublimation, as explained in Characterization, the MALDI-IMS measurements are started.

On the prepared ITO glass substrate, a small area ($\approx 1,0 \text{ cm} \times 0,5 \text{ cm}$) was scanned and analyzed by MALDI-IMS and from this the following average spectra of the whole area are obtained, shown in Figure 6.8. The top spectrum represents the obtained mass spectrum for all detected compounds and the two bottom images show for one specific mass peak, here for 1169 Da and 1799 Da, the intensities of it in the whole detected area of the sample. The color red indicates a high intensity of the detected mass peak in the area and the color blue a low intensity. For the detected area of Figure 6.8 can be stated that it looks quite homogeneous. Another area of the same glass slide was analyzed as well for which the average mass spectrum and two intensity images, at 1058 Da and 1661 Da are given in Figure 6.9. The distribution of compounds is different in Figure 6.9 compared to Figure 6.8. The images show a distribution in the range between 1-2 kDa where higher intensities are found in the right part of the detected area. There is no homogeneous distribution present. So from even just one sample can be stated that there is probably a difference in composition present within the latexes.

EMULSION POLYMERIZATION TOWARDS WATERBORNE HYDROPHOBIC DISPERSIONS

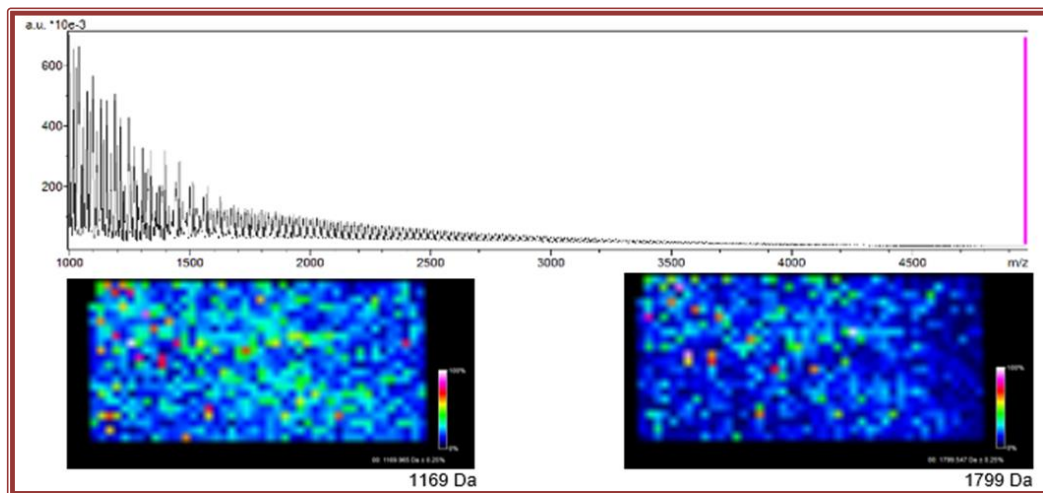


Figure 6.8. MALDI-IMS results ITO coated glass slide with epoxy resin, Azobis initiator at 150°C. Top spectrum = Mass spectrum, Images bottom = Intensities of specific mass peaks (1169 Da and 1799 Da) in top spectrum

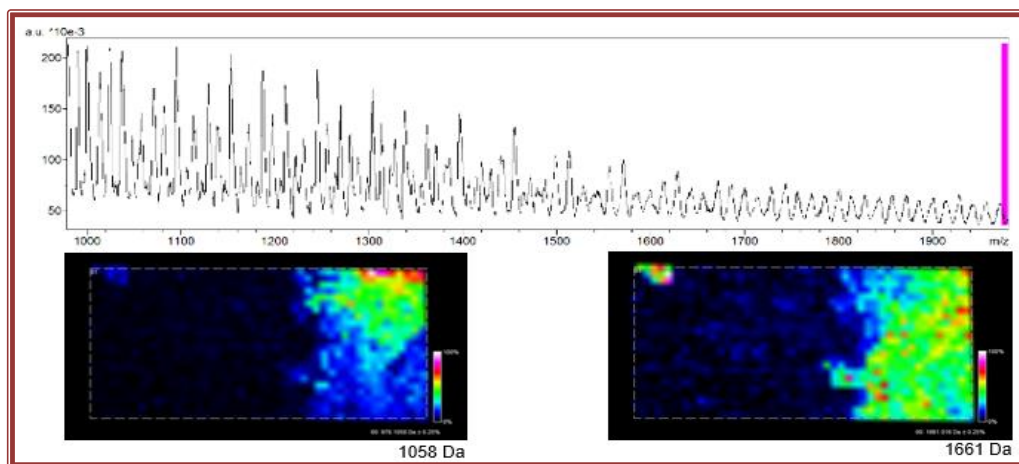


Figure 6.9. MALDI-IMS results ITO coated glass slide with epoxy resin, Azobis initiator at 150°C. Top spectrum = Mass spectrum, Images bottom = Intensities of specific mass peaks (1058 Da and 1661 Da) in top spectrum

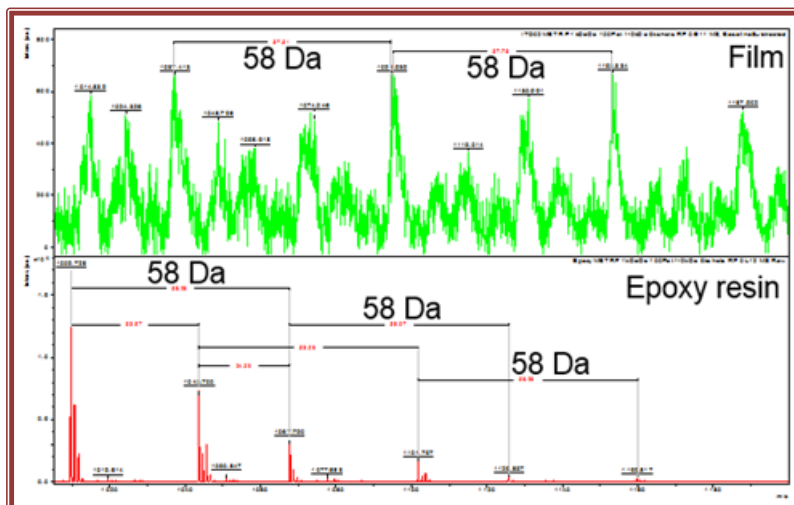


Figure 6.10. MALDI average mass spectra of film and pure epoxy resin

Furthermore, average mass spectra of the prepared film and pure epoxy resin, given in Figure 6.10, are made by MALDI to see whether the epoxy resin has reacted by checking similarities between peaks. Figure 6.10 shows that the film and the epoxy resin have peaks at different masses, which means that there are no pure epoxy groups inside the film. However, when looking at the possible molecular structure of the epoxy resin (Figure 6.1) and especially to the repeating unit polypropylene glycol (PPG), which has a molar mass of about 58 Da, that this unit is also found in the spectrum of the latex, again at different masses. This means that PPG chains are incorporated in the system and that copolymerization between acrylics and epoxy resin is indeed obtained, even in the low molecular chains analyzed here. Therefore the low molar masses in the bimodal distribution of molar masses from the GPC results are not just caused by not reacted surfactant or initiator, but contain small copolymers as well.

6.5 CONCLUSIONS

In this chapter the development of a method of high temperature batch emulsion polymerization initiated by microwave heating, which allows copolymerization in acrylics/hydrophobic resin hybrid systems, was investigated. The selected acrylic system was made of MMA/BA/AA and it was polymerized in presence of epoxy resin pre-polymer containing two epoxy functionality at each chain end.

The polymerization of MMA/BA/AA with epoxy resin was induced by thermal initiator (VA-086 and KPS) and MWH.

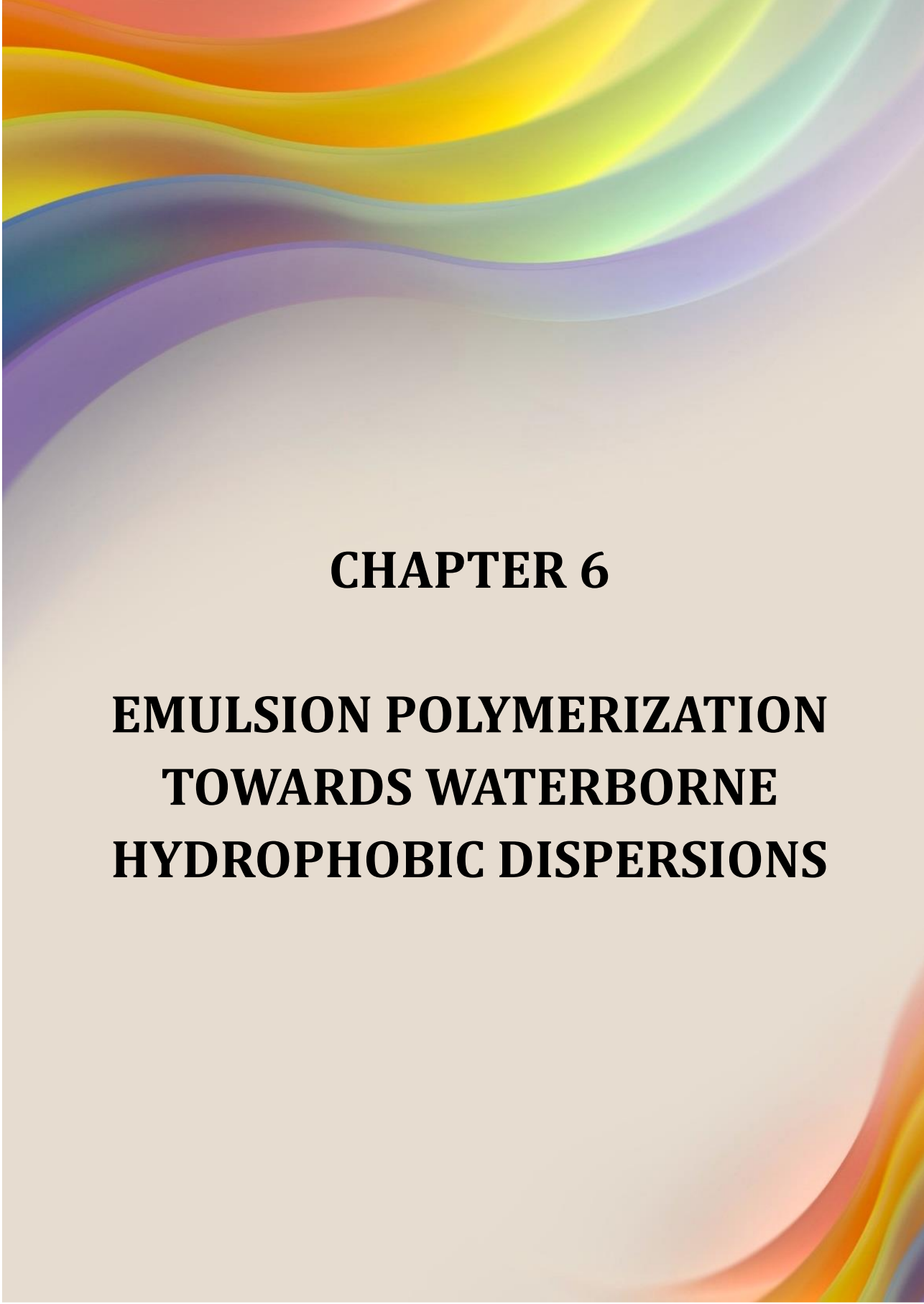
Both initiations V-089 and KPS at lower temperatures (80°C and 60°C) where enough to obtain a polymerizations with good characteristics like particle size, gel fraction and molecular weight. Probably the faster heating, accompanied with the pressure, and the initiator added before the reaction temperature was achieved. Is the ideal combination to obtain this type of polymers, with the advantage of reducing the costs for the used emulsion instead of miniemulsion, additionally the MW-energy consumption.

Polymer properties could not be performed due to a lack of time, but in the near future could be a future work, as well the more trails to add other resins like alkyd resins.

6.5 REFERENCES

- [1] P.A. Lovell, M.S. El-Aasser, Features of Emulsion Polymerization, in: Emuls. Polym. Emuls. Polym., 1997. [https://doi.org/10.1016/S1381-5148\(97\)84204-6](https://doi.org/10.1016/S1381-5148(97)84204-6).
- [2] M.J. Barandiaran, J.C. de la Cal, J.M. Asua, Emulsion Polymerization, in: Polym. React. Eng., John Wiley & Sons, Ltd, 2008: pp. 233–272. <https://doi.org/10.1002/9780470692134.ch6>.
- [3] Paint and Coatings Industry, Acrylic Hybrid Technology, (2002).

- <https://www.pcimag.com/articles/84118-acrylic-hybrid-technology>.
- [4] M. Goikoetxea, R.J. Minari, I. Beristain, M. Paulis, M.J. Barandiaran, J.M. Asua, A new strategy to improve alkyd/acrylic compatibilization in waterborne hybrid dispersions, *Polymer* (Guildf). (2010). <https://doi.org/10.1016/j.polymer.2010.09.052>.
- [5] H. Kawahara, T. Goto, K. Ohnishi, H. Ogura, H. Kage, Y. Matsuno, Preparation of epoxy resin/acrylic composite latexes by miniemulsion polymerization method, *J. Appl. Polym. Sci.* (2001). <https://doi.org/10.1002/app.1422>.
- [6] S.T. Wang, F.J. Schork, G.W. Poehlein, J.W. Gooch, Emulsion and miniemulsion copolymerization of acrylic monomers in the presence of alkyd resin, *J. Appl. Polym. Sci.* (1996). [https://doi.org/10.1002/\(SICI\)1097-4628\(19960620\)60:12<2069::AID-APP4>3.0.CO;2-K](https://doi.org/10.1002/(SICI)1097-4628(19960620)60:12<2069::AID-APP4>3.0.CO;2-K).
- [7] T.G.T. Jansen, J. Meuldijk, P.A. Lovell, A.M. van Herk, On the miniemulsion polymerization of very hydrophobic monomers initiated by a completely water-insoluble initiator: thermodynamics, kinetics, and mechanism, *J. Polym. Sci. Part A Polym. Chem.* (2016). <https://doi.org/10.1002/pola.28155>.
- [8] H. Zhang, Zhengfeng; Cheng, Qili; Wang, WO 2013/075293 A1: Process for emulsion polymerizing hydrophobic monomers, 2013.
- [9] C. Zhao, G. Zhang, L. Zhao, Effect of curing agent and temperature on the rheological behavior of epoxy resin systems, *Molecules.* (2012). <https://doi.org/10.3390/molecules17078587>.
- [10] E.M.S. Van Hamersveld, J.J.G.S. Van Es, F.P. Cuperus, Oil-acrylate hybrid emulsions, mini-emulsion polymerization and characterization, in: *Colloids Surfaces A Physicochem. Eng. Asp.*, 1999. [https://doi.org/10.1016/S0927-7757\(98\)00721-3](https://doi.org/10.1016/S0927-7757(98)00721-3).
- [11] C. Costa, A.L. Alberton, A.F. Santos, M. Fortuny, P.H.H. Araújo, C. Sayer, J.C. Pinto, Kinetic Parameters of the Initiator Decomposition in Microwave and in Conventional Batch Reactors - KPS and V50-Case Studies, *Macromol. React. Eng.* (2015). <https://doi.org/10.1002/mren.201500013>.
- [12] C. Costa, V.H.S. Santos, P.H.H. Araujo, C. Sayer, A.F. Santos, C. Dariva, M. Fortuny, Rapid decomposition of a cationic azo-initiator under microwave irradiation, *J. Appl. Polym. Sci.* (2010). <https://doi.org/10.1002/app.32409>.



CHAPTER 6

EMULSION POLYMERIZATION TOWARDS WATERBORNE HYDROPHOBIC DISPERSIONS

6.1 INTRODUCTION

Since the high demand for synthetic alternatives to natural rubber latexes boosted the research in this field during World War II, the emulsion polymerization technique is nowadays considered as the basis of a massive global industry that continues to expand, mainly due to the versatility of the reaction and the ability to control the properties of the polymer latexes produced [1]. With a yearly production of synthetic polymer dispersions of more than 25% of the overall polymer production, emulsion polymerization is important industrial process with divers applications in the main markets of polymer dispersions, like paints and coatings, paper coatings, adhesives, carpet backings and even in biomedical applications as drug delivery system [1,2].

Hybrid coatings based on combination of acrylics with another functional polymer, as for example, epoxies, alkyds, urethanes, or silicones are common class of polymer species known as high performance due to advantageous combination of the main properties of both polymer species. [3,4]. Incorporating of the hydrophobic components within acrylic systems results in producing, for example, protective coatings, which have not only a decorative purpose and excellent mechanical and thermal properties, but are also able to confer anti-fouling and water resistance properties to painted substrates.

The main problem in these systems is that physical blends of the two different polymer dispersions or emulsion polymerisation reaction of two different polymer systems can produce an incompatible mixture that exhibits the worst properties of each polymer. Therefore, the great challenge in this kind of material is to compatibilize the both phases. Previous studies show that the copolymerization of, for example, acrylic/alkyd and acrylic/epoxy resins have been performed by both emulsion and miniemulsion polymerization [5,6]. Although emulsion polymerization has several advantages over miniemulsion polymerization in terms of less complexity,

lower costs, easier scale-up, and better reproducibility, it is stated in both studies that miniemulsion polymerization proved to be the most effective in incorporating the hydrophobic resins into the acrylic coating copolymers. **The hydrophobic nature of the resin caused diffusion limitations**, which made it impossible for emulsion polymerization to succeed since, in this technique, diffusion of the hydrophobic component through the water phase into the polymer particles is needed. Miniemulsion overcomes this limitation, as the locus of polymerization are the small monomer droplets prepared from monomer and resins mixed previously. Therefore, no transport across the aqueous phase is necessary. The colloidal stability of miniemulsion is improved by use of a small amount of costabilizer, which is low molecular weight and highly water-insoluble component, which prevent Ostwald ripening process, by which small monomer droplets disappear by monomer diffusion to the large droplets. [2,7].

Even though miniemulsion polymerization enables the production of good quality hybrid latexes on a lab-scale, the implementation in the industry is still challenging, due to the requirement of additional energy to pre-form the small monomer droplets, which increases the irreproducibility and scale-up possibilities [2].

Alternatively, emulsion polymerization at increase temperature may be used, (≥ 100 °C) **aimed to increase the diffusion of the more hydrophobic component through the aqueous phase** and may be the clear road of scaling up the emulsion copolymerization in acrylic hybrid systems. This idea has been developed in a published patent was found, which stated that: "Although water solubility is not always a linear function of temperature, high temperature can increase diffusivity for low polar and non-polar monomers. By elevating the temperature, it is possible to increase the saturation concentration of hydrophobic monomers in water, which makes it possible for emulsion polymerizing hydrophobic monomers"[8]. Although some possible monomers to perform this kind of reaction are proposed, there are no

EMULSION POLYMERIZATION TOWARDS WATERBORNE HYDROPHOBIC DISPERSIONS

details about methods, results, or specifications, and the increase of the diffusivity of hydrophobic monomers at elevated temperatures was not proved.

Conventional heating reactors, however, are not convenient to perform the reactions in aqueous dispersed media at higher temperatures due to the use of water as a continuous phase. Therefore, in this work, it is intended to use a microwave (MW) reactor, which allows precise control of the temperature and pressure in the reaction system.

The main goal of this work will, therefore, be to develop a method of high-temperature emulsion polymerization assisted by microwave heating, which will allow copolymerization of the acrylics/hydrophobic resin hybrid systems. It is expected to obtain similar products as usually obtained by conventional miniemulsion polymerization at lower temperatures. Therefore, the main challenge lies in eliminating the distribution in chemical composition within the different particles by controlling the temperature and, subsequently, the diffusion of hydrophobic compounds throughout the water phase.

In this chapter, we explore this possibility taking advantage of the MW reactor with excellent control of temperature and pressure. The acrylic monomers (MMA/BA/AA) were copolymerized in emulsion polymerization either with epoxy or alkyd resin.

6.2 EXPERIMENTAL

6.2.4 MATERIALS

The materials are given in Appendix I.

6.2.2 POLYMERIZATIONS

Emulsion polymerization was carried out at 20% solids content (S.C.) of acrylic monomers and 10% of S.C. of resin, in 400 mL total volume emulsion. The water phase was prepared by mixing water and of sodium dodecyl sulfate (SDS, 1 wt%) surfactant and 1.5wt % based to acrylic monomers amount of the initiator 2,2'azobis[2-methyl-N-(2-hydroxyethyl)propionamide](VA-086) or potassium persulfate (KPS). The organic phase was by mixing MMA/BA/AA of 49.5/49.5/1 wt% ratio as the main monomers and 10% of epoxy resin D.E.R. 732.

Miniemulsion polymerization was performed for comparison under CH (ME 11^{CH}). Miniemulsion was prepared similarly as explained, with addition of 7% of stearyl acrylate (SA) polymerizable co-stabilizer to the oil phase. Both phases were stirring separately for 5 minutes at 200 rpm, mixed together, and stirred for 15 minutes at 300 rpm. For miniemulsion preparation, the emulsion containing SA was subjected to sonication by 10 minutes at 80% power output and 50% duty cycle under magnetic stirred at 250 rpm, sonication was carried out in an ice bath to avoid overheating.

When azo-initiator type was used, it was dissolved into the organic phase along with the monomers. On the other hand, the water-soluble initiator KPS was dissolved into the water phase. After that, the complete mixture was placed into MW reactor and polymerized in batch, several variables were changed along with the chapter, so the

EMULSION POLYMERIZATION TOWARDS WATERBORNE HYDROPHOBIC DISPERSIONS

different experiments are described in Table 6.1, where temperature, heating time, and reaction time was changed.

The initiator was added in the reaction mixture since the beginning, before the reaction starts it was subjected to just five minutes degasification. After that time, the nitrogen inlet was closed. The reactions were performed in hermetically closed MW reactor, so during the reaction the pressure increased.

Table 6.1. Reaction formulations for different co-polymerizations performed under microwave heating with different reaction parameters. (Exp^{CH}: Performed by conventional heating).

Exp.	Temperature (°C)	Initiator type	Heating program (min)	Reaction Time (min)
E1 ^{CH}	80	VA-086	10	120
2	80	VA-086	10	120
3	100	VA-086	10	120
4	120	VA-086	10	120
5	150	VA-086	10	60
6	100	VA-086	3	15
7	100	VA-086	3	30
8	60	KPS	3	120
9	80	KPS	3	120
10	100	KPS	3	120
ME11 ^{CH}	60	KPS	10	120

6.2.3 CHARACTERIZATIONS

The final acrylic conversions were measured gravimetrically. Particle size distribution of the latexes were determined by dynamic light scattering (DLS). The molar mass distribution (MMD) of the soluble fraction in THF was determined by gel permeation chromatography (GPC) at 35°C. To measure the MMD of samples, the sol part obtained after soxhlet extraction was concentrated and then directly analysed by GPC. The gel fraction was measured by soxhlet extraction, using THF as the solvent. In order to identify if the epoxy resin was present in the copolymer, the final latex was centrifuged at 10000 rpm of 4°C by 1 h, and after that their fractions were analysed by DLS and FT-IR.

More details about the methodology and characteristics of all equipment used are described in Appendix I.

6.3 RESULTS AND DISCUSSIONS

6.3.1 HYBRID LATEX CHARACTERISTICS

Hybrid polymer system made of MMA/BA/AA and bi-functional epoxy resin pre-polymer were copolymerized in situ, expecting to obtain crosslinking between the copolymer acrylic chains and the epoxy resin throughout COOH-epoxy reaction at increased temperature. The reactions were performed in emulsion system, and we increased slowly the reaction temperature, expecting to improve the epoxy resin diffusion and subsequently its incorporation in the hybrid polymer (Figure 6.1). The effect of the following parameters, the reaction time, the heating program in MW reactor, and the initiator type on the emulsion polymerization reaction, stability of the latex and incorporation of the epoxy in the hybrid polymer were studied.

EMULSION POLYMERIZATION TOWARDS WATERBORNE HYDROPHOBIC DISPERSIONS

The reactions were performed at four different temperatures for 10 min. The reaction performed at the lowest temperature (80°C) was performed under CH for comparison. In Table 6.2 the final conversion achieved and the latexes characteristics are shown. It may be observed that in CH reaction at 80°C in 120 min 44% acrylic monomer conversion was achieved, whereas, when performed under MWH, the conversion was as high as 96%. This difference in conversion is likely a result of the fact that the initiator was added to the reaction mixture in MWH reactor before heating was started, whereas in CH it was added after achieving the reaction temperature. Furthermore, the heating profiles were not equalized as in previous chapters and the heating program to achieve the reaction temperature in MW reactor was 10 min, which is rather long. These results clearly demonstrate our points of view, that most of the differences between CH and MWH polymerizations in published literature were result of the poor comparison conditions established between CH and MWH

Table 6.2. Characteristics of **MMA/BA/AA/Epoxy resin** latexes produced at different reaction temperatures, using **V-086** as initiator. Reaction time is 10 min. (Exp^{CH}: Performed by conventional heating).

Exp.	Temperature reaction (°C)	Overall Conversion (%)	Dp (nm)	Coagulum (%)	% Gel	Mw (kDa)	Đ
1 ^{CH}	80	44	92	0	6	---	---
2	80	96	114	0	49	1066	2.79
3	100	95	116	2	0	644	2.30
4	120	87	126	11	0	197	2.21
5	150	66	378	19	0	184	2.37

Table 6.2 demonstrates that by increasing of the temperature in the MWH reactor, the conversion decreased. However, simultaneously, coagulation appeared in the system and its amount increased with the temperature, which explained the lower conversions observed as part of the polymer was incorporated in the coagulum. The amount of coagulum obtained may be observed in Figure 6.2, where the photos of the reactor and the coagulum obtained at the end of each reactions are shown.

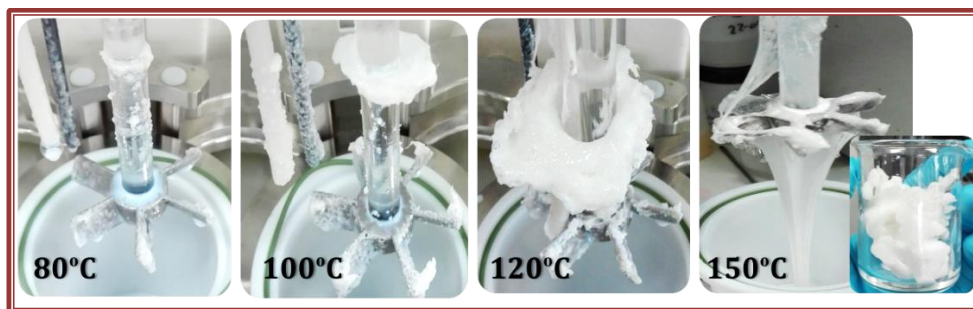


Figure 6.2. Coagulation of each reaction at different temperatures.

Table 6.2 shows that the average particle size of the latexes increased with temperature, probably due to the lower stability of the latexes at higher temperature. However, the increase coagulum production could be promoted as well due to the intensive mechanical stirring of the latex after achieving of full acrylic monomer conversion.

It is worth mentioning that the pressure was slightly increased during the higher temperature reaction. For reaction performed at 80°C, the pressure increased up to ~1.5 bar; for 100°C and 120°C the pressure was ~2 bar and, for 150°C the pressure increase up to ~3 bar..

According to Table 6.2, the insoluble polymer fraction in THF (% gel) of the latex produced at 80°C is 50%. This indicates that there is high incorporation of the epoxy

EMULSION POLYMERIZATION TOWARDS WATERBORNE HYDROPHOBIC DISPERSIONS

resin within the acrylic polymer. In the same reaction done under CH, there was no insoluble polymer produced. As it was mentioned, this difference was likely due to the difference in temperature in the initial reaction period. Even though at higher temperature due to faster initiator decomposition, it is expected to obtain lower molar masses, the higher temperature may promote the chain transfer to polymer process which leads toward increased branching and gel formation within the acrylic polymer [??]. Additionally the epoxy group reactions are as well promoted by increasing the temperature [9,10]. However, surprisingly the polymers produced at higher temperatures in MWG reactor did not contain any gel fraction and the produced molar masses were low, decreasing further with the temperature. The low molar mass is likely the reason for the lack of gel, and were obtained because of the promoted bimolecular terminations at high temperature. On the other hand, the gel obtained within these reactions was probably incorporate within the coagulum.

In the next attempts in order to decrease the coagulum formation, it was decided to shorten the heating program (to achieve the reaction temperature) in MW reactor from 10 min to 3 min and to decrease the reaction time from 120 min to 30 min, and to 15 min. The reactions were performed at 100°C and the results are presented in Table 6.3. As it may be observed in Figure 6.3, except the small amount of polymer adhered on the mechanical agitator, no coagulum was observed in the system. In the same reaction performed for 120 min (and with larger heating program of 10 min), apart of the polymer adhered on the agitator, there was 2% of the polymer present as solid coagulum.

Table 6.3. Characteristics of latexes produced by **MMA/BA/AA** copolymerization with **Epoxy resin**, using **V-086** as initiator at two different reaction times and, **100°C** reaction temperature.

Exp.	Reaction time (min)	Overall Conversion (%)	Dp (nm)	Coagulum (%)	% Gel	Mw (kDa)	Đ
6	15	84	121	0	17	609	2.1
7	30	85	115	0	10	611	2.2

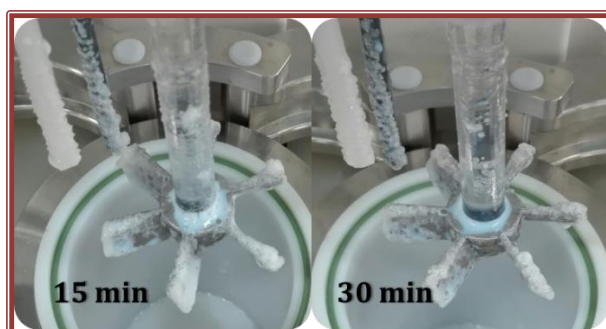


Figure 6.3. Photos of the coagulum of the reaction No.6 and No.7 at different reaction times.

Table 6.3 shows that very high acrylic monomer conversion was achieved, in both cases higher than 80%. The pressure into the reactor increased to ~2bar for both experiments, and the final particle size was similar between them (~118 nm). Under these conditions the incorporation of epoxy resin in the acrylic polymers, giving raise to formation of gel fraction was increased to about 17 % and 10 %, for both reactions, respectively. The sol molar masses were very similar of about 6000 kDa. These results indicate that the reaction was probably almost finished even in 15 min, and that the prolonged agitation was likely the reason of the creation of large coagulum. The lack

EMULSION POLYMERIZATION TOWARDS WATERBORNE HYDROPHOBIC DISPERSIONS

of full conversion can be a result on fast consumption of initiator due to very high decomposition rate at such high temperature, and possible solution could be addition of second shot of initiator to achieve full conversion.

The second advantage of shortening the reaction time is the decrease in the energy consumption. For example, for experiment No.3, the total MW-energy consumption was 1606.0 kJ and, for Exp. 6 and 7, the MW-energy consumed were for 252.2 kJ and 414.5 kJ, for a volume of 400 mL, at same temperature and pressure. However, the conditions should be found at which 100% conversion of acrylic monomers would be achieved.

In the so far presented results, VA-086 water-soluble azo initiator was used. It is known that azo-initiator decomposition rate is not affected by MW heating [11]. In the next attempts, KPS initiator was used, to check if the MW can affected the polymerization reaction not only through different way of heating, but as well through initiation step, as it was demonstrated that it decomposed faster under MW [11,12].

The heating time was kept at 3 minutes and reaction time was 120 min. The reactions were performed at three different temperatures, 60°C, 80°C and 100°C. For comparison, conventional heating miniemulsion polymerization was performed at 60°C.

Table 6.4 shown the characteristics of final latexes. High monomer conversions >95% were obtained by MWH method, whereas, for miniemulsion polymerization under CH 87% of conversion was achieved. No significant differences were observed in the final particle size, for all cases D_p of ~90 nm was obtained and no coagulum in neither case was observed (Figure 6.4). The similar particle size in the MW emulsion polymerization with that of CH miniemulsion and the lack of coagulum indicate that the reactions were successful and probably beside the diffusion limitation of epoxy resin it was probably incorporated into the polymer particles homogeneously.

Table 6.4. Characteristics of latexes produced by **MMA/BA/AA** copolymerization with **Epoxy resin** at different reaction temperatures and, **KPS** as initiator.

Exp.	Temperature reaction (°C)	Overall Conversion (%)	Dp (nm)	Coagulum (%)	% Gel	Mw (kDa)	Đ
8	60	96	87	1	48	2015	2.02
9	80	99	76	1	13	822	1.96
10	100	96	87	2	11	761	2.25
11 ^{CH}	60	87	91	0	7	---	---

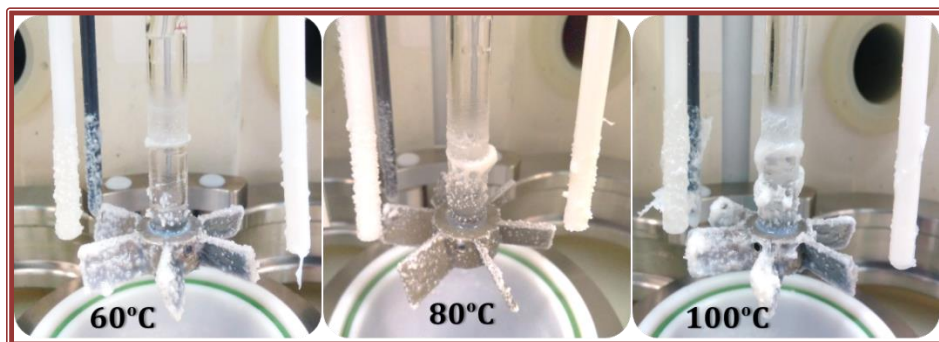


Figure 6.4. Coagulation of reaction No.6 and No.7 at different reaction times.

The gel content for MWH at 60°C was found to be almost 50%, which amount dropped at higher temperature to 13% and 11%. Surprisingly, the molar mass of the THF soluble fraction for 60°C reaction was very high (>2.000 kDa) and decreased at increased temperature in MW reactor. For CH miniemulsion polymerization just 7% gel was found, this could be due to a less epoxy resin incorporation into de polymer system, because of less COOH – epoxy reaction at lower temperature (60°C).

6.3.2 INCORPORATION OF EPOXY INTO THE CO-POLYMER

In order to identify if the composition of all polymer particles is similar and contain both components, the acrylics and the epoxy, the final latex was centrifuged at 10000 rpm of 4°C for 1 h, Different fractions along the length of the centrifugation tube were extracted the fractions and were analysed by DLS and FT-IR. FTIR spectra were used to distinguish the composition within each fraction, for which the ratio of the following bands were used as indicator for the composition: for acrylics C=O at 1721 cm^{-1} and for the epoxy resin C-O of oxirane group at 842 cm^{-1} . Representative FT-IR spectra of the neat epoxy, neat acrylics and their combination are shown in Figure 6.5, showing the characteristic peaks of both components used to calculate relative composition of the each fraction. The obtained results are shown in Table 6.5.

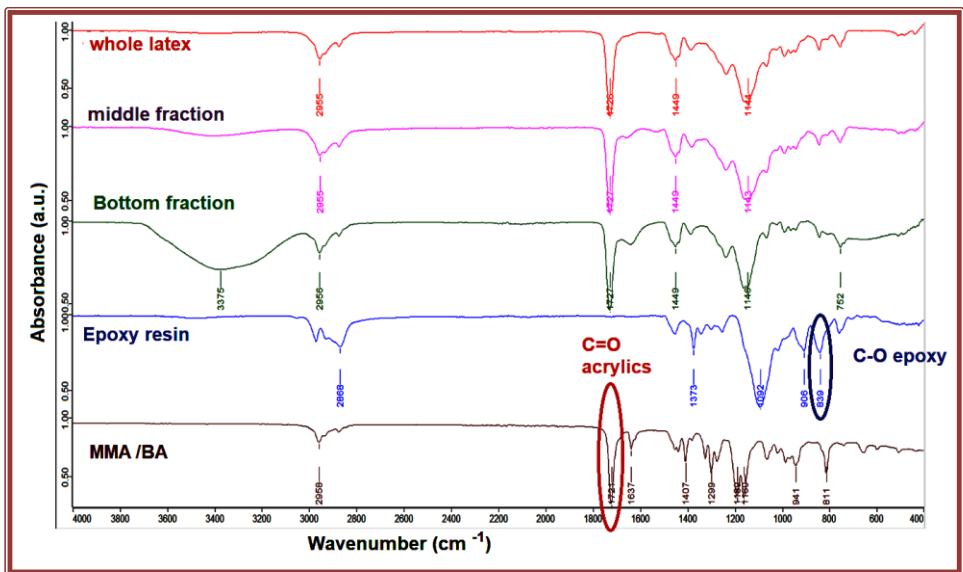


Figure 6.5. Representative FTIR spectra (reaction MW at 80°C with VA-086 initiator) and characteristic peaks used for evaluation of chemical composition of the polymer fraction after centrifugation.

In Figure 6.6 the particle size distribution from DLS (PSD) of the hybrid latex obtained at 80°C with VA-086 azo initiator. In the figure the PSD fraction after centrifugation of this latex are presented, too. By centrifugation of the latexes, 3 phases are obtained: a top fraction consisting mostly of water, a middle fraction containing the less dense particles and a bottom fraction consisting of more dense particles. The bottom fraction is not included in the Figure 6.6, because it was completely solid after centrifugation and could not be analyzed with DLS. Figure 6.6 presents that the whole latex and the middle fraction has completely same PSD, which indicates that the separation occurred during centrifugation is not due to the size of the particles but due to their composition.

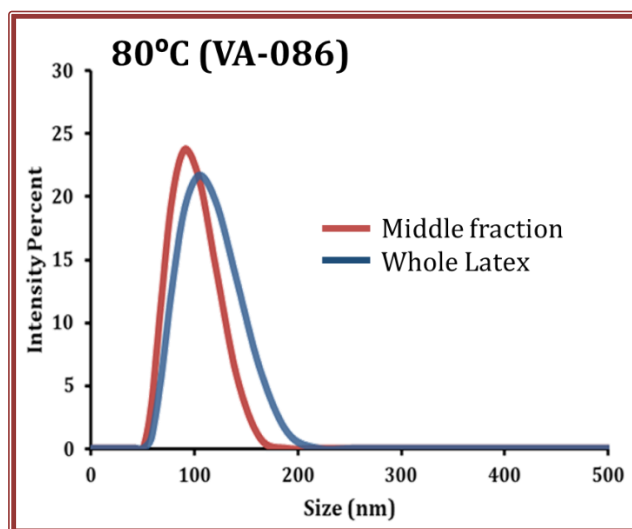


Figure 6.6. PSD of the latex obtained at 80°C with VA-086 and the middle fraction after its centrifugation.

EMULSION POLYMERIZATION TOWARDS WATERBORNE HYDROPHOBIC DISPERSIONS

Similar findings were obtained for all other latexes produced with VA-086 at different temperature, except the latex obtained at 150°C. As shown in Figure 6.7, there is an important difference in PSD between the middle fraction and the whole latex. The PSD of the middle fraction is shift towards the lower particle sizes with respect to the whole latex, indicating that the particles were separated in fractions with different sizes.

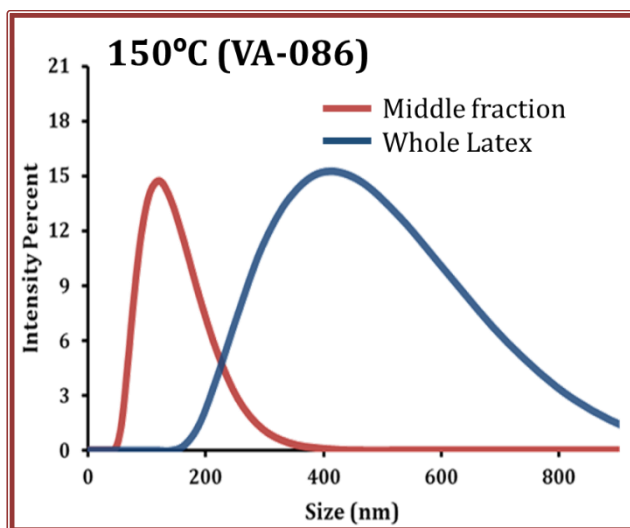


Figure 6.7. PSD of hybrid latex obtained at 150°C with VA-086 initiator and the middle fraction after its centrifugation.

The composition of the each of these fractions (including the bottom fraction that were not analyzed with DLS, was determined by FT-IR analysis and the intensity ratio of C=O representing acrylics and C-O representing epoxy resin. Table 6.5 shows the ratio of some of the representative materials obtained.

Table 6.5. Ratio of the FT-IR bands of acrylics and epoxy, of each latexes produced by MMA/BA/AA copolymerization with **Epoxy resin** at different reaction temperatures and, different **initiators** .

Exp.	Temperature (°C)	sample	Dp (nm)	Ratio between Acrylics/epoxy
1 ^{CH}	80	Final latex	92	7.35
2	80	Final latex	114	8.68
		Middle fracttion	112	8.46
3	100	Final latex	116	7.59
		Middle fracttion	109	7.47
		Coagulum	--	6.75
4	120	Final latex	126	8.045
		Middle fracttion	120	8.249
		Coagulum	--	8.448
5	150	Final latex	378	5.54
		Middle fracttion	119	2.32
		Coagulum	--	11.17
6	100	Final latex	121	6.493
		Middle fracttion	112	6.085
7	100	Final latex	115	5.89
		Middle fracttion	110	5.462
8	60	Final latex	87	6.528
		Middle fracttion	81	6.886
9	80	Final latex	76	7.00
		Middle fracttion	78	6.23
10	100	Final latex	87	7.953

EMULSION POLYMERIZATION TOWARDS WATERBORNE HYDROPHOBIC DISPERSIONS

		Middle fraction	77	6.24
11 ^{CH}	60	Final latex	91	9.12
		Middle fraction	67	5.63

In order to determine and visualize the distribution of compounds in the latexes by MALDI-IMS measurements, first the utilized latex is chosen from the GPC results. In this work the latex with epoxy resin and Azobis initiator performed at 150°C is chosen for all upcoming MALDI-IMS results, which has a bimodal distribution of molar masses of which the low molecular weights can be detected by MALDI-IMS. After preparing films of this latex on ITO glass slides by using a film applicator and a 2-MBT matrix deposited on it by sublimation, as explained in Characterization, the MALDI-IMS measurements are started.

On the prepared ITO glass substrate, a small area ($\approx 1,0$ cm x 0,5 cm) was scanned and analyzed by MALDI-IMS and from this the following average spectra of the whole area are obtained, shown in Figure 6.8. The top spectrum represents the obtained mass spectrum for all detected compounds and the two bottom images show for one specific mass peak, here for 1169 Da and 1799 Da, the intensities of it in the whole detected area of the sample. The color red indicates a high intensity of the detected mass peak in the area and the color blue a low intensity. For the detected area of Figure 6.8 can be stated that it looks quite homogeneous. Another area of the same glass slide was analyzed as well for which the average mass spectrum and two intensity images, at 1058 Da and 1661 Da are given in Figure 6.9. The distribution of compounds is different in Figure 6.9 compared to Figure 6.8. The images show a distribution in the range between 1-2 kDa where higher intensities are found in the right part of the detected area. There is no homogeneous distribution present. So from even just one sample can be stated that there is probably a difference in composition present within the latexes.

CHAPTER 6

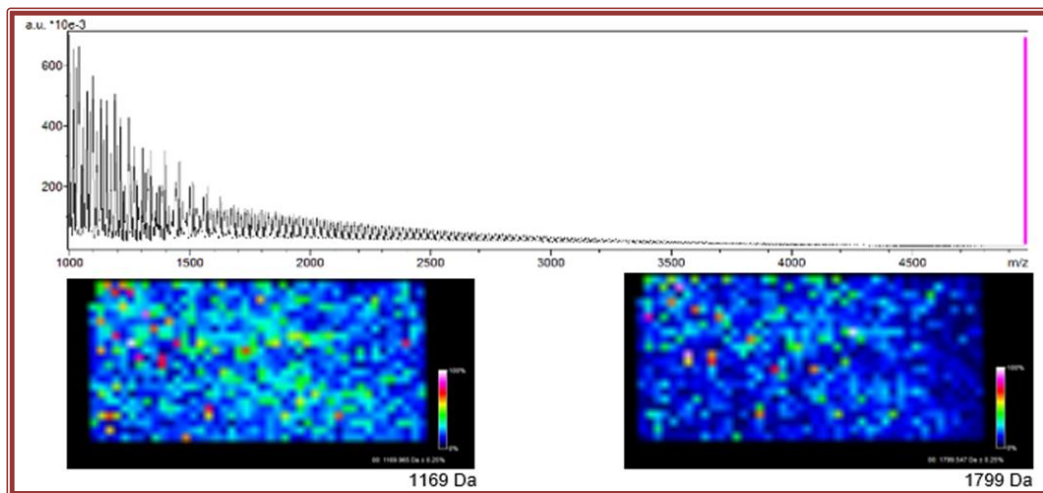


Figure 6.8. MALDI-IMS results ITO coated glass slide with epoxy resin, Azobis initiator at 150°C. Top spectrum = Mass spectrum, Images bottom = Intensities of specific mass peaks (1169 Da and 1799 Da) in top spectrum

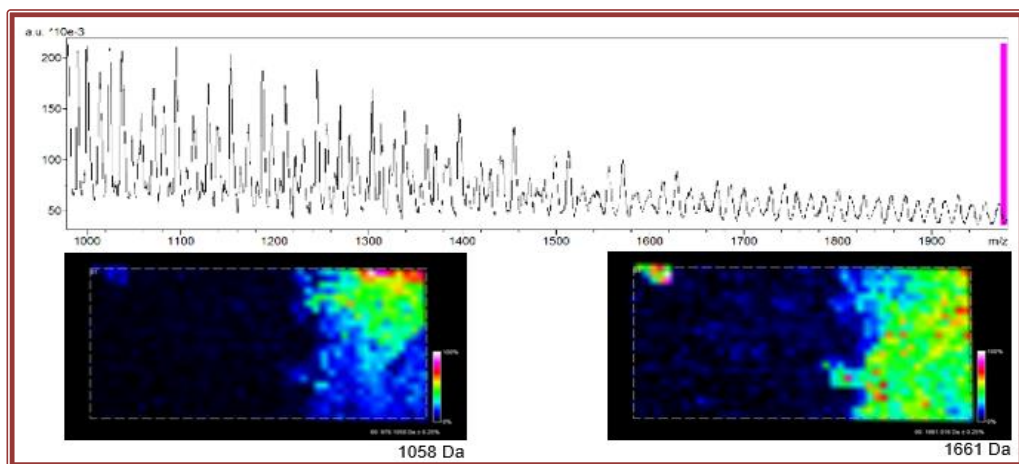


Figure 6.9. MALDI-IMS results ITO coated glass slide with epoxy resin, Azobis initiator at 150°C. Top spectrum = Mass spectrum, Images bottom = Intensities of specific mass peaks (1058 Da and 1661 Da) in top spectrum

EMULSION POLYMERIZATION TOWARDS WATERBORNE HYDROPHOBIC DISPERSIONS

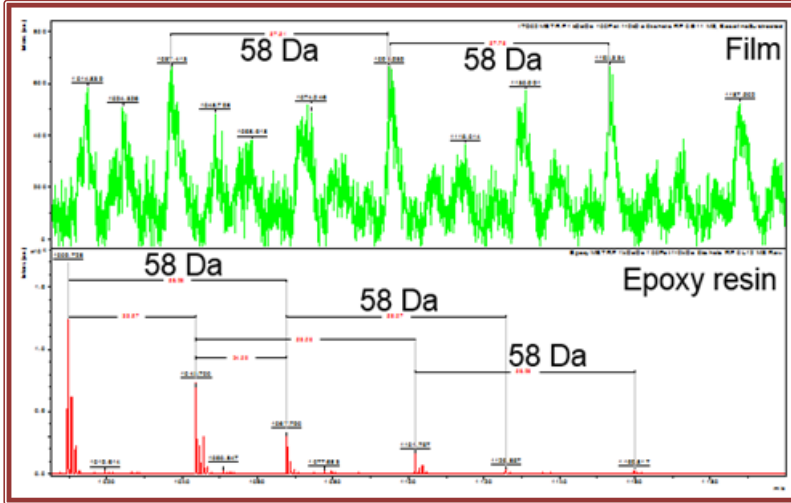


Figure 6.10. MALDI average mass spectra of film and pure epoxy resin

Furthermore, average mass spectra of the prepared film and pure epoxy resin, given in Figure 6.10, are made by MALDI to see whether the epoxy resin has reacted by checking similarities between peaks. Figure 6.10 shows that the film and the epoxy resin have peaks at different masses, which means that there are no pure epoxy groups inside the film. However, when looking at the possible molecular structure of the epoxy resin (Figure 6.1) and especially to the repeating unit polypropylene glycol (PPG), which has a molar mass of about 58 Da, that this unit is also found in the spectrum of the latex, again at different masses. This means that PPG chains are incorporated in the system and that copolymerization between acrylics and epoxy resin is indeed obtained, even in the low molecular chains analyzed here. Therefore the low molar masses in the bimodal distribution of molar masses from the GPC results are not just caused by not reacted surfactant or initiator, but contain small copolymers as well.

6.5 CONCLUSIONS

In this chapter the development of a method of high temperature batch emulsion polymerization initiated by microwave heating, which allows copolymerization in acrylics/hydrophobic resin hybrid systems, was investigated. The selected acrylic system was made of MMA/BA/AA and it was polymerized in presence of epoxy resin pre-polymer containing two epoxy functionality at each chain end.

The polymerization of MMA/BA/AA with epoxy resin was induced by thermal initiator (VA-086 and KPS) and MWH.

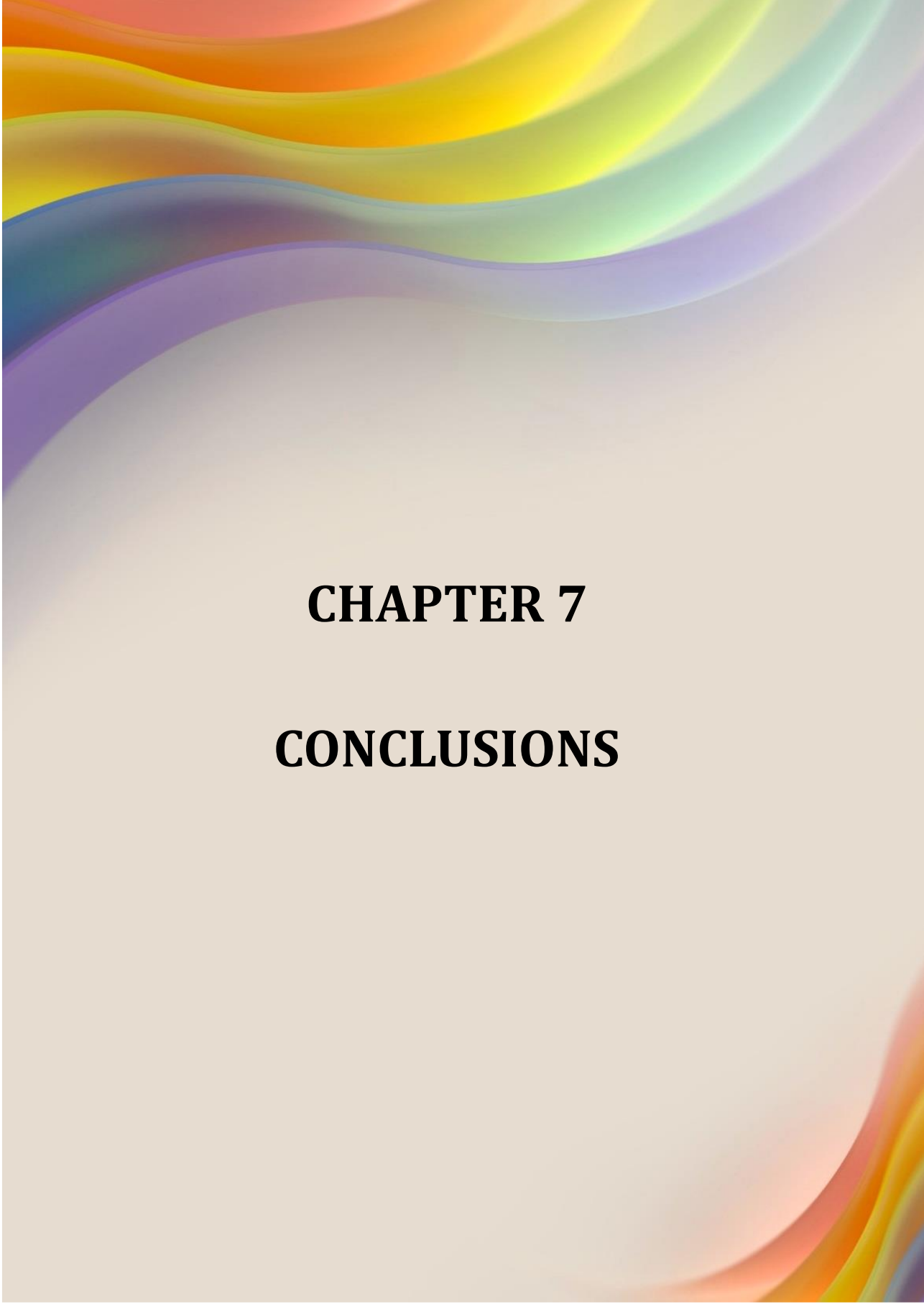
Both initiations V-089 and KPS at lower temperatures (80°C and 60°C) were enough to obtain a polymerizations with good characteristics like particle size, gel fraction and molecular weight. Probably the faster heating, accompanied with the pressure, and the initiator added before the reaction temperature was achieved. Is the ideal combination to obtain this type of polymers, with the advantage of reducing the costs for the used emulsion instead of miniemulsion, additionally the MW-energy consumption.

Polymer properties could not be performed due to a lack of time, but in the near future could be a future work, as well the more trails to add other resins like alkyd resins.

6.5 REFERENCES

- [1] P.A. Lovell, M.S. El-Aasser, Features of Emulsion Polymerization, in: *Emuls. Polym.* *Emuls. Polym.*, 1997. [https://doi.org/10.1016/S1381-5148\(97\)84204-6](https://doi.org/10.1016/S1381-5148(97)84204-6).
- [2] M.J. Barandiaran, J.C. de la Cal, J.M. Asua, *Emulsion Polymerization*, in: *Polym. React. Eng.*, John Wiley & Sons, Ltd, 2008: pp. 233–272. <https://doi.org/10.1002/9780470692134.ch6>.
- [3] Paint and Coatings Industry, *Acrylic Hybrid Technology*, (2002).

- <https://www.pcimag.com/articles/84118-acrylic-hybrid-technology>.
- [4] M. Goikoetxea, R.J. Minari, I. Beristain, M. Paulis, M.J. Barandiaran, J.M. Asua, A new strategy to improve alkyd/acrylic compatibilization in waterborne hybrid dispersions, *Polymer* (Guildf). (2010). <https://doi.org/10.1016/j.polymer.2010.09.052>.
- [5] H. Kawahara, T. Goto, K. Ohnishi, H. Ogura, H. Kage, Y. Matsuno, Preparation of epoxy resin/acrylic composite latexes by miniemulsion polymerization method, *J. Appl. Polym. Sci.* (2001). <https://doi.org/10.1002/app.1422>.
- [6] S.T. Wang, F.J. Schork, G.W. Poehlein, J.W. Gooch, Emulsion and miniemulsion copolymerization of acrylic monomers in the presence of alkyd resin, *J. Appl. Polym. Sci.* (1996). [https://doi.org/10.1002/\(SICI\)1097-4628\(19960620\)60:12<2069::AID-APP4>3.0.CO;2-K](https://doi.org/10.1002/(SICI)1097-4628(19960620)60:12<2069::AID-APP4>3.0.CO;2-K).
- [7] T.G.T. Jansen, J. Meuldijk, P.A. Lovell, A.M. van Herk, On the miniemulsion polymerization of very hydrophobic monomers initiated by a completely water-insoluble initiator: thermodynamics, kinetics, and mechanism, *J. Polym. Sci. Part A Polym. Chem.* (2016). <https://doi.org/10.1002/pola.28155>.
- [8] H. Zhang, Zhengfeng; Cheng, Qili; Wang, WO 2013/075293 A1: Process for emulsion polymerizing hydrophobic monomers, 2013.
- [9] C. Zhao, G. Zhang, L. Zhao, Effect of curing agent and temperature on the rheological behavior of epoxy resin systems, *Molecules.* (2012). <https://doi.org/10.3390/molecules17078587>.
- [10] E.M.S. Van Hamersveld, J.J.G.S. Van Es, F.P. Cuperus, Oil-acrylate hybrid emulsions, mini-emulsion polymerization and characterization, in: *Colloids Surfaces A Physicochem. Eng. Asp.*, 1999. [https://doi.org/10.1016/S0927-7757\(98\)00721-3](https://doi.org/10.1016/S0927-7757(98)00721-3).
- [11] C. Costa, A.L. Alberton, A.F. Santos, M. Fortuny, P.H.H. Araújo, C. Sayer, J.C. Pinto, Kinetic Parameters of the Initiator Decomposition in Microwave and in Conventional Batch Reactors - KPS and V50-Case Studies, *Macromol. React. Eng.* (2015). <https://doi.org/10.1002/mren.201500013>.
- [12] C. Costa, V.H.S. Santos, P.H.H. Araujo, C. Sayer, A.F. Santos, C. Dariva, M. Fortuny, Rapid decomposition of a cationic azo-initiator under microwave irradiation, *J. Appl. Polym. Sci.* (2010). <https://doi.org/10.1002/app.32409>.



CHAPTER 7

CONCLUSIONS

CONCLUSIONS

7.1. GENERAL CONCLUSIONS

Study of the comparison of polymerization process performed by two different methods: microwave heating (MWH) and conventional heating (CH), using identical: heating rates, stable temperature profiles, stirring rates and, initiator addition at the same time and, the temperature at atmospheric pressure was done. Three different polymerization techniques, such as solution, emulsion, and miniemulsion, were investigated to analyze the differences in polymerization rate, copolymer composition, polymer microstructure, and mechanical properties between MWH and CH methods. Additionally, more experiments performed under MWH as a proof of the concept were done, like the graphene surface modification and their polymer composites, waterborne hydrophobic polymerizations were performed.

A reliable comparison of free radical CH and MWH assisted solution polymerization was reached by creating similar reaction temperature profiles, eliminating the possibility to attribute the observed effects to thermal differences. The most common monomers for free-radical polymerization, such as MMA, BA, and St, as well as organometallic monomer VFc, presenting different polarities and dielectric properties, were selected. Two types of organic solvents were studied.

On the one hand, toluene an MW transparent solvent, and on the other, DMF is characterized by fast absorption, efficient heating under MWH. Finally, three different initiators have been studied: AIBN and two peroxides LPO and BPO.

It was found that under similar reaction temperature profiles in both CH and MWH reactors in the case of MMA/BA and MMA/St monomer couples, no changes were observed neither in polymerization rates nor in the polymer composition and molar masses. Nevertheless, in the case of MMA/VFc monomer couple in both investigated solvents, slightly enhanced polymerization rates were observed, especially in the

early reaction stages. This effect was accompanied by a difference in copolymer composition, suggesting altered reactivity ratios of MMA and VFc during polymerization under MWH. The observed effects were more pronounced in toluene, considered as MW transparent solvent, because the toluene system was exposed to more intense MW irradiation in order to keep the same temperature profile as one of the DMF systems. Increasing the concentration of VFc in the initial co-monomer mixture, the observed effects in DMF solvent increased, too. As a result, the copolymer obtained in MW irradiation in shorter reaction times was richer in VFc than the respective CH copolymer.

The observed effects were explained by the unique heat properties of the MW irradiation in a multi-component solution, which provided selective heating and the creation of dynamically distinct domains. Depending on the interaction of the components with MW irradiation within each domain, they will either absorb the MW irradiation and efficiently transfer it to heat or will remain in the configurational mode and accumulate the heat, which likely increased the mobility of the molecules within such domain. The last case results in the creation of microwave specific effects, as the ones observed in the case of MMA/VFc mixture. The MW energy requirement of MMA/VFc monomer system, which was higher than for other systems besides the high capability of VFc of MW absorption, demonstrates the inefficiency of VFc to convert the absorbed energy into heat.

A comparison of free-radical CH and MWH assisted emulsion polymerization was performed under similar reaction temperature profiles, decreasing the possibility to attribute the observed effect to thermal differences. Under such conditions, the copolymerization of MMA/BA as the main monomers were studied, modifying the amount of initiator (KPS), or type of functional monomer (HEMA, NaSS, and AM) added in a small amount (1%) to the MMA/BA formulation.

CONCLUSIONS

Very small differences were observed between CH and MWH reactions in the initial reaction period, which were diminished during the reaction. The polymerization rate was slightly higher under MWH than CH, which was attributed to the initial drop of temperature in CH reactor when the initiator solution was introduced. Despite the higher temperature initially in the MWH reactor, under which it was expected to produce faster decomposition of KPS, fewer particles were nucleated. We think that the higher temperature-induced postponed nucleation process due to increased free energy of nucleus formation or because of the higher volumetric growth rate of the particles. The particle size was a little bit larger in the MWH reaction, signifying that the average radical per particle is lower. Nevertheless, the molar masses of the polymer produced under MWH, in general, were larger than those obtained under CH. These effects were decreased when a higher amount of KPS initiator was used, and the effects were stronger when ionic functional monomers were, especially in the case of NaSS. These results even presented minor differences between both heating methods, a strong indication that there is an effect occurring under MW different from pure thermal effects.

In the case of functional monomers, the obtained results demonstrated that higher incorporation of the functional monomers was produced in the reaction under MWH, which was attributed to the improved partitioning of these highly hydrophilic monomers. DMTA results have shown that all polymers produced under MWH were slightly more mechanically stable; however, essential thermal stability was observed in MWH polymers. Namely, they kept the thermal stability at temperatures higher for about from 7°C to 27°C than that of CH polymers. Additionally, the MWH polymers absorbed up to from 5.7% to 30.1% less water absorption than their CH counter polymers.

Finally, this work demonstrated that the use of MWH to assist polymerization reaction in the emulsion is an important tool towards more sustainable polymer production, with eventually improved properties.

A reliable comparison of free-radical of CH and MWH assisted miniemulsion polymerization of MMA/BA/HEMA with the addition of the different amount of MWCNTs was reached by creating similar reaction temperature profiles.

It was found that, under similar reaction temperature profiles in both CH and MWH reactors, the polymerization rate was not significant, as well the number of particles and the final particle size, even with the addition of MWCNTs. In this polymer system, the use of KPS as initiator does not have any MW-effect in polymerization rate.

The insoluble polymer fraction in THF was strongly increased with the addition of MWCNTs for CH reactions, attributed to the possible grafting between polymer chains onto MWCNTs, whereas polymers synthesized by MWH is likely that they do not present the insoluble polymer fraction. This was confirmed with polymer mechanical properties evaluated in DMTA where the reinforcement of the polymer was done with the addition of MWCNTs synthesized by both heating methods.

Additionally, the latex stability of the polymer composites after two years of storage was significantly different between both heating methods, probably due to the high cross-linked between the polymer and MWCNTs the latex synthesized under CH present less stability than the MWH-latex.

In graphene surface modification it was demonstrated that MWH can provide facile way for surface modification of graphene, by simple irradiation in water either without any additives or in presence of water-soluble monomers and initiator. In all

CONCLUSIONS

these strategies, mild graphene surface modification was induced, which was demonstrated by RAMAN spectroscopy in which it was observed that the defect sites in graphene structure were increased. The hydrophobicity of the treated graphene dropped with respect to the non-treated one, as it was shown by measurements of water contact angles.

Such treated graphene were used to prepare miniemulsion using MMA/BA/HEMA monomer mixture and polymerized in MWH reactor. As a result nice composite films were obtained, in which the non-treated graphene was surprisingly dispersed better than the treated ones. This was the probable reason for the modest improvement of the mechanical and thermal properties.

The development of a method of high temperature batch emulsion polymerization initiated by microwave heating, which allows copolymerization in acrylics/hydrophobic resin hybrid systems, was investigated. The selected acrylic system was made of MMA/BA/AA and it was polymerized in presence of epoxy resin pre-polymer containing two epoxy functionality at each chain end.

The polymerization of MMA/BA/AA with epoxy resin was induced by thermal initiator (VA-086 and KPS) and MWH.

Both initiations V-089 and KPS at lower temperatures (80°C and 60°C) where enough to obtain a polymerizations with good characteristics like particle size, gel fraction and molecular weight. Probably the faster heating, accompanied with the pressure, and the initiator added before the reaction temperature was achieved. Is the ideal combination to obtain this type of polymers, with the advantage of reducing the costs for the used emulsion instead of miniemulsion, additionally the MW-energy consumption.

Polymer properties could not be performed due to a lack of time, but in the near future could be a future work, as well the more trails to add other resins like alkyd resins.

7.2. FUTURE WORK AND PERSPECTIVES

A Ph.D. thesis work has a limited period, and hence, there are some aspects that remain to be investigated. Here there are some suggestions for the next scientific, that want to continue this work.

Free-emulsifier polymerization was not studied, and according to state of the art (Chapter 1), some publications reported successful emulsifier-free water polymer dispersions, another possibility the incorporation into the formulation more amount of ionic monomer like NaSS, can be a possible solution. As well, it should be useful if other types of initiators could be used, like water-soluble azo-initiators.

In miniemulsion polymerization vinylferrocene could be another monomer to study, even, more initiators and different concentrations of surfactant could be possible to used.

Microwave-assisted polymerization is a wide area, and multidisciplinary scientific team could be much better to trying to elucidate more accurately all the science behind this topic.

Every year humanity grows and with it technology, therefore new and better materials will be required. In base on this work MWH could produce polymers with almost the same properties than CH, additionally, the control temperature is much better under MWH, and energy consumption could be reflected if the components of the reaction mixture are well selected.

CONCLUSIONS

7.3. PUBLICATIONS AND CONFERENCES PRESENTATIONS

Part of this thesis have been published or will be published as soon as possible; besides, part of the work described in the thesis have been presented at conferences as an oral or poster presentation. For manuscripts that are in preparation, the title and/or authors may still be adapted; hence, they could suffer some modification.

7.3.1. PUBLICATIONS

7.3.1.1. FIRST AUTHOR

- **Bertha T. Pérez-Martínez**, José M. Asua, Radmila Tomvska *et al.*, “Miniemulsion copolymerization of (meth)acrylates in the presence of functionalized multiwalled carbon nanotubes for reinforced coating applications” *Beilstein J. Nanotechnol.* (8) 2017,1328-1337.
- **Bertha T. Pérez-Martínez**, Ulrich S. Schubert, Radmila Tomvska, *et al.*, “Microwave irradiation versus conventional heating assisted free-radical copolymerization in solution” *Chemical Engineering Journal* (399) 2020, 125761.
- **Bertha T. Pérez-Martínez**, Radmila Tomovska, “Miniemulsion copolymerization of (meth)acrylates in the presence of functionalized multiwalled carbon nanotubes under microwave heating, an update” In preparation.
- **Bertha T. Pérez-Martínez**, Radmila Tomovska, “Microwave-assisted free-radical emulsion polymerization” In preparation.
- **Bertha T. Pérez-Martínez**, Radmila Tomovska, “Review of Microwave-assisted polymerization along the time” In preparation.

7.3.1.2. COLLABORATIONS

- Ana Trajcheva, **Bertha T. Pérez-Martínez**, Radmila Tomovska *et al.*, “QCM nanocomposites based on graphene nanoribbon” *Polymer Journal* 2020
- Marija Prosheva, **Bertha T. Pérez-Martínez**, Radmila Tomovska *et al.*, “Dry Sonication Process for Preparation of Hybrid Graphene/ Carbon Nanotubes Structures for Chemical Sensors Application” Submitted

7.3.2. CONFERENCES

7.3.2.1. ORAL PRESENTATIONS

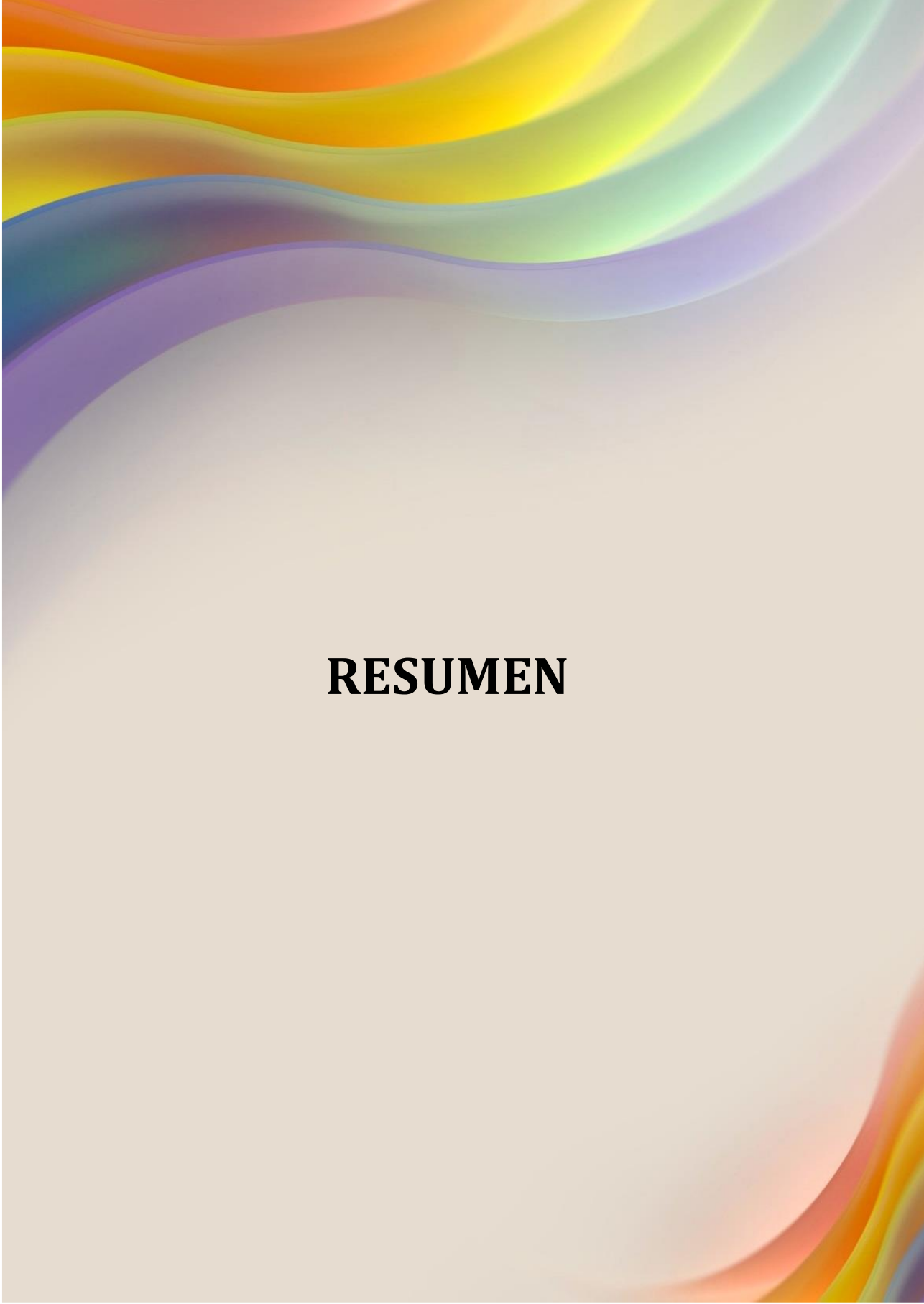
- Waterborne Multiwall Carbon Nanotubes/Polymer Composites Prepares by In-Situ Miniemulsion Polymerization; 10th World Congress of Chemical Engineering; **Barcelona, Spain; October 2017.**
- A comprehensive study of Microwave initiates solution copolymerization of MMA/BA: effect on reactivity ratios; XV Reunión del Grupo Especializado de Polímeros (GEP); **Huelva, Spain; September 2018.**

7.3.2.2. POSTER PRESENTATIONS

- Comparison of Conventional Heating and Microwave Initiated Polymerization Process, Performed in Solution an Emulsion; International Polymer Colloids Group Conference (IPCG/GRS); **Singapour; June 2019.**

7.3.2.3. AWARDS

- The video clip entitled: “Polymer nanocomposites: Microwave Heating Vs. Conventional Heating” into the call Exciting And Simple Experiments (EASE) in IPCG/GRS conference; **Singapour; June 2019.**



RESUMEN

8.1. RESUMEN Y CONCLUSIONES

El objetivo de este trabajo es comparar los procesos de polimerización asistidos por dos métodos diferentes: calentamiento por microondas (MWH) y calentamiento convencional (CH), utilizando idénticos: velocidades de calentamiento, perfiles de temperatura estables, velocidades de agitación así como la adición del iniciador al mismo tiempo y temperatura a presión atmosférica. Se investigaron tres técnicas de polimerizaciones diferentes, solución, emulsión y miniemulsión, para analizar si existen diferencias en la velocidad de polimerización, la composición del copolímero, la microestructura del polímero y las propiedades mecánicas entre los procesos y productos sintetizados bajo MWH y CH. Para ello se estudió la copolimerización de diversos tipos de monómeros, incluidos los monómeros funcionales, e incluso algunos sistemas híbridos acrílico-epoxi, así como la polimerización in situ en sistemas compuestos con grafeno y nanotubos de carbono.

En el **Capítulo 1** se describió la teoría principal detrás de los mecanismos de transferencia de calor del calentamiento por microondas y sus posibles efectos, así como el estado del arte de los diferentes métodos de polimerización en solución, emulsión y miniemulsión realizados bajo calentamiento por microondas, también se describe el objetivo general de este trabajo de investigación y la organización de todo el documento.

El **Capítulo 2**, se realizó la copolimerización por radicales libres en solución para estudiar si la forma de calentamiento (ya sea MWH o CH) afecta la cinética de copolimerización y las características del producto (la microestructura y la composición del copolímero). Para ello, se utilizaron diferentes sistemas de monómeros (diferente en polaridad y propiedades dieléctricas, así como el uso de monómero organometálico), diferentes iniciadores y la reacción se realizó en un solvente de alta absorción de MW como dimetilformamida (DMF) o un solvente



transparente al MW como lo es el tolueno. Se logró una comparación confiable de la polimerización vía radicales libres en solución asistida por MWH o CH mediante la creación de perfiles de temperatura de reacción similares. Se seleccionaron los monómeros más habituales para la polimerización por radicales libres, como metacrilato de metilo (MMA), acrilato de butilo (BA) y estireno (St), así como el monómero organometálico vinil ferroceno (VFc), que presenta diferentes polaridades y propiedades dieléctricas. También se estudiaron dos tipos de disolventes orgánicos, así como tres diferentes iniciadores: AIBN y dos peróxidos LPO y BPO. Se encontró que bajo perfiles de temperatura de reacción similares en reactores de CH y MWH en el caso de parejas de monómeros MMA/BA y MMA/St, no se observaron cambios ni en las velocidades de polimerización ni en la composición del polímero y tampoco en masas molares. Sin embargo, en el caso del par de monómeros MMA/VFc en ambos disolventes investigados, se observaron velocidades de polimerización ligeramente mejoradas, especialmente en las primeras etapas de reacción. Este efecto estuvo acompañado por una diferencia en la composición del copolímero, lo que sugiere relaciones de reactividad alteradas de MMA y VFc durante la polimerización bajo MWH. Los efectos observados fueron más pronunciados en tolueno, considerado como disolvente transparente de MW, ya que, el sistema con tolueno se expuso a una irradiación de MW más intensa para mantener el mismo perfil de temperatura a comparación con la reacción donde se usa DMF. Al aumentar la concentración de VFc en la mezcla de comonómeros inicial, también aumentaron los efectos observados en la reacción donde se utilizó DMF. Como resultado, el copolímero obtenido en irradiación de MW en tiempos de reacción más cortos era más rico en VFc que el copolímero de CH respectivo.

Los efectos observados se explicaron probablemente por las propiedades térmicas únicas de la irradiación de MW en una solución de múltiples componentes, que proporcionó un calentamiento selectivo y la creación de dominios dinámicamente

RESUMEN

distintos. Dependiendo de la interacción de los componentes con la irradiación de MW dentro de cada dominio, se puede absorber la irradiación de MW y la transferencia de calor será más eficiente o de lo contrario los componentes permanecerán en el modo configuracional y acumularán calor, lo que probablemente aumentará la movilidad de las moléculas dentro de dicho dominio. El último caso resulta en la creación de efectos específicos de microondas, como los observados en el caso de la mezcla MMA/VFc. El requerimiento de energía de MW del sistema de monómero MMA/VFc, que fue más alto que para otros sistemas además de la alta capacidad de absorción de MW de VFc, demuestra la ineficiencia de VFc para convertir la energía absorbida en calor.

El **Capítulo 3**, se realizó la comparación de los procesos de polimerización en emulsión asistida por CH y MWH. Los monómeros MMA/BA fue el copolímero principal adicionando un 1% de tres monómeros funcionales diferentes (metacrilato de 2-hidroxietilo (HEMA), estireno sulfonato de sodio (NaSS) y acrilamida (AM); Se utilizó persulfato de potasio (KPS) como iniciador y se estudió el efecto de su contenido. El objetivo principal fue evaluar si, al cambiar el tipo de monómero funcional o la cantidad de iniciador, se puede inducir un calentamiento selectivo y, por lo tanto, afectar la velocidad de polimerización, la distribución del tamaño de partículas, la microestructura del polímero, las propiedades mecánicas y la absorción de agua del polímero final obtenido.

Se observaron diferencias muy pequeñas entre las reacciones de CH y MWH en el período de reacción inicial, que disminuyeron durante la reacción. La velocidad de polimerización fue ligeramente más alta en MWH que en CH, lo que se atribuyó a la caída inicial de temperatura en el reactor de CH cuando se introdujo la solución de iniciador. A pesar de la temperatura más alta inicialmente en el reactor MWH, bajo la cual se esperaba que se produjera una descomposición más rápida de KPS, se nuclearon menos partículas. Probablemente en el proceso de nucleación pospuesto



inducido por una temperatura más alta se debe al aumento de la energía libre de formación del núcleo o debido a la mayor tasa de crecimiento volumétrico de las partículas. El tamaño de partícula fue un poco mayor para las reacciones de MWH, lo que significa que el promedio de radicales por partícula es menor. Sin embargo, las masas molares del polímero producido bajo MWH, en general, fueron mayores que las obtenidas bajo CH. Estos efectos disminuyeron cuando se usó una mayor cantidad de iniciador KPS, y los efectos fueron más fuertes cuando se utilizaron los monómeros funcionales iónicos, especialmente en el caso de NaSS. Estos resultados incluso presentaron diferencias menores entre ambos métodos de calentamiento, una fuerte indicación de que hay un efecto que ocurre bajo MW diferente de los efectos térmicos puros.

En el caso de los monómeros funcionales, los resultados obtenidos demostraron que se produjo una mayor incorporación de los monómeros funcionales en la reacción bajo MWH, lo que se atribuyó al mejor reparto de estos monómeros altamente hidrófilos. Los resultados de DMTA han demostrado que todos los polímeros producidos bajo MWH eran ligeramente más estables mecánicamente; sin embargo, se observó una estabilidad térmica esencial en los polímeros sintetizados por MWH. Es decir, mantuvieron la estabilidad térmica a temperaturas más altas durante aproximadamente entre 7°C y 27°C que la de los polímeros sintetizados por CH. Además, los polímeros por MWH absorbieron hasta un 5.7% a un 30.1% menos de agua que sus contra polímeros de CH.

Finalmente, este trabajo demostró que el uso de MWH para ayudar a la reacción de polimerización en la emulsión es una herramienta importante hacia una producción de polímeros más sostenible, con propiedades eventualmente mejoradas.

RESUMEN

El **Capítulo 4**, se realizó la comparación de los procesos de polimerización en miniemulsión asistida por CH y MWH. Los monómeros MMA/BA fue el copolímero principal adicionando un 1% de HEMA, además de adicionar nanopartículas inorgánicas como nanotubos de carbono de pared múltiple (MWCNTs) para la obtención de nanocompuestos poliméricos. Se realizó una comparación de las cinéticas de reacción, propiedades de los látex híbridos y películas de polímero obtenidos bajo MWH o CH.

Se logró una comparación confiable de la polimerización en miniemulsión asistida por radicales libres de CH y MWH de MMA/BA/HEMA con la adición de diferentes cantidades de MWCNTs creando perfiles de temperatura de reacción similares. Se encontró que, bajo perfiles de temperatura de reacción similares en CH y MWH, la velocidad de polimerización no era significativa, así como el número de partículas y el tamaño de partícula final, incluso con la adición de MWCNTs. En este sistema de polímero, el uso de KPS como iniciador no tiene ningún efecto de MW en la velocidad de polimerización.

La fracción de polímero insoluble en THF se incrementó fuertemente con la adición de MWCNT para reacciones de CH, lo que se atribuye al posible injerto entre cadenas de polímero y MWCNTs, mientras que los polímeros sintetizados por MWH es probable que no presenten la fracción de polímero insoluble. Esto se confirmó con las propiedades mecánicas del polímero evaluadas en DMTA donde el refuerzo del polímero se realizó con la adición de MWCNT sintetizados por ambos métodos de calentamiento.

Además, la estabilidad del látex de los compuestos poliméricos después de dos años de almacenamiento fue significativamente diferente entre ambos métodos de



calentamiento, probablemente debido a la alta reticulación entre el polímero y los MWCNT, el látex sintetizado bajo CH presenta menos estabilidad que el látex MWH.

En el **Capítulo 5**, se trataron de abordar dos objetivos, primero la modificación de la superficie de láminas de grafeno bajo calentamiento por microondas, utilizando diferentes monómeros como ácido acrílico (AA) y acrilamida (AM) con el fin de mejorar la compatibilidad entre el grafeno y el polímero. Después de la modificación con grafeno, se realizó la polimerización de MMA/BA/HEMA con la adición de 0.5% de grafeno modificado y sin modificar, mediante polimerización vía radicales libres por miniemulsión utilizando solo el método de MWH. Se estudiaron la cinética, la microestructura del polímero y las propiedades mecánicas de las películas del polímero.

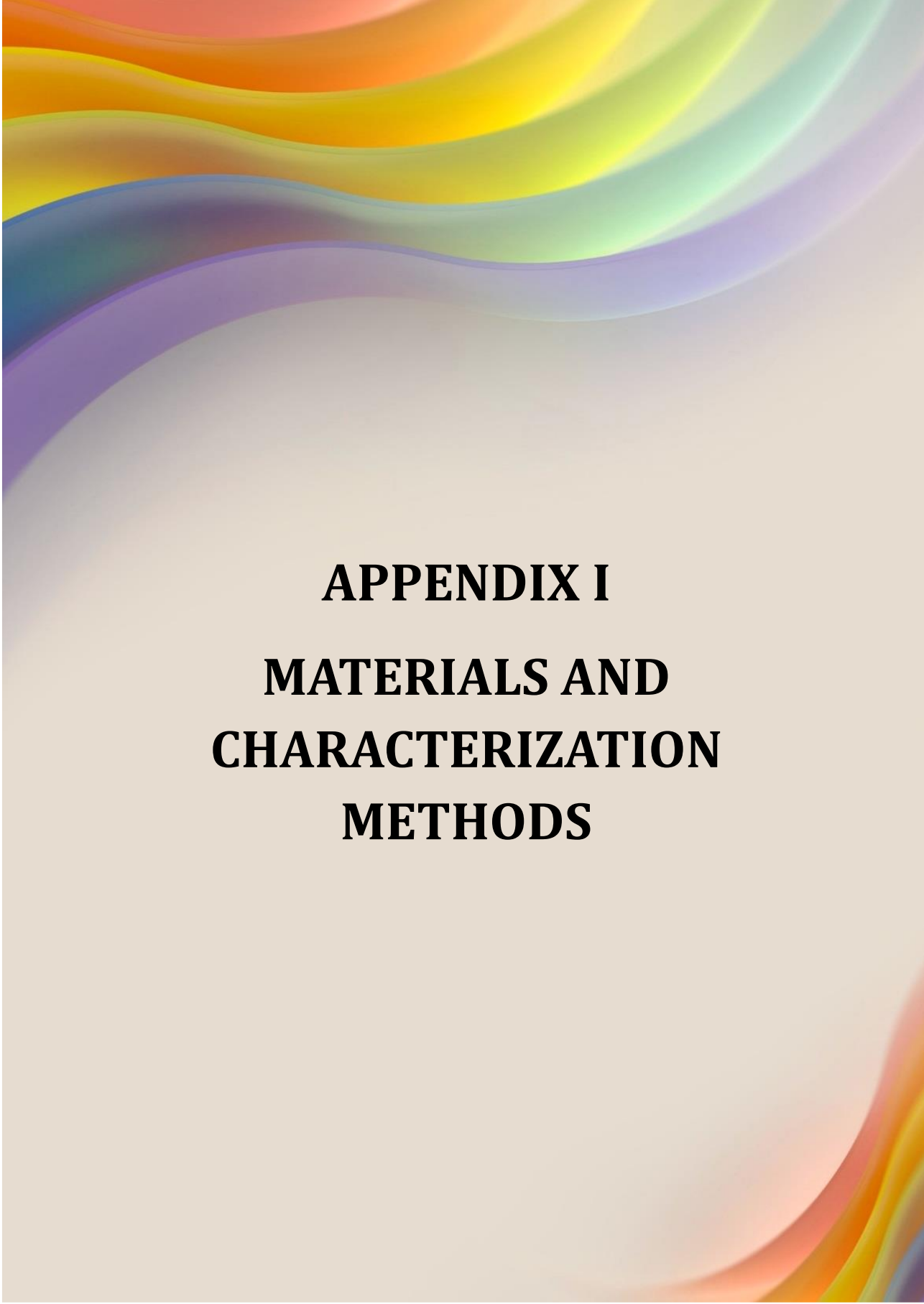
En la modificación de la superficie del grafeno se demostró que el MWH puede proporcionar una forma fácil de modificar la superficie del grafeno, mediante una simple irradiación de MW en agua, ya sea sin aditivos o en presencia de monómeros solubles en agua e iniciador. En todas estas estrategias, se indujo una leve modificación de la superficie del grafeno, lo que se demostró mediante espectroscopía RAMAN en la que se observó que los sitios de defectos en la estructura del grafeno estaban aumentados. La hidrofobicidad del grafeno tratado disminuyó con respecto al no tratado, como se demostró con las mediciones de los ángulos de contacto sobre la superficie del grafeno. Dicho grafeno tratado se usó para preparar una miniemulsión usando una mezcla de monómeros MMA/BA/HEMA y se polimerizó en un reactor MWH. Como resultado se obtuvieron películas poliméricas compuestas, en las que el grafeno no tratado se dispersó sorprendentemente mejor que los tratados. Esta fue la razón probable de la modesta mejora de las propiedades mecánicas y térmicas.

RESUMEN

En el **Capítulo 6** se investigó el desarrollo de un método de polimerización en emulsión por lotes a alta temperatura iniciado por calentamiento por microondas. Los sistemas híbridos, en los que se copolimerizan monómeros acrílicos en presencia de resinas altamente hidrófobas, tales como poliuretano, epoxi o alquidas, se polimerizan habitualmente en miniemulsión, porque las resinas tienen una difusión limitada a lo largo de la fase acuosa. Sin embargo, la polimerización en miniemulsión no es de importancia práctica para la producción a gran escala, debido a la etapa adicional de homogeneización de alta energía para producir pequeñas gotas de monómero o híbrido. En este capítulo, la idea era utilizar la ventaja del reactor MWH para lograr una temperatura alta y rápida, y en lugar de una miniemulsión, realizar la polimerización en emulsión de MMA/BA/AA con una resina epoxi altamente hidrófoba. A alta temperatura ($<70^{\circ}\text{C}$), se puede promover la difusión de los componentes hidrófobos. Por tanto, las reacciones se realizaron en el siguiente rango de temperatura: 80°C a 150°C , utilizando diferentes iniciadores (VA-086 o KPS).

Tanto las iniciaciones utilizando V-089 como KPS a temperaturas más bajas (80°C y 60°C) fueron suficientes para obtener polimerizaciones con buenas características como tamaño de partícula, fracción de gel y peso molecular. Probablemente el calentamiento más rápido, acompañado de la presión, y que el iniciador se haya añadido antes de que se alcanzara la temperatura de reacción, es la combinación ideal para obtener este tipo de polímeros, con la ventaja de reducir los costos de la emulsión utilizada en lugar de miniemulsión, adicionalmente el consumo de energía MW.

Las propiedades de los polímeros no se pudieron realizar por falta de tiempo, pero en un futuro cercano podría ser un tema a desarrollar para completar este estudio, así como más adicionar otras resinas tipo alquídicas en la formulación.



APPENDIX I

MATERIALS AND

CHARACTERIZATION

METHODS

APPENDIX I

I.1. MATERIALS

The next table is presented all materials that were used in this work, as well as their main characteristics.

Table I.1. Materials that were used throughout the Ph.D thesis.

Name	Acronyms	CAS No.	Purity	Supplier
Methyl methacrylate	MMA	80-62-6	99.9% 45-55ppm MEHQ	Quimidroga
n-butyl acrylate	BA	141-32-2	99.9% 10-20 ppm MEHQ	Quimidroga
Styrene	St	100-42-5	99.7% 10-20 ppm TBC	Quimidroga
Vinyl ferrocene	VFc	1271-51-8	>98%	Daken Chemical Limited
2-hydroxyethyl methacrylate	HEMA	868-77-9	97% ≤250 ppm MEHQ	Sigma- aldrich
Sodium styrene sulfonate	NaSS	2695-37-6	≥90%	Sigma- aldrich
Acrylamide	AM	79-06-1	≥98.0% (GC grade)	Sigma- aldrich
Acrylic acid anhydrous	AA	79-10-7	99% 200 ppm MEHQ	Sigma- aldrich
Octadecyl acrylate	SA	4813-57-4	97%	Sigma- aldrich
Sodium dodecyl sulfate	SDS	151-21-3	≥98.5% (GC)	Sigma- aldrich

MATERIALS AND CHARACTERIZATION METHODS

Polyvinylpyrrolidone	PVP	9003-39-8	mol.wt 10,000	Sigma- aldrich
Multi-walled carbon nanotubes	MWCNT	30806856 6	95% L:5-15 μ m OD:10-30 nm	Io-li tec nanomaterial s
Graphene	GP	1034343- 98-0	Nanopowder 8nm flakes	Graphene supermarket
Potassium persulfate	KPS	7727-21-1	\geq 99%	Fluka
Benzoyl peroxide	BPO	94-36-0	75% remainder water	Sigma- aldrich
Lauroyl peroxide	LPO	105-74-8	97%	Sigma- aldrich
2,2'Azobis(2-methyl propionitrile)	AIBN	78-67-1	98% (GC grade)	Sigma- aldrich
2,2'Azobis[2-methyl-N- (2-hydroxyethyl) propionamide]	VA-086	61551-69- 7	98%	Wako Chemicals
Toluene	---	108-88-3	Reagent grade	Fisher
Toluene GPC	---	108-88-3	\geq 99.9% (HPLC grade)	Sigma- aldrich
Toluene deuterated	Toluene-d ₈	2037-26-5	99.6 atom % D	Sigma- aldrich
Tetrahydrofuran	THF	109-99-9	GPC grade (250ppm BHT)	Schurlab
N,N-Dimetyl formamyde	DMF	68-12-2	Reagent grade	Sigma- aldrich

APPENDIX I

N,N-Dimetyl formamyde	DMF	68-12-2	HPLC grade	Sigma-aldrich
Deuteriochloroform	Chloroform-d	865-49-6	99.8% atom% D	Sigma-aldrich
Ethanol absolute	EtOH	64-17-5	Synthesis grade	Schurlab
1-pentanol	---	71-41-0	≥99.0% (GC grade)	Acros Organics
Hydroquinone	HQ	123-31-9	99.5%	Sigma-aldrich
Epoxy resin D.E.R 732	---	26142-30-3 (9072-62-2)	---	Fluka

MATERIALS AND CHARACTERIZATION METHODS

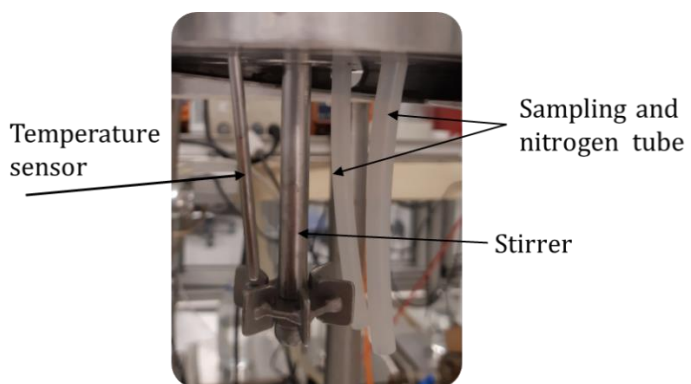
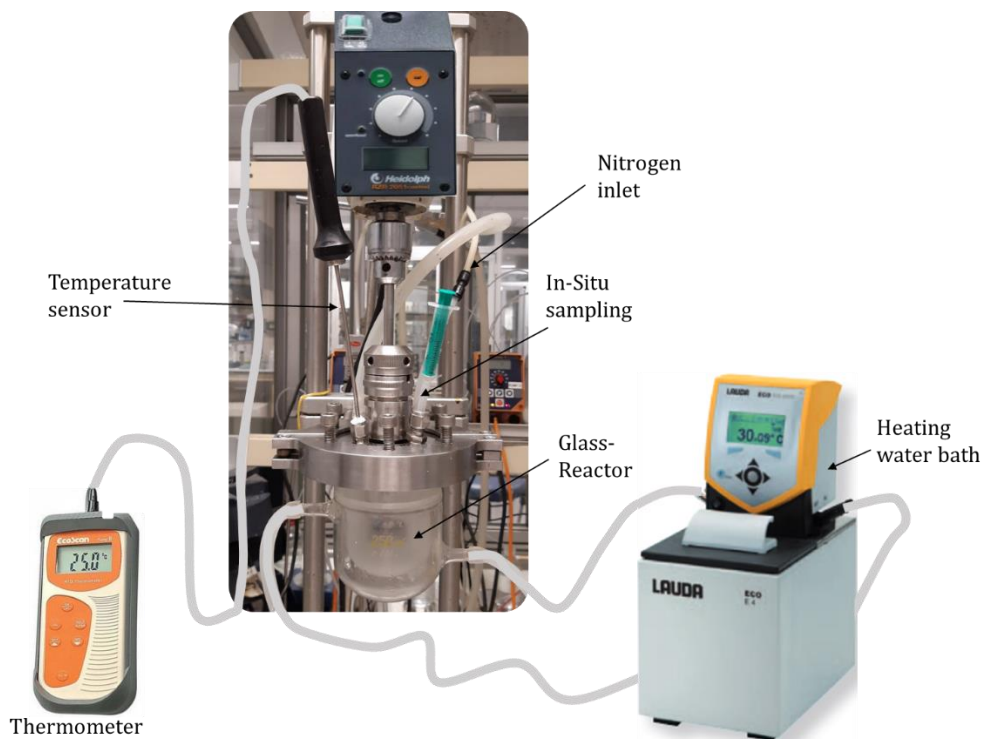
Throughout the experimental part, extreme care was taken to use the same equipment and laboratory material to ensure the reproducibility of the results. In the methodology section of each chapter, each one of them is specified. In the Table I.2 has presented the most used material along with the work, like glass beakers, magnetic stirrers, magnetic bars, and the balances that were used.

Table I.2. Standard laboratory material.

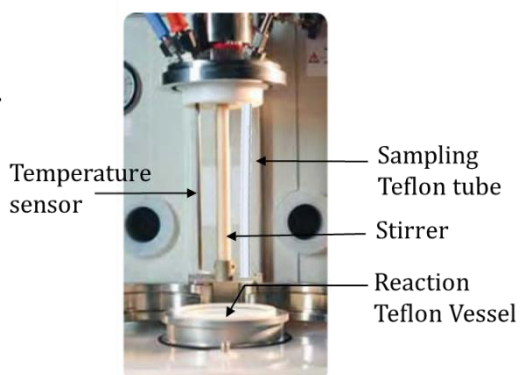
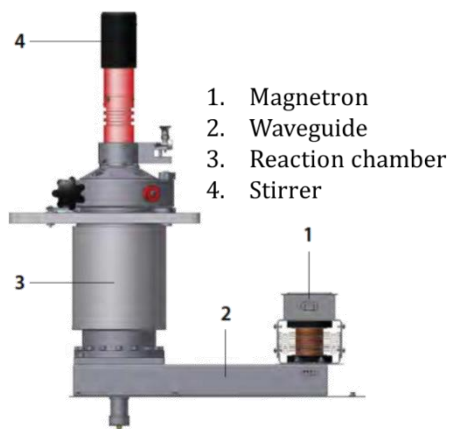
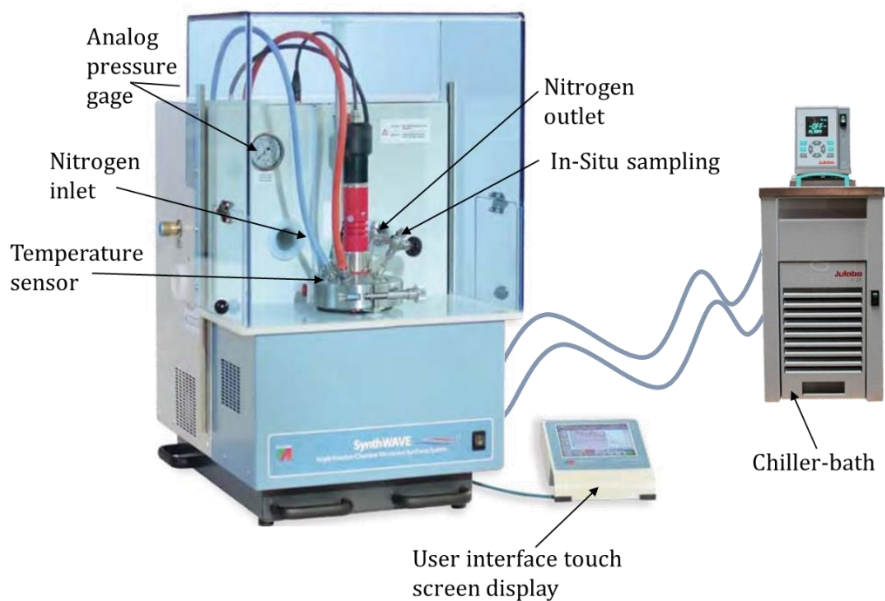
Material	Acronym	Characteristics
Balances	BL-1	Balance Mettler Toledo PM4000, two decimal places, Capacity 4100 g, std deviation ± 0.001 g
	BL-2	Balance Sartorius ED3235, three decimal places, Capacity 320 g, std deviation ± 0.001 g
	BL-3	Balance Sartorius ED224S, four decimal places, Capacity 220 g, std deviation ± 0.1 g
Beakers	V1	Scharlau, Capacity: 250mL, in \varnothing 7 cm
	V2	Ilmabor, Capacity:150mL, in \varnothing 5.6 cm
	V3	Scharlau, Capacity: 100mL, in \varnothing 4.8 cm
	V4	Scharlau, Capacity: 50mL, in \varnothing 4.1 cm
Magnetic stirrer	Str-1	Heidolph MR-3000, 100 to 1250 rpm (placed into big sonicator)
Magnetic bars	Mb-1	Length: 5.8 cm,thickness:1cm
	Mb-2	Length: 4 cm, thickness:0.8cm
	Mb-3	Length: 3 cm, thickness:0.8cm

APPENDIX I

I.2. CONVENTIONAL HEATING SET-UP



I.3. MICROWAVE HEATING SET-UP



I.4. CHARACTERIZATION METHODS OF DISPERSED POLYMERS

I.4.1. OVERALL CONVERSION AND COPOLYMER COMPOSITION

I.4.1.1. GRAVIMETRY

The gravimetric conversion was determined to measure about 0.8 grams of the latex directly received from the reactor during the polymerization process and transferred into pre-weighed aluminum cups; after that, immediately was added 3-4 drops of 1% hydroquinone solution. After this, the filled cup was put in an oven at 60°C to dried until achieving constant weight (approx by 30-42 hours), and the dried cup was weighted as well. The balance used in all gravimetric processes is the BL-2, which is better described in Table I.2. The overall conversion was determined using the next equation.

$$X_T = \frac{\frac{W_{dried\ sample}}{W_{sample}} - \frac{W_{non-polymeric\ solids}}{W_{total}}}{\frac{W_{monomers}}{W_{total}}} \times 100$$

I.4.1.2. GAS CHROMATOGRAPHY

Into Chapter 2, the overall conversion and copolymer composition of MMA/BA or MMA/St polymerizations using toluene or DMF as a solvent was determined by gas chromatography (GC) using 1-pentanol as internal standard and helium as a gas carrier.

During the reaction, aliquots were taken from the reactor and immediately put on ice at ~-5 to -7°C to stop the reaction. After that, it was weight the GC vial (using BL-3), with 250 µl sample, 50 µl of internal standard, and 8 µl of hydroquinone solution, and placed into the equipment.

MATERIALS AND CHARACTERIZATION METHODS

For each system of monomer and solvents, a calibration curve was performed separately, the set data was composed for 8 points along the line, and each point repeated twice.

A GC apparatus (HP 689 series) equipped with an HP 7694E headspace sampler and a BP capillary column was used. The zone temperature parameters were the following: Vial 130°C, Loop: 170°C, and T., Line 180°C. GC cycle of 26 min and Vial equilibrating time of 15 min. The method used during all measurements is well described in Figure I.1.

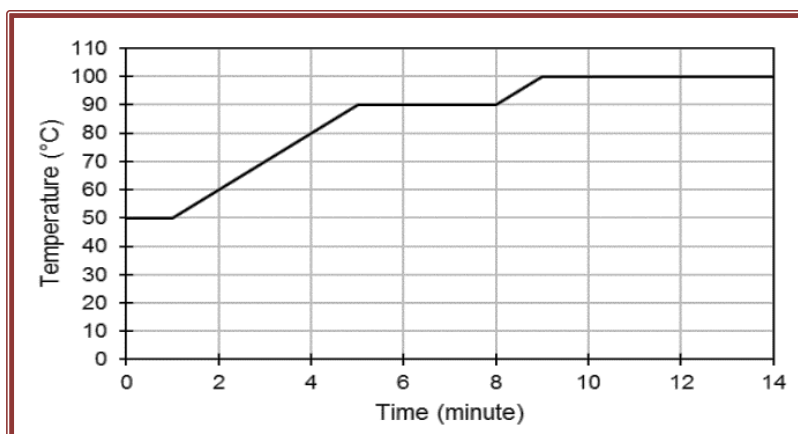


Figure I.1. Gas chromatography temperature profile.

Overall conversion and copolymer composition were calculated using the quantification of free monomer following these equations.

First, for calibration curve was plotted on axis x the relation between monomer (grams) and internal standard (grams) and on axis y , the relation between the area under the curve of monomer signal and the area under the curve of internal standard (obtained previously by GC) as follows:

APPENDIX I

$$X = \frac{g_{monomer}}{g_{int. standard}} \quad , \quad Y = \frac{Area_{monomer}}{Area_{int. standrad}}$$

From the resulted linear plot, the slope equation can be obtained

$$y = mx \pm b$$

Where y is given by the experimental (kinetics) results for the relation between the area under the curve for the quantified monomer and the area for internal standard; the terms for m and b are known for the equation resulted for the calibration curve, and the unknown term is the x , from which will determine the relationship between grams of quantified monomer and grams of the internal standard; hence the grams of monomer that has not been polymerized yet, it is quantified, following the next equations. Calculated from those equations, the copolymer composition ($X_{i-monomer}$) or each monomer separately, and then the global conversion (X_T).

$$X_{i-mon} = \frac{A_0 - A}{(A_0 - A) + (B_0 - B)}$$

$$X_T = \frac{(A_0 + B_0) - (A + B)}{A_0 + B_0}$$

I.4.1.3. PROTON NMR (^1H NMR)

Into Chapter 2, the overall conversion and copolymer composition of MMA/VFc polymerizations using toluene and DMF as a solvent was determined by ^1H NMR on a Bruker 500 NEO spectrometer were equipped with BBO probe and z-axis gradients at room temperature. The aliquot was taken directly from the reactor and transferred 500 μl of the sample into NMR-tube and adding 5 μl of 1% hydroquinone solution and 50 μl of deuterated solvent, which Toluene- d_8 for experiments where toluene was the main solvent and Chloroform- d where DMF was the solvent were used. All samples were carefully weighed using an analytical balance (BL-3).

Kinetics of the NMR spectrum was recorded with a constant gain value and a pulse of 5 degrees. They were recorded without solvent removal, and the number of recorded points was 32K for a spectral width of 10 kHz. The relaxation time was 1 s, and the acquisition time for 3.27 s.

I.4.2. PARTICLE SIZE AND NUMBER OF PARTICLES

I.4.3. DYNAMIC LIGHT SCATTERING

During kinetics of polymerizations in Chapters 3, 4, 5, and 6, particle Z-average diameters were measured by dynamic light scattering (DLS) in a Zetasizer Nano from Malvern Instruments. Which determines the particle size by measuring the rate of fluctuation in laser light intensity scattered by particles as they diffuse through a fluid. The analyses were carried out at 25°C using 1 min of temperature equilibration followed by three size measurements of 300 seconds each.

All of the samples were prepared at the same concentration by diluting 15 μl of the sample into 2 mL of double deionized water. Plastic disposal cuvetts with their respective top were used as cells.

APPENDIX I

The Z-average obtained was used to determine the evolution of the number of particles (N_p) during the reactions, following the next equation.

$$N_p = \frac{6 w}{\pi \rho_{pol} (Z_{ave})^3}$$

Where w is the amount of monomer (g), the density of the polymer is ρ_{pol} (g/mL) using their correspond ponderation for each monomer, and Z_{ave} is the diameter obtained from the DLS in centimeters (cm).

1.4.3. GEL CONTENT FRACTION

Gel fraction is defined as the fraction of polymer that is not soluble in a suitable solvent (tetrahydrofuran, THF, in this case). The gel fraction was measured by Soxhlet extraction, using THF as the solvent. A glass fiber square pad (10 x 10 cm) was impregnated with a polymer sample in the center of the pad (a few drops) and dried approx. 12 h at room temperature and then 4 hours at 60°C. After that, the pad was folded, as shown in Figure I.2, and placed into the soxhlet extractor. The extraction was carried out for 24 h under THF reflux conditions (about 70°C). The gel remained in the glass fiber after drying in the oven at 60°C, whereas the sol polymer was recovered from the THF solution. The fraction of gel was calculated as follows:

$$gel(\%) = \frac{w_g}{w_p} \times 100$$

where w_g is the weight of insoluble fraction of the sample (dried sample), and w_p is the weight of the whole polymer sample.

In this process, the analytical balance (BL-3) was used.

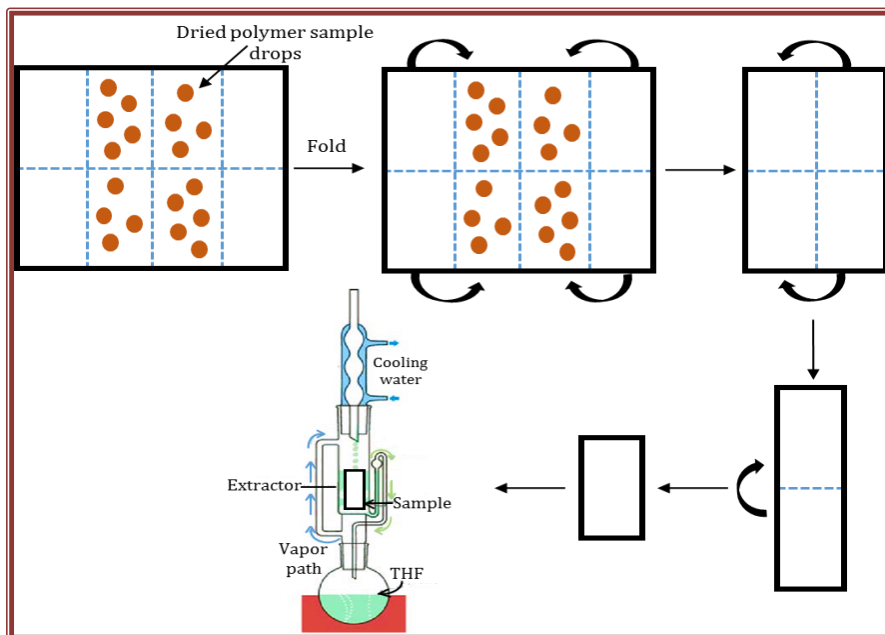


Figure I.2. Scheme of a soxhlet extraction method for gel fraction measurements.

I.4.4. MOLECULAR WEIGHT AND MOLECULAR WEIGHT DISTRIBUTION

I.4.4.1. GPC

The molar mass distribution (MMD) of the soluble fraction was determined by size exclusion chromatography/gel permeation chromatography (SEC-GPC). The samples taken out from the Soxhlet were first dried and redissolved in THF (GPC grade) to achieve a concentration ~ 1 or 0.5 mg per milliliter, and filtered before injection into the instrument (polyamide filter $\phi = 45 \mu\text{m}$).

The GPC instrument consisted of a pump (Shimadzu LC-20a), three columns in series (Styragel HR2, HR4, and HR6 with pore sizes ranging from 10^2 to 10^6 \AA), an autosampler (Waters 717), and a differential refractometer (Waters 2410), and, a dual

APPENDIX I

λ absorbance detector (Waters 2487). THF was used as a mobile phase at a flow rate of 1 mL min⁻¹, and all measurements were performed at 35°C. Polystyrene (PS) standards (5th order universal calibration) were used to calibrate the equipment, and the reported molar masses are related to PS.

I.4.4.2 SEC/MALS

The absolute molar mass distribution (MMD) of the soluble fraction of the polymer composites with MWCNTs (Chapter 4) was determined by size exclusion chromatography with a multi angle light scattering detector (SEC/MALS). The instrument was composed of a pump (Shimadzu LC-20a), three columns in series (Styragel HR2, HR4, and HR6 with pore sizes ranging from 10² to 10⁶ Å) coupled to a DAWN Heleos II multiangle (18 angles) light scattering laser photometer equipped with an HE-Ne laser ($\lambda=658$ nm), and an Optilab Rex differential refractometer. THF was used as a mobile phase at a flow rate of 1 mL min⁻¹, and all measurements were performed at 35°C. The SEC/MALS data were analyzed by using the ASTRA software version 6.1 (Wyatt Technology, USA).

I.4.5. TURBIESCAN

To measure the stability of the miniemulsions in Chapter 4, as well as the MWCNTs water dispersions in Appendix III, it was used as a Turbiscan Lab ^{expert} apparatus. This instrument measures the evolution of the light backscattered of the sample through the vial. The sample is placed into the device and is scanned by a light source, which is an electroluminescent diode in the near-infrared ($\lambda=880$ nm). Two synchronous detectors collect the transmission from the incident light at 180° and

backscattered from the incident radiation at 45° . Figure I.3 shows the scheme of turbiescan device.

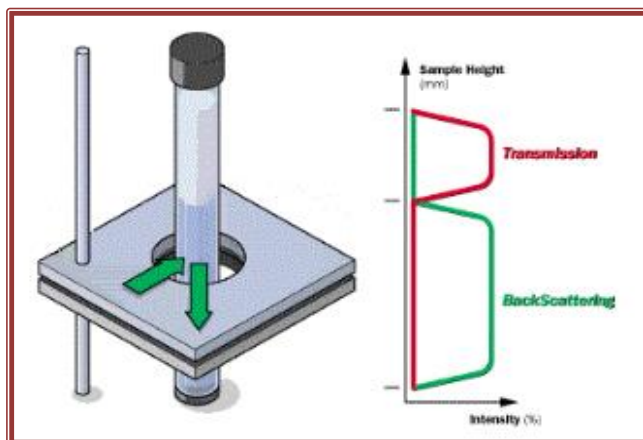


Figure I.3. Scheme of Turbiescan.

I.4.6. INFRARED SPECTROSCOPY

Fourier transform infrared spectroscopy (FT-IR) was used in Chapter 5 in order to follow the possible incorporation of epoxy or alkyd resin into depolymerization and, in Chapter 7, where samples of polyamide were treated under microwave irradiation, in order to a possible degradation or not.

The infrared spectra were obtained by device Alpha FT-IR spectrometer, with Platinum ATR operated with OPUS software.

I.4.7. STATIC WATER CONTACT ANGLE

The water contact angle measurements were performed in Chapter 5 and Appendix III, where MWCNTs and graphene samples were measured. Apparatus Data Physics OCA 20 model goniometer was used, and all measurements were performed according to the standard sessile drop method with dynamic tracking function (1 frame s⁻¹ during one minute).

The films of MWCNTs or graphene dispersions samples were prepared by drop cast method on glass substrates and dried for 24 hours at standard conditions (23°C and 55% relative humidity). After that, a drop of 5 μ l of deionized water was placed on the surface of the film, and with the software of the device, it can be possible to take the photo and measure the contact angle. For the reported result, ten repetitions of the measurement were done.

I.5. CHARACTERIZATION METHODS OF POLYMER FILMS

I.5.1. WATER UPTAKE MEASUREMENTS

For the water uptake test that was performed for Chapter 3, rectangular samples of dimensions 2.8 cm x 4.6 cm and 0.5 mm thickness were prepared in Teflon molds and dried at 25°C and 55% of relative humidity for seven days, using a humidity chamber (SH-641 Espec Bench-TopType).

Films were weighted (m_0), and each film separately was immersed into a plastic bottle with 100 mL double deionized water at room temperature. At some intervals, films were taken out of the plastic bottle, smoothly blotted with paper and weighed (m_t), and put back again into their corresponding bottle with water. The water uptake measurements were calculated in relation to the initial dry weight of the samples using the next equation.

$$\text{Water uptake (\%)} = \frac{m_t - m_0}{m_0} \times 100$$

After the water uptake test, samples were taken, dried at 65°C for seven days, then samples were reweighed to calculate the weight loss compared to the initial weight of the sample before the test. For each reported data, an average of 3 films for each sample was necessary. Throughout the weighing process, analytical balance (BL-3) was used.

1.5.2. DYNAMIC-MECHANICAL THERMAL ANALYSIS (DMTA)

The DMTA measurements were carried out using a dynamic mechanical thermal analyzer (DMTA) from Triton 2000 DMA, Triton Technology Ltd brand. Films were cast from coatings at different conditions using a humidity chamber (SH-641 Espec Bench-TopType). For Chapter 3, 25°C or 45°C, both of them at 55% of relative humidity for seven days, and for Chapter 4, 25°C at 80% of relative humidity for seven days. After that, all borders of the films were carefully cut with sharp scissors and cut samples of 0.5 cm width, 2.5 cm length, and the thickness was 0.5 mm. It is essential to mention that, for all film manipulation wearing gloves is necessary to avoid sample contamination.

A single cantilever tension geometry was used. The real (storage modulus, E') and imaginary (loss modulus, E'') components of the complex shear modulus $E^*=E'+iE''$ and the internal friction coefficient $\tan(\delta)=E''/E'$ (mechanical loss) were measured over the temperature range from -40°C to 90°C (-40°C to 150°C in Chapter 4) in the constant frequency of 1Hz. The heating rate was 4°C/min. To decrease the temperature of the polymer sample, liquid nitrogen was used. The results reported were the average of 3-4 repeated measurements.

I.5.3. DIFFERENTIAL SCANNING CALORIMETRY (DSC)

The glass transition temperature (T_g) was determined by Differential scanning calorimetry (DSC) in a TA instrument Q1000. Sample of film polymer was weighed (BL-3) around 3-5 mg and placed in aluminum hermetic pans. DSC was analyzed in the air atmosphere at the heating rate of 10°C/min; the scanning cycles consisted of first cooling to -80°C and heating to 120°C. The second heating run was used to determine the glass transition temperature of the polymer.

I.5.4. MICROSCOPIC TECHNIQUES

The fractured composite films (Chapter 4) were prepared under liquid nitrogen, and scanning electron microscopy (**SEM**) images were taken in a Hitachi S-4800. For latexes with and without MWCNTs (Chapter 4) and graphene samples for Chapter 5 were determined by transmission electron microscopy (**TEM**) using a Jeol TM-1400 Plus series 120 kV electron microscope.

I.6 CALCULATION OF MW-ENERGY CONSUMPTION

In this work, the MW-energy consumption is related to the electric energy needed for the magnetron of the equipment. The software used was easyControl-640 from the reactor SynthWAVE (Milestone Srl-MLS GmbH), showing the energy uses in watts (W) applied for the magnetron according to the program, as shown in Figure I.4.

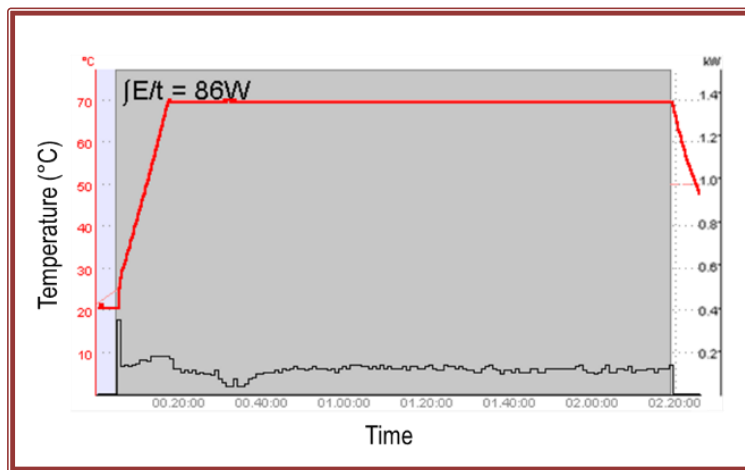
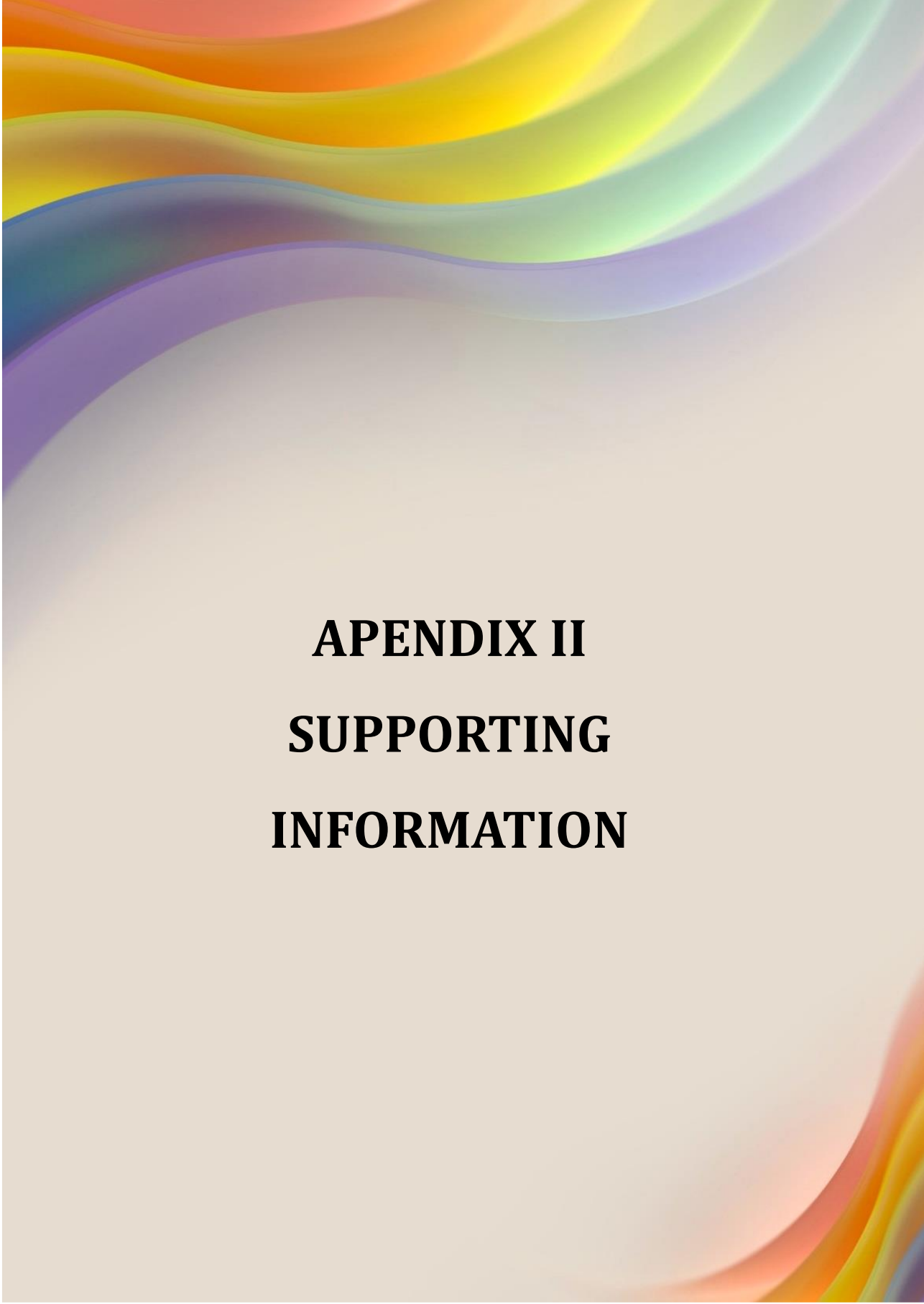


Figure I.4. Microwave irradiation profile (black line) and temperature profile (red line) for a standard polymer reaction.

As shown in the figure, the temperature is well defined by the power applied to the system; hence, the power applied can not be constant; for that, an integral of energy is taken with a tool of the software ($\int E/t$) obtaining the power applied by the second. After this, the power obtained should be multiplied by the time of microwave irradiation exposure to obtain the energy, following the next equation.

$$E = P \times t$$

Where E is the energy in joules (J), P is the power in watts (W), and t is the time in seconds (s). The energy date showed in this work was reduced as kilojoules (kJ). For Chapter 2 and Chapter 3, this energy was divided by the volume in milliliters (mL) to obtain the energy spent during the polymerization per mL (kJ/mL).



APENDIX II
SUPPORTING
INFORMATION

II.1 SUPPORTING INFORMATION OF CHAPTER I

II.1.1 STATE OF THE ART SOLUTION POLYMERIZATION

Table II.1.1. Summary of the different published works in solution polymerization by free radical polymerization

Ref.	Monomers	Microwave reactor	Temperature & Reaction time	Power (watts)	Solvent	Initiator	Mn(kDa) ^a	D ^a	Polymer Conversion
[42]	NPA	CEM Discover	70°C to 120°C 20 min	N.R.	DMSO	AIBN	60 to 290	1.53 to 1.67	30% to 68%
[43]	MMA	Domestic oven	~70°C Cyclos 20 sec	700 w	Chloro-benzene	BPO	20 to 35	1.4 to 2.2	N.R.
[44]	AcPheBz+DMA	CEM Discover	100°C 40 min	250 w	Dioxane	ACHN	38.5	N.R.	18% of QD ^b
[45]	NPMI+PFS	CEM Discover	70°C±1 5 to 270 min	150 w	Anisole	AIBN	14.7 to 22	1.57 to 2.09	41% to 58%
[48]	AM	Domestic Oven Kenstar	98°C 25 to 125 sec	0-800w	Water	KPS	N.R.	N.R.	25.8% to 98.5%
[49]	AA+AM+starch	N.R.	30°C to 70°C 1-3.5 h	N.R.	Water	KPS	N.R.	N.R.	N.R.
[50]	MMA	Biotage Emrys L. (small scale)	100°C 20 min	150 w	IL-1, IL-2	AIBN	19.6 to 26.4	2.05 to 3.75	56% to 95%
		N.R.		IL-2					
[51]	MMA St St+AN MMA+NPMI	MLS micro PREP 1500	60°C, 80°C 90 to 420 min	N.R.	DMF, Methanol, IL-3 IL-4	AIBN, BPO	4.5 to 38.9	N.R.	25% to 98.5%

Table II.1.1. (continued) Summary of the different published works in solution polymerization by free radical polymerization

Ref.	Monomers	Microwave reactor	Temperature & Reaction time	Power (watts)	Solvent	Initiator	Mn(kDa) ^a	Đ ^a	Polymer Conversion
[52]	St	CEM	100°C 45 min	50 w, 150 w, 300 w	Toluene, DMF	BPO, DtBP, tBPB, DCP, LPO	13.3 to 199	1.85 to 2.25	2.8% to 50.11%
	St+MMA	Discover	100°C 60 min				11.8 to 184	1.53 to 2.39	1.82 to 91.6%
[53]	St+ MMA	CEM Discover	100°C 60 min	50 w, 150 w, 300 w	Toluene, DMF	BPO, tBPB, DCP	6.7 to 38.2	1.79 to 2.38	12% to 75%

Monomers: NPA 4-nitrophenyl acrylate, MMA methyl methacrylate, AcPheBz n-acryloyl-(S)-phenylalanine benzyl ester, DMA 2-(n,n-dimethylamino)ethyl acrylate, NPMI n-phenylmaleimide, PFS 2,3,4,5,6-pentafluorostyrene, AM acrylamide, AA acrylic acid, St styrene, AN acrylonitrile.

Solvents: DMSO dimethyl sulfoxide, DMF n,n-dimethyl formamide, IL-1 1-butyl-3-methylimidazolium trifluoromethane sulfonate, IL-2 1-butyl-3-methylimidazolium tetrafluoroborate, IL-3 1-ethyl-3-methylimidazolium ethylsulfate, IL-4 1-butyl-3-methylimidazolium tetrafluoroborate.

Initiators: KPS potassium persulfate, AIBN 2,2'-azobisisobutyronitrile, ACHN 1,1'-azobis(cyclohexane-1-carbonitrile), BPO benzoyl peroxide DtBP di-tert-butyl peroxide, tBPB tert-butylperbenzoate, DCP dicumyl peroxide, LP lauroyl peroxide.

^aMn(kDa) and Đ: Molecular weights and dispersities of the polymers, determined by gel permeation chromatography

^bQB %: Quaternization degree

N.R.: Not reported

II.1.2 STATE OF THE ART EMULSION POLYMERIZATION

Table II.1.2. Summary of the different published works in emulsion polymerization by free-radical polymerization

Ref.	Monomers	Microwave reactor	Temperature & Reaction time	Power (watts) $\lambda=2.45$ GHz	Solvent	Initiator	Surfactant	Dp (nm)	Polymer Conversion
57	St	Self-designed MW-apparatus	70±4°C 7 cycles 20s on, 10s off	175 W or 800 W	Water	KPS	SLS	N.R.	~90% (140 s)
58	MMA	Self-designed MW-apparatus	65±1°C 20 to 40 min	2-350 W ($\lambda=1.25$ GHz)	Water	KPS	SDS	N.R.	16% to 91.3%
59	St	Self-designed MW-apparatus	72±3°C 40 min	N.R. ($\lambda=1.25$ GHz)	Water	KPS	SDS	71.3 & 70.2 (DLS)	>90%
60	BA or St BA+St	Korea Microwave Instrument Co.	70°C 240 min	300 W	Water	KPS	SLS	58 & 41nm (SEM)	~100%
62	MMA	Portland DMR-41 MW Oven	50±2°C 10 min	50 W	Water	KPS	SDS	~80 to 100 (Coulter)	~85% to 100%
63	MMA or BA	Synthos 3000 Anton Paar	80°C <15 min or 70°C <40min	1400 W	Water	KPS	Disponil, FES32 A3065	50 to 60 (DLS)	PMMA=93% PBA= 91%
65	MMA	Synthos 3000 Anton Paar	80°C <25 min	Máx. 1400 W	Water	V-50	DTAB	~80 to 100 (DLS)	~100%

Table II.1.2. (continued) Summary of the different published works in emulsion polymerization by free-radical polymerization

Ref.	Monomers	Microwave reactor	Temperature & Reaction time	Power (watts) $\lambda=2.45$ GHz	Solvent	Initiator	Surfactant	Dp (nm)	Polymer Conversion
65	St	Milestone-Start-S-model	60°C to 85°C 7.5 to 90 min	<55 W	Water	KPS	SDS	N.R.	~50% to 97%
67	MMA+diff. Functional monomers	Initiator Eight Biotage	70°C 1 h	23±2 W	Water Or Wt/At	KPS	N.R.	~55 to 230 (DLS)	N.R.
69	St	Whirlpool-VIP20	70±2°C 1 h	~80 W	Water	KPS	SDS	20 to 80 (LLS)	~97% (40 min)
70	St	Whirlpool-VIP20	~70°C 1 h	80 W	Water	KPS	SDS or without	~60 (LLS)	98%
71	St	Whirlpool-VIP20	~70°C 1 h	80 W	Water	KPS	Surf-free	~69.4 (LLS)	98% (40 min)
72	BMA	Modified-MW device	70±2°C 1.5 h	N.R.	Water Or Wt/Et	KPS	Surf-free	88 to 299.8 (LLS)	68% to 99%
73	St+(MMA or BMA or EA or BDA)	N.R.	T = N.R. 8 h	650 W	Wt/At	KPS	Surf-free	16 to 280 (LLS)	N.R.
74	MMA MMA+EOA	Modified-MW device	~80°C 5 h	450 W 80 W	Water	KPS	Surf-free	~84 to 280 (LLS)	N.R.
75	MMA	Whirlpool T120	70°C 2 h	0-700 W	Water Or Wt/At	KPS	Surf-free	215 or 100 (TEM)	~80% or 100%

Table II.1.2. (continued) Summary of the different published works in emulsion polymerization by free-radical polymerization

Ref.	Monomers	Microwave reactor	Temperature & Reaction time	Power (watts) $\lambda=2.45$ GHz	Solvent	Initiator	Surfactant	Dp (nm)	Polymer Conversion
77	St-NIPAAm	SANLE-MP 650D	70°C 1 h	650 W & 130 W	Water	KPS	Surf-free	109 to 130 (TEM)	N.R.
78	St-NIPAAm	SANLE-MP 650D	70°C 1 h	650 W & 130 W	Water	KPS	Surf-free	136 to 149 (TEM)	N.R.
79	MMA+St+ NMA	XH-100A MW- Reactor	T = N.R. 8 h	100- 1000 W	Water	KPS	Surf-free	114 to 233 (TEM)	~90%

Monomers: **MMA** methyl methacrylate, **BA** butyl acrylate, **St** styrene, **BMA** butyl methacrylate, **EA** ethyl acrylate, **BDA** maleic anhydride, **EOA** europion octanate, **NIPAAm** N-isopropylacrylamide, **EGDMA** ethylene glycol dimethacrylate, **NMA** N-hydroxymethyl acrylamide.

Solvents: **Wt** water, **At** acetone, **Et** ethanol.

Initiators: **KPS** potassium persulfate, **V-50** 2'-2'-azo(2-methylpropionamide) dihydrochloride.

Dp: Particle diameter.

Dp Characterized by: **LLS** laser light scattering, **DLS** dynamic light scattering, **TEM** transmission electron microscopy, **COULTER** He/Ne 4mW Coulter Counter.

N.R.: Not reported.

Table II.1.3. Summary of the different published works in miniemulsion polymerization by free-radical polymerization

Ref.	Monomers	Microwave reactor	Temperature & Reaction time	Power (watts)	Initiator	Surfactant/ Co-surfactant	Dp (nm)	Polymer Conversion
80	St	MLS-Ethos 1600	T= 75 and 95°C Cycles of 9-12 s or <30 min	1000 W or 110 W	AIBN KPS V-59 PEGA 200	SDS/HD	N.R.	~30% to 90.3%
81	St	MLS-Ethos 1600	T= 75 and 95°C Cycles of 9-12 s or <30 min	1000 W or 110 W	AIBN PEGA 200	SDS/HD or O-terphenyl	N.R.	~30% to 90.3%
82	MMA/BA/ DFHMA	AH-100A	80°C, 2h	400 W	AIBN	SDS or OP- 10/ HD	56 &75	N.R.
83	MMA or St	Anton Paar MW-300	T= 80°C or 90°C 2,5,10 & 15 min	850 W	KPS AIBN	SDS/HD	N.R.	~20% to 100%
84	Urea- urethane	CEM Discover-S	T= 50,60,70, &80°C; 5h	50,100,150 &300 W	N.R.	SDS/N.R.	~110 to 120	~90%
85	MMA or St with MWCNTs	Modified- MW device WP750L23	T= N.R. 25-30 min	136 W	KPS	SLS	N.R.	~19% to 40%

Monomers: MMA methyl methacrylate, BA butyl acrylate, St styrene, DFHMA Dodecafluoroheptyl methacrylate

MWCNTs: Multi-wall carbon nanotubes

Initiators: KPS potassium persulfate, AIBN 2,2'-azobis(2-methylpropanitrile), V-59 2,2'-azobis(2-methylbutyronitrile) PEGA 200 symmetrical poly(ethylene glycol).

Surfactant and Co-surfactant: SDS sodium dodecyl sulfate, SLS sodium lauryl sulfonate, HD hexadecane,

OP-10 polyoxyethylene alkylphenol ether.

Dp: Particle diameter.

N.R.: Not reported.

II.2 SUPPORTING INFORMATION OF CHAPTER II

II.2.1 MOLECULAR WEIGHT DISTRIBUTION OF MMA/BA

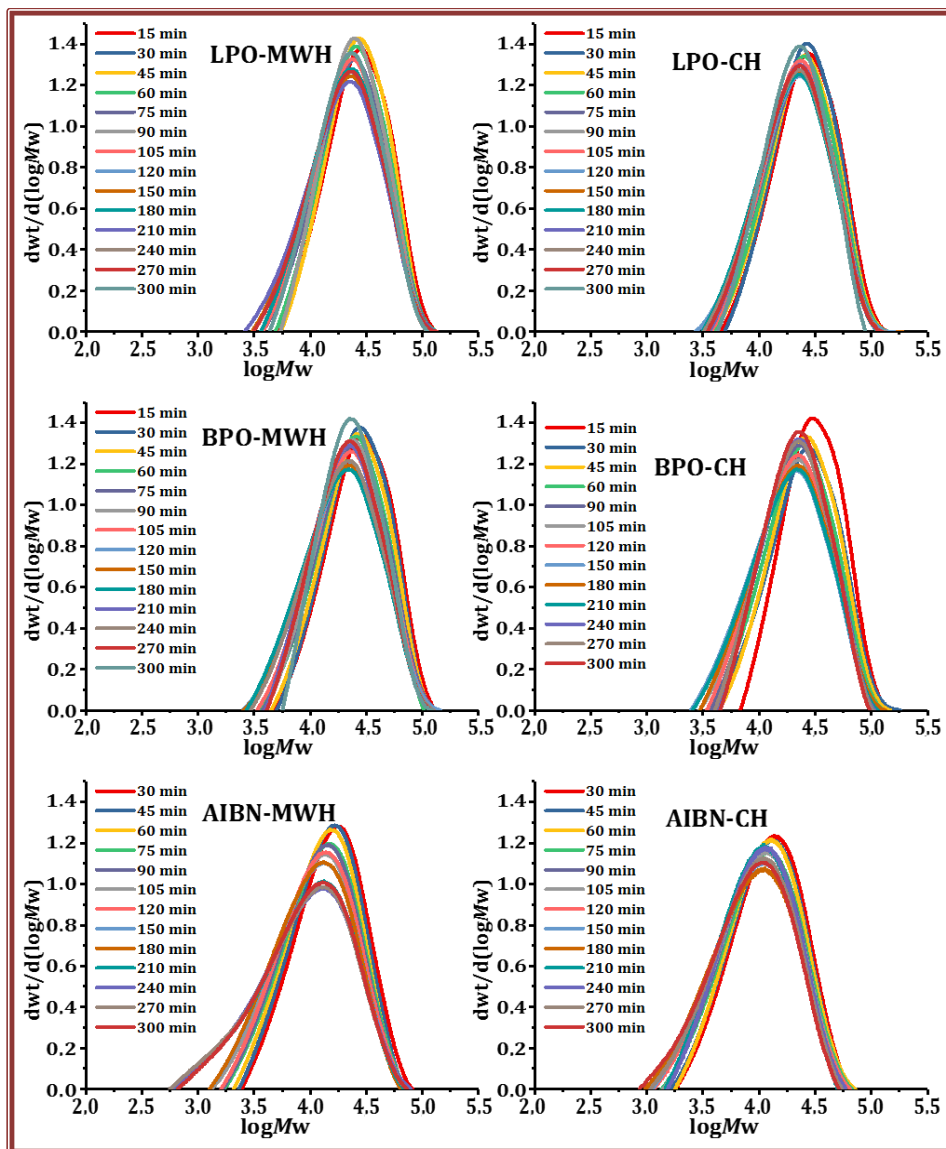


Figure II.2.1. Molecular weight distributions of MMA/BA polymerization in toluene using LP, BPO, and AIBN as initiators; under MWH and CH methods.

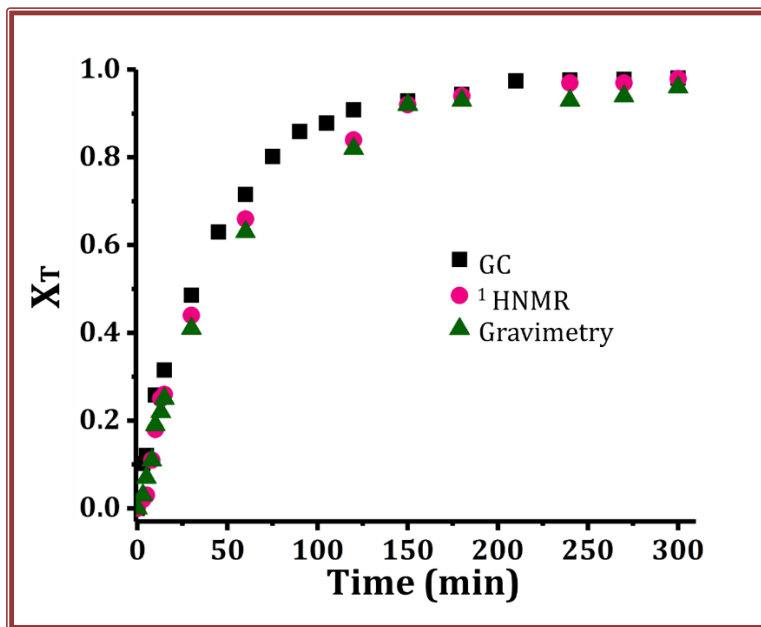
II.2.2. COMPARISON BETWEEN GRAVIMETRY, GC AND, $^1\text{HNMR}$ OVERALL CONVERSIONS

Figure II.2.2. The overall conversion of MMA/BA in DMF was characterized by three different methods, gas chromatography, $^1\text{HNMR}$, and gravimetry.

II.3. SUPPORTING INFORMATION OF CHAPTER III

II.3.1. MOLECULAR WEIGHT DISTRIBUTION BETWEEN MWH AND CH.

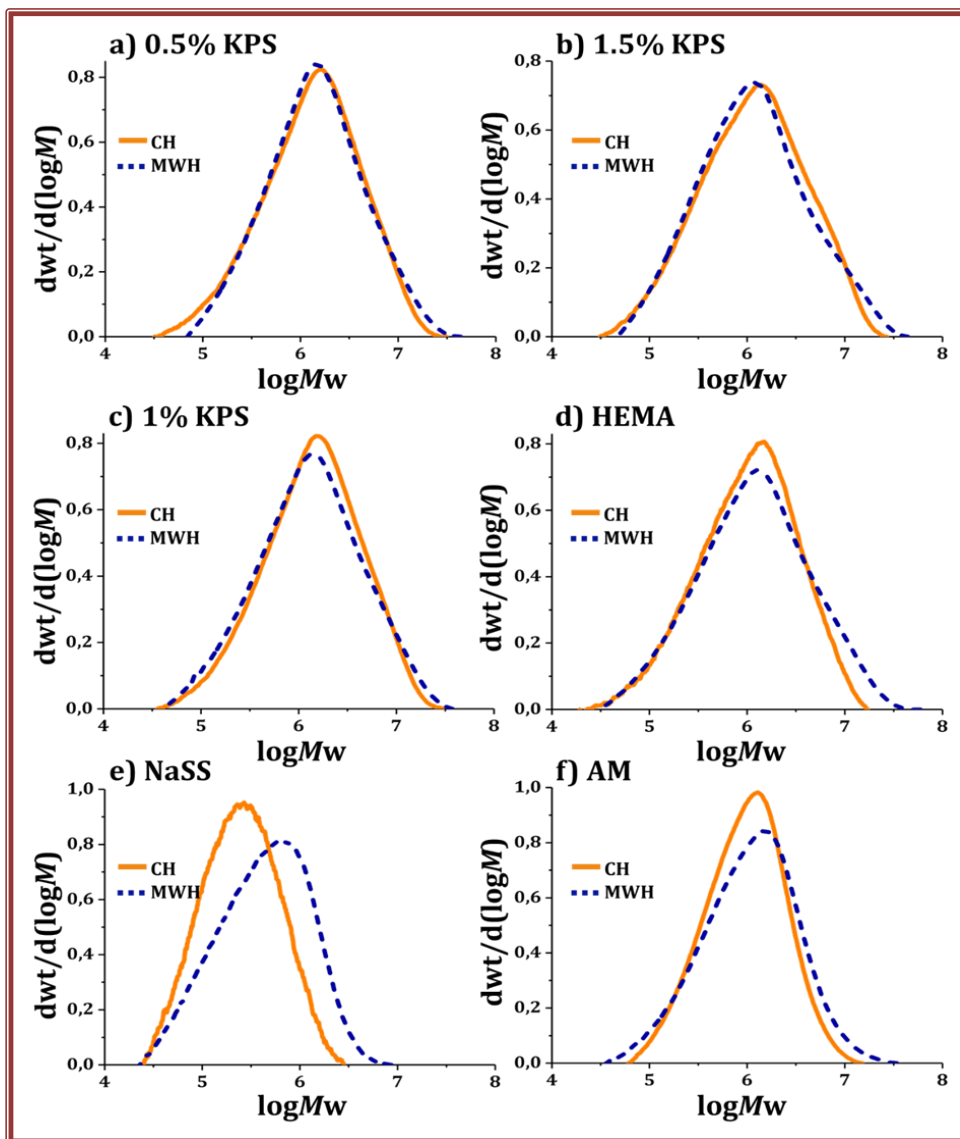


Figure II.3.1. Molecular weight distribution between MWH and CH polymer latexes of MMA/BA copolymers using different amounts of KPS or functional monomers.

II.3.2. POLYMER FILMS DRIED AT 25°C AND 55% HUMIDITY.

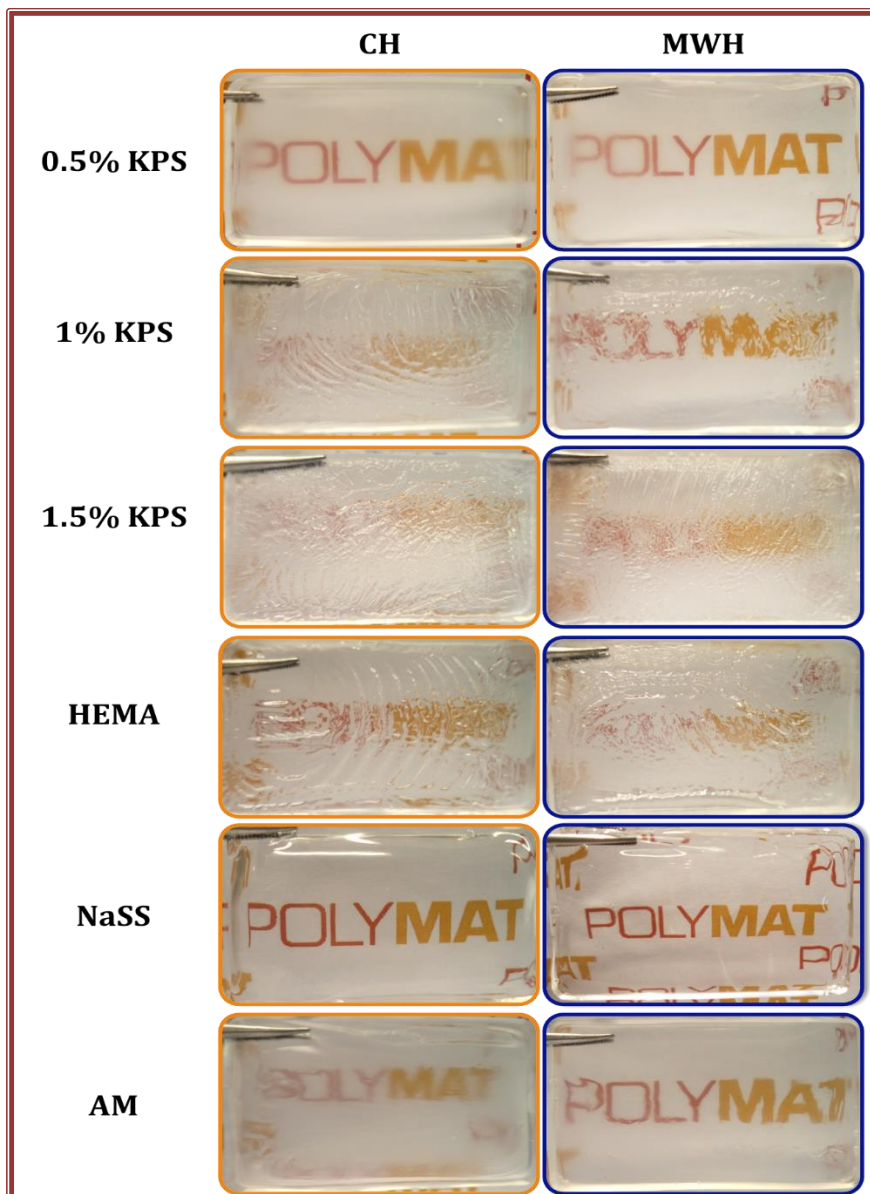


Figure II.3.2. Polymer films dried at 25°C and 55% relative humidity.

SUPPORTING INFORMATION

II.3.3. DMTA MEASUREMENTS FOR FILMS DRIED AT 25°C and 55% HUMIDITY.

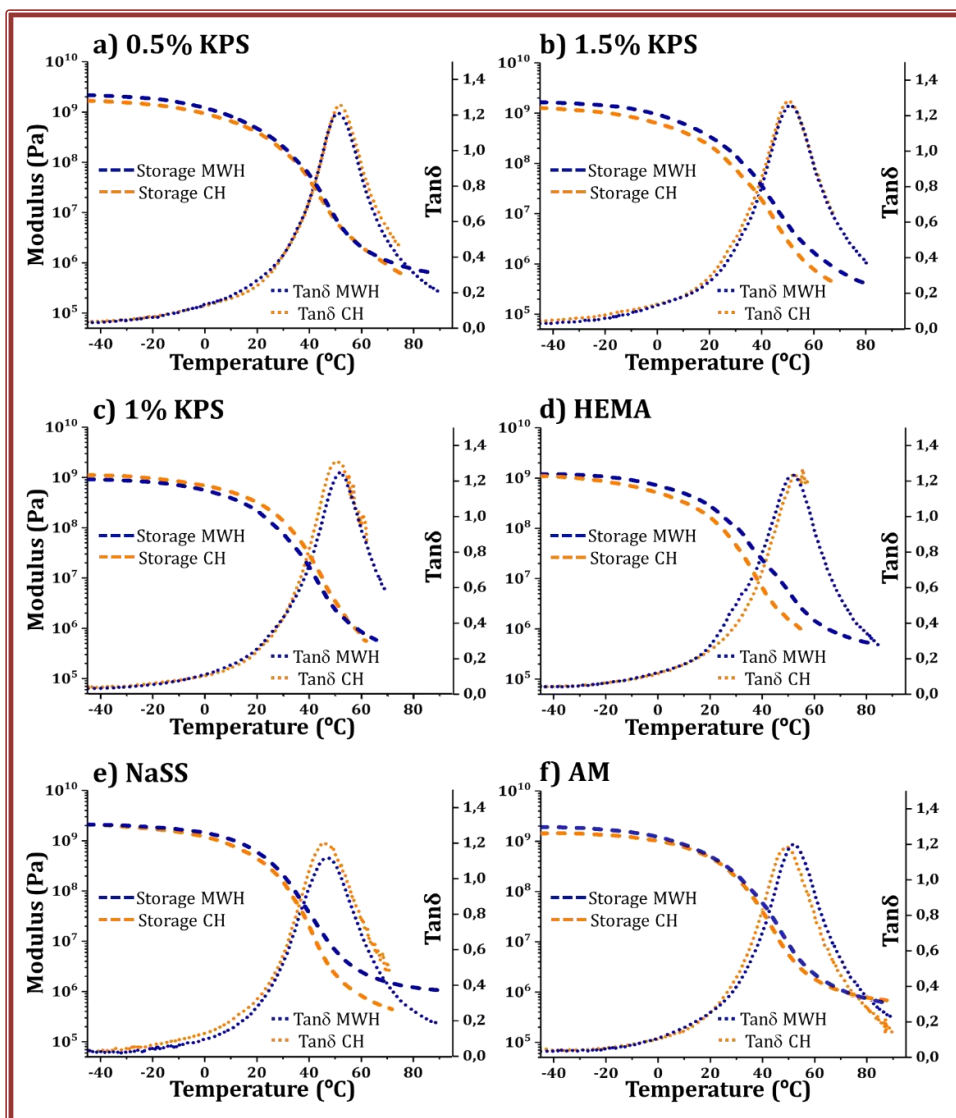


Figure II.3.3. DMTA measurements between MWH and CH polymer films dried at 25°C and 55% of relative humidity.

II.3.4. POLYMER FILMS DRIED AT 25°C, AFTER WATER UPTAKE

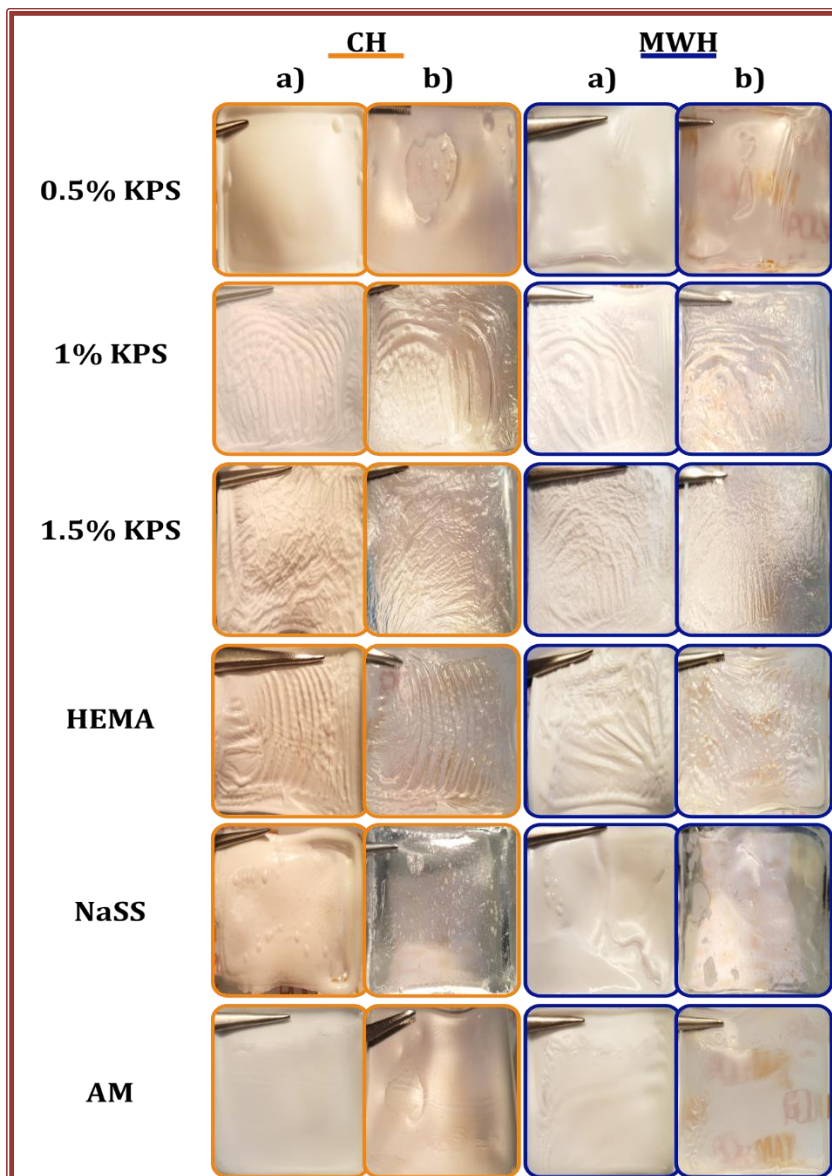


Figure II.3.4. Polymer films dried at 25°C. a) after 52 days immersed water; b) after dried at 60°C, orange color for CH and blue color for MWH method.

II.4. SUPPORTING INFORMATION OF CHAPTER 4

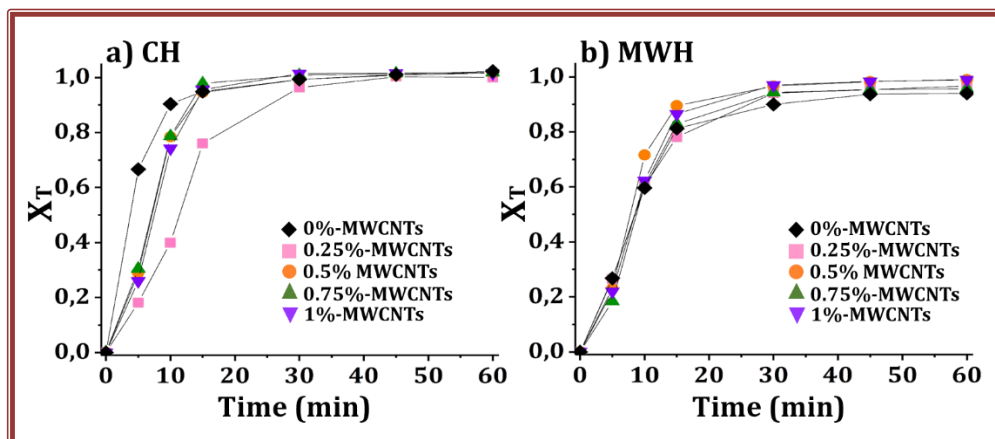


Figure II.4.1. The overall polymer conversion for miniemulsion polymerization in the presence of different MWCNTs by both methods a) CH and b) MWH.

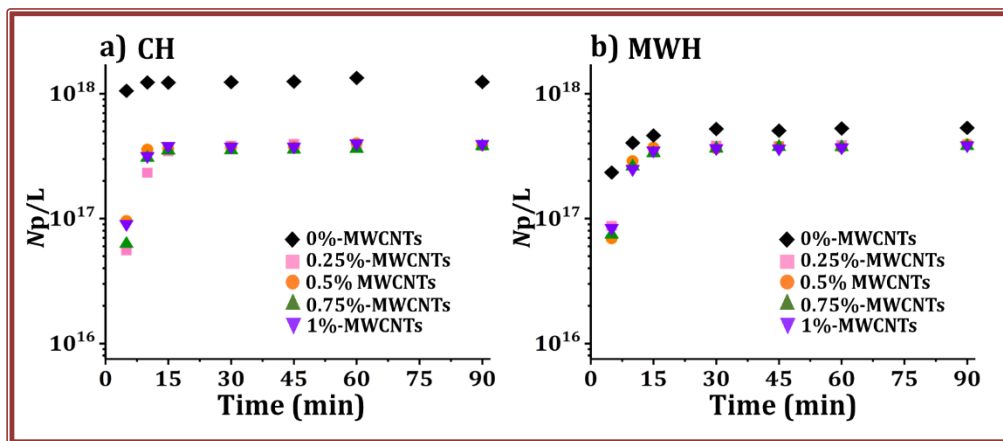


Figure II.4.2. The number of particles per liter for miniemulsion polymerization in the presence of different MWCNTs by both methods a) CH and b) MWH.

II.4.3. POLYMER COMPOSITES FILMS.

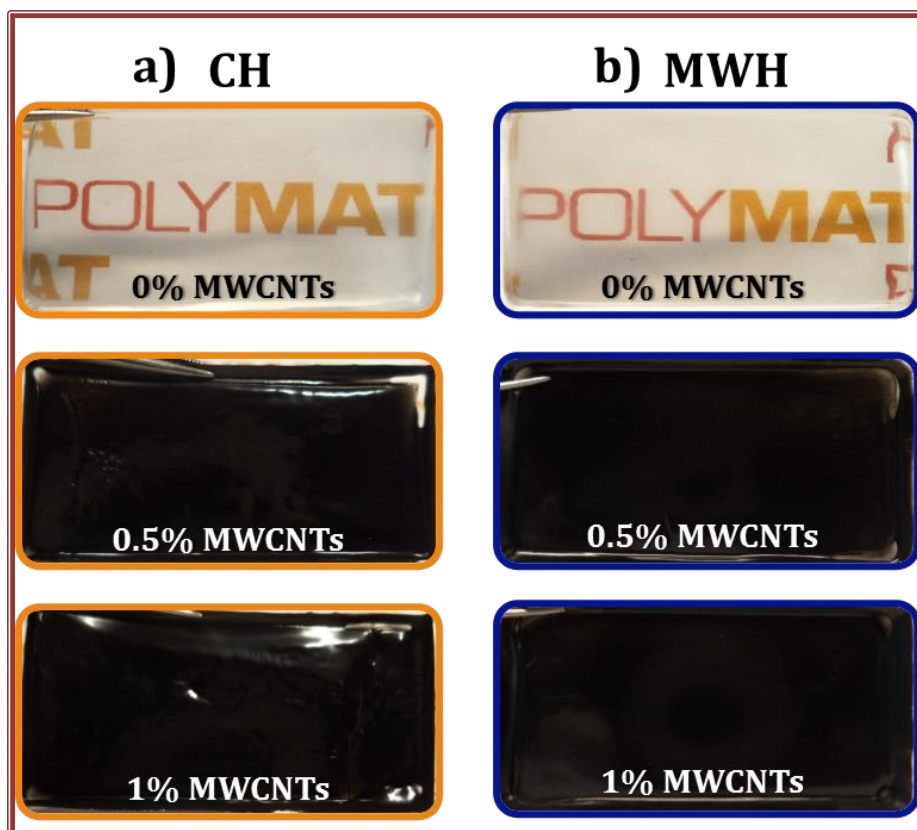


Figure II.4.3. Comparison of the polymer films of MMA/BA/HEMA copolymer, using different amounts of MWCNTs between a)CH (orange color) and b)MWH(blue color).



APENDIX III

**DISENTANGLEMENT OF
LARGE MWCNTs BY
SONICATION**

III SUPPORTING INFORMATION FOR CHAPTER 4

III.1. INTRODUCTION

Due to the huge specific surface area, important surface interactions, and significant rise of surface energy, nanoparticles in engineered or environmental systems are prone to remarkable aggregation, which has been a bottleneck in obtaining the full functional advantage of nanosize of the particles. To find solutions, researchers have developed various wet-methods of nanoparticle treatment, consisting of the use of high-pressure homogenizers [1], high speed/high shear stirring [2], and ultrasonicators of the dispersions/solutions of nanoparticles in various solvents [3–6].

The main drawback of wet methods is the use of solvents, but as well, the production of dry powders from the dispersions/solutions have been shown to be highly energy-intensive, long, and difficult to scale-up process [7]. This has led to the development of dry and environmentally benign methods, such as various processes in supercritical fluids [7–9] or magnetically assisted impaction mixing, and missing by fluidization of nanopowders [10]. Most of these methods have been developed with the aim of efficient mixing of different nanopowders, which is challenging to achieve unless adequate disaggregation is attained first. The main drawback is extensive size distribution and difficulty in attaining nanosize dimensions. Therefore, there is still a need for an efficient and straightforward dry method for nanoparticle disaggregation.

As stated by Komarov and Hirasawa [11], the ability of a sound wave to propagate through gasses make the ultrasonication process an attractive non-contact method in providing energy to the material. This idea was used in this work, for the first time up to the best knowledge of the authors, to deagglomerate large nanoparticles' aggregates by applying ultrapower sonication to the nanomaterial in air.

Sonication of solid particles dispersed in liquid mediums is a well-described process [4–6]. The changes of the solids occurred due to two phenomena, cavitation collapse that drives high-speed jets and associated shock waves of liquid into the solid surface. Besides, high-velocity interparticle collisions may induce dramatic alteration in surface morphology and composition [12]. Furthermore, if performed in water, ultrasound creates aggressive $\text{OH}\cdot$ radicals [13], which may significantly alter the surface chemistry of nanoparticles. However, no reports were found about the ultrasonication of solids particles in the air. It is well known that acoustic streaming (forced air current) is created in the air above the vibrating beam [14]. As a result, vigorous turbulent currents are generated by powerful ultrasonication in air, which induces strong thermal convection or radiation to and from the particles [11]. We expected that this air current would effectively disaggregate the nanoparticle aggregates and induce mild surface changes.

The proof of concept of the ultrasonication of nanomaterials in the air for disaggregation has been demonstrated using multi-walled carbon nanotubes (MWCNTs) that were clustered in large bundles up to a few μm . Highly entangled products are difficult to disperse uniformly in fluids and melt, and they would lead to a heterogeneous distribution of the MWCNTs in the composite film with lower improvements in their mechanical and transport properties. Therefore, in order to develop applications for these MWCNTs it is necessary to disentangle the MWCNTs agglomerates. For that aim, the MWCNTs powder was subjected to ultrasonication performed in air. With the aim of comparison, the ultrasonication of the MWCNTs bundles was performed in water, as well. Ultrasonication is a very common method used to break up agglomerates in solution processing techniques, and additionally, it provides the surface of MWCNTs with oxygen functionalities that later on prevent the re-aggregation of the tubes and increases their dispersibility [15,16].

DISENTANGLEMENT OF LARGE MWCNTs BY AIR SONICATION

The sonication treatments of CNTs were usually performed in the solvent [17–19], often in water [20–22]. Except for the introduction of oxygen functionalities at CNTs surface, the introduction of disorders and damages in the graphene structures of the CNTs occurred and shortening of the CNTs (decreasing the aspect ratio) [16,17,22], up to complete transformation of CNTs into amorphous carbon nanofibres [21]. It is likely due to the creation of aggressive OH· radicals during high power sonication in water [13], which process was expected to be reduced significantly when the sonication is performed in air.

In order to demonstrate that **air sonication** is a viable alternative for **efficient disentanglements of MWCNTs**, sonication in water dispersions as one of the most frequently utilized method was used as a reference.

III.2 EXPERIMENTAL

III.2.1 MATERIALS

Multiwalled Carbon Nanotubes (MWCNTs, length = 5 to 10 μm ; diameter = 10 to 20 nm) were purchased from IoLiTec Nanomaterials Co. (98.5%, Germany).

III.2.2 METHODS

MWCNTs were treated by sonication in the air according to the following procedure: 0.35g of MWCNTs were poured into a 50 ml beaker with a magnetic stirrer and sealed. In order to improve the efficiency of magnetic mixing, the magnetic stirrer was modified by adding metal extensions that gave a form of a cross to the stirrer (Figure III.1-c); after that, an ultrasound tip (Branson 450 instrument, Danbury, CT) was introduced into the beaker (keeping a separation between the ultrasound tip and magnetic stirrer of approximately 1.7 cm and 2.5 cm separation between the tip and

APPENDIX III

the bottom of the beaker). Afterward, ultrasound was applied (70% of power output and 50% duty cycle) under mixing with a magnetic stirrer of 200 rpm. For the aim of comparison, ultrasonication of MWCNTs was performed in water. The same amount of MWCNTs (0.35g) was dispersed in 30 mL of water within the same baker as for air sonication. The sonication was applied under the same conditions as explained for sonication in air. Figure III.1 shows the set-up for sonication in air and water.

MWCNTs sonicated in the air (0.15 g) were dispersed in water (15 g) under magnetic stirring (200 rpm), and the aqueous dispersion of both air and water sonicated MWCNTs were compared. These dispersions were used to prepare samples for characterization.

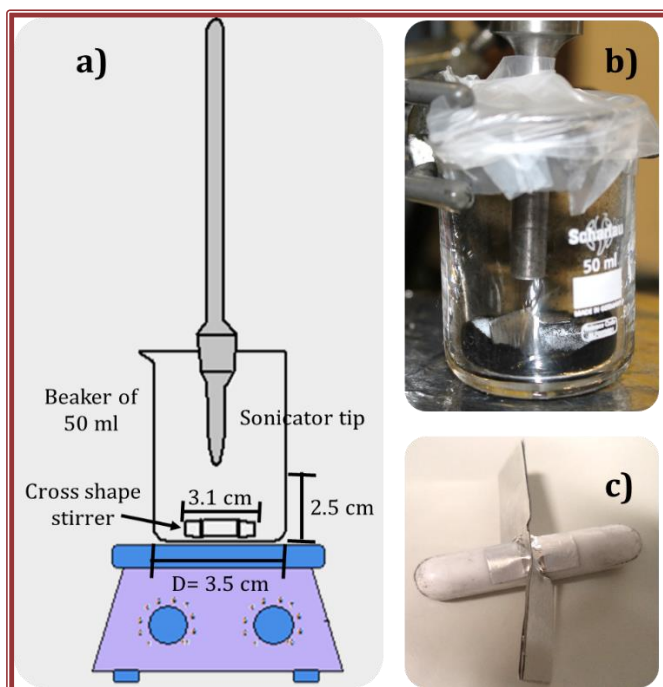


Figure III.1. a) Set-up for MWCNTs air or water sonication; b) Picture of the sonication in the air; c) Cross shape stirrer used.

III.2.3 CHARACTERIZATIONS

MWCNTs were analyzed by Raman spectroscopy (Horiba, Xplora) of the films prepared from aqueous dispersions of MWCNTs. Water contact angles on films of MWCNTs prepared by drop cast method on glass substrates were determined in goniometer (system Dataphysics OCA 20) using the sessile drop method with dynamic tracking function (1 frame s⁻¹ during one minute). The reported values of contact angles are the average of five measurements. SEM analyses of MWCNTs were carried out using Quanta FEG 250 in high vacuum mode at 5 and 10 KV. The sonicated stub on top of self-adhesive carbon tape. This means that water sonicated MWCNTs should be dried before analysis, whereas air sonicated MWCNTs were analyzed directly after treatment. The electrical conductivity of the films prepared from aqueous dispersion by drop cast method on glass substrate was measured by Four Point Probe Resistivity Meter (Miller Inc. Model FP500). The measurement was performed at several points in the film. The presented conductivities are the average of at least five measurements.

III.3 RESULTS AND DISCUSSIONS

III.3.1 MWCNTs SONICATION TREATMENT IN AIR AND WATER

In Figure III.2-a an optical image of the neat MWCNTs dispersed in water and dropped cast to a substrate is shown. Obviously, a wide distribution of different sizes of MWCNTs' bundles is presented, ranging from a few μm to a few mm.

SEM image of dried MWCNTs after sonication in water is presented in Figure III.2-b, and that of MWCNTs after sonication in the air in Figure III.2-c. The difference in the disentanglement is astonishing. By comparison of Figure III.2-b and III.2-c, it becomes obvious that while water sonication resulted in a wide distribution of the bundles'

APPENDIX III

diameter (up to 200 μm), air sonication resulted in round objects with quite uniform sizes of up to maximum 50 μm .

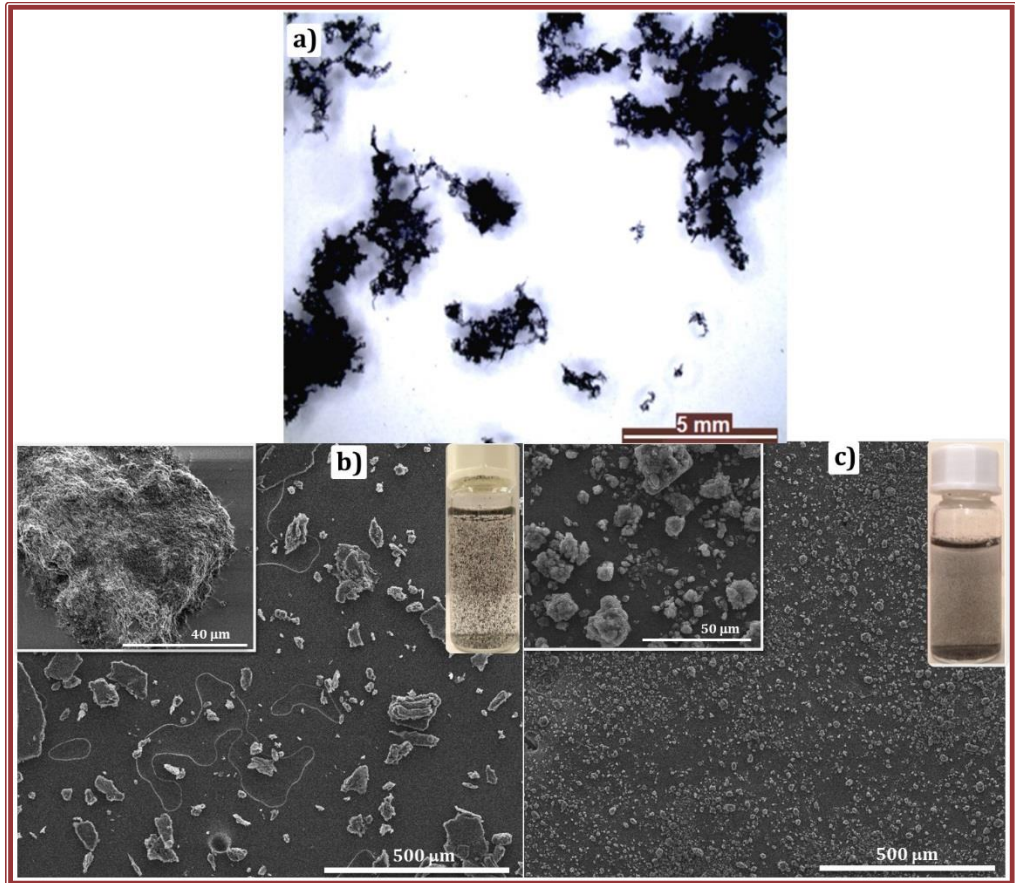


Figure III.2. a) Optical micrograph of neat MWCNTs; b) MWCNT sonicated in water for 1.5 h, and c) MWCNT sonicated in the air for 1.5 h. In the insets: aqueous dispersions of a) neat MWCNTs b) water sonicated and c) air sonicated MWCNTs (the photos were taken immediately after the addition of MWCNTs into water).

DISENTANGLEMENT OF LARGE MWCNTs BY AIR SONICATION

Similar findings were noticed after the preparation of aqueous dispersions of MWCNTs as received water sonicated dispersion is presented in the inset of Figure III.2-b and shows visible aggregates that after shaking off the dispersions sedimented fast on the vial bottom. The inset of Figure III.2-c shows air sonicated MWCNTs dispersed in water. The dispersion is much uniform and more stable, as after shaking MWCNTs deposited slowly on the vial bottom. These observations were demonstrated additionally by measuring of light backscattered and transmitted from these dispersions, presented in Figure III.3.

The aqueous dispersion of water sonicated MWCNTs (Figure III.3-a) is significantly less stable than the air sonicated ones (Figure III.3-b). The changes of the light backscattered (or transmitted) in time (30 min) and height of the sample (55 mm) by the dispersion of water treated MWCNTs denotes sedimentation as a result of which the light transmitted throughout the dispersions was increased significantly (Figure III.3-a). Complete sedimentation may be observed in the images of the water treated MWCNTs, shown on the left (at time 0) and on the right (at time 30 min) side of Figure III.3-a. There is a slight change in the light backscattered in time by the aqueous dispersion of air sonicated nanotubes, meaning more stable dispersions significantly in the period of time measured (30 minutes), although the transmittance was slightly increased (Figure III.3-b), especially to the vial top indicating the start of sedimentation process within the time of measurements (30 min). It may be observed in the images of the dispersions, as on the right side, there is some precipitation of MWCNTs although one part of them is still in the dispersion.

APPENDIX III

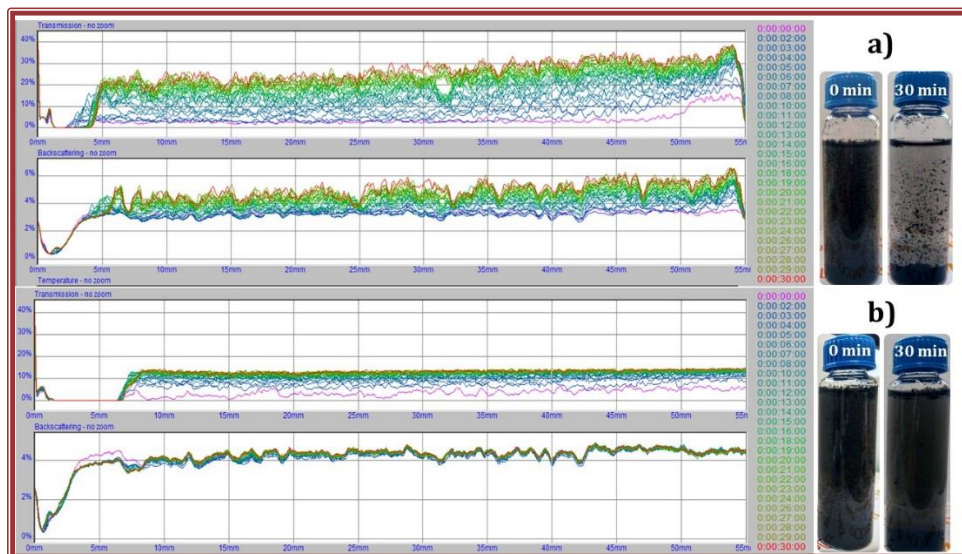


Figure III.3. Light backscattered and transmitted measured each minute during 30 minutes from the dispersions of MWCNTs sonicated in a) water; and b) air.

In order to check the nature of the changes induced in the sonication treated MWCNTs, they were analyzed by Raman spectroscopy. Figure III.4 shows the Raman spectra of the neat and the treated MWCNTs in water and air. These spectra have three characteristic peaks, peak G corresponds to planar vibrations of carbon atoms, peak D is due to structural defects coming from the presence of sp^3 hybridized carbons within the graphene network, and peak 2D is the second overtone of the peak D. Table III. 1 shows the changes in the ratios D/G and 2D/G of MWCNTs treated 1.5 h. The decrease of the D/G ratio during the sonication indicates that there was no creation of defects but rather the restoration of sp^2 carbon hybridized structure, which is unexpected, especially underwater sonication, where MWCNTs are likely exposed to a high concentration of $OH\cdot$ radicals. On the other hand, the comparison of the Raman spectra in Figure III.4 shows that there is a change in the intensity of both the G and

DISENTANGLEMENT OF LARGE MWCNTs BY AIR SONICATION

the D peak after sonication processes, which changes become hidden within the ratio of the peaks. In order to quantify these changes, in Table III.1 the normalized intensity of the characteristic peaks are presented. For normalization, the radial breathing mode centered (RBM) at around 250 cm^{-1} was used, which is related to the thickness or number of layers in MWCNTs, thus, expected not to be changed during these treatments.

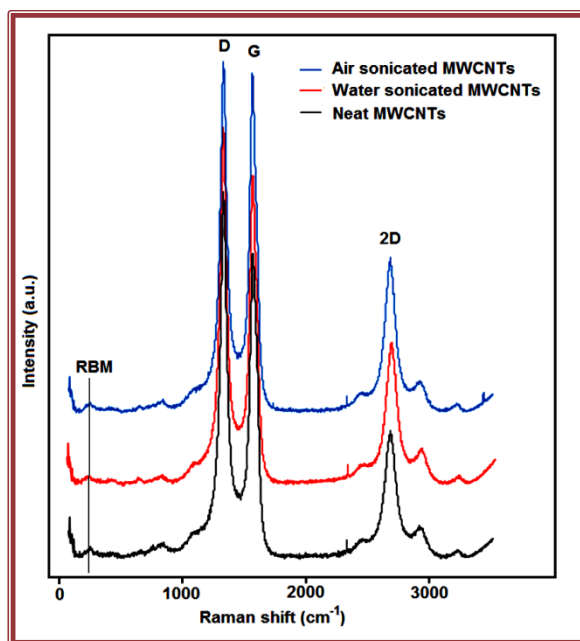


Figure III.4. Raman spectra of MWCNTs.

Obviously, the 1.5 h air sonicated MWCNTs have increased intensity of both D and G peaks. The relative increment of D peak denotes an increase in sp^3 hybridized carbons, or the introduction of functional groups, whereas the rise in G peaks denotes recovering of the structural defects (for example atomistic vacancy defects, five or

APPENDIX III

seven carbon rings) due to the high temperature to which the MWCNTs were exposed during the sonication. In the water sonicated MWCNTs the augmentation of D peak is more pronounced because of the presence of OH· radicals, demonstrating more intensive functionalization. The G peak was slightly raised still presenting some improvement of the structure when compared to neat MWCNTs, however less than air sonicated ones.

Table III.1. Intensity ratios of characteristic Raman peaks of the air and water treated MWCNTs.

Sample	D/G	2D/G	D/RBM	G/RBM	2D/RBM	EC (S·m ⁻¹)
Neat MWCNTs	1.20	0.40	50.98	43.29	17.91	94.24
Air (1.5 h)MWCNTs	1.01	0.42	58.57	56.67	25.71	37.99
Water (1.5 h)MWCNT	1.14	0.42	63.94	54.31	24.72	23.61

The measurement of the electrical conductivity (EC) was in line with the presented observations; thus, it dropped from 94.24 S·m⁻¹ for the untreated to 37.99 S·m⁻¹ for the MWCNTs sonicated for 1.5 h in air and to 23.61 S·m⁻¹ for MWCNTs sonicated 1.5 h in water (Table III.1). The electrical conductivity dropped due to two reasons. The first one is the functionalization of the treated MWCNTs that introduce a higher number of sp³ hybridized carbon atoms within the graphene structure of the CNT, which limits the free movement of the π electrons between carbon atoms. The second reason for the conductivity drop is the decrease in the MWCNTs aspect ratio. Air treated MWCNTs, as shown in Figure III.2, seem to be broken in smaller aggregates and likely with a higher decrease in aspect ratio than water treated ones. Thus the final difference in the electrical conductivity seems to be the results of two simultaneous effects from the treatments: functionalization and change in aspect ratio.

DISENTANGLEMENT OF LARGE MWCNTs BY AIR SONICATION

To demonstrate the decrease in aspect ratio, the treated MWCNTs were analyzed by SEM under higher magnifications. By comparison of SEM images of the MWCNTs before (Figure III.5-a, where some smaller bundles of 30 μm size are presented) and after ultrasonication treatment in the air (Figures III.5-b-d) it is clear that the size of the agglomerates decreased after the treatment, leading to rather smooth and regular agglomerates. In the insets of Figure III.5, the images and the water contact angles of the films prepared from the air treated nanotubes dispersions are shown. However, these observations differ a lot for the MWCNT sonicated in water, as it is shown in Figures III.5-e-g. First of all, no significant changes in the bundles' size were noticed during various periods of sonication. In addition, there was no change in the water contact angles with respect to the non-treated MWCNTs. At first sight, this may be contradictory to the previous results (Raman spectra) and the expectation; however, during multiplied repeating of these measurements it was noticed that water treated MWCNTs aggregated visibly, which did not occur for air treated MWCNTs. The obvious reason for this is the aspect ratio, as, after the treatment in water, the MWCNTs are still too long and entangled easily.

The presented results showed that the aspect ratio of the MWCNTs decreased more significantly during sonication in air. This is advantageous for the dispersions of the MWCNTs in water, as shorter structures are easier to disperse and stabilize. This is the probable reason why the air sonicated MWCNTs presented better water dispersibility (Figure III.3). Water contact angle varied from 136° for the untreated MWCNTs to 81° for the film formed with MWCNTs that were subjected to 1.5 h of sonication. The high contact angle observed for the untreated MWCNTs is a typical of rough surfaces of hydrophobic materials (materials that have a water contact angle higher than 90° on a flat surface) [23,24]. The decrease observed for the first 1 h of sonication ($136^\circ \rightarrow 107^\circ$) can be attributed to the smoother surface of the MWCNTs films formed with shorter and disentangled MWCNTs. However, contact angle

measured after 1.5 h of sonication (82°), indicated that MWCNTs became hydrophilic (water contact angle lower than 90° on a flat surface), as already shown in Raman spectra (Figure III.4) [24].

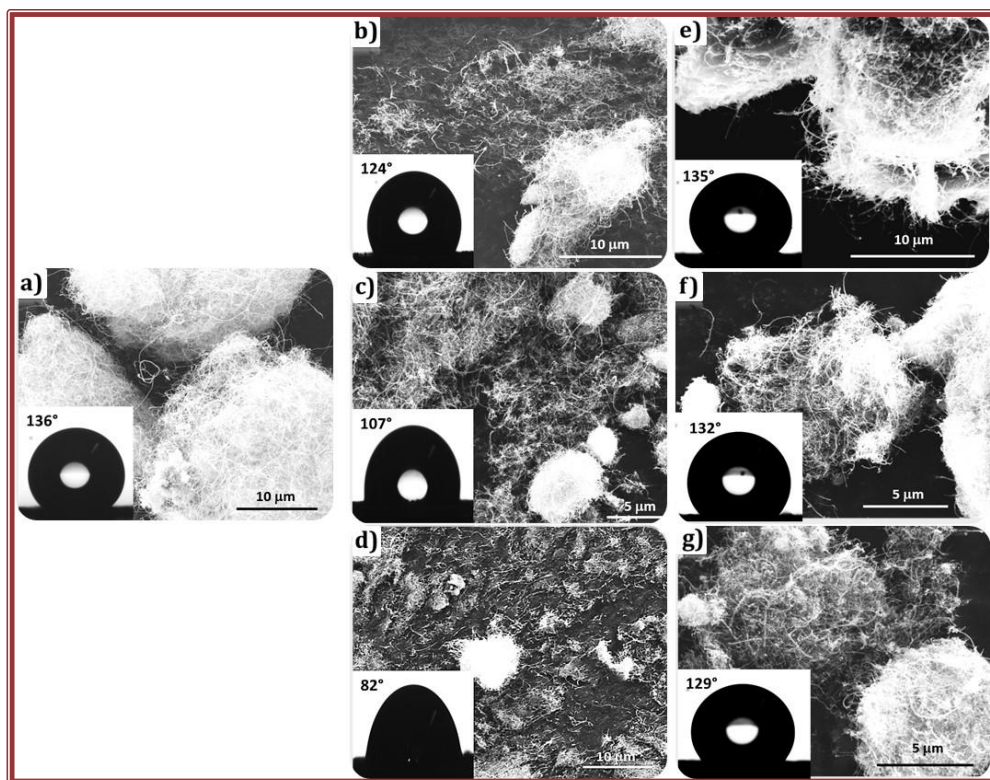


Figure III.5. SEM images of **a)** untreated MWCNTs; **b)** MWCNTs after 0.5 h of sonication in air; **c)** MWCNTs after 1 h of sonication in air; **d)** MWCNTs after 1.5 h of sonication in air; **e)** MWCNTs after 0.5 h of sonication in water; **f)** MWCNTs after 1 h of sonication in water; **g)** MWCNTs after 1.5 h of sonication in water.

DISENTANGLEMENT OF LARGE MWCNTs BY AIR SONICATION

All these results demonstrate that the air sonication process is much more efficient in the disentanglements of MWCNTs than the water sonication process and that the functionalization of the MWCNTs in the air is milder (as proved by the smaller augmentation of the D-peak in Raman spectra). Better disentanglement process in the air may be explained by the fact that during passage through the medium, the sound wave suffers from attenuation due to energy loss through different mechanisms [25], one of them being frictional (viscous) loss. Obviously, even sonicated under the same conditions, MWCNTs in the air would be exposed to a higher energy than in water. Likely, during sonication in the air, the MWCNTs are exposed to a current of very hot air that induced collisions between the solid particles that induce breakage of the large aggregates. Within such a harsh atmosphere, one may expect that radicals will be formed from the molecules presented in air, between them humidity that may be the reason behind the functionalization.

III.3.1 PERFORMANCE OF THE TREATED MWCNTS IN POLYMER COMPOSITES

In order to compare the performance of the treated MWCNTs, they were introduced into polymer matrix by emulsion mixing procedure, which means a physical blend of stable aqueous dispersions of MWCNTs with polymer latex produced by emulsion polymerization. Prior to being introduced into a polymer matrix, the pre-treated MWCNTs by sonication in air and in water were dispersed in the aqueous solution of PVP. Figure III.6 shows the stability of both dispersions, measured as a light backscattered through the dispersions versus the height of sample 45 mm) in time (3 hours). Both dispersions have shown to be stable in time; however, the water sonicated MWCNTs dispersion (Figure III.6-b) show unusually increased light scattering towards the top of the vial. Probably, this dispersion presents distribution in size of MWCNTs bundles through the height of the vial, although there are no visible destabilization effects.

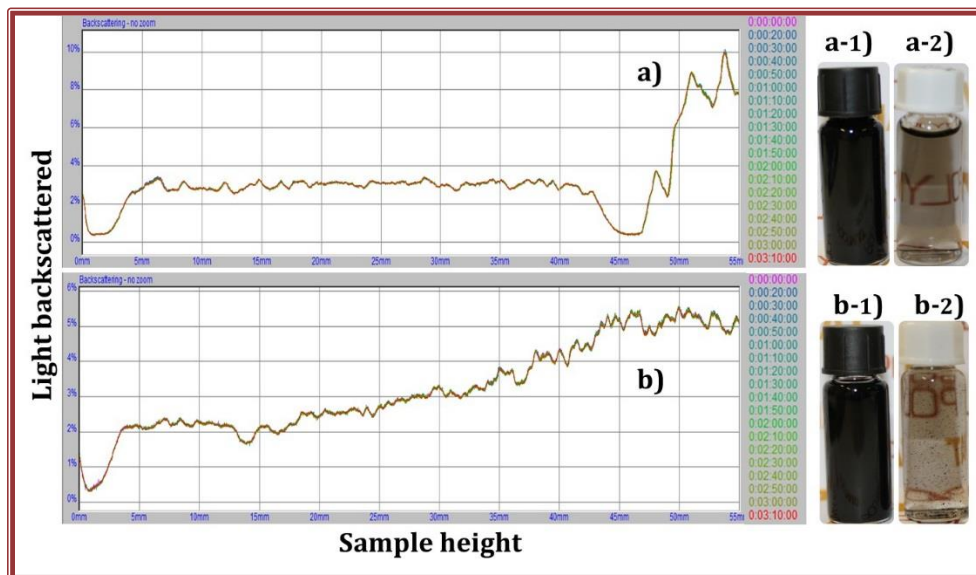


Figure III.6. Light backscattered from the aqueous dispersions of MWCNTs (0.3 wt%) sonicated in: **a) air; b) water**. In the insets, the images of concentrated-1 (0.3 wt%) and diluted-2 with water (1:100) dispersions are shown.

Figure III.6 shows the images of the dispersions. The concentrated ones (0.3 wt%), which were subject to the measurements of light backscattered, are black colored and not transparent. In order to observe the dispersions, they were diluted with water (1:100). As Figure III.6 show, air treated MWCNT (Figure III.6-a-2) show very nice powder dispersed in water, likely due to the combined effect of introduced hydrophilicity that reduced the tendency to aggregation and the smaller size that reduced sedimentation. Water sonicated MWCNTs presents small aggregates, and some of them immediately after preparation of the dispersions sedimented on the bottom of the vial. Although water sonicated MWCNTs have higher hydrophilicity (observation based on Raman spectra), the larger dimension of these nanotubes seems to be determined for their stabilization in water (Figure III.6-b-2).

DISENTANGLEMENT OF LARGE MWCNTs BY AIR SONICATION

A thin film was prepared from the diluted dispersions, and the electrical conductivity was determined to be $1.23 \times 10^{-6} \text{ S} \cdot \text{m}^{-1}$ for air sonicated and $5.00 \times 10^{-7} \text{ S} \cdot \text{m}^{-1}$ for water sonicated MWCNTs. Having in mind that the electrical conductivity of the naked MWCNTs, after treating by ultrasonication in air and water were $38 \text{ S} \cdot \text{m}^{-1}$ and $24 \text{ S} \cdot \text{m}^{-1}$, obviously, the presence of PVP adsorbed onto the MWCNT surface-induced significant drop of the conductivity, even more, important for the water sonicated MWCNTs. This behavior is quite unexpected and difficult to explain since the interaction between the PVP and the MWCNTs are π - π stacking between the aromatic rings in both that have even shown increased electrical conductivity in the case of graphene [26].

PVP stabilized MWCNTs were mixed with MMA/BA/HEMA latex, as a result of which, hybrid dispersions were obtained, containing both MWCNTs and polymer nanoparticles dispersed in water. The content of MWCNTs was 0.5 wt% with respect to the polymer. The composite films were prepared from the hybrid dispersions by water evaporation under controlled temperature (25°C) and relative humidity (80%). Both polymer films have very low values of electrical conductivity of an order of $10^{-8} \text{ S} \cdot \text{m}^{-1}$, which is only one order of magnitude raised with respect to neat polymer film ($10^{-9} \text{ S} \cdot \text{m}^{-1}$). This result is explained by the significant drop in electrical conductivity of MWCNTs stabilized by PVP.

Morphology of the composite films containing air or water sonicated MWCNTs is presented in Figure III.7. Which in polymer film containing water, sonicated MWCNTs (Figure II.7-b) show that during the preparation of the films from the dispersion certain phase separation has occurred, and some neat polymeric areas are visible. Whereas for polymer film prepared using MWCNTs air sonication treatment (Figure III.7-a) present a good film formation and homogeneous distribution of MWCNTs along with the films. Confirming that for composite preparation, the sonication of MWCNTs performed in the air is a much better method than using water.



Figure III.7. Images of polymer films cast from **a)** hybrid dispersion containing 0.5 wt% air sonicated MWCNTs; **b)** hybrid dispersion containing 0.5% water sonicated MWCNTs.

The same was confirmed from the SEM images of the top surfaces of the composite films (Figure III.8).

Figures III.8-a and b, where the top view of composite with air sonicated MWCNTs is presented under different magnification, show the very nice distribution of the nanotubes (white objects) within the dark polymer matrix. The presence of some small aggregates is noticeable. However, SEM images of the top surface of composites with water sonicated MWCNTs show a completely different distribution (Figures III.8-c and d). The nanotubes in the aggregated form are distributed within the matrix, showing areas very rich with nanotubes and others with few nanotubes and neat polymer. The morphology of the surface is completely distinct. While films with air sonicated MWCNTs are smooth, the films with water sonicated nanotubes show wrinkled morphology. The last may be an indication of the formation of the skin during the drying of the film that is characteristic of lower viscosity dispersions. In the dispersions containing water sonicated MWCNTs, the bigger aggregates of nanotubes precipitated, which decrease the viscosity of the dispersions, so bad quality films were formed.

DISENTANGLEMENT OF LARGE MWCNTs BY AIR SONICATION

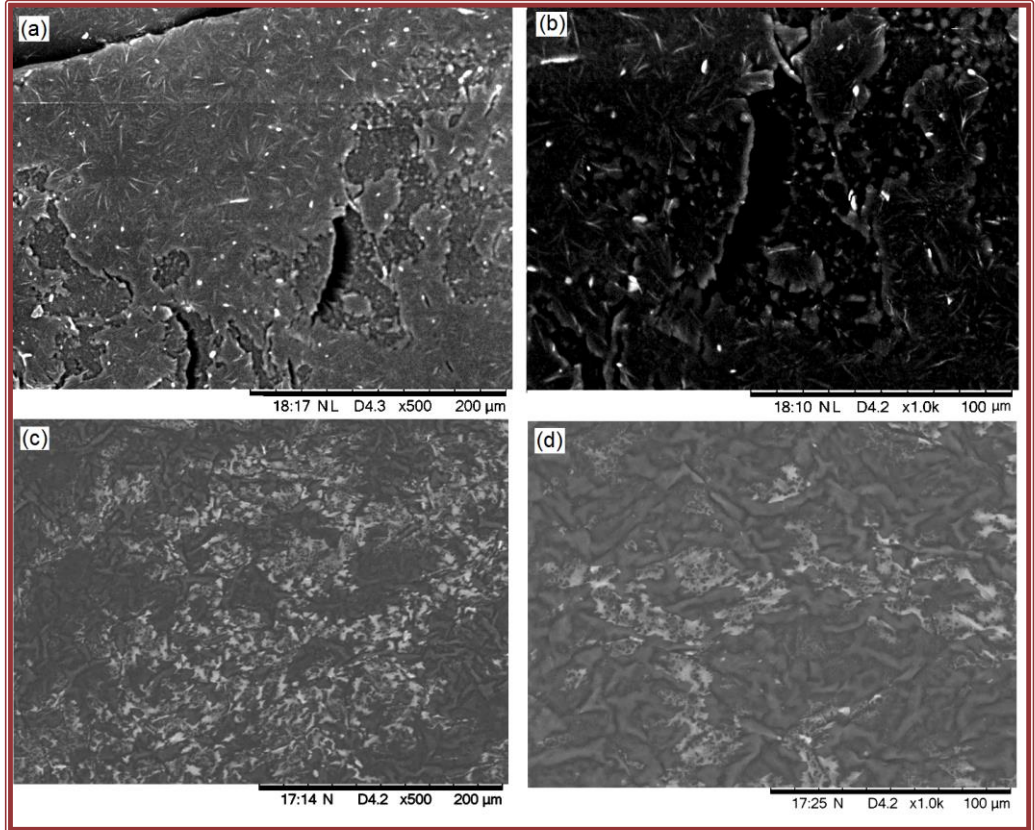


Figure III.8. SEM images of the top surface of the composite films containing 0.5 wt% a) and b) air sonicated MWCNTs and c) and d) water sonicated MWCNTs.

III.4 CONCLUSIONS

The viability of a novel dry method of disaggregation of MWCNTs based on ultrapower sonication in the air has been proved. The results have been compared with the sonication of MWCNTs performed in aqueous dispersions, as one of the most often used method for nanotubes disentanglement.

The air sonicated MWCNTs has shown better dispersibility in water, more stable dispersions, and much smaller aggregates than the water sonicated ones. By Raman spectra measurements, it was demonstrated that by the exposure to high temperature during air sonication, some defects in the graphene structures of the tubes were recovered, and MWCNTs were mildly functionalized on the surface, additionally confirmed by the measurements of the water contact angles that dropped from 136° on neat MWCNT to 82° on-air treated ones. The electrical conductivity of the treated MWCNTs dropped, an effect that was expected due to the two simultaneous changes: aspect ratio decrease and functionalization on the surface that increase the presence of sp^3 hybridized carbons. However, shorter MWCNTs are much easier to stabilize in dispersions, which means that always a compromise between the conductivity and aspect ratio should be found, depending on the possible application.

The presented results demonstrate that the air sonication process is more efficient in the disentanglements of MWCNTs than the water sonication process due to exposure of the nanotubes on higher energy in air than in water, as the attenuation of ultrasound radiation is higher in water, which is much more viscous medium. This offers an advantage of more efficient utilization of ultrasound energy in the air, as the same effect may be achieved with less energy if the sonication is performed in air.

The sonicated MWCNTs were mixed with MMA/BA/HEMA polymer latex resulting in hybrid latexes from which composite films were prepared. Water sonicated MWCNTs containing films presented larger aggregates of less homogeneous films than the films with air sonicated MWCNTs, confirming that for composite preparation, the sonication of MWCNTs performed in the air is a much better method.

III.5 REFERENCES

- [1] I.N. Seekkuarachchi, H. Kumazawa, Aggregation and disruption mechanisms of nanoparticulate aggregates. 2. Dispersion of aggregates using a motionless mixer, *Ind. Eng. Chem. Res.* (2008). doi:10.1021/ie0714955.
- [2] G. Carotenuto, M. Valente, G. Sciumè, T. Valente, G. Pepe, A. Ruotolo, L. Nicolais, Preparation and characterization of transparent/conductive nano-composites films, *J. Mater. Sci.* (2006). doi:10.1007/s10853-006-0253-y.
- [3] J.H. Bang, K.S. Suslick, Applications of ultrasound to the synthesis of nanostructured materials, *Adv. Mater.* (2010). doi:10.1002/adma.200904093.
- [4] T. Hielscher, Ultrasonic Production of Nano-Size Dispersions and Emulsions, (2005) 138–143.
- [5] J.S. Taurozzi, V.A. Hackley, M.R. Wiesner, Preparation of Nanoparticle Dispersions from Powdered Material Using Ultrasonic Disruption, *NIST Spec. Publ.* (2012).
- [6] K.S. Suslick, Sonochemistry, in: *Kirk-Othmer Encycl. Chem. Technol.*, 2000. doi:10.1002/0471238961.1915141519211912.a01.
- [7] D. To, R. Dave, X. Yin, S. Sundaresan, Deagglomeration of nanoparticle aggregates via rapid expansion of supercritical or high-pressure suspensions, *AIChE J.* (2009). doi:10.1002/aic.11887.
- [8] D. Wei, R. Dave, R. Pfeffer, Mixing and characterization of nanosized powders: An assessment of different techniques, *J. Nanoparticle Res.* (2002). doi:10.1023/A:1020184524538.
- [9] J. Yang, Y. Wang, R.N. Dave, R. Pfeffer, Mixing of nano-particles by rapid expansion of high-pressure suspensions, in: *Adv. Powder Technol.*, 2003. doi:10.1163/156855203769710681.
- [10] J. Scicolone, A. Mujumdar, S. Sundaresan, R.N. Davé, Environmentally benign dry mechanical mixing of nano-particles using magnetically assisted impaction mixing process, *Powder Technol.* (2011). doi:10.1016/j.powtec.2011.02.021.
- [11] S. Komarov, M. Hirasawa, Enhancement of gas phase heat transfer by acoustic field application, *Ultrasonics.* (2003). doi:10.1016/S0041-624X(02)00454-7.
- [12] S.J. Doktycz, K.S. Suslick, Interparticle collisions driven by ultrasound, *Science*

- (80-). (1990). doi:10.1126/science.2309118.
- [13] M. Kohno, T. Mokudai, T. Ozawa, Y. Niwano, Free radical formation from sonolysis of water in the presence of different gases, *J. Clin. Biochem. Nutr.* (2011). doi:10.3164/jcfn.10-130.
- [14] M. Legay, N. Gondrexon, S. Le Person, P. Boldo, A. Bontemps, Enhancement of heat transfer by ultrasound: Review and recent advances, *Int. J. Chem. Eng.* (2011). doi:10.1155/2011/670108.
- [15] P.C. Ma, N.A. Siddiqui, G. Marom, J.K. Kim, Dispersion and functionalization of carbon nanotubes for polymer-based nanocomposites: A review, *Compos. Part A Appl. Sci. Manuf.* (2010). doi:10.1016/j.compositesa.2010.07.003.
- [16] F. De Nicola, P. Castrucci, M. Scarselli, F. Nanni, I. Cacciotti, M. De Crescenzi, Exploiting the hierarchical morphology of single-walled and multi-walled carbon nanotube films for highly hydrophobic coatings, *Beilstein J. Nanotechnol.* (2015). doi:10.3762/bjnano.6.34.
- [17] C.J. Kerr, Y.Y. Huang, J.E. Marshall, E.M. Terentjev, Effect of filament aspect ratio on the dielectric response of multiwalled carbon nanotube composites, *J. Appl. Phys.* (2011). doi:10.1063/1.3569596.
- [18] Q. Cheng, S. Debnath, E. Gregan, H.J. Byrne, Ultrasound-Assisted swnts dispersion: Effects of sonication parameters and solvent properties, *J. Phys. Chem. C.* (2010). doi:10.1021/jp101431h.
- [19] L. Dumée, K. Sears, J. Schütz, N. Finn, M. Duke, S. Gray, Influence of the Sonication Temperature on the Debundling Kinetics of Carbon Nanotubes in Propan-2-ol, *Nanomaterials.* (2013). doi:10.3390/nano3010070.
- [20] K. Yang, Z.L. Yi, Q.F. Jing, R.L. Yue, W. Jiang, D.H. Lin, Sonication-assisted dispersion of carbon nanotubes in aqueous solutions of the anionic surfactant SDBS: The role of sonication energy, *Chinese Sci. Bull.* (2013). doi:10.1007/s11434-013-5697-2.
- [21] L. Vaisman, H.D. Wagner, G. Marom, The role of surfactants in dispersion of carbon nanotubes, *Adv. Colloid Interface Sci.* (2006). doi:10.1016/j.cis.2006.11.007.
- [22] Y.Y. Huang, E.M. Terentjev, Dispersion of carbon nanotubes: Mixing, sonication, stabilization, and composite properties, *Polymers (Basel).* (2012). doi:10.3390/polym4010275.

DISENTANGLEMENT OF LARGE MWCNTs BY AIR SONICATION

- [23] A.B.D. Cassie, S. Baxter, Wettability of porous surfaces, *Trans. Faraday Soc.* (1944). doi:10.1039/tf94444000546.
- [24] R.N. Wenzel, Resistance of solid surfaces to wetting by water, *Ind. Eng. Chem.* (1936). doi:10.1021/ie50320a024.
- [25] V.S. et al. Moholkar, Chapter 2. Physical and Chemical Mechanisms of Ultrasound in Biofuel Synthesis, in: Springer (Ed.), *Prod. Biofuels Chem. with Ultrasound*, Netherlands, 2015: pp. 35–86.
- [26] M.J. Deka, D. Chowdhury, Tuning Electrical Properties of Graphene with Different π -Stacking Organic Molecules, *J. Phys. Chem. C.* (2016). doi:10.1021/acs.jpcc.5b12403.